

1-1-1979

# Rheology and rheo-optics of concentrated solutions of helical polypeptides.

Gabor, Kiss

*University of Massachusetts Amherst*

Follow this and additional works at: [https://scholarworks.umass.edu/dissertations\\_1](https://scholarworks.umass.edu/dissertations_1)

---

## Recommended Citation

Kiss, Gabor, "Rheology and rheo-optics of concentrated solutions of helical polypeptides." (1979). *Doctoral Dissertations 1896 - February 2014*. 643.

[https://scholarworks.umass.edu/dissertations\\_1/643](https://scholarworks.umass.edu/dissertations_1/643)

This Open Access Dissertation is brought to you for free and open access by ScholarWorks@UMass Amherst. It has been accepted for inclusion in Doctoral Dissertations 1896 - February 2014 by an authorized administrator of ScholarWorks@UMass Amherst. For more information, please contact [scholarworks@library.umass.edu](mailto:scholarworks@library.umass.edu).



RHEOLOGY AND RHEO-OPTICS OF CONCENTRATED  
SOLUTIONS OF HELICAL POLYPEPTIDES

A Dissertation Presented

By

GABOR KISS

Submitted to the Graduate School of the  
University of Massachusetts in partial fulfillment  
of the requirements for the degree of

DOCTOR OF PHILOSOPHY

May

1979

Department of Polymer Science and Engineering

© Gabor Kiss 1979  
All Rights Reserved

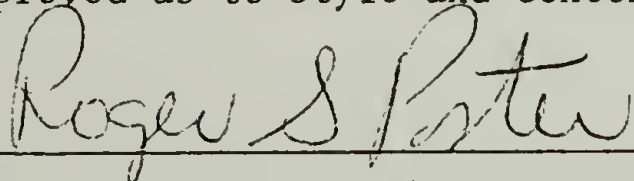
RHEOLOGY AND RHEO-OPTICS OF CONCENTRATED  
SOLUTIONS OF HELICAL POLYPEPTIDES

A Dissertation Presented

By

GABOR KISS

Approved as to style and content by:



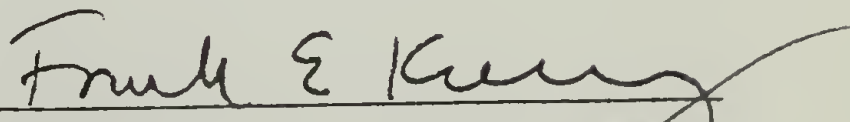
Roger S. Porter, Chairperson of Committee



Richard S. Stein, Member



Richard Farris, Member



Frank E. Karasz, Acting Department  
Head  
Department of Polymer Science and  
Engineering

I dedicate this thesis to:

My father, Kornel D. Kiss

My mother, Klara Kiss

My advisor, Prof. Roger S. Porter

My good friends, Eva Andor

Jackie Davidson

David Glaser

Steve and Jan Grossman

ABSTRACT

Rheology and Rheo-Optics of Concentrated Solutions  
of Helical Polypeptides

May 1979

Gabor Kiss

B.S., Case Western Reserve University

Ph.D., University of Massachusetts

Directed by: Professor Roger S. Porter

Concentrated m-cresol solutions of poly- $\gamma$ -benzyl-glutamate (PBG) (both the L-enantiomer alone and a racemic mixture), poly- $\epsilon$ -carbobenzyl-oxy-L-lysine (PCBZL), and poly- $\beta$ -benzyl-aspartate (PBA) were the subjects of rheological and rheo-optical investigation. Steady shear viscosity and first normal stress difference ( $N_1$ ) were measured in a cone-and-plate rheometer over a shear rate range of .025-16,000  $\text{sec}^{-1}$ . Dynamic viscosity and dynamic storage modulus were measured via oscillatory shear and eccentric rotating disc over a frequency range of .1-400 rad/sec and .1-63 rad/sec respectively. Photomicrographs during shear were obtained by use of a shearing stage and polarized stroboscopic illumination. Dried films made from sheared drops of concentrated solutions of a volatile solvent were also investigated.

All samples gave liquid crystalline (birefringent) solutions at concentrations beyond a critical value. The transition to the liquid-crystalline state was manifested rheologically as a peak in all material functions at concentrations close to the critical value for the PBG and

PCBZL samples. An unusual normal stress effect consisting of negative values of the first normal stress difference,  $N_1$ , was observed at intermediate shear rates in many of the liquid crystalline PBLG and PCBZL solutions. All normal force measurements were corrected for the negative inertial contribution. At low and very high shear rates values of  $N_1$  were positive. Both the shear stress at the changes in sign of  $N_1$  and the maximum values within the first positive and the negative regimes of  $N_1$  were concentration dependent.

At high shear rate the peak in steady shear viscosity vs. concentration was suppressed but the peak in  $N_1$  vs.  $C$  was not, indicating that shear orientation does not overwhelm the structure inherent in the fluid, as had previously been thought.

The effect of helix flexibility in the PCBZL was to increase the value of critical concentration for the formation of the anisotropic phase. In fact, the observation of liquid crystalline behavior in concentrated PCBZL solutions indicates that the inverse coil-helix transition which occurs at 30°C in dilute *m*-cresol solution is shifted to a lower temperature in concentrated solutions.

Three shear-dependent textures were observed in the liquid-crystalline solutions, corresponding to the three regimes of first normal stress difference (positive-negative-positive). Negative values of  $N_1$  were found to correlate with a texture consisting of striations perpendicular to the shearing direction. Similar structures were observed in sheared dried films.

The PBA sample behaved differently than the PBG and PCBZL sam-



ples, forming an anisotropic gel at high concentration. Values of the material functions were strongly dependent on shear history and behavior was consistent with the existence of a shear-sensitive and healable network.

## TABLE OF CONTENTS

	Page
ABSTRACT . . . . .	v
LIST OF TABLES . . . . .	x
LIST OF FIGURES . . . . .	xi
FOREWORD . . . . .	xviii
 Chapter	
I. RHEOLOGY OF SYSTEMS CONTAINING ROD-LIKE MACROMOLECULES AND PARTICLES . . . . .	1
 Rheology of Dilute Solutions and Suspensions of Rod-Like Molecules and Particles . . . . .	
Introduction . . . . .	1
Viscosity of Suspensions of Elongated Particles Exclusive of Brownian Motion . . . . .	4
Viscosity of Solutions of Elongated Particles Considering Brownian Motion . . . . .	9
Flow Birefringence of Dilute Solutions of Elongated Particles . . . . .	35
Viscoelastic Properties of Solutions of Rod-Like Molecules . . . . .	41
Concentrated Solutions of Rigid Rods . . . . .	49
Theory for Formation of Anisotropic Solutions . . . . .	49
Observations of Liquid Crystalline Order in Concentrated Solutions of Rod-Like Solutes . . . . .	57
Flow Properties of Concentrated Solutions of Rod-Like Molecules . . . . .	66
Commercial Aspects of Anisotropic Solutions . . . . .	96
Rod Systems in Bulk . . . . .	102
Low Molecular Weight Liquid Crystals . . . . .	102
Liquid Crystal Phenomena in Bulk Polymers . . . . .	110

Chapter	Page
II. RHEOLOGY OF CONCENTRATED SOLUTIONS OF POLY- $\gamma$ -BENZYL-GLUTAMATE . . . . .	120
Abstract . . . . .	120
Introduction . . . . .	120
Experimental . . . . .	122
Results . . . . .	124
Birefringence . . . . .	124
Steady Shear and Dynamic Viscosities . . . . .	125
Dynamic Modulus . . . . .	134
First Normal Stress Difference . . . . .	138
Discussion . . . . .	150
Conclusion . . . . .	156
III. RHEOLOGY OF CONCENTRATED SOLUTIONS OF PBLG AND PCBZL . . . . .	158
Abstract . . . . .	158
Introduction . . . . .	159
Experimental . . . . .	160
Results . . . . .	163
Steady Shear Viscosity . . . . .	163
First Normal Stress Difference . . . . .	174
Dynamic Viscosity . . . . .	198
Dynamic Modulus . . . . .	212
Discussion . . . . .	220
IV. RHEO-OPTICS OF CONCENTRATED SOLUTIONS OF HELICAL POLYPEPTIDES . . . . .	229
Introduction . . . . .	229
Experimental . . . . .	229
Results . . . . .	233
During Shear . . . . .	233
After Cessation of Shear . . . . .	236
Dried Films . . . . .	241
Discussion . . . . .	243
V. RHEOLOGY AND RHEO-OPTICS OF ANISOTROPIC PBA GEL . . . . .	250
Discussion . . . . .	257
VI. FUTURE WORK . . . . .	260
REFERENCES . . . . .	266
APPENDIX I. INERTIAL NORMAL FORCE CORRECTIONS IN ROTATIONAL RHEOMETRY . . . . .	277
APPENDIX II. DOCUMENTATION OF COMPUTER PROGRAMS . . . . .	291

LIST OF TABLES

Table	Page
1. Particle Lengths of Poly- $\gamma$ -Benzyl-L-Glutamates . . . . .	117
2. Some Polypeptides which Form Liquid Crystals in Suitable Solvents . . . . .	118
3. Mechanical Properties of Organic and Inorganic Fibers . . .	119
4. Indication of Liquid Crystalline Order of 335,000 M.W. PBG . . . . .	157
5. Values of Critical Concentration for Liquid Crystal Formation . . . . .	228

## LIST OF FIGURES

Figure	Page
1. Rotation of Elongated Molecules in a Shear Field . . . . .	2
2. Log $\alpha_1$ vs. Log $\alpha_0$ . . . . .	6
3. Viscosity of Suspension, $\eta$ , as a Function of Shear Rate $\dot{\gamma}$ . . . . .	8
4. Effect of Concentration on Relative Viscosity . . . . .	10
5. Effect of Fiber Curvature on Viscosity . . . . .	11
6. Dependence of $\nu$ on $\alpha$ for Prolate Ellipsoids of Axial Ratio, $p$ . . . . .	13
7. Theoretical Curves Showing Viscosity as a Function of Gradient for Monodisperse and Polydisperse Systems . . . . .	15
8. Master Curve for Reduced Steady State Viscosity of Dilute Collagen Solutions . . . . .	16
9. Reduced Viscosity for Dilute Solutions of Sodium Desoxyribonucleate in Water Plotted Against Product of Shear Rate and Zero-Shear Viscosity . . . . .	18
10. Effect of Shear Rate Upon Reduced Viscosity of DNA Solutions in Capillary Flow . . . . .	19
11. (a) Comparison of Experimental Curves of $[\eta]/[\eta]_0$ Against $\dot{\gamma}$ for DNA with Curves Calculated According to Kuhn and Kuhn for Linear Gaussian Coil with High Internal Viscosity. (b) Comparison of Experimental Curve of $[\eta]/[\eta]_0$ Against $\dot{\gamma}$ of DNA with Curves Calculated for Rigid Prolate Ellipsoid of Rotation ( $p > 100$ ) . . . . .	21
12. Viscosity-Shear Rate Curves . . . . .	22
13. Plots of Diochoism, $\Delta\epsilon$ , of DNA of D. Pneumoniae Against $\beta^2$ . . . . .	23
14. Relative Viscosity of TMV Solution vs. Shear Rate Concentrations . . . . .	25
15. Shear Dependence of the Intrinsic Viscosities for Tobacco Mosaic Virus . . . . .	26
16. Viscosity vs. Stress for PBLG in m-Cresol and in Dichloroacetic Acid at 25° . . . . .	28
17. Viscosity Versus Shear Rate for PBLG as Coils and Rods . . . . .	30
18. $[\eta]/[\eta]_0$ vs. Shear Rate for PBLG in Coil and Rod Form . . . . .	32
19. Effect of Solvent and Temperature on the Shear Dependence of Intrinsic Viscosities of PBLG . . . . .	33
20. Shear Stress Dependence of the Intrinsic Viscosities of Rods Obeying Hypothetical Molecular Weight Distributions . . . . .	34

Figure	Page
21. Orientation of Particles in a Doubly Refractive Fluid Between Concentric Cylinders . . . . .	36
22. (a) Extinction Angle, $\chi$ , vs. $\alpha$ and Dependence on Axial Ratio, p. (b) Orientation Factor, f, vs. $\alpha$ and Dependence on Axial Ratio, p. . . . .	38
23. (a) Dependence of Extinction Angle on Axial Ratio for $\alpha = 5$ . (b) Dependence of Orientation Factor on Axial Ratio for $\alpha = 5$ . . . . .	39
24. Hydrodynamic Lengths of Tobacco Mosaic Virus from non-Newtonian Viscosity and Flow Birefringence . . . . .	40
25. Intrinsic Viscosity of the Infinite Rod as a Function of the Rate of Shear . . . . .	43
26. Master Curves of Dynamic Viscosity $\eta_r'$ and Dynamic Rigidity $\mu_r$ , reduced to 1 g/100 ml and 26°C for Collagen in Dilute HCl . . . . .	45
27. Contributions of a Macromolecular Solute to the Components of the Complex Shear Modulus, as Predicted by the Theories of Kirkwood and Auer for Rigid Rods and Zimm for Flexible Coils . . . . .	47
28. Plots of $G'$ and $G'' - \omega\phi\eta_s$ for 1% Poly- $\gamma$ -benzyl-L-glutamate in m-methoxy-phenol . . . . .	48
29. Viscoelastic Response of Solutions of $\alpha$ -Helical Molecules . . . . .	50
30. The Onsager Model . . . . .	51
31. Concentration of Phases in Equilibrium in Relation to p for Athermal Mixtures . . . . .	54
32. Intrinsic Viscosity of DNA in H <sub>2</sub> O/DMF Solutions . . . . .	56
33. Reverse Spiral Arrangement in Tobacco Mosaic Virus Solution in Capillary Flow . . . . .	58
34. Comparison of Lines from Flory Theory with Experimental Determinations of A and B Points . . . . .	60
35. The Change in the Pitch of the Polypeptide Cholesteric Structure with Temperature . . . . .	61
36. Cholesteric Supramolecular Structure . . . . .	63
37. (a) Turbidity Points for the System PBLG-DMF-CH <sub>3</sub> OH at 10 and 30°C. (b) Phase Diagram for PBLG . . . . .	64
38. Model for Networks of Cellulose Microcrystals Formed by Almost Parallel Aggregation of Rodlike Particles . . . . .	68
39. Flow Curves for Gels of Cotton Cellulose Microcrystals of Different Concentrations . . . . .	69
40. Flow Curves for a Dilution Series of a Gel Containing Microcrystals Prepared from Wood Level - off DP Cellulose Gel . . . . .	70
41. Viscosity of Fibrinogen Solutions . . . . .	71
42. Viscosity of Poly- $\gamma$ -Benzyl-L-Glutamate in m-Cresol . . . . .	73
43. Schematic Representation of the Configuration of the Solutions at Rest and at Two Shear Rates . . . . .	74

Figure	Page
44. Solutions of PBG in m-Cresol, Plotted as $\log(\eta_{sp}/c)$ Versus Concentration, at Various Shear Stresses . . . . .	75
45. Volume Fraction of Solute at Isotropic-Anisotropic Transitions Versus Degree of Polymerization . . . . .	77
46. (a) Reduced Viscosity Measured at $\dot{\gamma} = 3.4 \text{ sec}^{-1}$ Versus Polymer Concentration. (b) Dynamic Elastic Modulus Measured at $\omega = .33 \text{ Hz}$ Versus Polymer Concentration . .	78
47. Dynamic Properties vs. Frequency Relationships. . . . .	79
48. Typical Weissenberg Effect for 10 vol. % PBLG in Dioxane at $22^\circ\text{C}$ . . . . .	80
49. Viscosity Versus Concentration for Poly(p-Benzamide) in Hydrofluoric Acid . . . . .	84
50. Critical Concentration for Formation of Anisotropic Phase Versus Molecular Weight (as Measured by Inherent Viscosity) for PPT . . . . .	85
51. Phase Diagram of PPT in $\text{H}_2\text{SO}_4$ . . . . .	86
52. Viscosity vs. Concentration for PPTA at 20 and $40^\circ\text{C}$ . . .	88
53. Relative Viscosity of PPTA Solutions of Varied Concentration as a Function of the Sulphuric Acid Content . .	90
54. Viscosity vs. Shear Stress for Solutions of PBA in DMAC . . . . .	91
55. Concentration Dependence of Viscosity at $20^\circ\text{C}$ for Solutions of PBA Samples . . . . .	92
56. Reduced Viscosities for PBA in DMAC . . . . .	94
57. Flow Curves for PBA Solutions in Reduced Coordinates . .	95
58. Viscosity-Temperature Behavior of a Concentrated Solution of PBA in DMAC . . . . .	97
59. Correlation of Modulus and Orientation Angle for PTA Fibers . . . . .	100
60. (a) Viscosity of Nematic p-Azoxyanisole at $121.8^\circ\text{C}$ . (b) Flow Data on Nematic p-Azoxyanisole at $121.8^\circ\text{C}$ . . .	106
61. Envisaged Orientation Patterns in the (a) Cholesteric and (b) Smectic Case . . . . .	108
62. Apparent Melt Viscosity of Polyester X7G . . . . .	112
63. (a) Flow Curves for Polystyrene Melts of Different Histories at $190^\circ\text{C}$ . (b) Comparison of the Flow Curves of Melts of Original Polypropylene and Samples Modified by Introducing 0.1% of Polyethylsiloxane Fluid PES-5, Introduced by Mechanical Mixing or by Codissolution in a Single Solvent . . . . .	116
64. Low Shear Limit of Steady Shear Viscosity and Low Frequency Limit of Dynamic Viscosity Versus Concentration for 335,000 M.W. PBG . . . . .	126
65. Steady Shear Viscosity Versus Shear Rate for 335,000 M.W. PBG Solutions . . . . .	128
66. Steady Shear Viscosity Versus Shear Rate for 335,000 M.W. PBG Solutions . . . . .	129

Figure	Page
67. Concentration Dependence of Steady Shear Viscosity at Several Shear Rates for 335,000 M.W. PBG . . . . .	130
68. Dynamic Viscosity Versus Frequency for 335,000 M.W. PBG Solutions . . . . .	131
69. Dynamic Viscosity Versus Frequency for 335,000 M.W. PBG Solutions . . . . .	132
70. Dynamic Modulus Versus Frequency for 335,000 M.W. PBG Solutions . . . . .	135
71. Dynamic Modulus Versus Frequency for 335,000 M.W. PBG Solutions . . . . .	136
72. Dynamic Modulus at $\omega = 4$ rad/sec Versus Concentration for 335,000 M.W. PBG . . . . .	137
73. First Normal Stress Difference Versus Shear Rate for 335,000 M.W. PBG Solutions . . . . .	139
74. First Normal Stress Difference Versus Shear Rate for 335,000 M.W. PBG (11.0 wt%) . . . . .	141
75. First Normal Stress Difference Versus Shear Rate for 335,000 M.W. PBG (14.0 wt%) . . . . .	142
76. First Normal Stress Difference Versus Shear Rate for 335,000 M.W. PBG (16.4 wt%) . . . . .	143
77. First Normal Stress Difference Versus Shear Rate for 335,000 M.W. PBG (19.0 wt%) . . . . .	144
78. First Normal Stress Difference Versus Shear Rate for 335,000 M.W. PBG (22.1 wt%) . . . . .	145
79. First Normal Stress Difference Versus Shear Rate for 335,000 M.W. PBG (25.3 wt%) . . . . .	146
80. Shear Stress at Points of Change in Sign of First Normal Stress Difference Versus Concentration for 335,000 M.W. PBG . . . . .	147
81. First Normal Stress Difference Versus Shear Rate for 2% Aqueous Polyacrylamide Solution . . . . .	149
82. Chemical Structures of Poly- $\gamma$ -Benzyl Glutamate, Poly- $\epsilon$ -Carbobenzyloxy-L-Lysine, Poly- $\beta$ -Benzyl-Aspartate . . . . .	161
83. Steady Shear Viscosity vs. Shear Rate for 150,000 M.W. PBLG Solutions . . . . .	164
84. Steady Shear Viscosity vs. Shear Rate for 150,000 M.W. PBLG Solutions . . . . .	165
85. Steady Shear Viscosity vs. Shear Rate for 200,000 M.W. PCBZL Solutions . . . . .	166
86. Steady Shear Viscosity vs. Shear Rate for 200,000 M.W. PCBZL Solutions . . . . .	167
87. Steady Shear Viscosity at Various Shear Rates vs. Concentration for 150,000 M.W. PBLG Solutions . . . . .	169
88. Steady Shear Viscosity at Various Shear Rates vs. Concentration for 200,000 M.W. PCBZL Solutions . . . . .	170
89. First Normal Stress Difference Versus Shear Rate for 150,000 M.W. PBLG Solutions . . . . .	175



Figure	Page
90. First Normal Stress Difference Versus Shear Rate for 200,000 M.W. PCBZL Solutions . . . . .	176
91. First Normal Stress Difference Versus Shear Rate for 14.0 wt% 150,000 M.W. PBLG Solution . . . . .	178
92. First Normal Stress Difference Versus Shear Rate for 16.2 wt% 150,000 M.W. PBLG Solution . . . . .	179
93. First Normal Stress Difference Versus Shear Rate for 18.0 wt% 150,000 M.W. PBLG Solution . . . . .	180
94. First Normal Stress Difference Versus Shear Rate for 20.6 wt% 150,000 M.W. PBLG Solution . . . . .	181
95. First Normal Stress Difference Versus Shear Rate for 22.5 wt% 150,000 M.W. PBLG Solution . . . . .	182
96. First Normal Stress Difference Versus Shear Rate for 25.4 wt% 150,000 M.W. PBLG Solution . . . . .	183
97. First Normal Stress Difference Versus Shear Rate for 27.6 wt% 200,000 M.W. PCBZL Solution . . . . .	184
98. First Normal Stress Difference Versus Shear Rate for 31.0 wt% 200,000 M.W. PCBZL Solution . . . . .	185
99. First Normal Stress Difference Versus Shear Rate for 33.4 wt% 200,000 M.W. PCBZL Solution . . . . .	186
100. First Normal Stress Difference Versus Shear Rate for 16.0 wt% 335,000 M.W. PBG Solution for Three Different Edge Conditions . . . . .	188
101. First Normal Stress Difference Versus Shear Rate for 17.0 wt% 350,000 M.W. PBLG Solution for Three Different Edge Conditions . . . . .	189
102. First Normal Stress Difference Versus Shear Rate for 17.0 wt% 350,000 M.W. PBLG Solution for Two Different Sample Geometries . . . . .	190
103. Shear Stress at Points of Change in Sign of First Normal Stress Difference vs. Concentration for 150,000 M.W. PBLG and 200,000 M.W. PCBZL Solu- tions . . . . .	193
104. Maximum Positive and Negative Values of First Normal Stress Difference vs. Concentration for 150,000 M.W. PBLG and 200,000 M.W. PCBZL Solutions . . . . .	194
105. First Normal Stress Difference vs. Concentration at One Low and One Very High Shear Rate for 150,000 M.W. PBLG Solutions . . . . .	196
106. First Normal Stress Difference vs. Concentration at One Low and One Very High Shear Rate for 200,000 M.W. PCBZL Solutions . . . . .	197
107. Dynamic Viscosity vs. Frequency (Oscillatory Shear) for 150,000 M.W. PBLG Solutions . . . . .	199
108. Dynamic Viscosity vs. Frequency (Oscillatory Shear) for 150,000 M.W. PBLG Solutions . . . . .	200

Figure	Page
109. Dynamic Viscosity vs. Frequency (Eccentric Rotating Disc) for 150,000 M.W. PBLG Solutions . . . . .	202
110. Limiting Viscosity Values vs. Concentration for 150,000 M.W. PBLG Solutions . . . . .	203
111. Steady Shear Viscosity vs. Shear Rate and Dynamic Viscosity vs. Frequency (Oscillatory Shear and Eccentric Rotating Disc) for Newtonian Viscosity Standard . . . . .	204
112. Dynamic Viscosity vs. Frequency (Oscillatory Shear) for 200,000 M.W. PCBZL Solutions . . . . .	206
113. Dynamic Viscosity vs. Frequency (Oscillatory Shear) for 200,000 M.W. PCBZL Solutions . . . . .	207
114. Dynamic Viscosity vs. Frequency (Eccentric Rotating Disc) for 200,000 M.W. PCBZL Solutions . . . . .	210
115. Limiting Viscosity Values vs. Concentration for 200,000 M.W. PCBZL Solutions . . . . .	211
116. Dynamic Storage Modulus vs. Frequency (Oscillatory Shear) for 150,000 M.W. PBLG Solutions . . . . .	213
117. Dynamic Storage Modulus vs. Frequency (Oscillatory Shear) for 150,000 M.W. PBLG Solutions . . . . .	214
118. Dynamic Storage Modulus vs. Frequency (Eccentric Rotating Disc) for 150,000 M.W. PBLG Solutions . . . . .	216
119. Dynamic Storage Modulus vs. Concentration for 150,000 M.W. PBLG and 200,000 M.W. PCBZL Solutions . . . . .	217
120. Dynamic Storage Modulus vs. Frequency (Oscillatory Shear) for 200,000 M.W. PCBZL Solutions . . . . .	218
121. Dynamic Storage Modulus vs. Frequency (Oscillatory Shear) for 200,000 M.W. PCBZL Solutions . . . . .	219
122. Dynamic Storage Modulus vs. Frequency (Eccentric Rotating Disc) for 200,000 M.W. PCBZL Solutions . . . . .	221
123. Exploded Schematic Diagram of Shearing Stage Apparatus . . . . .	230
124. Steady Shear Viscosity and First Normal Stress Difference versus Shear Rate for 17.0% 350,000 PBLG . . . . .	232
125. Polarized Light Micrographs of 17.0% 350,000 M.W. PBLG at Various Shear Rates 170X . . . . .	234
126. Polarized Light Micrographs of 14.1% 150,000 M.W. PBLG at Various Times after Shearing at $3.3 \text{ s}^{-1}$ 170X . . . . .	237
127. Polarized Light Micrographs of 14.1% 150,000 M.W. PBLG at Various Times after Shearing at $19 \text{ s}^{-1}$ 170X . . . . .	238
128. Polarized Light Micrographs of 14.1% 150,000 M.W. PBLG at Various Times after Shearing at $100 \text{ s}^{-1}$ 170X . . . . .	240
129. (a) Dried Film from 6.8% 350,000 M.W. PBLG in Dioxane 100X. (b) Dried Film from 15.0% 350,000 M.W. PBLG in Dioxane 100X--High Shear. (c) Dried Film from 15.0% 350,000 M.W. PBLG in Dioxane 100X--Low Shear. . . . .	242

Figure	Page
130. Helical Transverse Striations in Dried Film of 350,000 M.W. PBLG in Dioxane 100X . . . . .	244
131. Proposed Model Linking "Row-Nucleated" Texture and Negative Normal Stress Effect in Cone-and-Plate Rheometer . . . . .	247
132. Steady Shear Viscosity versus Shear Rate for 33.2% 60,000 M.W. PBA . . . . .	251
133. First Normal Stress Difference versus Shear Rate for 33.2% 60,000 M.W. PBA . . . . .	252
134. Dynamic Viscosity at Various Strain Amplitudes versus Frequency for 33.2% 60,000 M.W. PBA . . . . .	255
135. Dynamic Storage Modulus at Various Amplitudes versus Frequency for 33.2% 60,000 M.W. PBA . . . . .	256
136. Polarized Light Micrographs of 33.2% 60,000 M.W. PBA 170X . . . . .	258

## FOREWORD

The organization of this thesis is essentially chronological, reflecting the fact that each chapter is based on a free-standing paper which, except for the introduction, has appeared or will appear in the open literature. One consequence of this strategy is a certain amount of duplication among chapters, especially of introductory material. The advantages of this strategy are that the process of discovery which took place in the laboratory is accurately reflected in the thesis, and also that each chapter can be read separately. Thus the interested reader can read the entire thesis, yet others can select free-standing chapters treating topics of interest.

The first chapter is an extensive review of the rheology of rod-like molecules, starting with dilute solutions, then going to concentrated solutions and finally to bulk (melts). Low molecular weight compounds are treated also, but the bias of the review is towards polymers. A section dealing with high modulus fibers spun from liquid crystalline solutions reveals the motivation behind the work presented in the rest of the thesis. The choice of topics is far-ranging, some might say idiosyncratic, but it is an excellent introduction to the background of one of the glamour fields in polymer science (if this is not a contradiction in terms); that of obtaining excellent mechanical properties from extended chain polymers

by exploiting liquid crystalline order.

Chapter II presents an investigation of the rheological properties of a series of m-cresol solutions of a racemic mixture of PBLG and PBDG with a molecular weight of  $\sim 335,000$ . A peak in various material functions when plotted against concentration is shown to correlate with the onset of liquid crystalline order, and the surprising discovery of negative first normal stress difference in liquid crystalline solutions is revealed.

In Chapter III two different polymer samples, a  $\sim 150,000$  M.W. PBLG and a  $\sim 200,000$  M.W. PCBZL, are investigated in the same way. Peaks in material functions vs. concentration and the negative normal stress effect are confirmed. Another surprising effect in normal stress is presented, the observation of a peak in  $N_1$  vs.  $C$  but not in  $\eta$  vs.  $C$  at very high shear rates.

In Chapter IV the results of a rheo-optical investigation utilizing a shearing microscope stage and polarized stroboscopic illumination are presented. The negative normal stress effect is shown to correlate with a texture composed of striations perpendicular to the shearing direction. It is shown also that solutions sheared at rates below that necessary to observe the negative normal stress effect gradually develop the perpendicular striations after the cessation of shear. A model of molecular orientation consistent with the observations is proposed.

The rheology and rheo-optics of an anisotropic gel of a  $\sim 60,000$  M.W. PBA is presented in Chapter V. This sample is treated separately since the behavior is different from the other three

polypeptide samples, suggesting the existence of a network of temporary, "healable" cross-links of various strengths.

Suggestions for future work arising naturally from the work presented in this thesis are advanced in Chapter VI.

Appendix One describes the inertial correction to the normal force which was made to all data reported in this thesis. This correction is in the direction of reducing the magnitude of the negative normal stress effect but is by far insufficient to explain it away. This appendix has also been published separately.

Appendix Two documents various computer programs developed during the course of this work to facilitate the manipulation of large quantities of data, for the benefit of future users of the mechanical spectrometer.

C H A P T E R    I  
RHEOLOGY OF SYSTEMS CONTAINING ROD-LIKE  
MACROMOLECULES AND PARTICLES

Rheology of Dilute Solutions and Suspensions of  
Rod-Like Molecules and Particles

Introduction. Elongated molecules in a shear field will rotate about an axis perpendicular to both the direction of flow and the velocity gradient, that is, they will tumble end over end (Fig. 1).

The rate of rotation depends on the torque produced by the velocity gradient through viscous forces exerted on particle surfaces moving in a direction different from the adjacent medium. This torque is a maximum when the particle is perpendicular to the flow direction. However, the presence of the suspended particle results in a viscosity increase by virtue of the energy dissipated by the particle and this is at a maximum when the particle is at 45° to the flow direction (1). The particle thus contributes most to the viscosity as it is turning over. If one neglects the inertial effects and Brownian motion, the frequency of rotation is equal to one half of the shear rate and the suspension has a Newtonian viscosity given by:

$$\eta = \eta_s (1 + v\phi)$$

$\eta_s$  = viscosity of suspending medium

$\phi$  = volume fraction of suspended particle

$v$  is a constant depending on particle geometry.

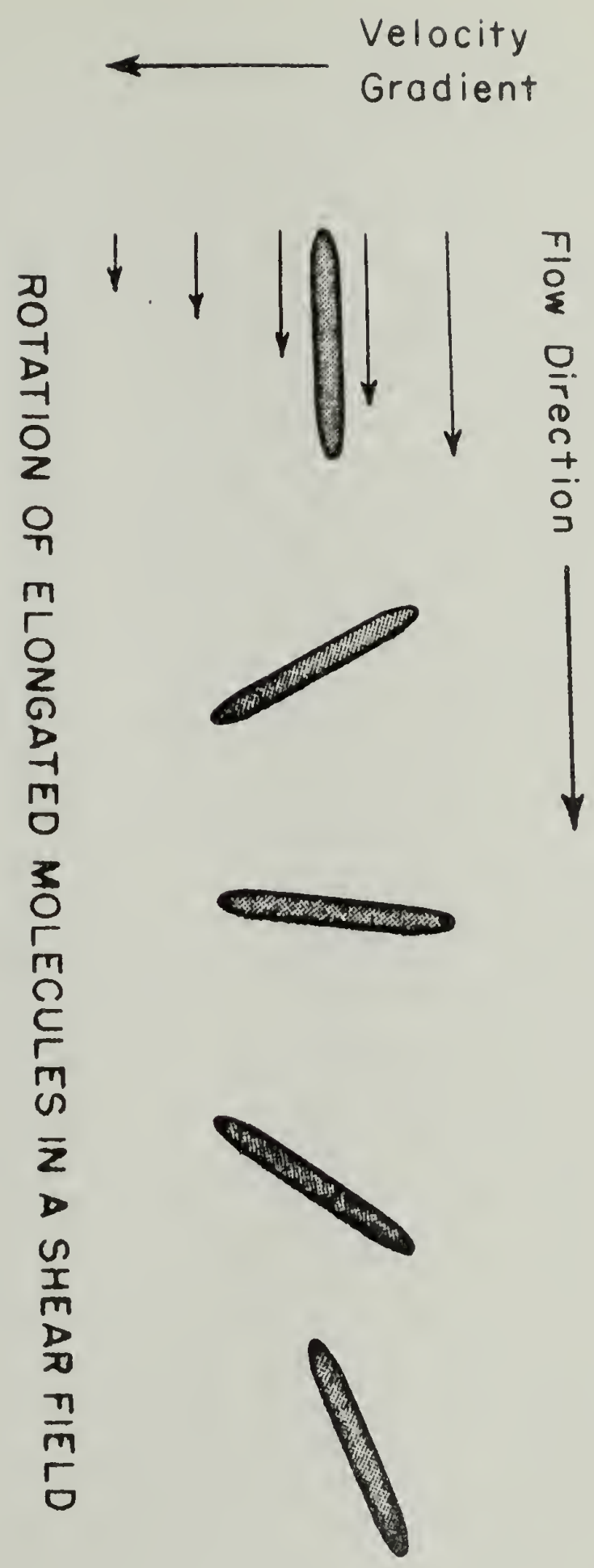


Figure 1. Rotation of Elongated Molecules in a Shear Field.



This behavior was deduced by Jeffrey (2) from hydrodynamic considerations. Jeffrey was able to specify only the maximum and minimum limits of  $\nu$  for oblate and prolate ellipsoids. In every case the minimum value was below the value of 2.5 obtained by Einstein for suspensions of spherical particles (3). Jeffrey has criticized a statement by Smoluchowski to the effect that 2.5 was necessarily a minimum for  $\nu$  since a spherical particle would least perturb the flow field by saying, "This argument is not valid, for we have shown that for any spheroid there are possible motions for which the increase in the dissipation of energy is less than it is for a sphere of the same volume." Subsequent work, e.g., Simha (4) revealed that 2.5 is indeed the minimum  $\nu$  and that anisotropic particles invariably require a greater value.

Although anisotropic particles in a shear field rotate end-to-end and with a periodicity of half the shear rate, they do so at a rate which varies throughout the course of a rotation. Most of the rotation period is spent parallel to the shearing direction and the least time is spent perpendicular to the shearing direction.

If a suspended particle is small enough that the Brownian motion is significant, particle orientation will tend to be randomized, reducing the time fraction spent parallel to the shearing direction. The balance between the randomizing and orienting influences will shift towards orientation as the shear rate is increased, thus reducing the amount of energy dissipated by the suspended particle. Hence if particle size is such that Brownian motion is significant, the effect will be a reduction in apparent suspension viscosity as shear

rate is increased (2).

Viscosity of suspensions of elongated particles exclusive of Brownian motion. Jeffrey's work on viscosity of suspensions of elongated particles in the absence of Brownian motion (that is, for particles large enough that Brownian motion may be neglected) was extended by Eisen-schitz, Taylor, Guth, Kuhn and others, and reviewed by Burgers (5).

In general the viscosity of a suspension of elongated par-ticles may be written as a series:

$$\frac{\eta_{sp}}{c} = \alpha_0 + \alpha_1 c + \dots \quad (2)$$

$\eta_{sp}$  = specific viscosity

$c$  = particle volume concentration

$\alpha_0, \alpha_1$  = constants

Since  $\alpha_0$  is the value of  $\frac{\eta_{sp}}{c}$  at zero concentration, it is thus identi-cal to the intrinsic viscosity.

Guth derived the following expressions for  $\alpha_0$  and  $\alpha_1$  (6):

$$\alpha_0 = \frac{p}{2\ell\eta 2p-3} + 2 \quad (3)$$

$$\alpha_1 = \frac{.04p^3}{2\ell\eta 2p-3}$$

where  $p$  is the ratio of a particle length-to-diameter. He assumed that the particles be in the X-Y plane. Burgers extended Jeffrey's theory to other orientations of the particles and obtained:

$$\alpha_0 = \frac{p^2}{6(\ell\eta 2p-1.8)} \sin^4 \theta \sin^4 \phi \quad (4)$$

where  $\theta$  and  $\phi$  are the orientation angles of spherical coordination.

A possible pitfall in the application of such theories is the modeling of suspended cylindrical particles by ellipsoids of revolution. Zimm and Haltner (7) found that the rotational friction coefficients of rods were 50% greater than ellipsoids of same length and axial ratio. Nawab and Mason (8) studied castor oil suspensions of rayon fibers of diameter  $3.5 \mu$  and with axial ratios between 43 and 356. They found that viscosity increased with axial ratio and was independent of shear rates between  $9.9$  and  $93.5 \text{ S}^{-1}$  for axial ratios below 113. Suspensions of particles with greater axial ratios showed shear thinning to an extent which was also not in agreement with theory. However, there was evidence of particle deformation in shear to which the particle orientation factor was sensitive. Fibers plasticized with water were more deformable which resulted in a higher viscosity. A simple exponential relationship between  $\alpha_0$  and  $\alpha_1$  was found:

$$\alpha_1 = 1.15 \alpha_0^{2.2} \quad (5)$$

(See Fig. 2)

Glass fibers of  $14 \mu$  in diameter and  $530 \mu$  length suspended in silicone oil were studied by Nicodemo and Nicolais (9). They employed an equation given by Brodnyan (10).

$$\eta_{\text{rel}} = \exp \frac{[\eta]\phi}{1-K\phi} \quad (6)$$

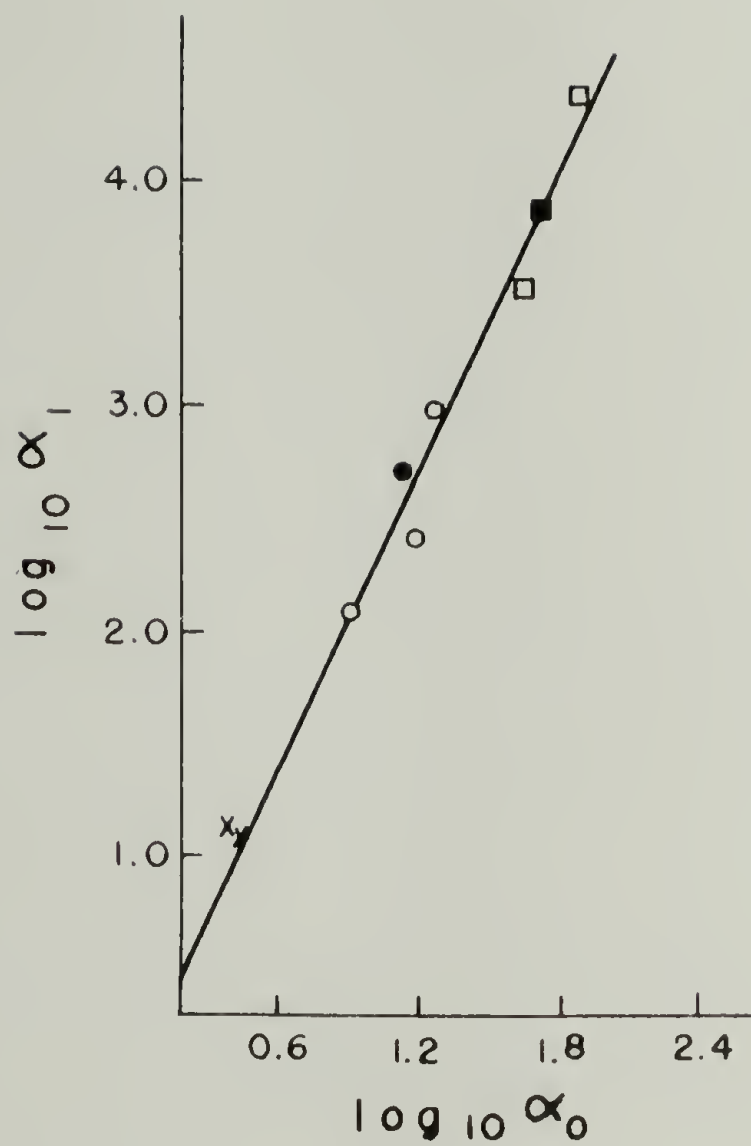


Figure 2.  $\log \alpha_1$  vs.  $\log \alpha_0$ .

○ Shear-Independent  $\alpha_1$  values, Unswollen Samples.

□,  $\alpha_1$  Extrapolated to  $\dot{\gamma} = 0$ , Unswollen Samples.

●, ■ Same Quantities for Swollen Samples.

x,  $\alpha_1$  for Rigid Spheres.

$\eta_{rel}$  = relative viscosity

$[\eta]$  = intrinsic viscosity

$\phi$  = volume fraction of suspended particles

K = a "crowding factor"

to obtain  $[\eta]$  from a plot of  $\log \eta_r$  versus  $\phi$ . The value of  $[\eta]$  obtained in this way agreed well with the value calculated for  $\alpha_0$  from the equation of Guth (Eqn. 3). Shear thinning was observed in the shear rate range of approximately  $1-100 \text{ s}^{-1}$ , above which a high shear Newtonian plateau was evident (See Fig. 3). This effect became more pronounced with increasing particle concentration. Calculations were made using the viscosities for the high shear Newtonian region. They did not, however, take data at low enough shear rate to observe a low shear Newtonian region.

Blakeney (11) studied suspensions of nylon fibers of diameter  $43.1 \mu$  and axial ratio  $20.3 \mu$  in a mixture of tetrachloroethylene and parafin oil, in a couette viscometer at shear rates from  $.1$  to  $.5 \text{ S}^{-1}$ . Measurements were made at volume concentrations up to  $.009$ . The orientation factor of Burgers's theory ( $\sin^4 \theta \sin^2 \phi$  where  $\theta$  and  $\phi$  are the orientation angles of a spherical coordinate system) was determined photographically. It was observed that below a critical volume concentration,  $C_o$ , at which particle interference becomes significant,

$$C_o = \frac{1.5}{p^2} \quad (7)$$

the orientation factor was constant and Burgers's theory predicted viscosity within experimental error. Above this concentration, the

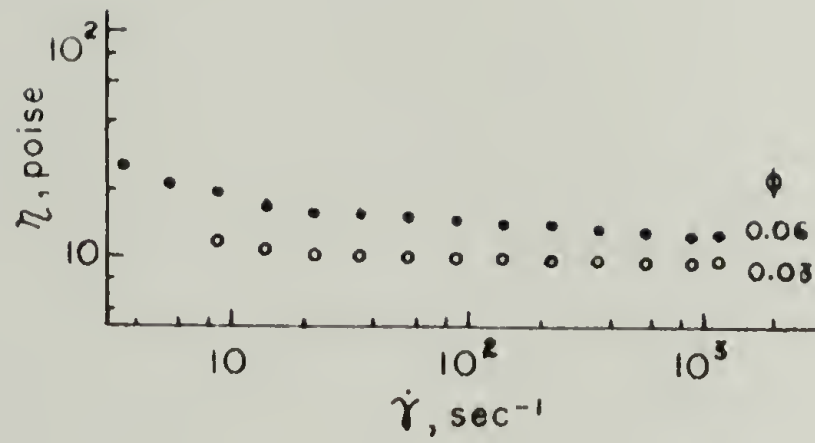


Figure 3. Viscosity of Suspension,  $\eta$ , as a Function of Shear Rate  $\dot{\gamma}$ .

orientation factor first increased and subsequently decreased. Viscosity changes showed parallel behavior (See Fig. 4). Burgers's theory assumes no interparticle interference and is not valid above  $C_0$ . However, by adding a quadratic concentration term:

$$\eta_{rel} = 1 + \alpha_0 C + K'(\alpha_0 C)^2 \quad (8)$$

Blakeney was able to fit the observed viscosity behavior to concentrations greater than  $C_0$ .

Blakeney speculated that previous studies on suspensions of rods in this concentration and size regime were at variance with Burgers's theory because of the tremendous effect of slight curvature in the particle on the period of rotation (and hence the energy dissipation leading to the increase in apparent viscosity) (12). This was confirmed by deliberately using curved fibers (See Fig. 5).

Viscosity of solutions of elongated particles considering Brownian motion. The effect of Brownian motion on the viscosity of ellipsoidal particles has been treated by many investigators (13-18). Scheraga (19) concluded that treatments of both Kuhn and Kuhn and Saito were theoretically satisfactory for the non-Newtonian viscosity for solutions of ellipsoidal particles.

The general solution of Jeffrey's hydrodynamic equations can be written for the viscosity increment  $\nu$  (defined in Eqn. 1) as:

$$\nu = a - b\alpha^2 + c\alpha^4 \quad (9)$$

where  $\alpha$  is the ratio of the shear rate,  $\dot{\gamma}$ , to the rotary diffusion

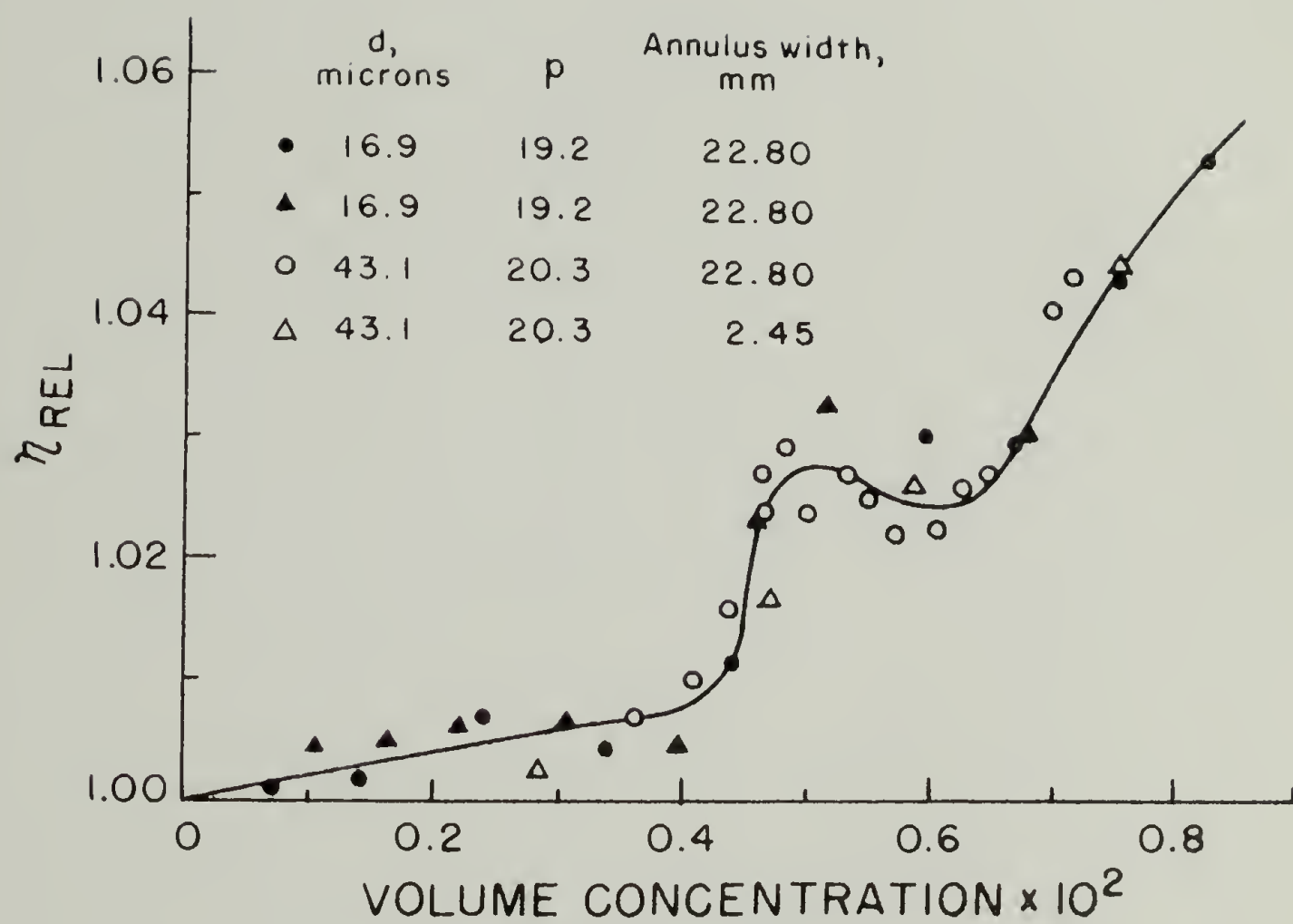


Figure 4. Effect of Concentration on Relative Viscosity.



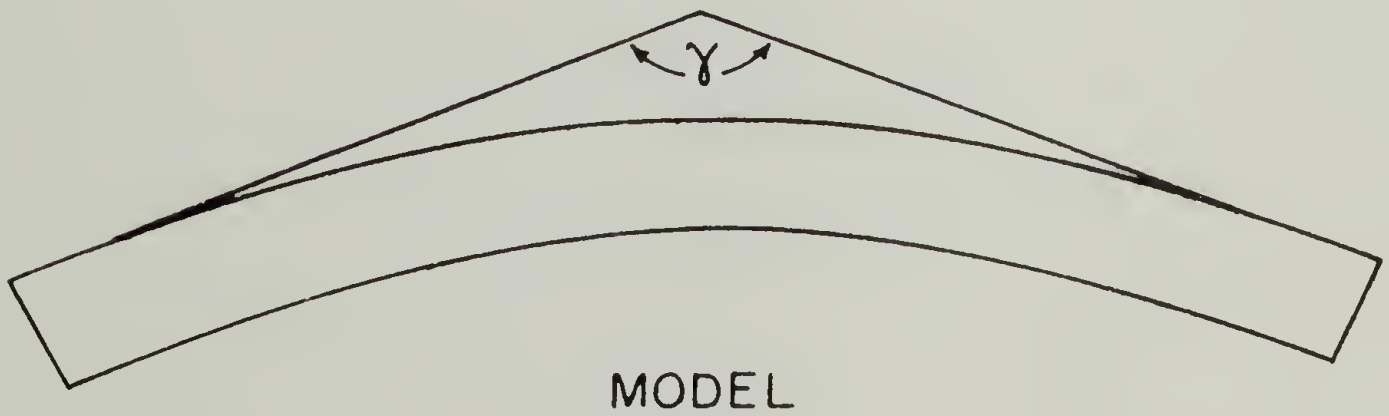
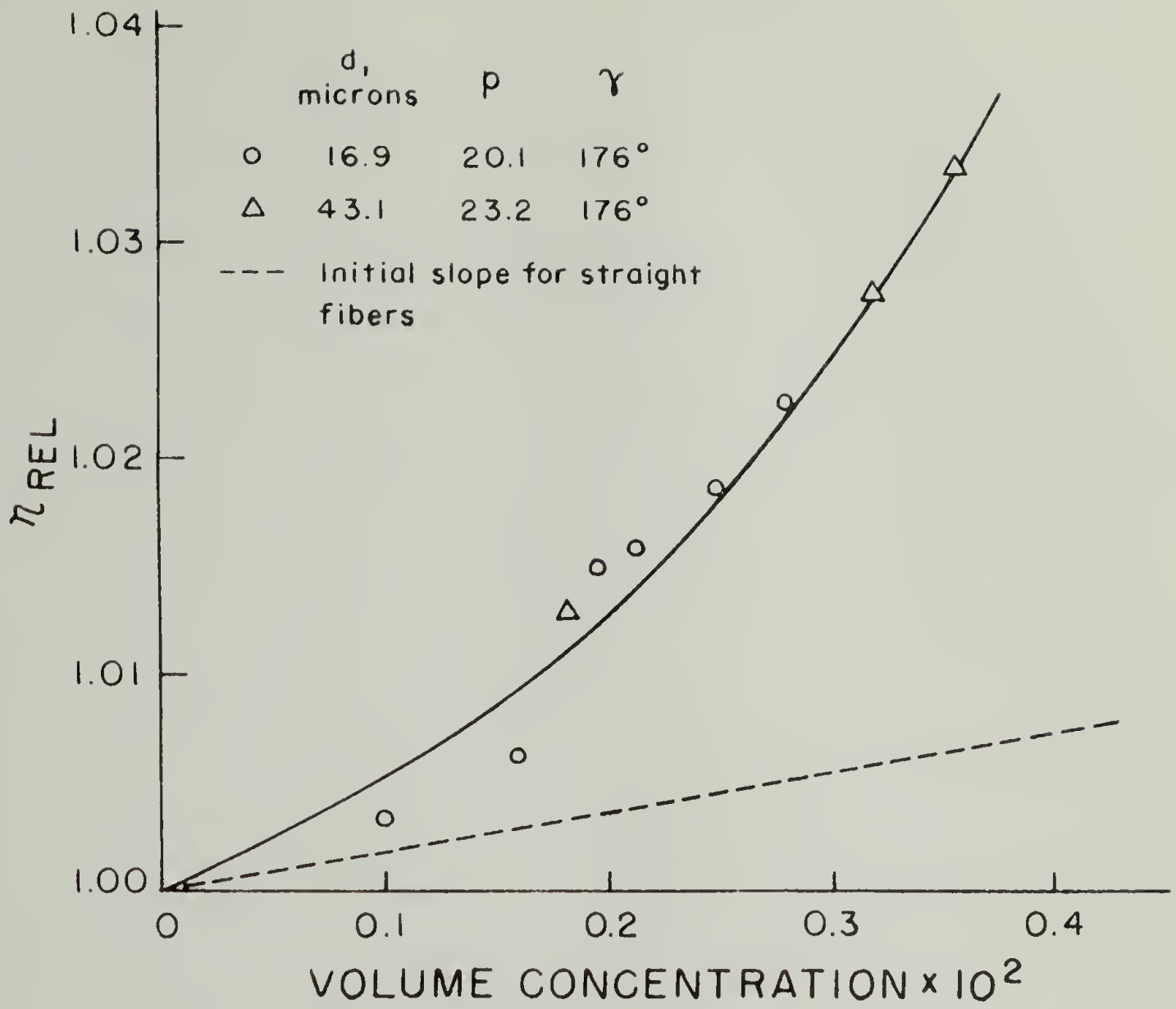


Figure 5. Effect of Fiber Curvature on Viscosity.

coefficient,  $\theta$ . Simha (20) derived an expression for  $\nu$  as a function of axial ratio,  $p$ , in the limit  $\alpha \rightarrow 0$  (i.e., zero shear stress), a situation in which the particles would be randomly oriented. Values of  $\nu$  for various axial ratios were tabulated by Mehl using the Simha expression (21).

Using Saito's results, Scheraga (19) tabulated  $\nu$  for various values of  $\alpha$  and  $p$ , for both prolate and oblate spheroids. This information is presented graphically in Figure 6 (and also as tables in the original paper). The results for  $\alpha = 0$  are identical to the aforementioned results obtained by Mehl. Although the calculations were carried out only up to  $\alpha = 60$ , Yang (22) found that a double log plot of  $\nu$  versus  $\alpha$  at constant  $p$  is 1 near; so that extrapolation can provide an upper limit of  $\alpha$ . The values of  $\nu$  obtainable from these calculations can be related to experimental quantities by the equation:

$$[\eta] = \lim_{\substack{C \rightarrow 0 \\ \dot{\gamma} \rightarrow 0}} \frac{\eta - \eta_0}{\eta_0 C} = \left( \frac{N V_e}{100M} \right) \nu \quad (10)$$

or

$$\frac{(\eta)_a}{(\eta)_{a=0}} = \frac{(\nu)_a}{(\nu)_{a=0}} \quad (23) \quad (11)$$

$N$  = Avogadro's number

$V_e$  = Equivalent hydrodynamic volume

$M$  = Molecular weight

A theoretical calculation for the effect of polydispersity on

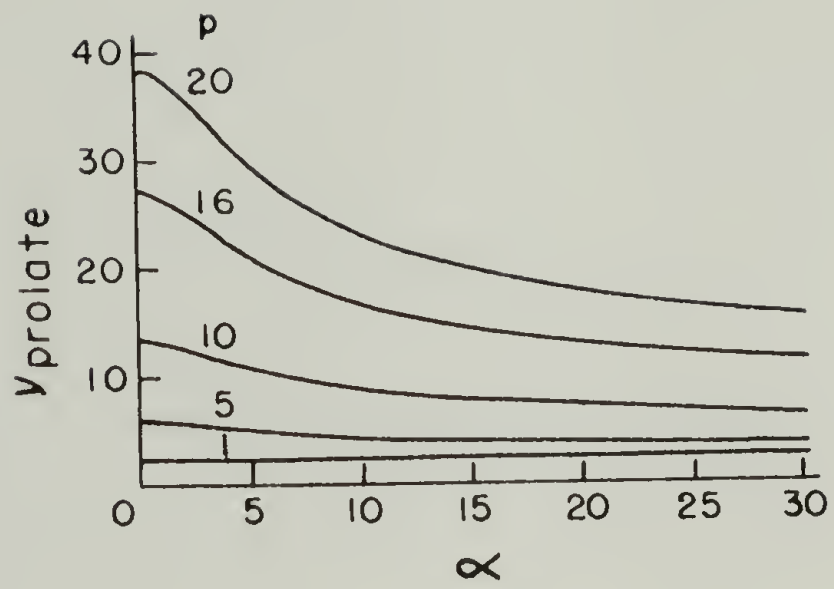


Figure 6. Dependence of  $\nu$  on  $\alpha$  for Prolate Ellipsoids of Axial Ratio,  $p$ .

the non-Newtonian flow of ellipsoids was carried out by Reichmann (24). The results were presented as the fractional viscosity reduction due to shear versus  $\alpha$  for monodisperse systems and for polydisperse systems modeled by allowing random end-to-end aggregation for 10% and 20% of the particles; see Fig. 7. It is seen that viscosity decreases more rapidly with  $\alpha$  with increasing polydispersity. Reichmann also stated that the rotary diffusion constant of the polydisperse system increases with increasing velocity gradient since a small gradient would not orient small particles, whereas a larger gradient would orient all particles.

Experimental observations of shear thinning in solutions of particles small enough to be affected by Brownian motion have been made on solutions of collagen, nucleic acids, tobacco mosaic virus, and helix-forming synthetic polypeptides.

In a study of dilute solutions of collagen in .01N aqueous HCl, Fukada and Date (25) obtained non-Newtonian flow data at various concentrations that were superimposable, see Fig. 8, by the use of reduced variables:

$$\eta_r = \eta \frac{\eta_s}{\eta_0}, \quad \dot{\gamma}_r = \dot{\gamma} \frac{\eta_0 C_s}{\eta_s C} \quad (12)$$

$\eta_r, \dot{\gamma}_r$  = Reduced viscosity and shear rate

$\eta$  = Viscosity of solution at non-zero shear rate

$\eta_0, C$  = Concentration and zero shear viscosity of solution

$\eta_s, C_s$  = Concentration and zero shear viscosity of reference solution

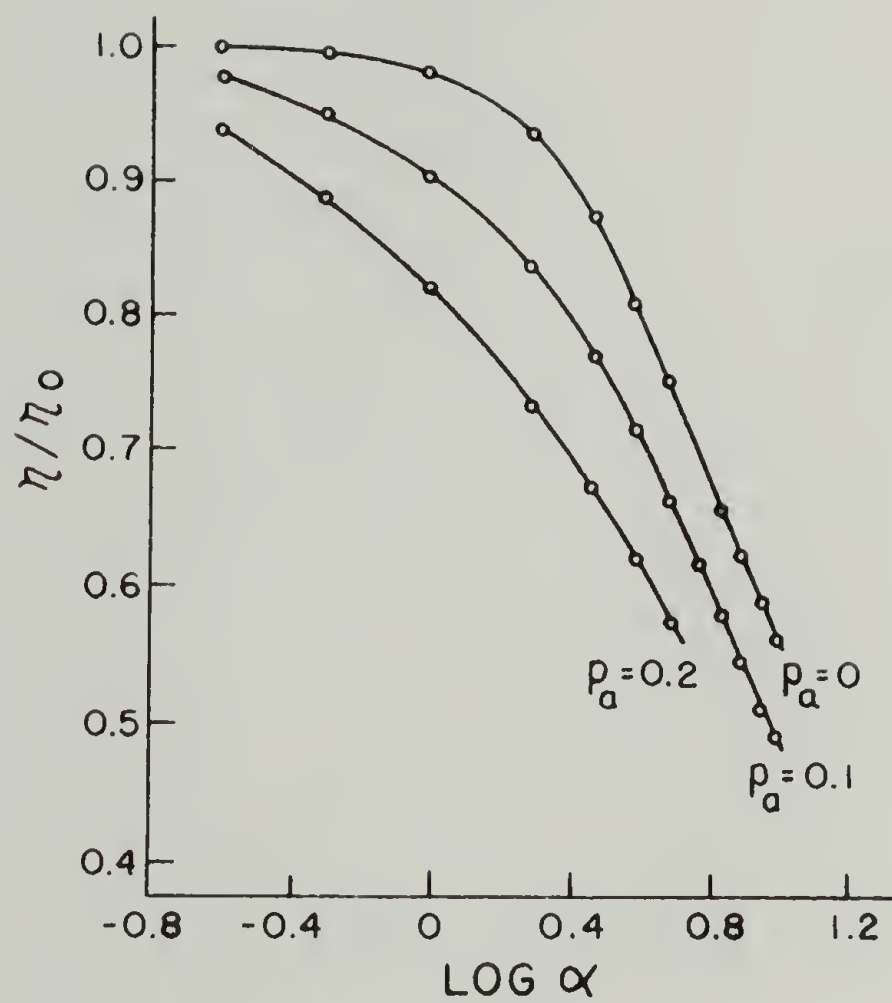


Figure 7. Theoretical Curves Showing Viscosity as a Function of Gradient for Monodisperse and Polydisperse Systems.

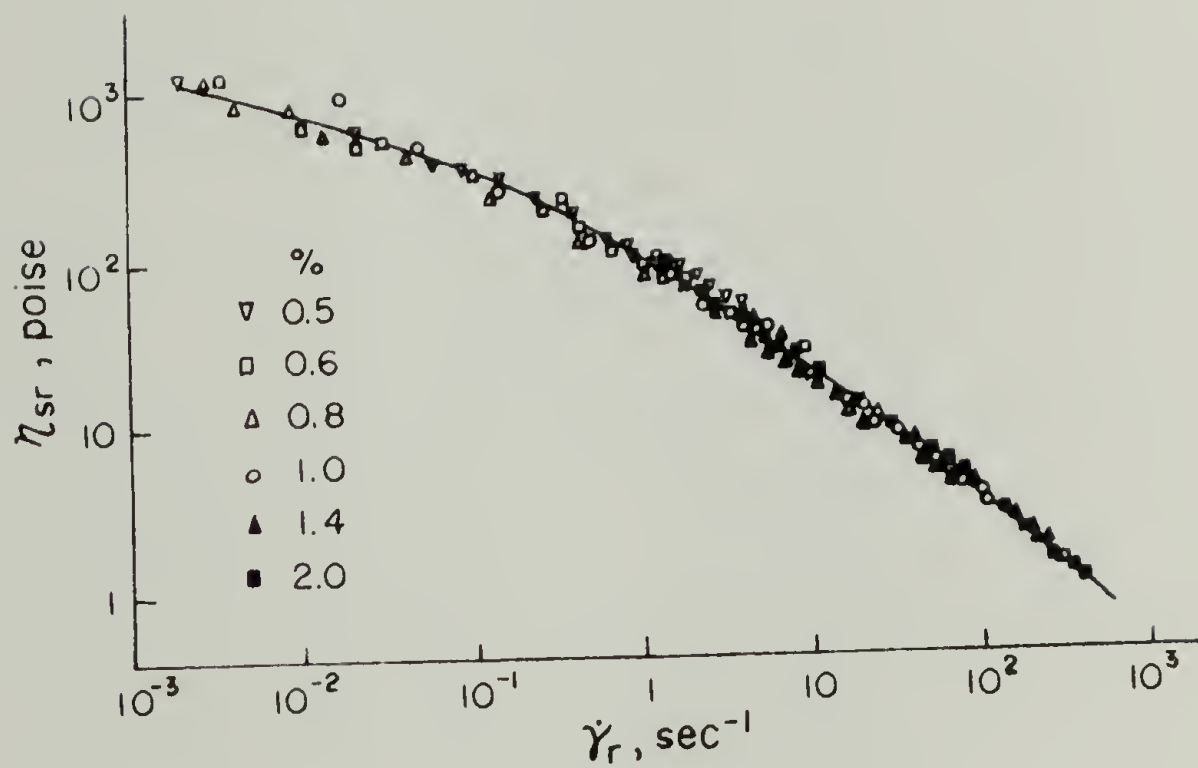


Figure 8. Master Curve for Reduced Steady State Viscosity of Dilute Collagen Solutions.

The shear rate did not extend down to a low-shear Newtonian limit so that although the ratio  $\eta_0/\eta_{s0}$  was accessible through the reduced variable treatment the absolute value of  $\eta_0$  was not determined. Viscosity was found to vary as the sixth power of concentration up to 2g/100ml.

Helders and Ferry (26) studied the viscosity/shear rate behavior of sodium deoxyribonucleate in aqueous solutions over an intermediate concentration range. Data at the upper end of the concentration range were expressed as reduced variables which matched reasonably the predictions of Bueche for "freely draining" flexible coils (27). At lower concentrations ( $.38 \times 10^{-3}$  and  $.19 \times 10^{-3}$  g/ml), the degree of overlap was insufficient to permit application of this model. Such data did fit the predictions of Saito for  $p = 300$  and  $\theta = 20.4 \text{ S}^{-1}$ , see Fig. 9. The flow activation energy increased only slightly with concentration while the relative viscosity increased tremendously, indicating that the high viscosities were due primarily to steric interference and not to reversible associations or network formation by the macromolecules.

Robins (28,29) observed that depending on the source of DNA, viscosities of very dilute solutions were constant up to a shear rate of  $3\text{-}150 \text{ S}^{-1}$  and then decreased, see Fig. 10. Concentrations were less than  $5 \times 10^{-5}$  g/ml in aqueous solution with enough NaCl added to suppress electrostatic effects. In order to determine the stiffness of the DNA helix, Robins utilized the equation:

$$\frac{[\eta]_{\dot{\gamma}=0} - [\eta]_{\dot{\gamma}}}{\dot{\gamma}^2} = K[\eta]_{\dot{\gamma}=0}^{K'} + \dots \quad (13)$$

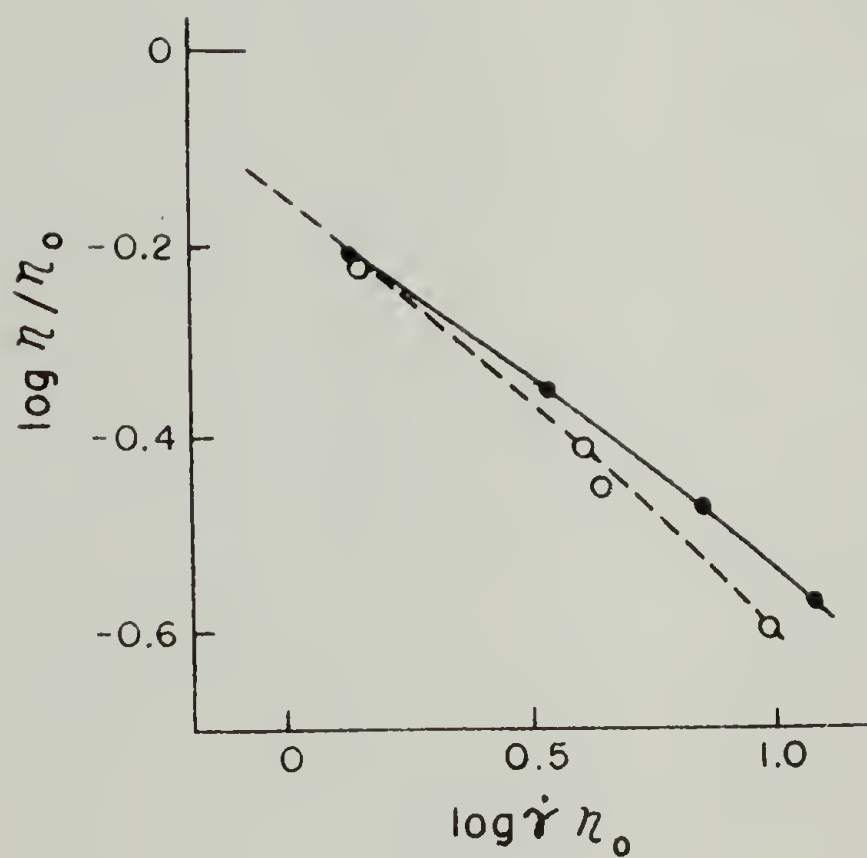


Figure 9. Reduced Viscosity for Dilute Solutions of Sodium Deoxyribonucleate in Water Plotted Against Product of Shear Rate and Zero-Shear Viscosity. ●,  $0.19 \times 10^{-3}$ ; ○,  $0.38 \times 10^{-2}$  g/ml. Dashed Curve; Saito Theory, Axial Ratio 300,  $\theta = 20.4 \text{ sec}^{-1}$ .



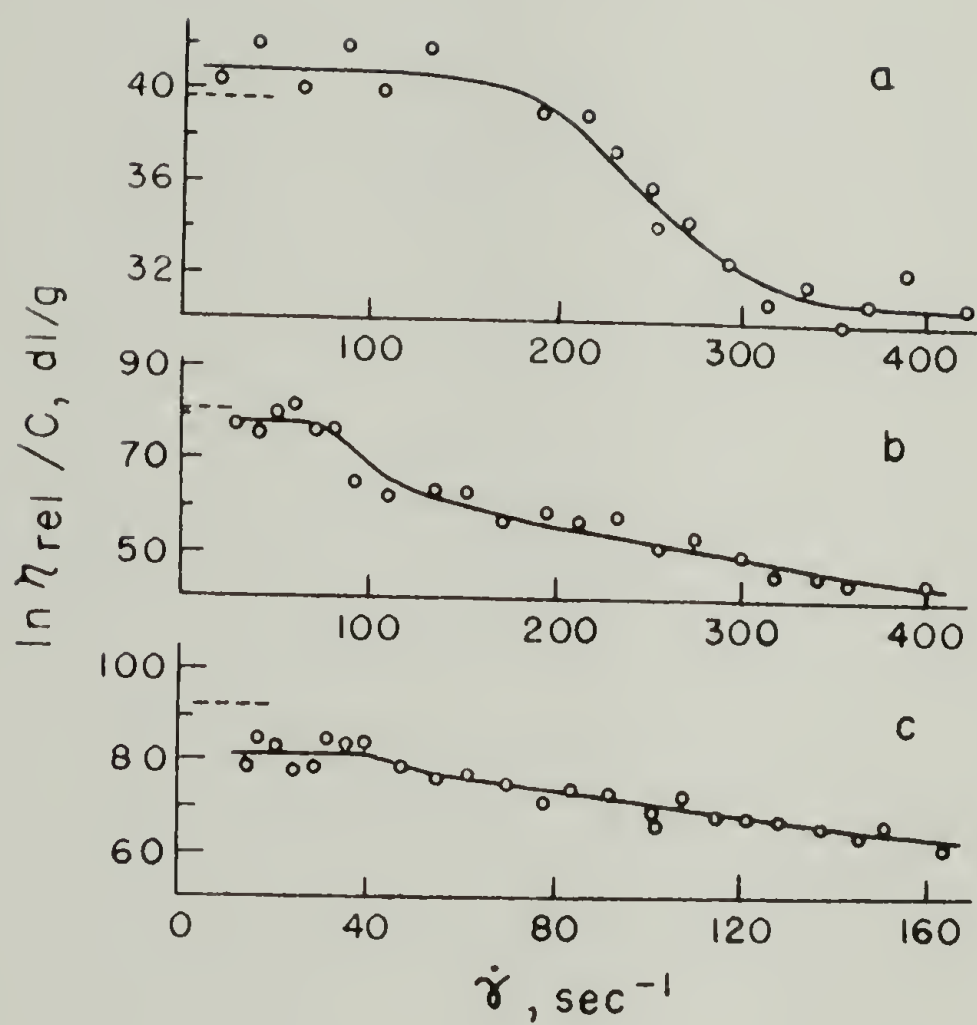


Figure 10. Effect of Shear Rate Upon Reduced Viscosity of DNA Solutions in Capillary Flow (a) 0.0025% Calf Thy-mus; (b) 0.00132% Herring Sperm; (c) 0.0016% E. coli B/r; ----- Indicates Couette Value Before Shear.

$K' = 4$  for a "soft" coil

$K' = 5$  for a "stiff" coil

After evaluating this exponent graphically, Robins concluded that DNA in dilute salt solution is a "soft" coil and, therefore, not amenable to model treatment either as a flexible coil or as a rigid particle.

Eisenberg (30) came to a similar conclusion in a viscosity study of dilute ( $1-6 \times 10^{-5}$  g/ml) solutions of DNA in  $10^{-3}$  M NaCl by plotting

$$\frac{(\eta_{sp})_{\dot{\gamma}}}{(\eta_{sp})_{\dot{\gamma}=0}}$$

versus  $\dot{\gamma}$  and comparing with predictions of Scheraga (for rigid ellipsoids) and Kuhn and Kuhn (31) (for Gaussian chains with high internal viscosity) for particles of different  $\theta$ . The experimental curve followed the Kuhn and Kuhn prediction for a single rotary diffusion constant, but cut across lines obtained from the Scheraga predictions for several values of  $\theta$  (see Figure 11). Eisenberg also observed the onset of shear thinning at a lower value of  $\dot{\gamma}$ , about  $1 \text{ S}^{-1}$  (see Figure 12).

The conclusion that DNA is a "soft" coil is at odds with the flow dichroism study of Wada (32) who indicated that DNA is even stiffer than cellulose trinitrate, which is considered a stiff, highly extended polymer, see Figure 13. Light scattering data supported this assertion since the persistence length of DNA is  $500\text{\AA}$  compared to cellulose trinitrate ( $117\text{\AA}$ ) and a typical flexible coil polymer,

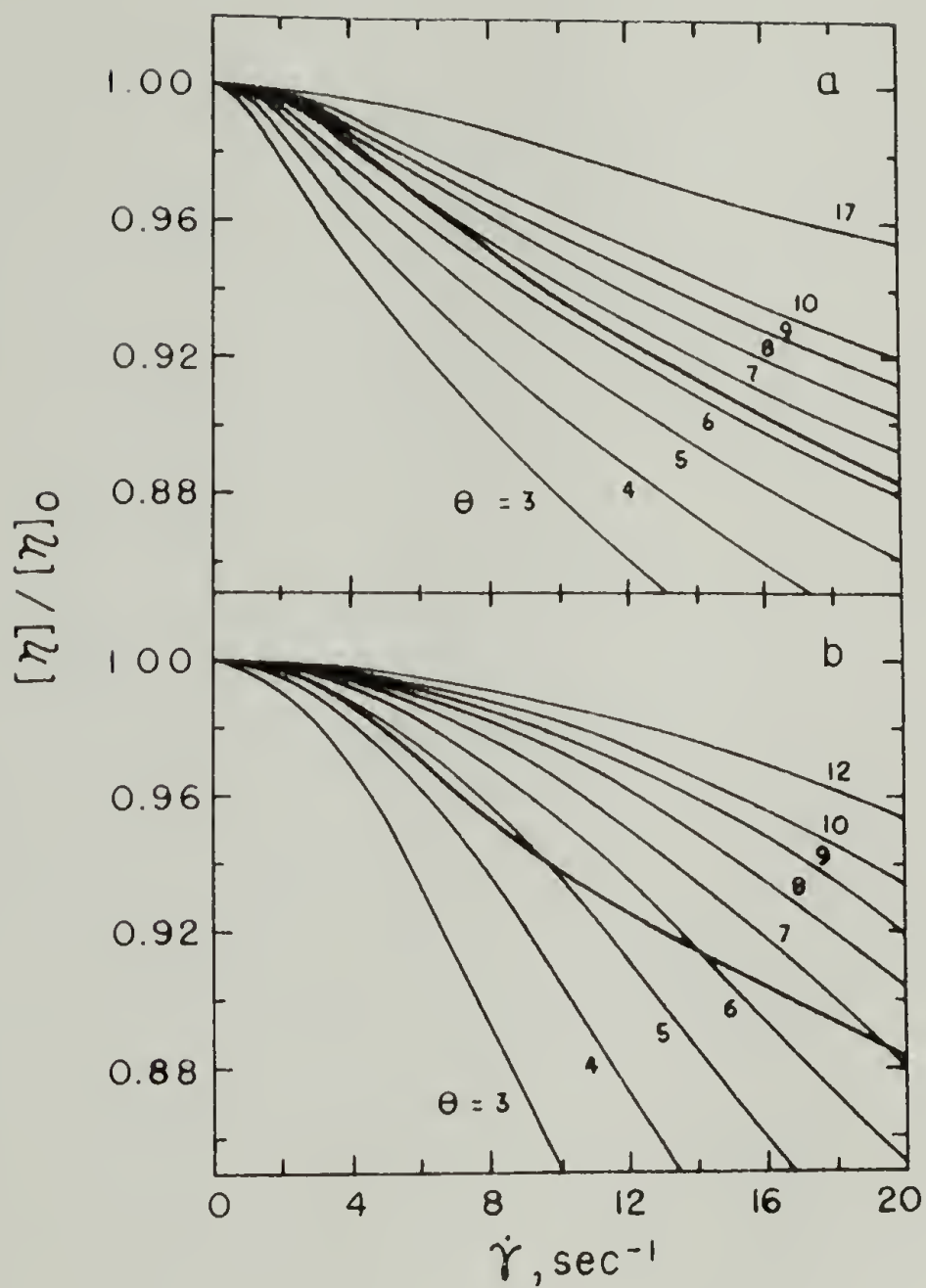


Figure 11. (a) Comparison of Experimental Curves of  $[\eta]/[\eta]_0$  Against  $\dot{\gamma}$  for DNA with Curves Calculated According to Kuhn and Kuhn for Linear Gaussian Coil with High Internal Viscosity. (b) Comparison of Experimental Curve of  $[\eta]/[\eta]_0$  Against  $\dot{\gamma}$  of DNA with Curves Calculated for Rigid Prolate Ellipsoid of Rotation ( $p > 100$ ).

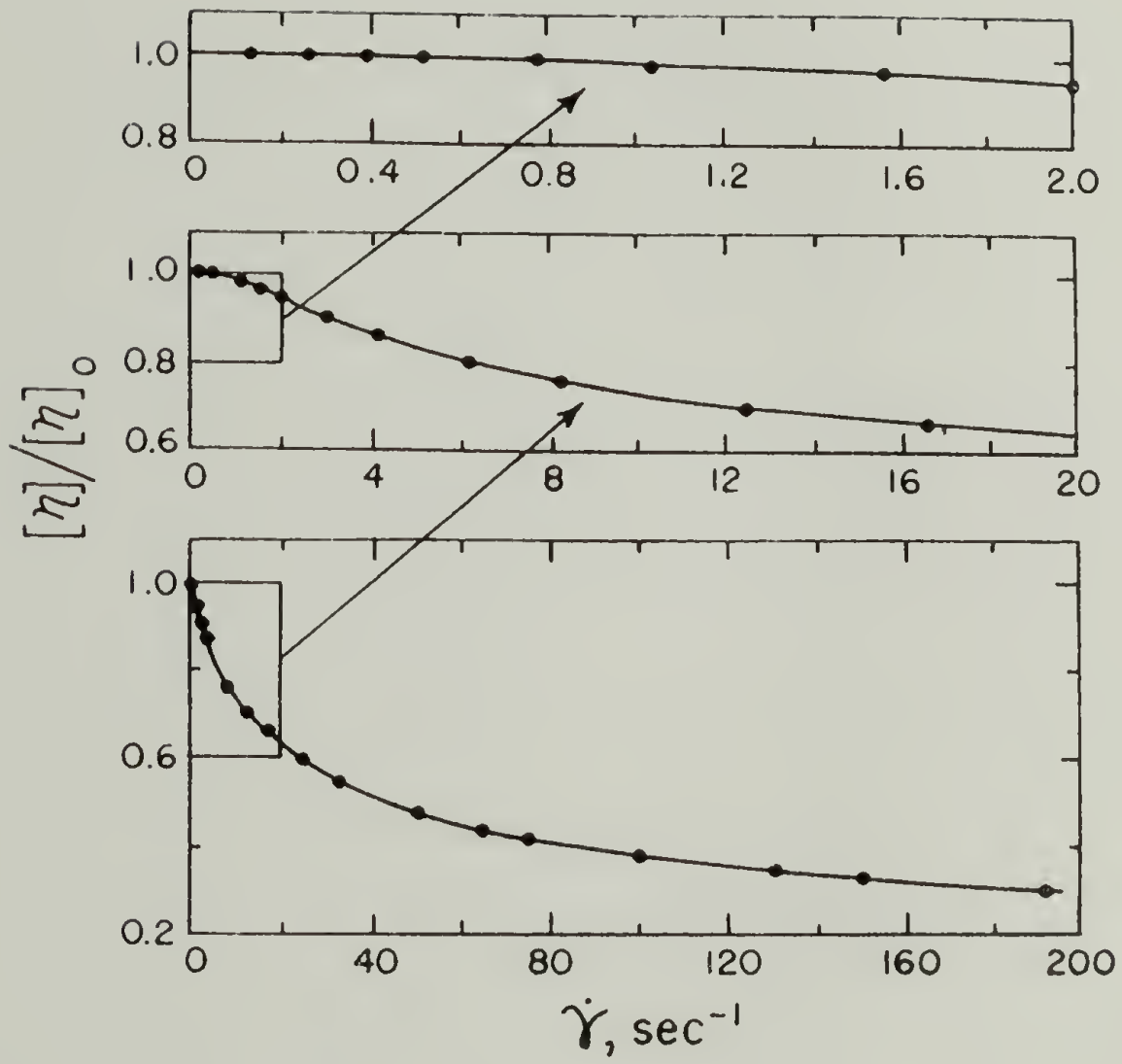


Figure 12. Viscosity-Shear Rate Curves.

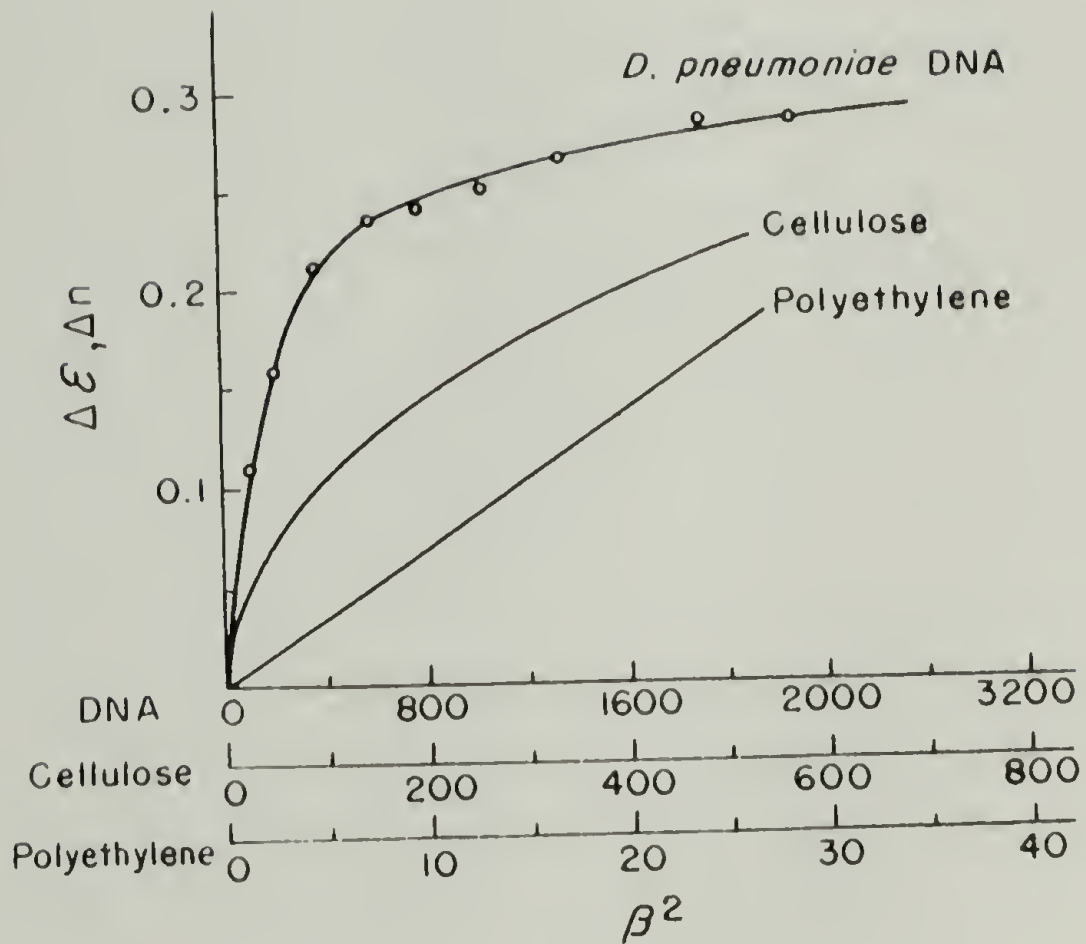


Figure 13. Plots of Dichroism,  $\Delta\varepsilon$ , of DNA of *D. Pneumoniae* Against  $\beta^2$ . The Same Kind of Relation Between Birefringence,  $\Delta n$ , and  $\beta^2$  for Cellulose and Polystyrene are also plotted.

polyethylene (7A).

Viscosity measurements on solutions of tobacco mosaic virus were made by Wada (33) and by Yang (34). Wada found the shear thinning behavior shown in Figure 14. From this information and an assumption of 15  $\mu$  for the length of the minor axis of the equivalent ellipsoid, Saito's theory predicted a p value of 20 compared to 18.8 determined from light scattering.

Yang's measurement of the dependence of intrinsic viscosity on shear stress is presented in Figure 15. Using the tables given by Scheraga to obtain values for  $\alpha$  and  $\theta$  from the viscosity data, Yang calculated p and the length of the equivalent ellipsoid using Perrin's (35) equation

$$\frac{\eta_s \theta}{T} = \frac{3k}{16\pi a^3} (2 \ln 2p-1) \quad (14)$$

T = Absolute temperature

k = Boltzmann's constant

a = length of semi-major axis

The length of the hydrodynamically equivalent ellipsoid was found to be 3610 $\overset{\circ}{\text{A}}$ , in agreement with the value of 3630 $\overset{\circ}{\text{A}}$  from sedimentation coefficient. Yang applied the Zimm and Haltner correction to obtain the length of the rod-shaped tobacco mosaic virus from the equivalent ellipsoid. Yang computed a length of 3100 $\overset{\circ}{\text{A}}$  which is in good agreement with his light scattering value of 3200  $\pm$  160 $\overset{\circ}{\text{A}}$  and also with a length obtained by electron microscopy (36).

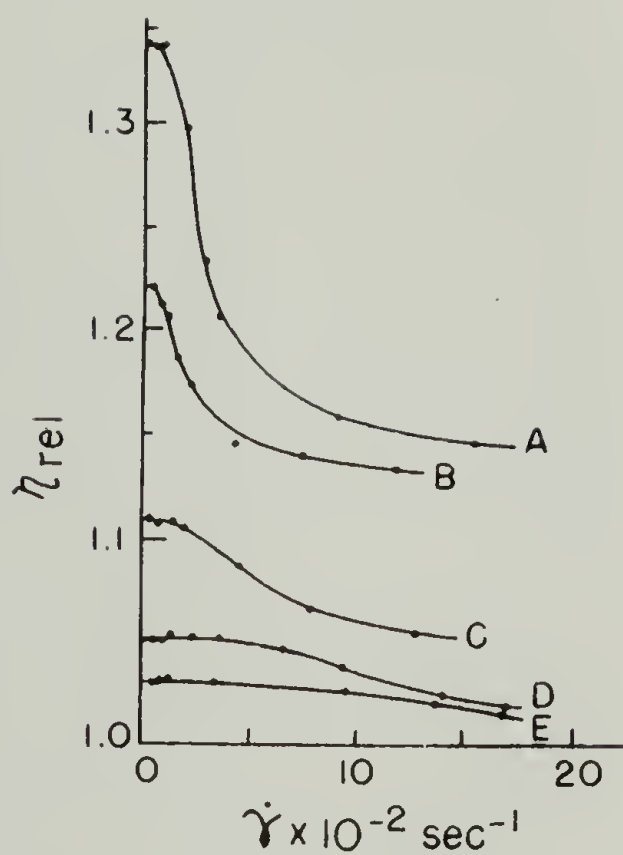


Figure 14. Relative Viscosity of TMV Solution vs. Shear Rate. Concentrations: A = 10 g/l, B = 7 g/l, C = 5 g/l, D = 1.7 g/l, E = 1.14 g/l.

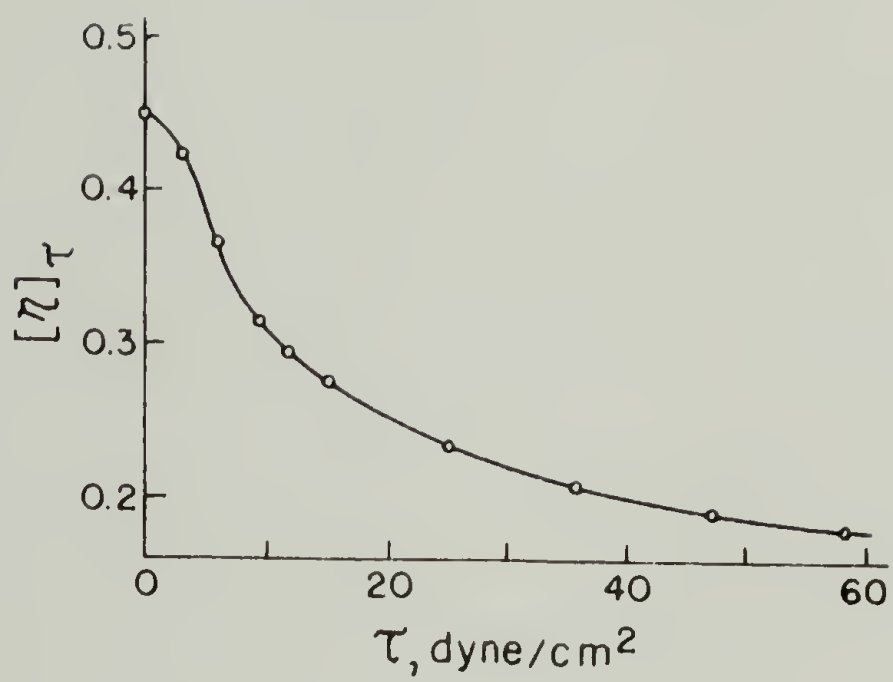


Figure 15. Shear Dependence of the Intrinsic Viscosities for Tobacco Mosaic Virus.



Poly- $\gamma$ -benzyl-L-glutamate (PBLG) is a synthetic polypeptide which adopts an  $\alpha$ -helical conformation in many solvents. In such helicoidal solvents PBLG may thus be considered as a rigid rod. In some solvents, such as chloroform, benzene, and dioxane, considerable association occurs leading to a high viscosity and Huggins constant. In DMF, m-cresol and pyridine the Huggins constant shows more usual values but viscosity remains high due to particle shape (37). Viscosity measurements in a hydrogen-bonding-breaking solvent, e.g., 8 M urea, confirm that the high viscosity can be due to particle shape and not to intermolecular hydrogen bonding (38). Dichloroacetic acid (DCA) is a denaturing solvent, i.e., one in which PBLG adopts a random coil configuration (37). This option of controlling molecular conformation by solvent choice plus the availability of PBLG as a nearly monodisperse polymer (39) makes it ideal for testing the theories for rigid coils.

Philippoff and Gaskins (40) remarked that the theory for shear thinning for rigid ellipsoids calls for a viscosity decrease proportional to the square of the shear stress for monodisperse polymers. Previous experiments had in most cases resulted in a linear dependence of viscosity on shear stress rather than quadratic. In this study viscosity data at shear stress in the range of 6 to 65,000 dyne/cm<sup>2</sup> for solutions of .5 to 1.1 wt% were found to be superimposed by the use of reduced variables both for a helicoidal solvent (m-cresol) and for a denaturing solvent (DCA), see Figure 16. The data for m-cresol were best fit by a quadratic formula of the form:

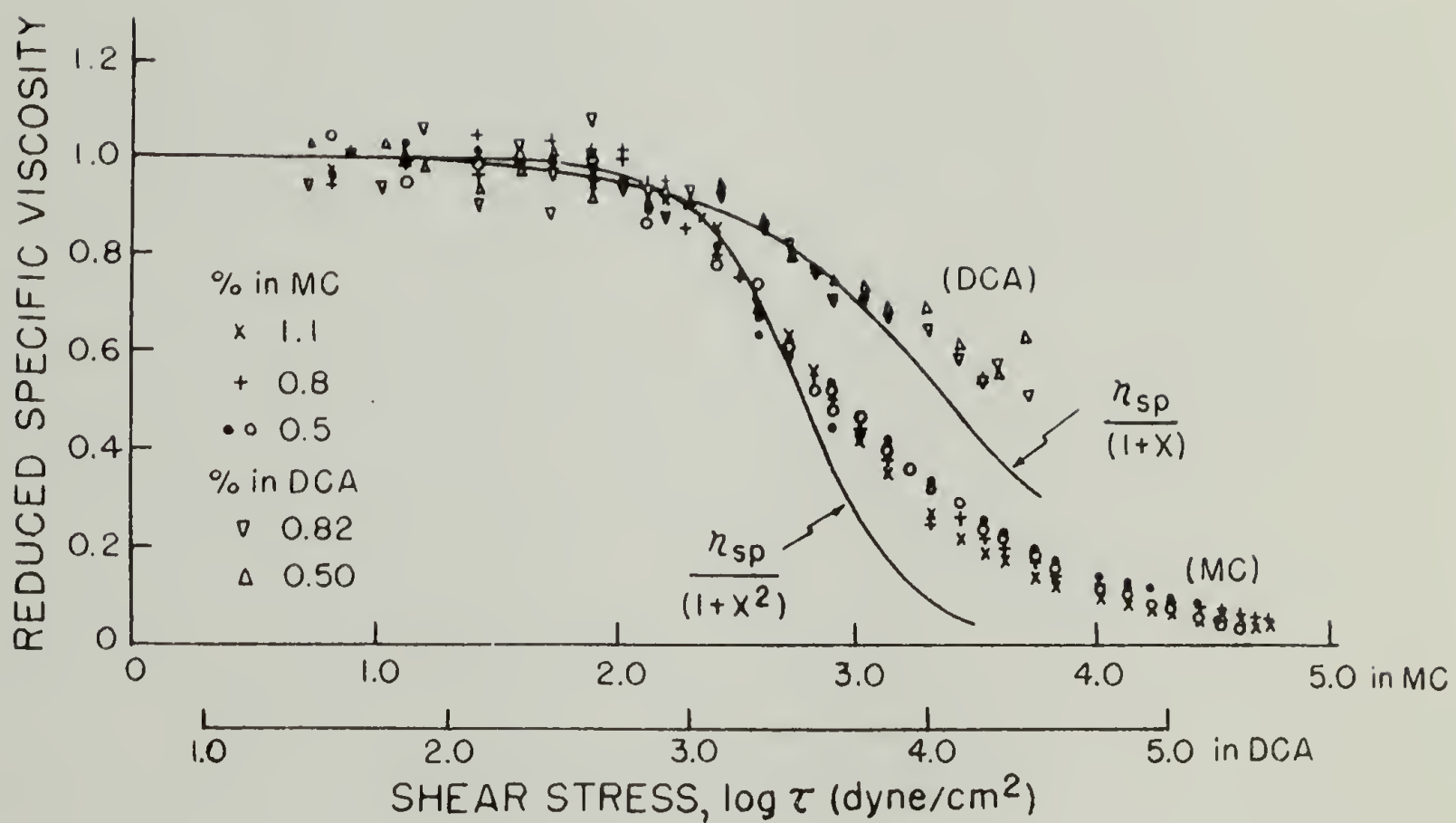


Figure 10. Viscosity vs. Stress for PBLG in m-Cresol and in Dichloroacetic Acid at 25°.

$$\eta = \frac{\eta_{sp}}{1+\chi^2} \quad (15)$$

up to about 40% viscosity reduction, thus vindicating the theory of Saito. The data obtained from DCA solutions were fit by a linear formula of the form:

$$\eta = \frac{\eta_{sp}}{1+\chi} \quad (16)$$

up to a viscosity decrease of about 35%. This was regarded as a consequence of the "internal polydispersity" of coiled macromolecules. That is, since the behavior of flexible chains in solution is a superposition of a large number of mechanisms, this behavior would appear to be that of a polydisperse system even if all of the macromolecules had the same molecular weight (41).

Yang (39) also employed PBLG as a model to test the rigid ellipsoid theory. He observed that reduced viscosity ( $\frac{\eta_{sp}}{C}$ ) dropped 10-fold over the shear stress range studied for m-cresol solutions whereas the DCA solutions dropped only about 30% from the low shear limit (see Figure 17). Two interesting features of these curves are the coincidence of the shear stress  $\tau_c$  at which the viscosity decrease commenced, regardless of temperature or concentration, and the fact that the curves for m-cresol (helical solvent) and DCA (random coil solvent) cross over. This latter observation indicates that the molecular helices are not disrupted by shear stress up to at least  $5 \times 10^4$  dyne/cm<sup>2</sup>. A comparison of experimental points with the curve from Scheraga's tabulated viscosity increments yields excellent agree-

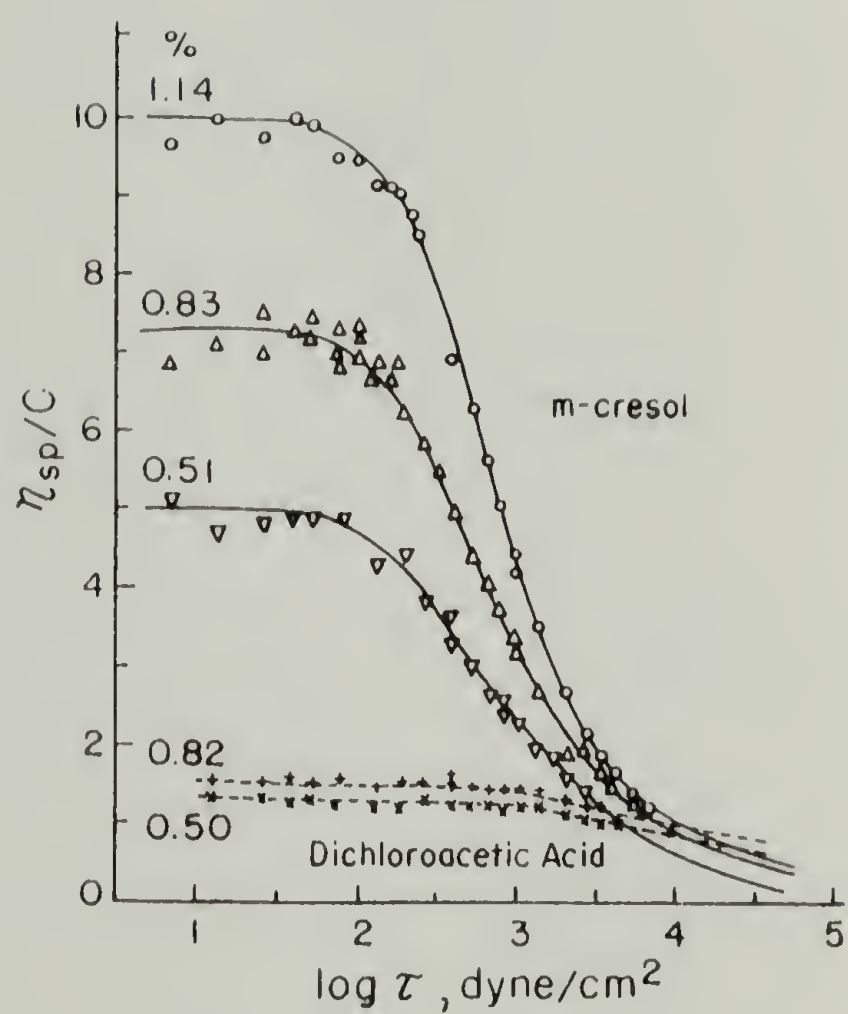


Figure 17. Viscosity Versus Shear Rate for PBLG as Coils and Rods.

ment in the case of the m-cresol solutions (see Figure 18). The results for PBLG in the coil form does not agree with the theories of Kirkwood, Rouse or Zimm for freely rotating chains which predict Newtonian viscosity, nor with Bueche's theory for freely draining coils.

In a more recent publication (42) Yang extended this investigation by considering the effect of solvent viscosity, temperature, and solute polydispersity. Viscosity data at different shear stresses and temperatures and with various (helical) solvents could be superimposed by plotting

$$\frac{[\eta]_{\gamma}}{[\eta]_{\gamma=0}}$$

versus  $\log \left( \frac{\tau}{T} \right)$  (see Figure 19). The effect of polydispersity was demonstrated by comparison with a 72/25 wt% blend of high with low molecular weight PBLG ( $\bar{M}_w = 336,000$  and  $\bar{M}_n = 253,000$ ) PBLG ( $\bar{M}_w = 130,000$  and  $\bar{M}_n = 117,000$ ). The curves for monodisperse polymer follow a quadratic dependence of viscosity on shear stress (or shear rate) as predicted by Saito. The mixture, however, exhibited a linear dependence. Thus a polydisperse system may exhibit a pseudo-linear dependence which is the composite of quadratic dependences for individual components. Theoretical curves for a Gaussian and a most probable distribution of molecular weights are compared with a monodisperse system in Figure 20. The calculated curves for each distribution spread over a wider non-Newtonian region than that for a monodisperse system. Furthermore, the apparent rotary diffusion

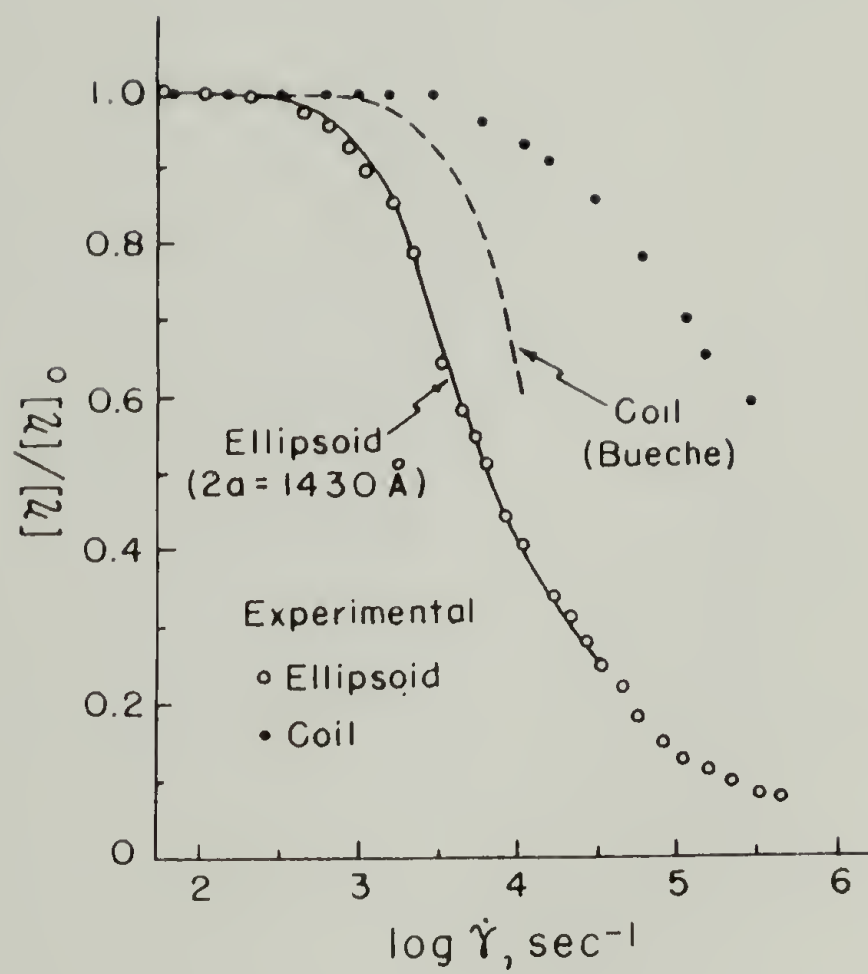


Figure 18.  $[\eta]/[\eta]_0$  vs. Shear Rate for PBLG in Coil and Rod Form; Lines are Theoretical Curves.

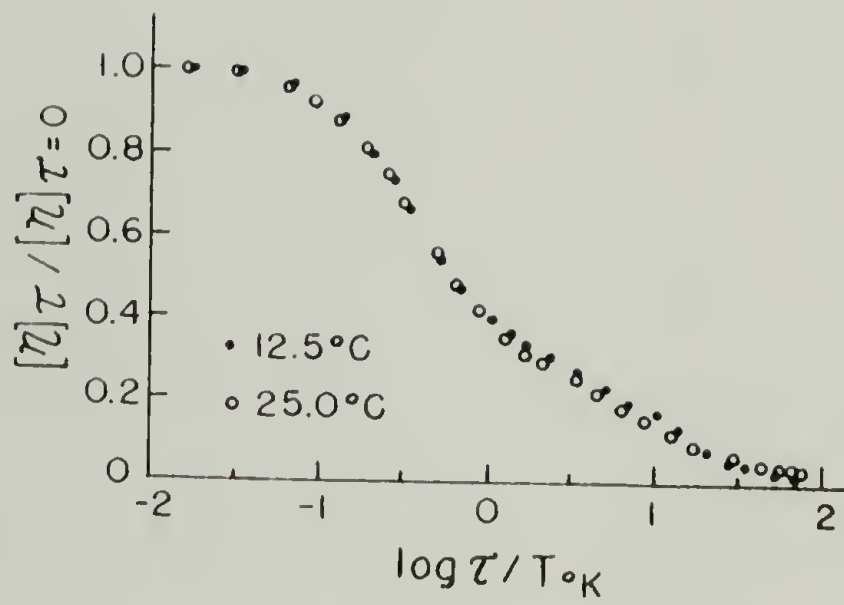


Figure 19. Effect of Solvent and Temperature on the Shear Dependence of Intrinsic Viscosities of PBLG; Closed Circles, m-Cresol at 12.5°; Open Circles, m-Cresol at 25.0°C.

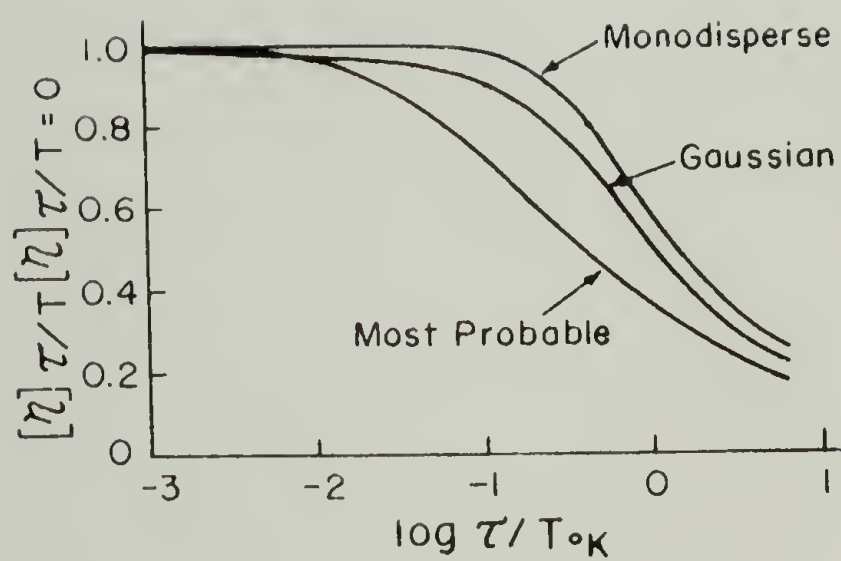


Figure 20. Shear Stress Dependence of the Intrinsic Viscosities of Rods Obeying Hypothetical Molecular Weight Distributions.



coefficient,  $\theta$ , is always higher for a monodisperse distribution than for polydisperse system of the same length. At low shear, longer particles are more readily oriented, leading to a low value of  $\theta$ . As shear stress is increased, the shorter particles can also be oriented, leading to a gradually increasing  $\theta$  until finally at infinite shear,  $\theta$  approaches that of the monodisperse distribution for particles of the same length.

Flow birefringence of dilute solutions of elongated particles. The study of flow birefringence of elongated particles is parallel to that of non-Newtonian viscosity since the same two opposing effects are involved, viz. the orienting effect of the velocity gradient and the disorienting effect of the rotary Brownian motion which is characterized by the rotary diffusion coefficient. The flow birefringence experiment generates two kinds of data, the extinction angle  $\chi$ , see Figure 21, and the magnitude of birefringence  $\Delta n$ , i.e., the difference in refractive index for light transmitted with its electric vector parallel and perpendicular to the optic axis of the molecules. At zero velocity gradient,  $\chi$  approaches  $45^\circ$  and  $\Delta n$  is zero. As  $\dot{\gamma}$  is increased,  $\chi$  decreases toward zero and  $\Delta n$  increases to a limiting value. Particles of very large  $p$  approach  $\chi = 0$  and high values of  $\Delta n$  at low shear.

Scheraga, Edsall and Gadd (43) numerically solved the expressions given by Peterlin and Stuart (44) for  $\chi$  and  $f$  in terms of  $\alpha$  and  $p$ .  $f$  is an orientation factor related to  $\Delta n$  by:

$$n = \frac{2\pi C}{n} (g_1 - g_2) f \quad (17)$$

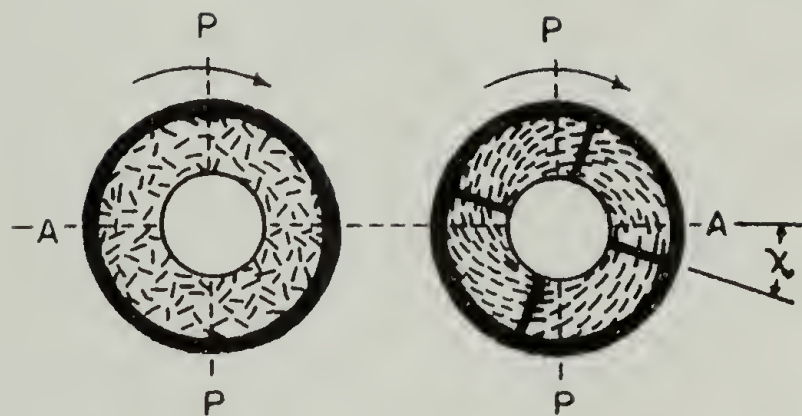


Figure 21. Orientation of Particles in a Doubly Refractive Fluid Between Concentric Cylinders. A and P Indicated the Orientation Directions of the Analyzer and Polarizer.

$C$  = volume concentration of particles

$n$  = index of refraction of the solution at rest

$(g_1 - g_2)$  = an optical factor depending on axial ratio and indices of refraction.

This information is presented graphically in Figure 22 for two values of  $p$  as a function of  $\alpha$  and in Figure 23 for a single value of  $\alpha$  as a function of  $p$ . The optical factor  $(g_1 - g_2)$  may be evaluated by plotting experimental values of  $\chi$  against  $\Delta n$  and then fitting a theoretical curve  $\chi$  vs.  $Kf$  by adjusting  $K$ . The optical factor is then given by:

$$(g_1 - g_2) = \frac{nK}{2\pi C} \quad (18)$$

In his paper on the non-Newtonian viscosity of TMV, Yang (45) also performed flow birefringence experiments in order to obtain an independent measurement of the rotary diffusion constant,  $\theta$ , using tables such as those given by Scheraga, and thus the hydrodynamic length from the Perrin equation. A comparison of the lengths calculated by the two methods is presented in Figure 24. The difference between the curves was explained by the fact that both methods are sensitive to polydispersity and give different averages for the hydrodynamic length: non-Newtonian viscosity giving the viscosity average and flow birefringence a complex average more heavily weighted to longer particles than weight average. It also appears that the flow birefringence average changes with shear rate.

Subsequently Yang (46) compared the flow birefringence method

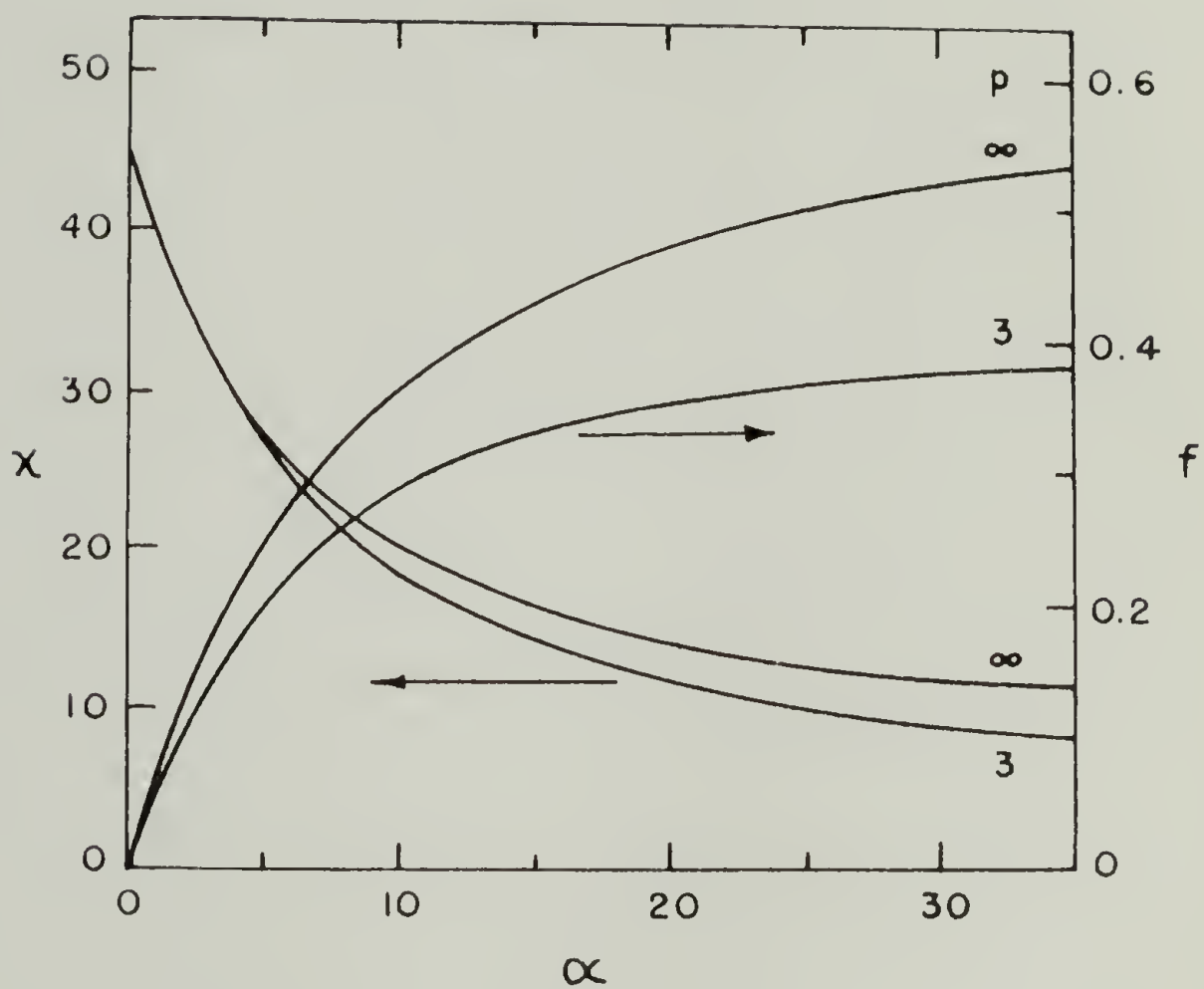


Figure 22. (a) Extinction Angle,  $\chi$ , vs.  $\alpha$  and Dependence on Axial Ratio  $p$ . (b) Orientation Factor,  $f$ , vs.  $\alpha$  and Dependence on Axial Ratio,  $p$ .

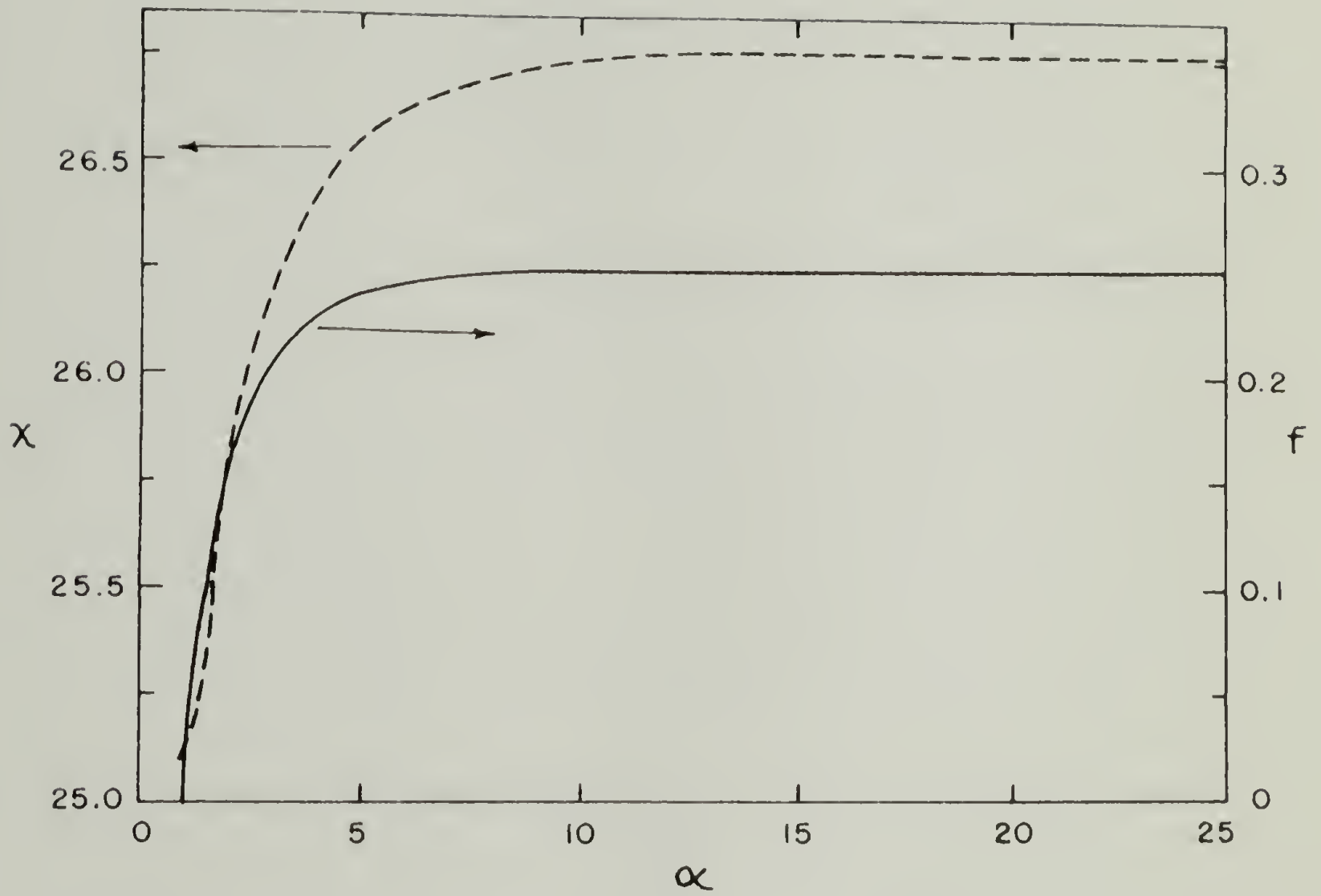


Figure 23. (a) Dependence of Extinction Angle on Axial Ratio for  $\alpha = 5$ .  
 (b) Dependence of Orientation Factor on Axial Ratio for  $\alpha = 5$ .

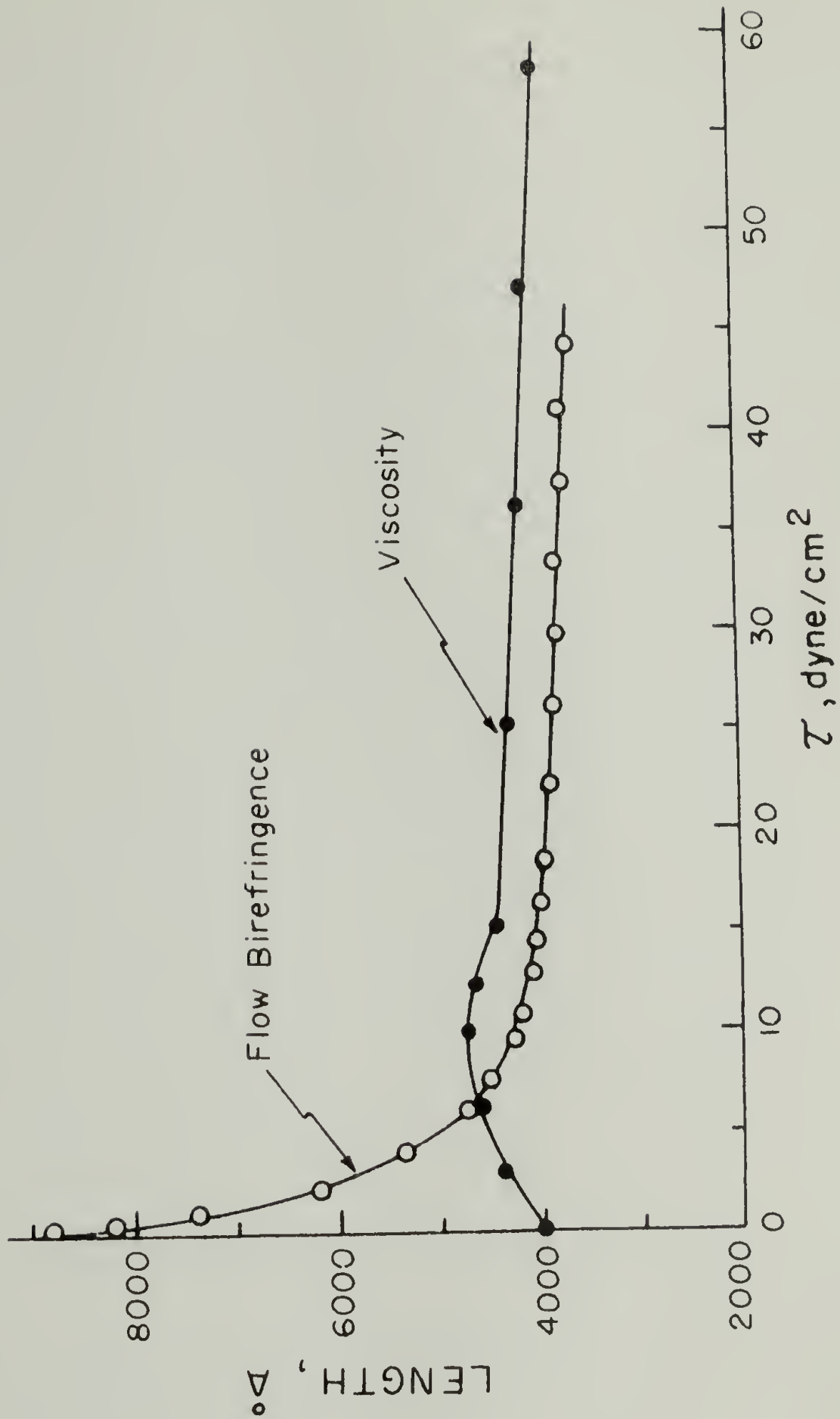


Figure 24. Hydrodynamic Lengths of Tobacco Mosaic Virus from non-Newtonian Viscosity and Flow Birefringence.

of determining particle length with a method he proposed involving intrinsic viscosity at zero shear. The latter has the advantage of being insensitive to polydispersity and being applicable to relatively short particles. A knowledge of the molecular weight is required, however:

$$L = 6.82 \times 10^{-8} ([\eta]_0 M)^{1/3} [p^2/\nu]^{1/3} \quad (19)$$

L = particle length.

The reliability of this method is demonstrated by comparison with lengths calculated on the basis of 1.5Å per residue and also those obtained from light scattering. The agreement is excellent: see Table 1. Finally, this method gives a direct measure of particle length rather than that of an equivalent ellipsoidal, as is given by flow birefringence or by non-Newtonian flows.

Viscoelastic properties of solutions of rod-like materials. A theory for the viscoelasticity of rod-like molecules in solution has been developed by Kirkwood and Auer (47) using the general theory of irreversible processes for solutions of macromolecules. The results were presented as a function of frequency which allows comparison with data on the propagation of shear waves. This theory predicts that the intrinsic viscosity  $[\eta]$  drops with increasing frequency to one fourth of the zero-frequency value, while intrinsic rigidity  $[\mu]$  increases from zero to an asymptotic value of  $\frac{3RT}{5}$  per mole/cm<sup>3</sup> of solute. The equations presented were

$$[\eta] = \frac{\pi n L^2}{9000 M_o \log \frac{L}{b}} \left[ 1 + \frac{3}{1 + \omega^2 \tau^2} \right] \quad (19)$$

$$[\mu] = \frac{6NKT}{1000M} \frac{\omega^2 \tau^2}{1 + \omega^2 \tau^2} \quad (19)$$

$[\mu]$  = Intrinsic rigidity

$b$  = Spacing of units along this length

$\omega$  = Frequency

$M$  = Molecular weight

The quantity  $\tau$  is the relaxation time given by

$$\tau = \frac{\pi n_s L^3}{18kT \ell n \frac{L}{b}} \quad (20)$$

Kirkwood and Plock (48) extended this theory to include the effect of shear rate. Results were given for two extremes, the dumb-bell model and the infinite rod. It was seen that the velocity perturbation function and hence both intrinsic viscosity and intrinsic rigidity are even functions of shear rate. Also this theory agrees with Saito for viscosity of ellipsoids of revolution in the limit of infinite  $p$ . Figure 25 shows that  $[\eta]$  approaches a zero-shear value with zero slope and decreases to an asymptotic value at high  $\dot{\gamma}$  (note that since  $\tau$  is related to the rotary diffusion constant,  $\tau \dot{\epsilon}$  is proportional to the  $\alpha$  used by Scheraga).

The theory developed by Kirkwood and Auer was applied by Kotaka (49) to the components of normal stress in a solution of rod-



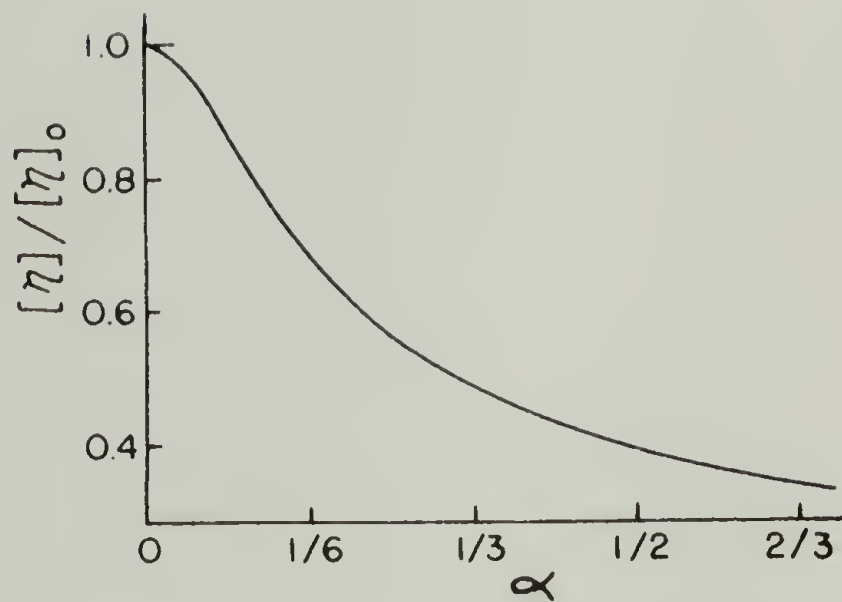


Figure 25. Intrinsic Viscosity of the Infinite Rod as a Function of the Rate of Shear.

like macromolecules. When hydrodynamic interaction between elements of the molecules are considered all normal stresses ( $\sigma_{xx}$ ,  $\sigma_{yy}$ ,  $\sigma_{zz}$ ) appear. The relationships among the normal stresses is given approximately by

$$(\sigma_{yy} - \sigma_{zz}) = -\frac{1}{6}(\sigma_{xx} - \sigma_{zz}) \quad (21)$$

Thus the effect of normal stress in a solution of rod-like macromolecules is mainly tension in the direction of flow.

The viscoelasticity of solutions of collagen in dilute HCl was investigated by Fukada and Date (50). Collagen molecules are rods of diameter  $13.6\text{\AA}$  and length  $3000\text{\AA}$  and are able to associate laterally to form a gel in the concentration range studied. The use of the following reduced variables allowed the superposition of dynamic viscosity and dynamic rigidity data for various concentrations (see Figure 26):

$$\text{Reduced dynamic rigidity } \mu_r = \frac{\mu T_s C_s}{TC} \quad (22)$$

$$\text{Reduced dynamic viscosity } \eta_r' = \eta' \frac{\eta'_{so}}{\eta'_0}$$

$$\text{Reduced frequency } \omega_r = \omega \eta'_0 \frac{T_s C_s}{TC}$$

$T_s, C_s$  = Temperature and concentration of reference solution

$T, C$  = Temperature and concentration of solution being measured

$\eta'_{so}$  = Zero frequency viscosity of reference solution

$\eta'_0$  = Zero frequency viscosity of measured solution.

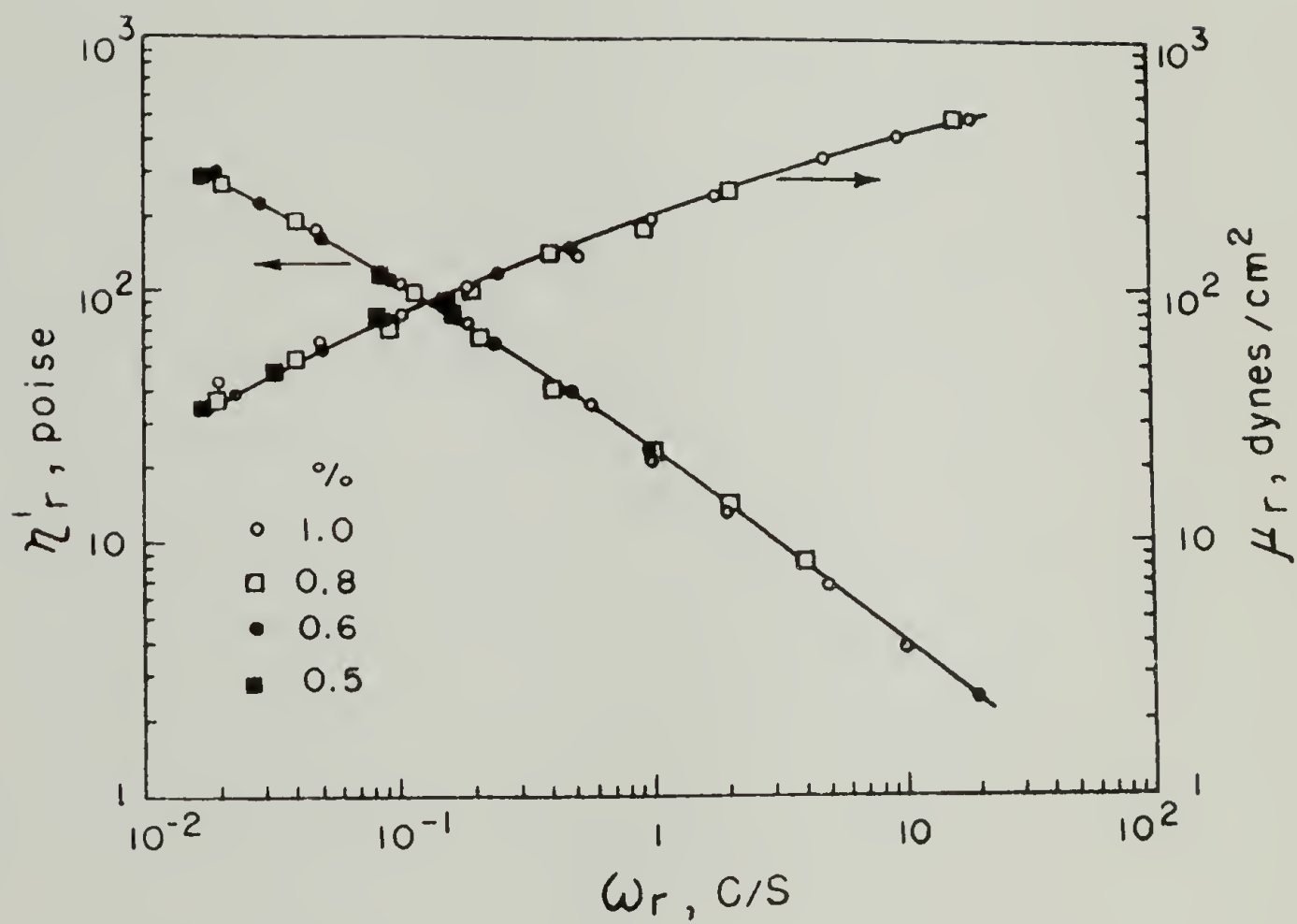


Figure 26. Master Curves of Dynamic Viscosity  $\eta'_r$  and Dynamic Rigidity  $\mu_r$ , reduced to 1 g/100 ml and 26°C for Collagen in Dilute HCl.

It was also found that plotting dynamic viscosity versus frequency on the same axes as steady shear viscosity versus shear rate show virtual coincidence as called for by theory. The concentration dependence of rigidity was found to depend on the 3.3 power of concentration rather than the 3.67 power as given by theory for dilute gels (51). Dynamic viscosity also varied exponentially with concentration; however, the exponent varied with frequency, from 3.2 at .5 Hz to 2.2 at 20 Hz. Similar behavior was observed for steady shear viscosity, the exponent varying from 4.8 at  $.015 \text{ S}^{-1}$  to 1.5 at  $100 \text{ S}^{-1}$ . The variation of  $\mu$  and  $\eta'$  with frequency for collagen solutions was more pronounced than for solutions of gelatin derived from denatured collagen, corresponding to behavior of PBLG in helicoidal and denaturing solvents.

The viscoelastic behavior of solutions of PBLG in a helicoidal solvent of high viscosity (m-methoxyphenol) at concentrations of 1.0 and 2.0 wt% were studied by Tschoegl and Ferry (52) and compared to the Kirkwood-Auer prediction for rigid rods and the Zimm theory for dilute solutions of random coil polymers (53), see Figures 27 and 28. Data fall between the best fit for the two theories; a fit to the K-A theory required a molecular weight about twice actual whereas fitting the Zimm theory required a molecular weight about ten times too high. This is even more favorable than it seems for the K-A theory, as it is heavily weighted to high molecular weight species, so that a slight polydispersity can easily cause the apparent molecular weight to be twice the nominal monodisperse molecular weight. Calculation of the relaxation time from the K-A theory also leads to reasonable results.

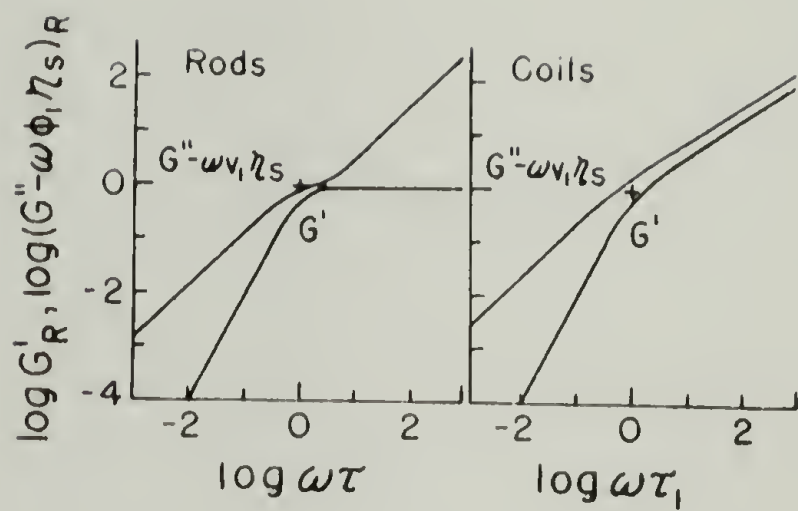


Figure 27. Contributions of a Macromolecular Solute to the Components of the Complex Shear Modulus, as Predicted by the Theories of Kirkwood and Auer for Rigid Rods and Zimm for Flexible Coils.

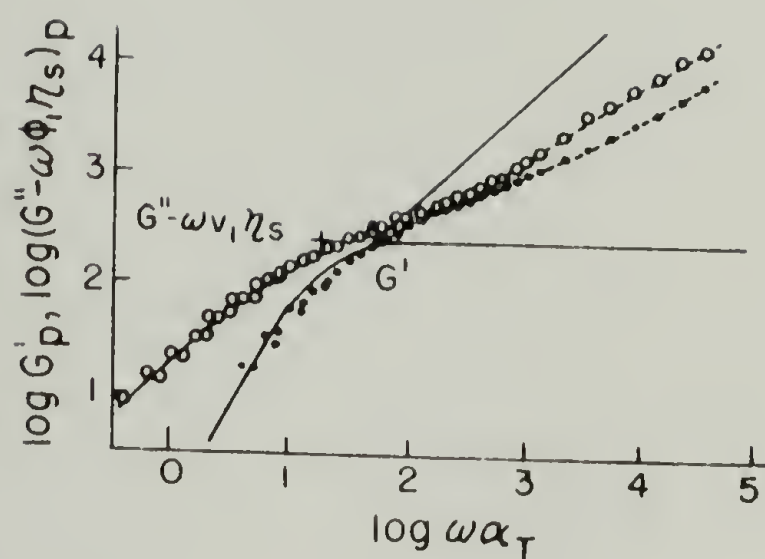


Figure 28. Plots of  $G'$  (black circles) and  $G''-\omega\phi\eta_s$  (open circles) for 1% Poly- $\gamma$ -benzyl-L-glutamate in *m*-methoxy-phenol. Measured at  $0^\circ$ ,  $25^\circ$ , and  $50^\circ\text{C}$  and reduced to  $25^\circ\text{C}$ . Solid Curves Represent Kirkwood-Auer Theory. The Subscript  $p$  Denotes Multiplication by  $T_s\rho_s/T_p$ .

A slight flexibility in the helix is indicated by the deviation from the K-A theory at higher frequency. Measurements in a denaturing solvent (dichloroacetic acid) gave results inconsistent with the K-A theory and in only fair agreement with the Zimm theory.

The dynamic viscoelasticity of solutions of helical polypeptides has also been investigated by Tanaka et al. (54,55). It was found that  $\frac{G''-\omega\eta_s}{C}$ ,  $\frac{G'}{C}$ , and  $\frac{\tau}{K}$  (where  $G''-\omega\eta_s$  is dynamic loss modulus minus the solvent contribution,  $G'$  is dynamic storage modulus and  $\tau$  is relaxation time) all increased linearly with concentration from .1 to .5 g/cc and the K-A theory qualitatively describes the viscoelasticity of  $\alpha$ -helices in solution (PBLG in  $\text{CHCl}_3$ , poly- $\gamma$ -methyl-D-glutamate in  $\text{CHCl}_3$ ) (see Figure 29). Preliminary results for D, L-copoly- $\gamma$ -benzylglutamate (PBDLG) indicated that a small percentage of D residues result in imperfections of the  $\alpha$ -helix. These measurements were obtained by means of a "torsional crystal" method at frequencies from 19.6 and 117.7 KHz, compared to .016 to 400 Hz for the oscillating rod and cup used by Tschoegl and Ferry (56).

#### Concentrated Solutions of Rigid Rods

Theory for formation of anisotropic solutions. The first section of this paper was concerned with the behavior of solutions of rod-like particles which were sufficiently dilute that the particles could be assumed not to interact. In some of the studies cited, this condition was not met; as concentration is increased, inter-particle interaction becomes more important and eventually dominates behavior. This problem was first treated theoretically by Onsager (57) and

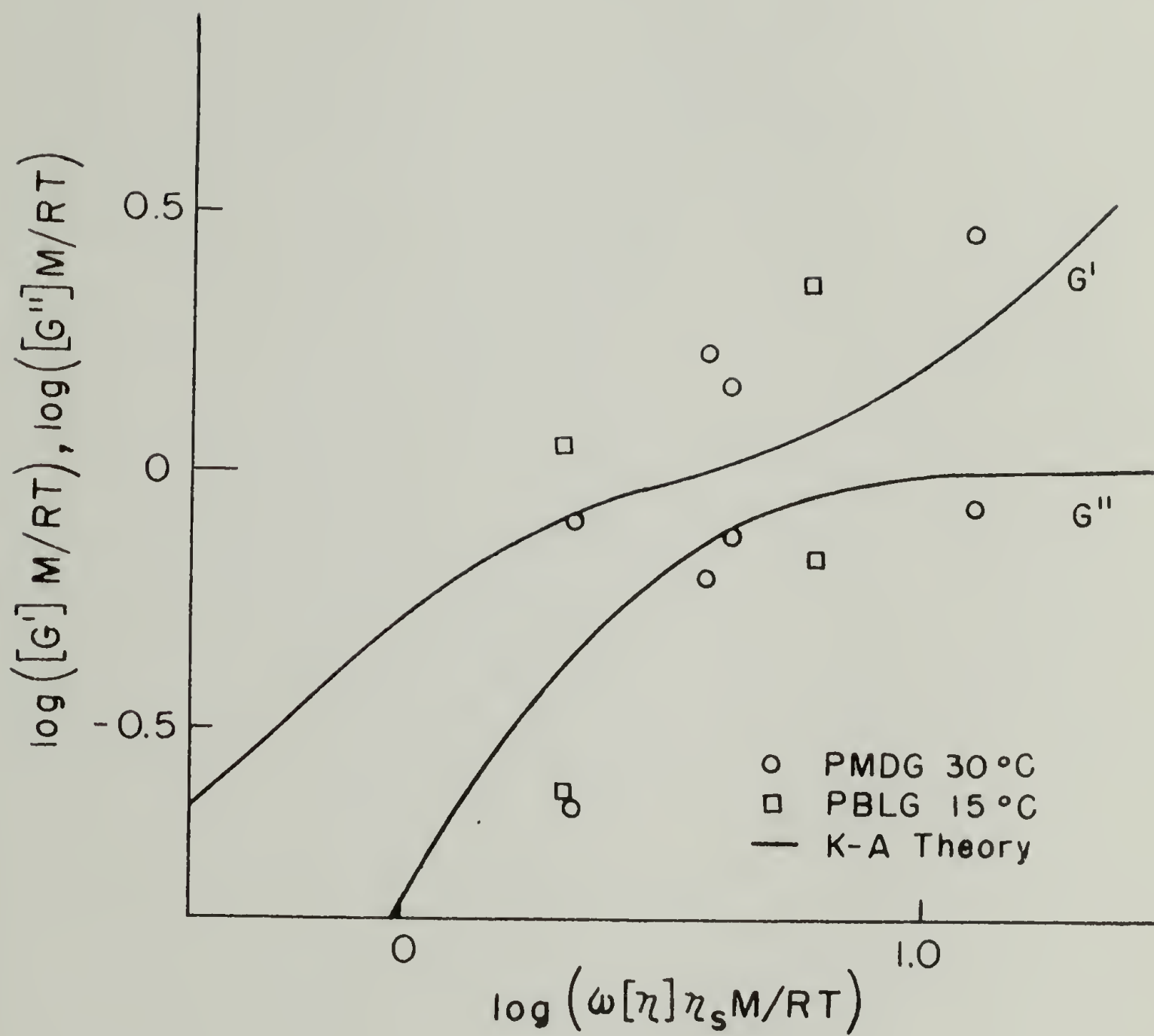


Figure 29. Viscoelastic Response of Solutions of  $\alpha$ -Helical Molecules.



Isihara (58), who considered rigid anisotropic solutes separated by a repulsive force. The equilibrium orientation of the solute particles is determined by the competition between the orienting effect due to repulsion and the disorienting effect of thermal agitation. This is evaluated by writing the free energy as a virial expansion in the distribution function of orientations of the anisotropic particles in space and then finding the <sup>(minimum?)</sup> maximum. To simplify the mathematics, the expansion was truncated at the second term. The result is that phase separation should occur with one phase containing a low concentration of unoriented particles and the other containing a higher concentration of oriented particles; see Figure 30. The critical concentration at which this occurs is inversely proportional to  $p$ , the axial ratio. This approach is limited to low concentrations by the disregard of higher terms in the virial expansion. Its accuracy for concentrations in the range of the anisotropic phase is open to question.

A combinatorial approach was adopted by Flory (59) and by DiMarzio (60). The number of ways in which rigid rods can be packed on a lattice is counted, the partition function is constructed, and free energy is calculated as a function of orientation. This method offers the advantage of applicability over the entire concentration range. The results are qualitatively similar to the Onsager theory with phase separation occurring at a volume fraction of solute.

$$\phi_2^* \approx \frac{8}{p} \left( 1 - \frac{2}{p} \right) \quad (23)$$

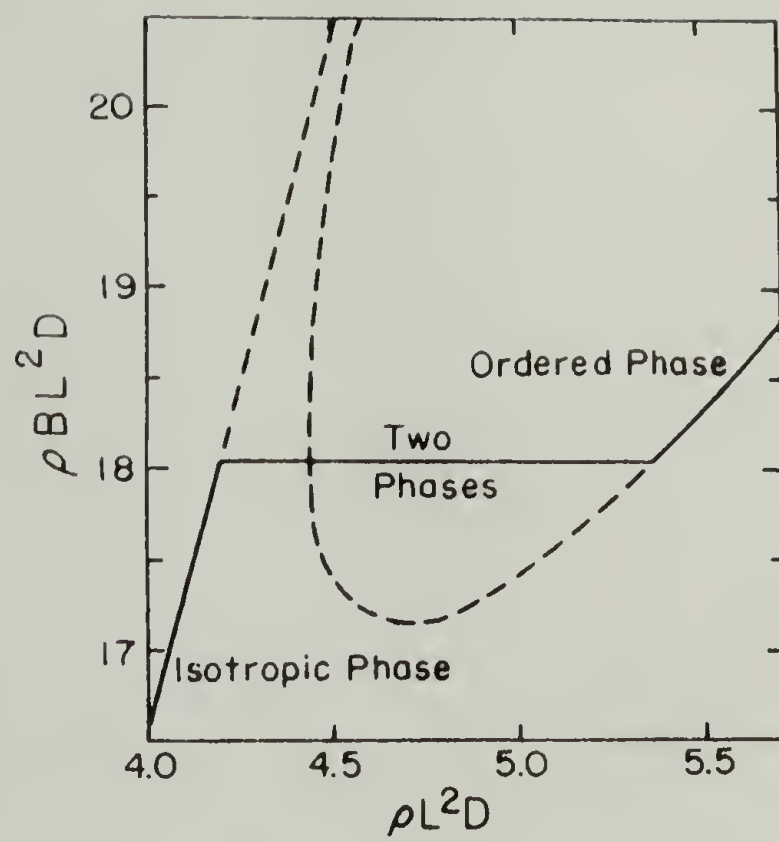


Figure 30. The Onsager Model.

Here, however, phase separation is entirely a consequence of particle asymmetry and an inter-particle force is not required. As the aspect ratio is increased, the concentration in both phases drops and the ratio of concentrations approaches 1.56; see Figure 31. DiMarzio deduced the possibility of a third phase (tentatively identified as a cholesteric mesophase) which is metastable unless there is an additional energy term which would cause it to be preferred. This energy would be available only if the molecules were plate-like or ribbon-like, rather than as rods.

A review by Straley (61) criticized the Flory theory as having made an avoidable approximation. Straley reworked Flory's treatment without using the questionable approximation and found that for any suspension of asymmetric objects, however dilute, an anisotropic distribution of orientations exists which minimizes the free energy, hence spontaneous ordering occurs. Straley concluded that the Flory theory is incorrect and that the Onsager theory is qualitatively correct. Despite this, the Flory theory is widely accepted.

Frenkel (62) extended the purely entropic formalism of Flory and DiMarzio by considering the effect of temperature and environment on the flexibility parameter,  $f$ , which ranges from 0 for a rigid rod to 1 for a flexible chain. Molecules for which  $f < .63$  are too flexible to form liquid crystals but the addition of energy, such as by a shear or magnetic field, can reduce  $f$  below the critical value. Lowering  $f$  by such means also reduces the critical concentration for liquid crystal formation in the case of molecules with  $f > .63$ . Frenkel stated an equivalence principle, i.e., that the thermodynamic

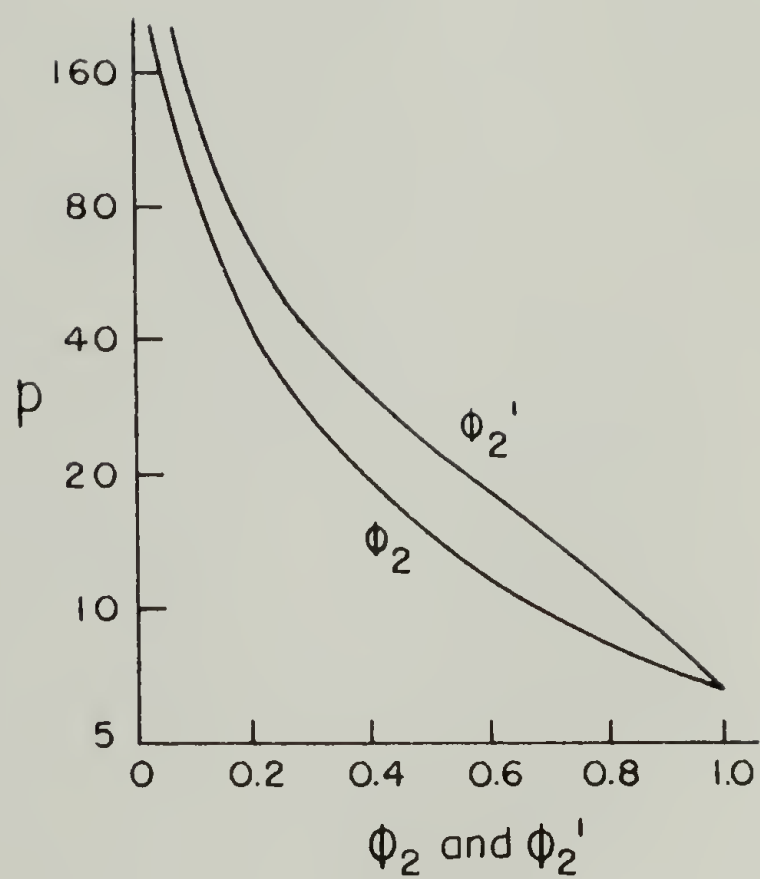


Figure 31. Concentration of Phases in Equilibrium in Relation to  $p$  for Athermal Mixtures.

behavior of a system of molecules under the influence of a "stiffening" field is indistinguishable from that of a more rigid molecule in the absence of the field. He also noted that in elongational flow, in contrast to shear flow, positive feedback is established between orientation and deformation. Thus elongational flow would be more effective at producing a liquid crystal from a melt or solution of a flexible polymer (62).

Possible approaches for increasing the rigidity of semi-flexible rod-like molecules in order to obtain anisotropic solutions have been discussed by Ciferri (63). The pertinent variables were considered to be solvent type, polymer concentration and solution temperature. Experimental evidence was cited to support the contention that these variables can influence the rigidity of rod-like molecules in solution. Variation of rigidity due to solvent effects was revealed by intrinsic viscosity measurements on DNA in a binary solvent ( $H_2O/DMF$  with 1% LiCl to suppress polyelectrolyte effects); see Figure 32, and by a large variation in intrinsic viscosity of solutions of poly-L-proline with addition of KCl (64). These effects were considered not due to aggregation, polyelectrolyte effects, or conventional helix-coil transitions. Variation of rigidity with polymer concentration was observed for PBLG in DCA which, as discussed earlier, is a denaturing solvent, yet optical rotation measurements revealed that at concentrations greater than 15g/100cc, PBLG molecules revert to a rigid helical conformation (65). The effects of shear and elongational flow on the orientation of semi-flexible molecules in solution were also discussed.

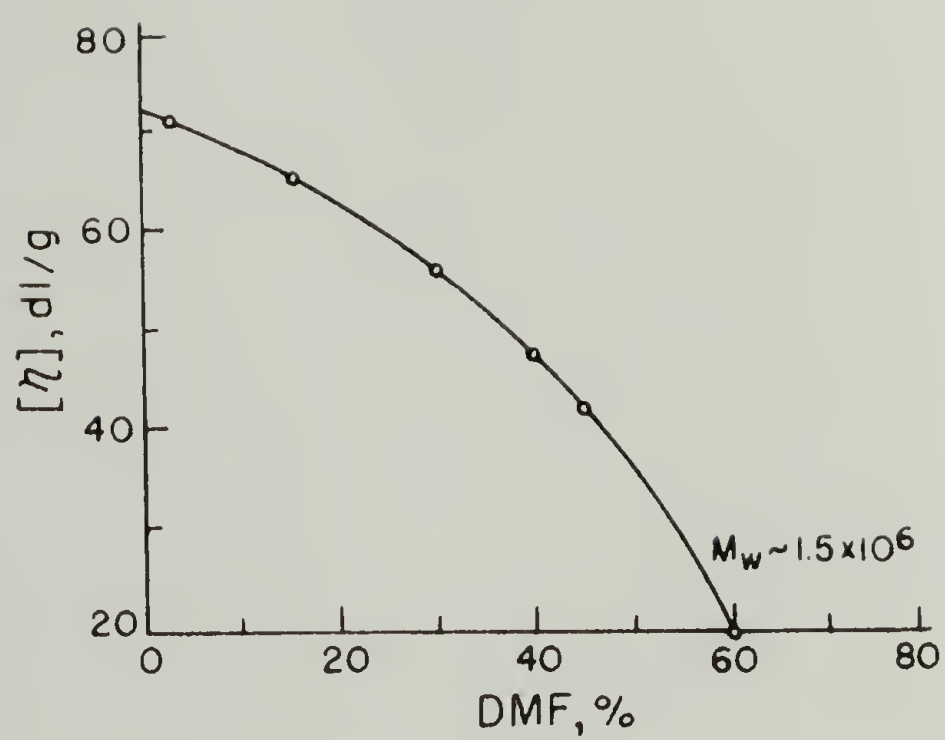


Figure 32. Intrinsic Viscosity of DNA in H<sub>2</sub>O/DMF Solutions, 0.1 M in LiCl, pH 7 at 14°C.

Observations of liquid crystalline order in concentrated solutions of rod-like solutes. Tobacco mosaic virus, TMV, is a rod-like particle with length 2800Å and diameter 150Å. In solutions of low ionic strength, the surrounding electrical double layer causes an increase in the effective diameter up to five-fold (66). Solutions of TMV at >2% concentrations separate into two phases as observed as early as 1937 by Bawden and Pirie (67). Bernal and Frankuchen (68) reported that suspensions of anisotropic solutions of TMV in isotropic solution can form spindle shaped tactoids since the interface acts as if it possessed an anisotropic surface tension. When the solution was made to flow rapidly through a tube, a reverse spiral pattern appeared when viewed between cross-polars. This effect was considered a consequence of a periodic change of orientation of the virus particles; see Figure 33.

When  $\alpha$ -helix forming synthetic polypeptides such as those enumerated in Table 2 are dissolved in sufficient concentration in helicoidal solvents such as doixane, chloroform and m-cresol, a process occurs which has been described by Frenkel (69) on the basis of low angle light scattering as consisting of four stages:

- (1) Formation of liquid spherulites
- (2) Oversaturation of liquid by spherulites leading to collapse
- (3) Orientational order begins to appear
- (4) Orientation order completely established

This spontaneous sequence takes up to 30 hours to form an optically anisotropic solution.

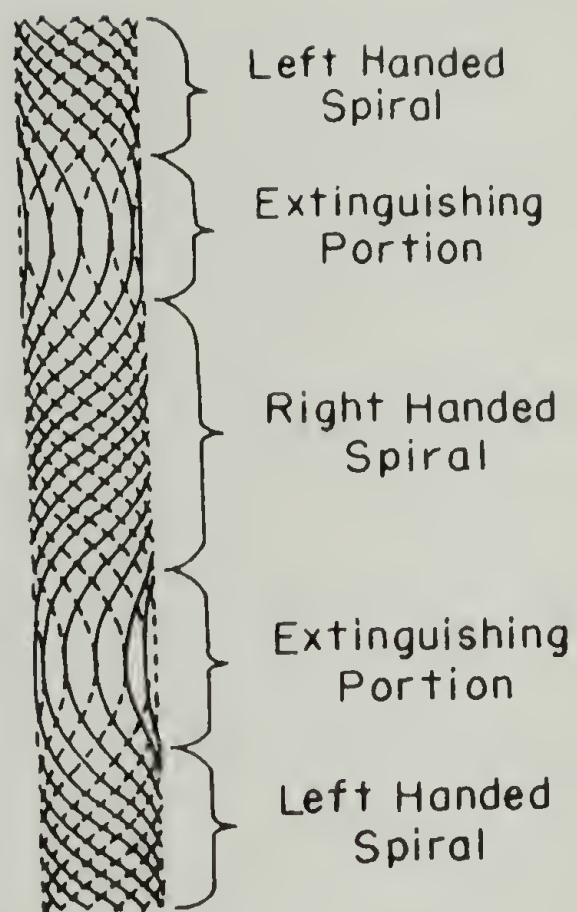


Figure 33. Reverse Spiral Arrangement in Tobacco Mosaic Virus Solution in Capillary Flow.



The concentration of PBLG at which the anisotropic phase first appears ("A-point") and that at which the solution becomes completely anisotropic ("B-point") as a function of molecular weight was determined by Robinson, Ward, and Beevers (70), both by optical measurement and by viscosity measurements. In the latter case the A-point was taken to be the peak in the viscosity vs. concentration curve; see Figure 34. These results were found to be independent of the choice of (helical) solvent. The predictions of the Flory theory were borne out qualitatively but the critical concentrations were somewhat over-estimated; see Figure 34. Periodic structures were visible even in un-polarized light which had large (100,000Å) and regular spacings (71). Solutions of single enantiomers of helix-forming polypeptides (i.e., all helices in the solution having the same optical rotary sense) were identified as cholesteric liquid crystals since these solutions were found to obey the theoretical expression derived by DeVries (72) for the high optical rotary power of cholesteric liquid crystals:

$$\theta = \frac{-\Delta n^2 P}{\lambda^2} \times 4.5 \times 10^4 \quad (24)$$

$\theta$  = optical rotation in deg/mm

$\Delta n$  = birefringence of the untwisted structure

$\lambda_0$  = wavelength of light in vacuum

P = pitch of the helices in microns

The pitch of the helices varied with temperature or concentration (73); see Figure 35.

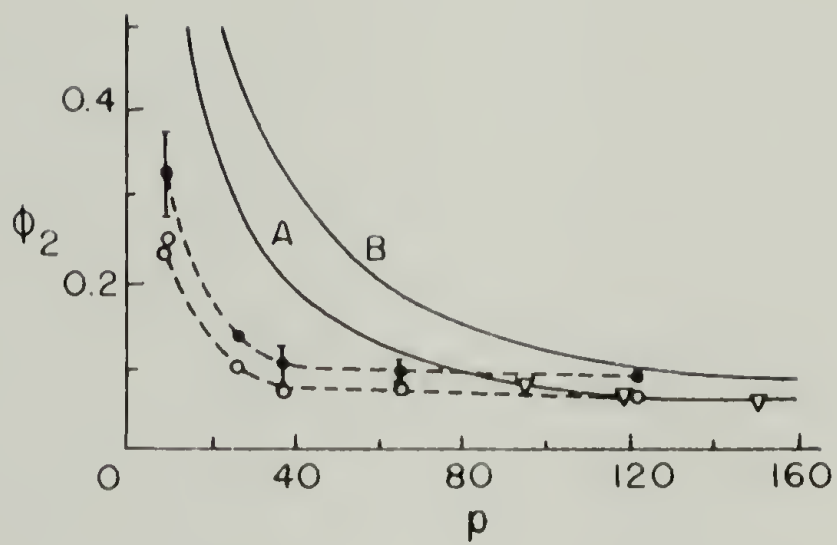


Figure 34. Comparison of Lines from Flory Theory with Experimental Determinations of A and B Points.  $\phi_2$  = PBIG Vol. Fraction;  $\rho = D.P. \times 1.5 \text{ \AA} / 15.5 \text{ \AA}$ .  $\circ$  A Points,  $\bullet$  B Points; Optical Measurements.  $\nabla$  Shear Rate Values for A Points. Solid Line is Flory Theory.

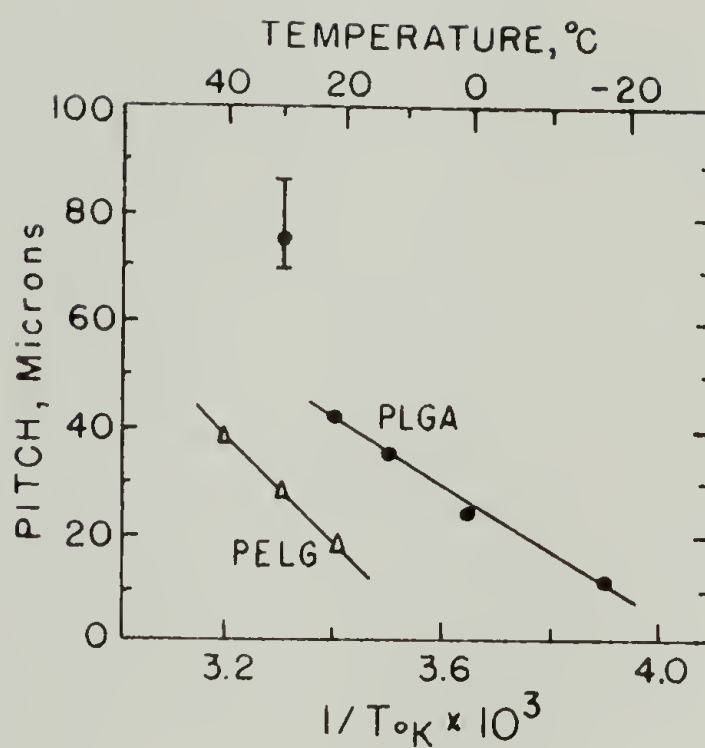


Figure 35. The Change in the Pitch of the Polypeptide Cholesteric Structure with Temperature. Liquid Crystals:  
 ● Molar Ratio of PLGA with respect to the Number of Monomer Units in the Polypeptide: DMF: H<sub>2</sub>O (1:6:5).  
 △ PELG-ethylacetate,  $\phi_2 = 0.3$ .

Solutions of equimolar mixtures of the D and L enantiomers of PBLG do not pack into the super-helices which give rise to cholesteric liquid crystals; see Figure 36. These solutions exhibit properties characteristic of nematic liquid crystals, including the "nemata" or thread-like structures. A nematic liquid crystal can also be produced from a cholesteric solution of PBLG by imposing a magnetic field which aligns the molecules and disrupts the macro-helices (74).

As discussed earlier, PBLG is denatured by dichloroacetic acid into a random coil configuration, but if the concentration is raised beyond 15g/100cc, an isothermal coil to  $\alpha$ -helix transition occurs and a cholesteric liquid crystal is obtained (63). Frenkel (65) reported that a 31% solution of PBLG in DCA undergoes an "orientational melting" at 71.5°C in which long range order disappears but optical anisotropy is not completely eliminated. At 95°C a second "melting" occurs and the solution becomes optically isotropic; however, the  $\alpha$ -helices still persist.

Ternary systems of PBLG in a helicoidal solvent plus a miscible non-solvent have been studied by Nakajima et al. (75) and Wee and Miller (76). The Flory theory was found to fit quite well both the ternary phase diagrams and the temperature-composition phase diagrams; see Figure 37.

Other examples of lyotropic polymer liquid crystals are systems in which polymer chain segments are capable of order in solution. Polymers such as polyphenyl methacrylic esters of oxybenzoic acids

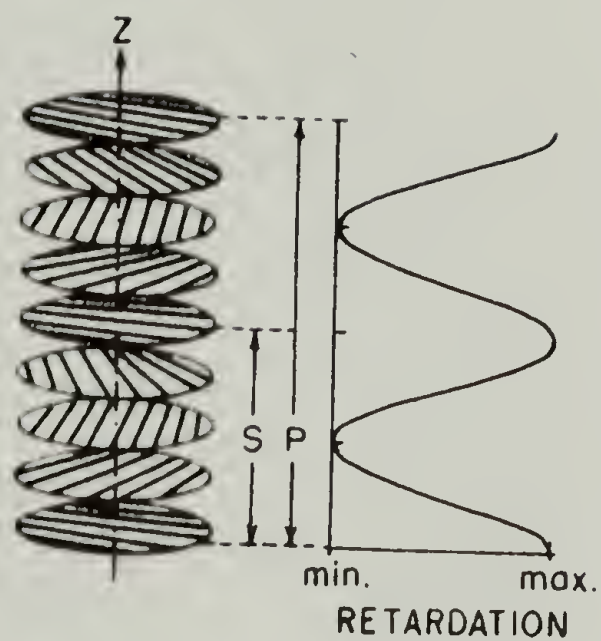


Figure 36. Cholesteric Supramolecular Structure.  $Z$  is the Optic Axis (axis of torsion),  $P$  is the Pitch and  $S = 1/2P$  is the Visible Periodicity. Polypeptide Molecules are Represented by the Parallel Lines.

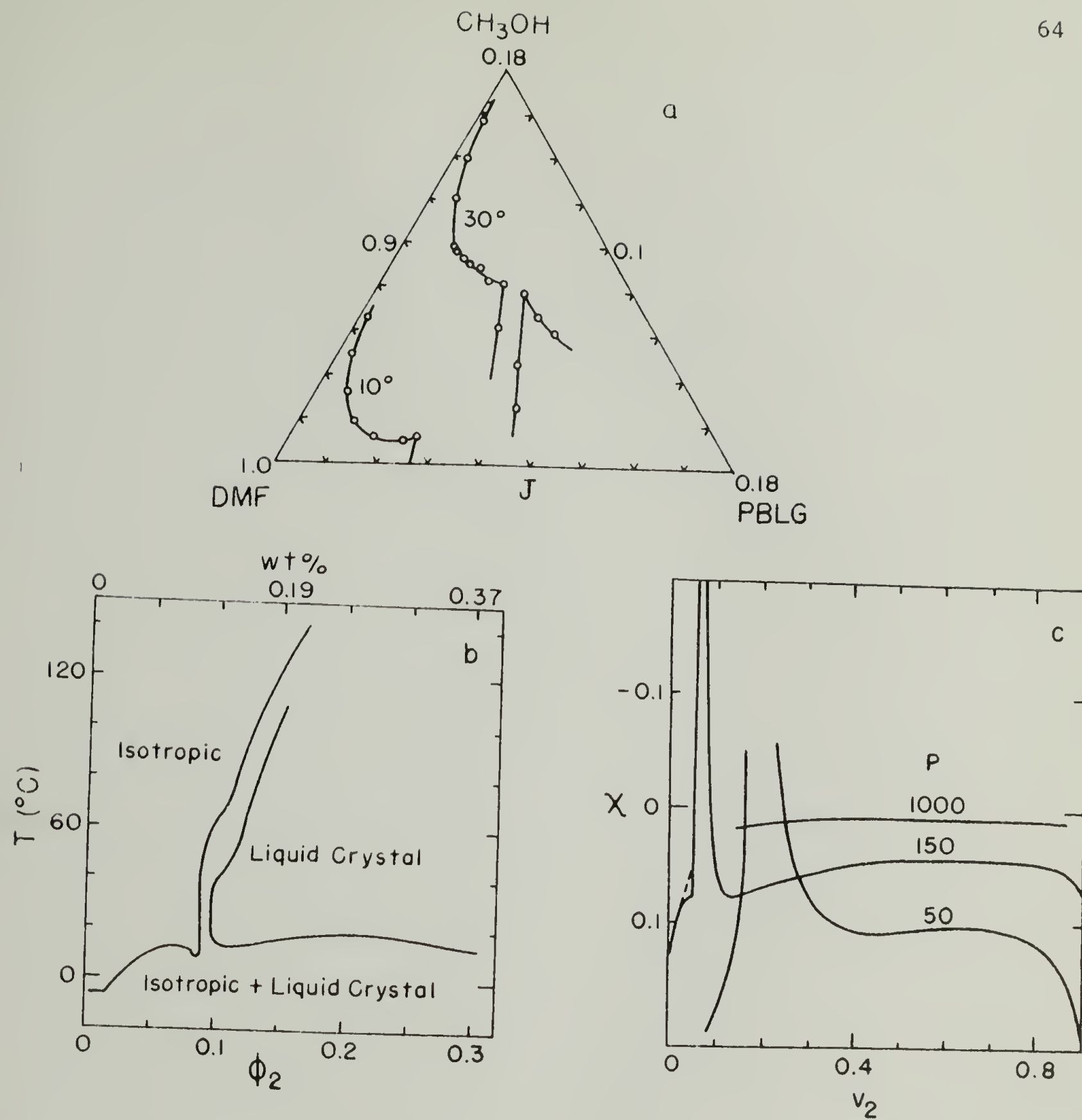
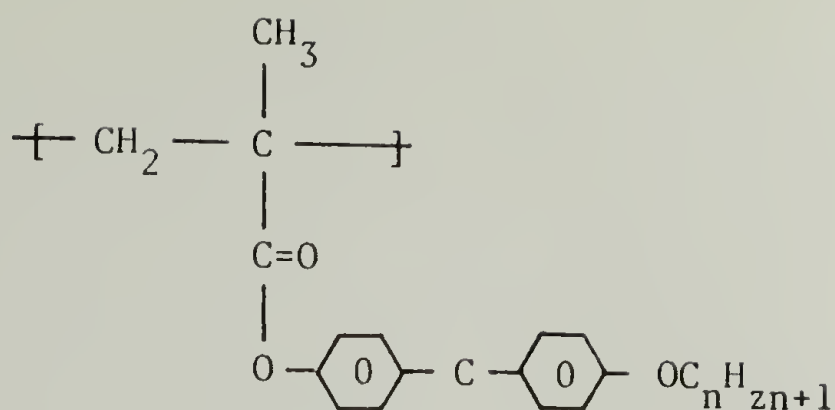


Figure 37. (a) Turbidity Points for the System PBLG-DMF-CH<sub>3</sub>OH at 10 and 30°C. Solid Line Calculated from the Flory Model. (b) Phase Diagram for PBLG ( $M_w$  310,000) Equilibrium Line Bounding the Liquid Crystal Phase was Determined by NMR; Line Bounding the Isotropic Phase was Determined by Polarizing Microscope. (c) Flory Phase Diagram as a Function of Axial Ratio  $p$ . For  $p = 150$  Dashed Portion Results from Assuming Equilibrium Degree of Disorientation as Unity. Only the High Concentration End of  $p = 1000$  Diagram is shown.



were investigated by Tsvetkov (77) and were found to exhibit intramolecular orientational order due to sidegroup formation of nematic liquid crystals.

If block copolymers are dispersed in a non-solvent for one of the blocks, such as polystyrene/polyethylene oxide in dibutyl phthalate/styrene, the insoluble blocks aggregate in parallel layers. The structures formed can be dispersed by agitation, but gradually reform. Two types of structures were identified by Skoulios and Finaz (78), a cylindrical structure and a leaf-like structure. Sadron (79) obtained a micellar structure which could be preserved by polymerization of the styrene in the solvent.

Systems have been reported which are not liquid crystalline per se but which require the aid of a solvent to form three-dimensional crystalline structures. For example, films of poly(2,6-dimethyl-1,4 phenylene) oxide (commonly known as "polyphenylene oxide") cast from chloroform are non-crystalline but upon exposure to  $\alpha$ -pinene or tetraline formed spherulites (80). Upon drying of the films, the spherulites collapsed again. Frenkel and Ginsburg (81) observed that annealing in formic acid vapor was required to crystallize amorphous poly-2-2'-octamethylene-5,5' dibenzimidazole, and

concluded that the role of the formic acid was to form a crystallizable polymer-solvent complex.

Flow properties of concentrated solutions of rod-like molecules.

Microcrystals of cellulose can be obtained by hydrolysis with strong sulfuric acid. Depending on the source, these microcrystals are rod-like with length dimensions ranging from 2000-4000 $\overset{\circ}{\text{A}}$  and lateral dimensions of 150-160 $\overset{\circ}{\text{A}}$  by 40-50 $\overset{\circ}{\text{A}}$  (82). These microcrystals are susceptible to lateral association but ultrasonic treatment is effective in breaking up aggregates (83). Addition of salt to dilute aqueous suspensions produces several types of precipitate, depending on cellulose type and NaCl concentration. One type of precipitant is birefringent (84). At higher concentrations of cellulose, the interparticle attractions act like weak crosslinks, causing gel formation.

The elasticity and flow properties of such gels were studied by Hermans (84,85). The shear modulus was found to vary with  $C^{3.5}$  which differs from the first power prediction for a network of rods in which the number of links per rod is large (86). In order to reconcile these results with the known propensity of cellulose microcrystals for parallel aggregation, a model was proposed in which cross-linking occurs by the forking and rejoining of sheaflike aggregates; see Figure 38A, so that the number of crosslinks is small compared to the number of rods. This model also accounts for the peculiar yield stress behavior of the gels. Gels which had a history of shearing at less than  $0.5 \text{ S}^{-1}$  exhibited a low yield stress but gels



with a higher prior shearing (e.g.,  $80 \text{ S}^{-1}$ ) exhibited a higher yield stress; see Figure 39. This was explained by postulating the formation of an oriented gel; see Figure 38B, in which the orientation produced by shearing is retained after the cessation of shear. Shear rates around  $0.5 \text{ S}^{-1}$  are insufficient to produce this oriented gel and consequently do not change the yield stress. Shear stress versus shear rate curves are shown in Figure 40. At constant shear rate, viscosity increased regularly with concentration.

Fibrinogen is a globular protein with an aspect ratio of 31.0 and molecular weight of 339,700. Kovinski and Kizior (87) found that at a concentration of 21 wt% of fibrinogen in water a nematic liquid crystal was formed (no evidence of optical rotation) in reasonable agreement with the Flory prediction. The viscosity-concentration correlation shown in Figure 41 follows the pattern which will be shown to be typical of solutions of rigid rods in the region of the isotropic-anisotropic transition. The point of discontinuity in this curve occurs at the same concentration as that of the isotropic-anisotropic transition observed at zero shear by birefringence. Note in Figure 41 that increasing the shear stress causes the discontinuity to occur at a lower viscosity due to the shear thinning effect and also at slightly lower concentration as shear-induced orientation of the isotropic solution reinforces the space-filling effects which lead to spontaneous formation of anisotropic solutions (c.f. the prior discussion of Frenkel).

PBLG in solutions of helicoidal solvent constitute an ideal model system for the study of flow properties of anisotropic solutions

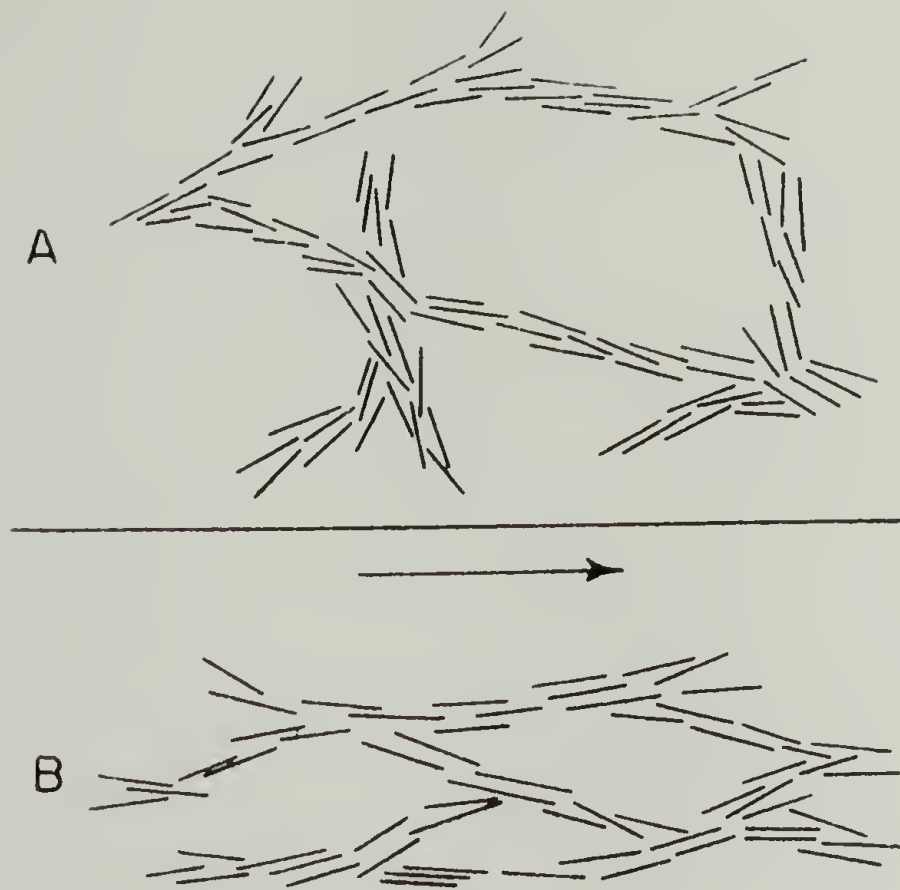


Figure 38. Model for Networks of Cellulose Microcrystals Formed by Almost Parallel Aggregation of Rodlike Particles. A. Gel in Which Aggregates are Oriented at Random. B. Gel in Which Aggregates have a Nearly Parallel Orientation from a Shearing Motion Applied Before Gel Allowed to Set.

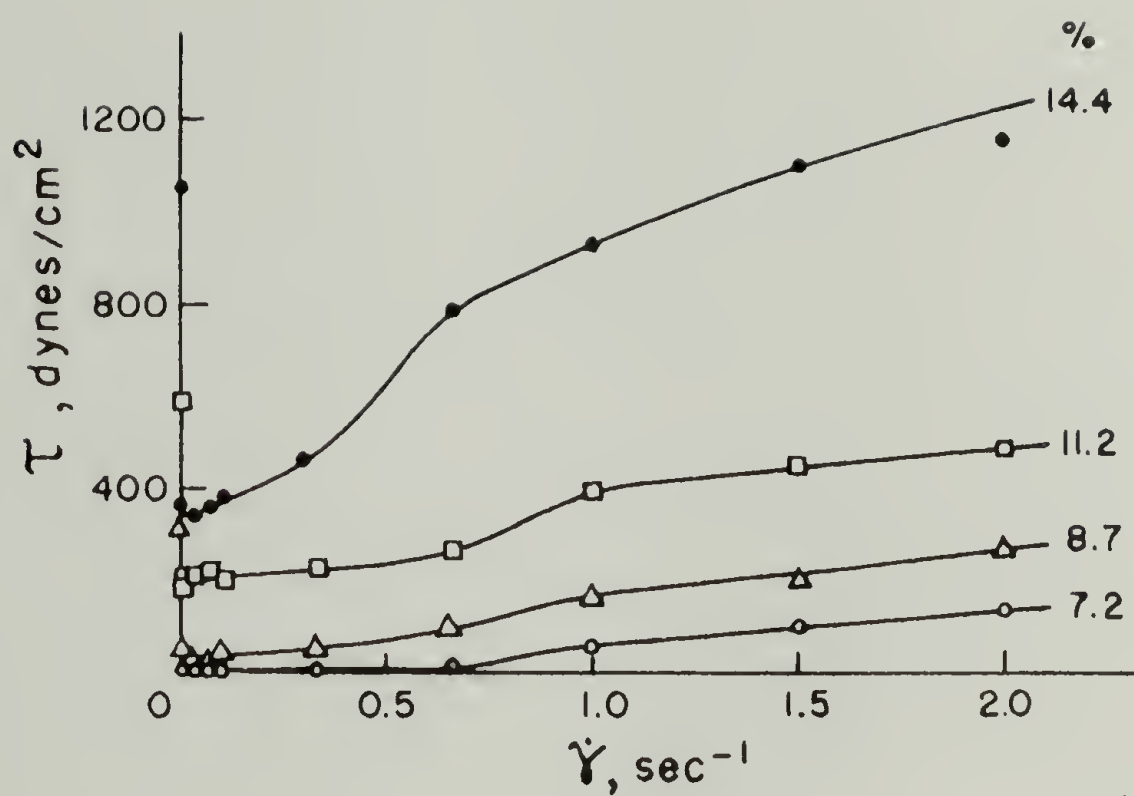


Figure 39. Flow Curves for Gels of Cotton Cellulose Microcrystals of Different Concentrations.

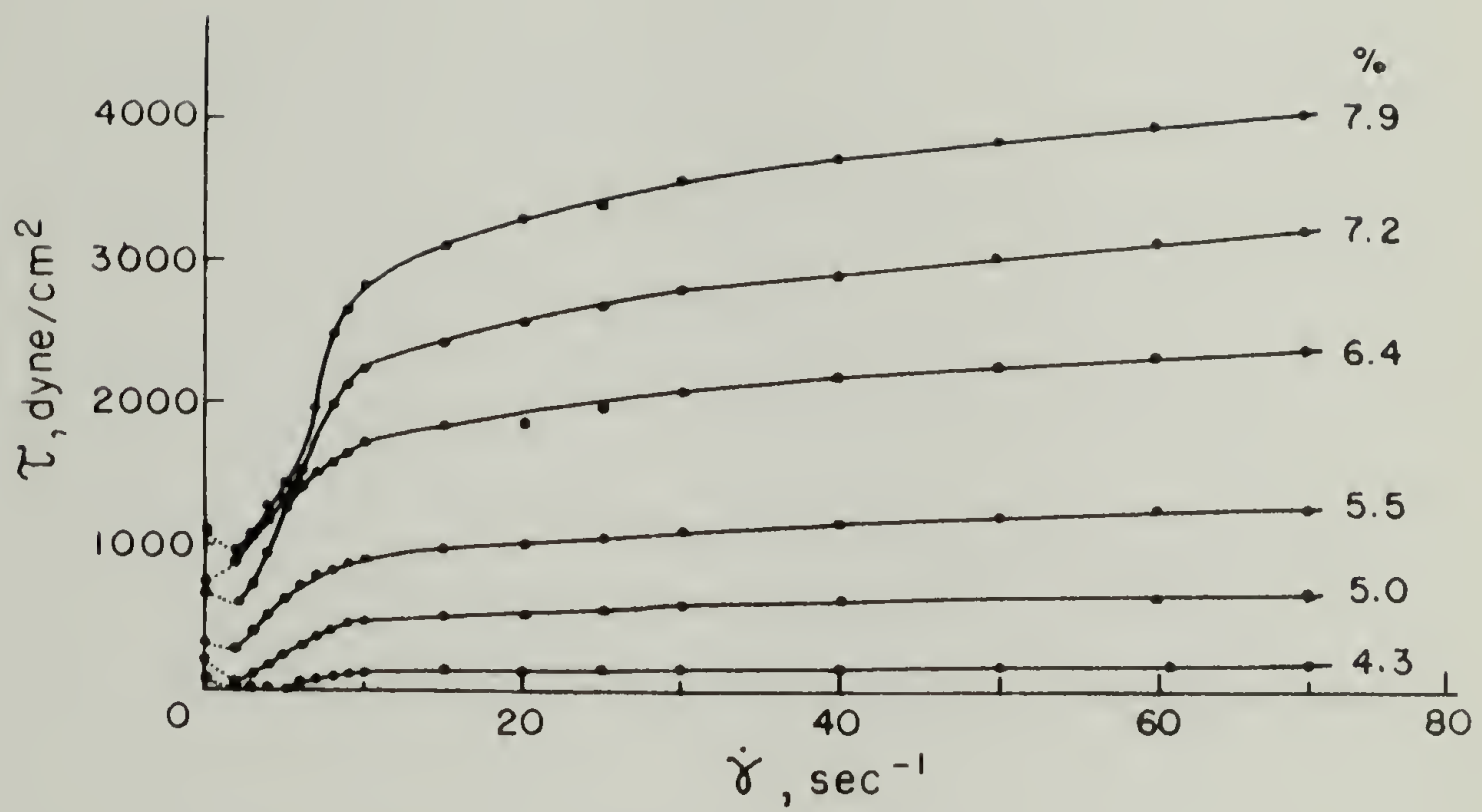


Figure 40. Flow Curves for a Dilution Series of a Gel Containing Microcrystals Prepared from Wood Level-off DP Cellulose Gel.

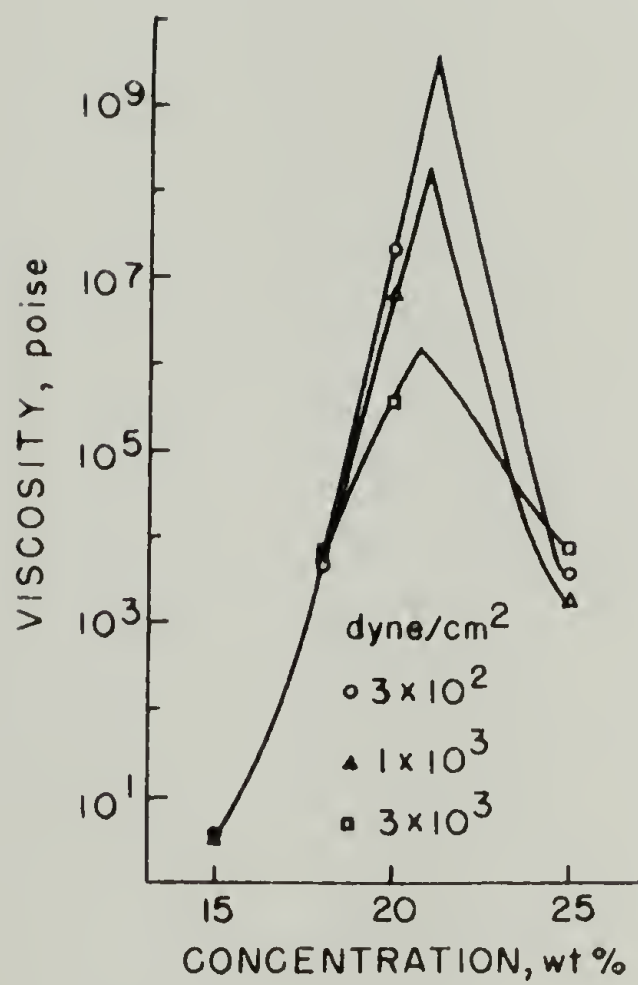


Figure 41. Viscosity of Fibrinogen Solutions.

for the reasons mentioned in the section dealing with non-Newtonian viscosity and also because of its widespread use in other studies of anisotropic solutions. Hermans (88) chose to study PBLG in m-cresol (possibly because many other helicoidal solvents are too volatile to allow confidence in concentration values). Figure 42 shows viscosity vs. concentration data for three molecular weights of PBLG. The viscosity drops dramatically upon formation of the anisotropic phase because a lower shear stress is required to orient the anisotropic phase than to orient individual molecules in the isotropic phase (89). The effect of shear rate on this process is illustrated schematically in Figure 43; supporting data are in Figure 44. Note that the discontinuity in  $\frac{\eta_{sp}}{C}$  vs.  $C$  shifts with shear to lower concentrations and is made less prominent, disappearing completely by  $\tau = 5 \times 10^3$  dyne/cm<sup>2</sup>. This indicates that the ordering induced at this level of shear stress is approximately the same as that produced by space-filling requirements at concentrations greater than the critical concentration.

Ordering in the anisotropic solutions is not perfect as is indicated by two lines of evidence. First, the viscosity versus concentration curve peaks but does not drop discontinuously; that is, viscosity continues to drop with concentration after the break point indicating that the statistical ordering becomes yet more perfect. Secondly, there is a shear dependence of viscosity for the anisotropic solutions which indicate that shear-induced orientation can enhance the order in the anisotropic solution.

Hermans also compared the volume fraction at which phase separation occurs (from the viscosity data) versus  $p$ , axial ratio (using

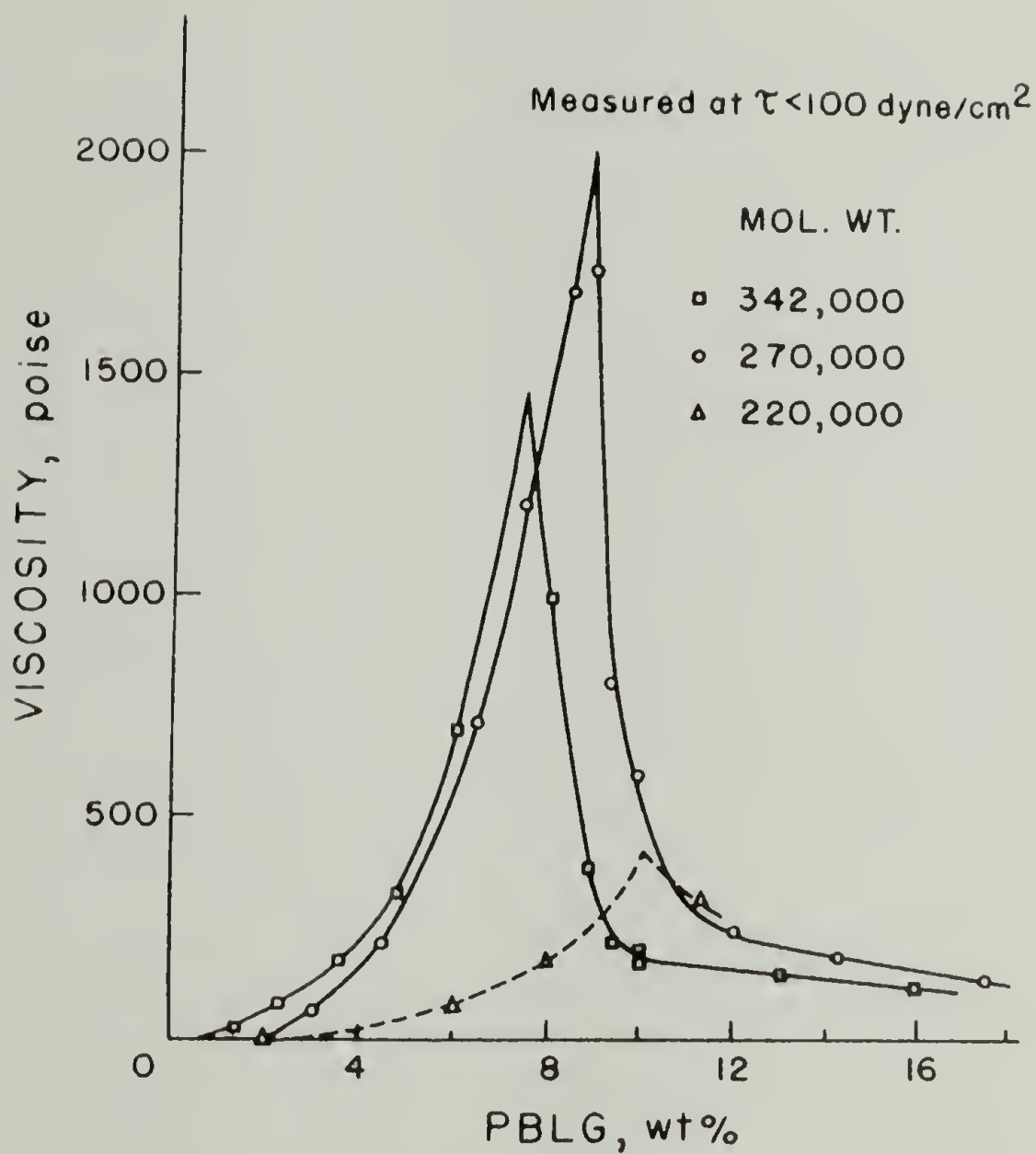


Figure 42. Viscosity of Poly- $\gamma$ -Benzyl-L-Glutamate in *m*-Cresol.

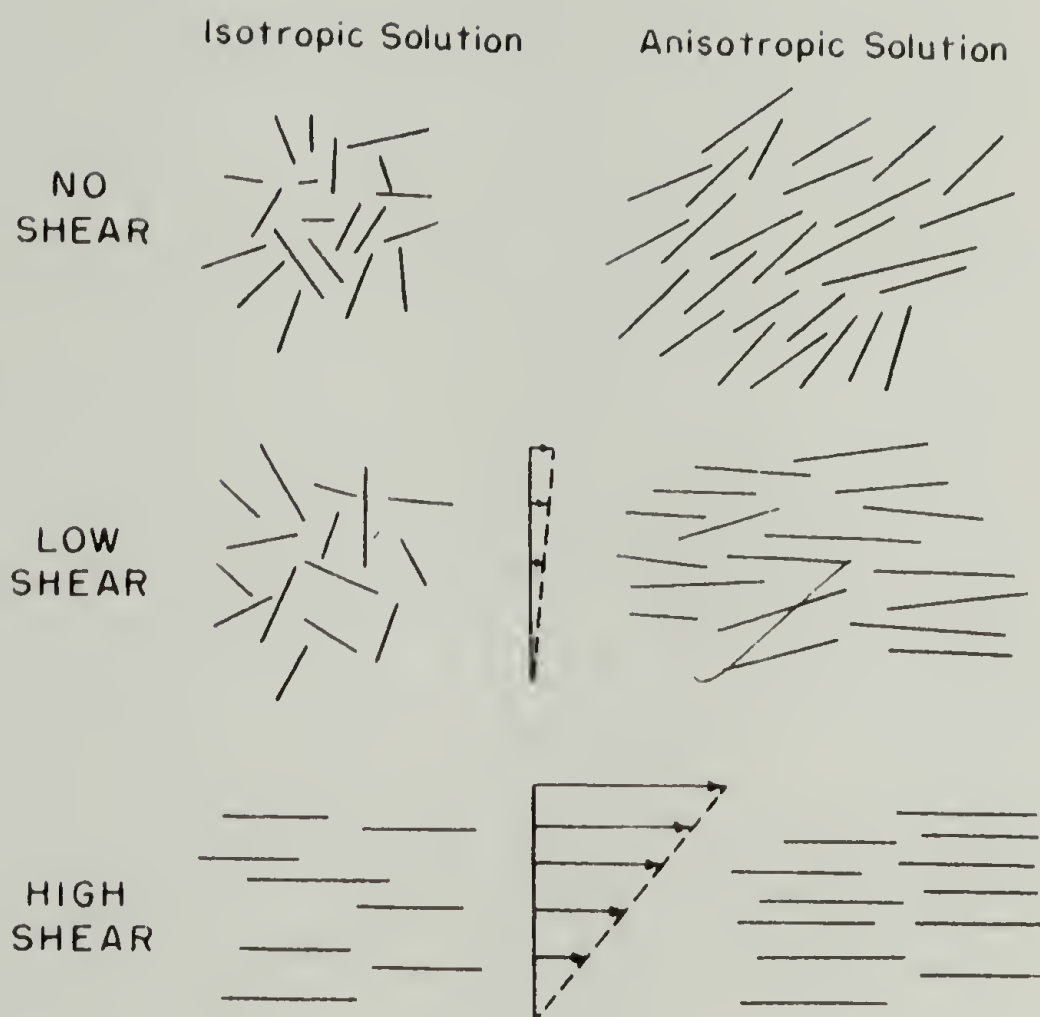


Figure 43. Schematic Representation of the Configuration of the Solutions at Rest and at Two Shear Rates.



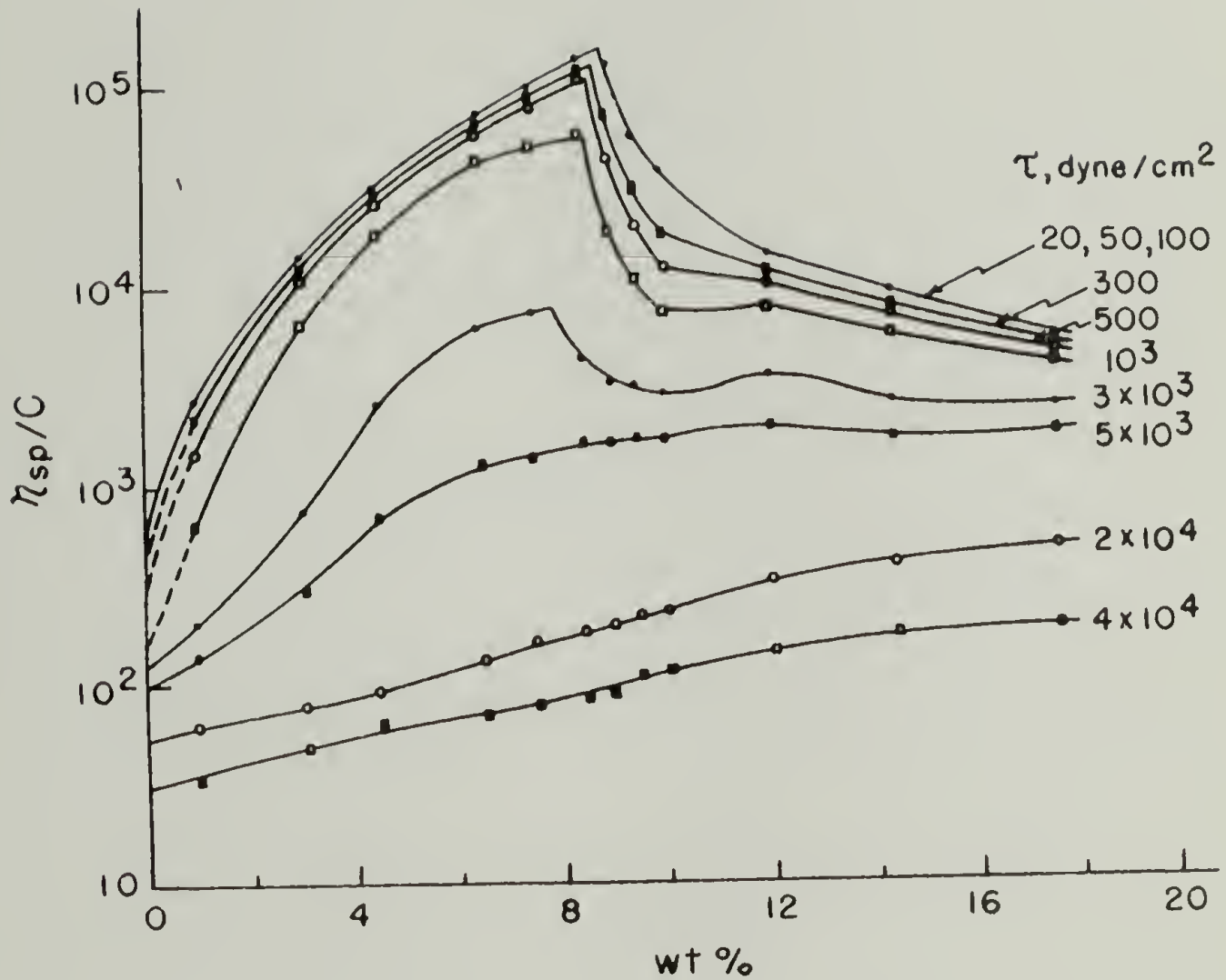


Figure 44. Solutions of PBG in m-Cresol, Plotted as  $\log(\eta_{sp}/c)$  Versus Concentration, at Various Shear Stresses.

for PBLG  $D.P. = \frac{M}{219}$  and  $p = .0968DP$  where  $M$  = molecular weight;  $D.P.$  = degree of polymerization), with the Flory theory. He got excellent agreement for the three molecular weights studied, see Figure 45.

Iizuka (90) performed similar studies on poly- $\gamma$ -ethyl-L-glutamate in 1,4-dioxane and  $CH_2Br_2$  and on equimolar mixtures of PELG and PEDG in  $CH_2Br_2$  as well as on PBLG in dioxane and  $CH_2Br_2$ . Results for all three systems were similar, showing identical A-points and also showing shoulders on the high concentration side of the  $\frac{\eta_{sp}}{C}$  vs.  $C$  curves, attributed to a predicted region of coexistence for isotropic and anisotropic phases. The reduced viscosity became constant at a concentration corresponding to the B-point; see Figure 46. The dynamic elastic modulus,  $G'$ , at constant frequency versus concentration showed the same features as reduced viscosity except that it started to rise sharply again after the B-point rather than remaining constant; see Figure 46. The viscosity measurements were made in a cone-and-plate instrument which gave lower and more homogeneous shear rates than the capillary results of Hermans. The dynamic shear storage and loss moduli were reported over about two decades of frequency; see Figure 47. The data were not analyzed save for a comment that the increase in storage and decrease in loss moduli with increasing frequency were more noticeable in the isotropic than in the anisotropic solutions.

Normal stresses were also measured by Iizuka (91); see Figure 48, and converted to the extinction angle,  $\chi$ , by the use of an equation given by Timoshenko (92):

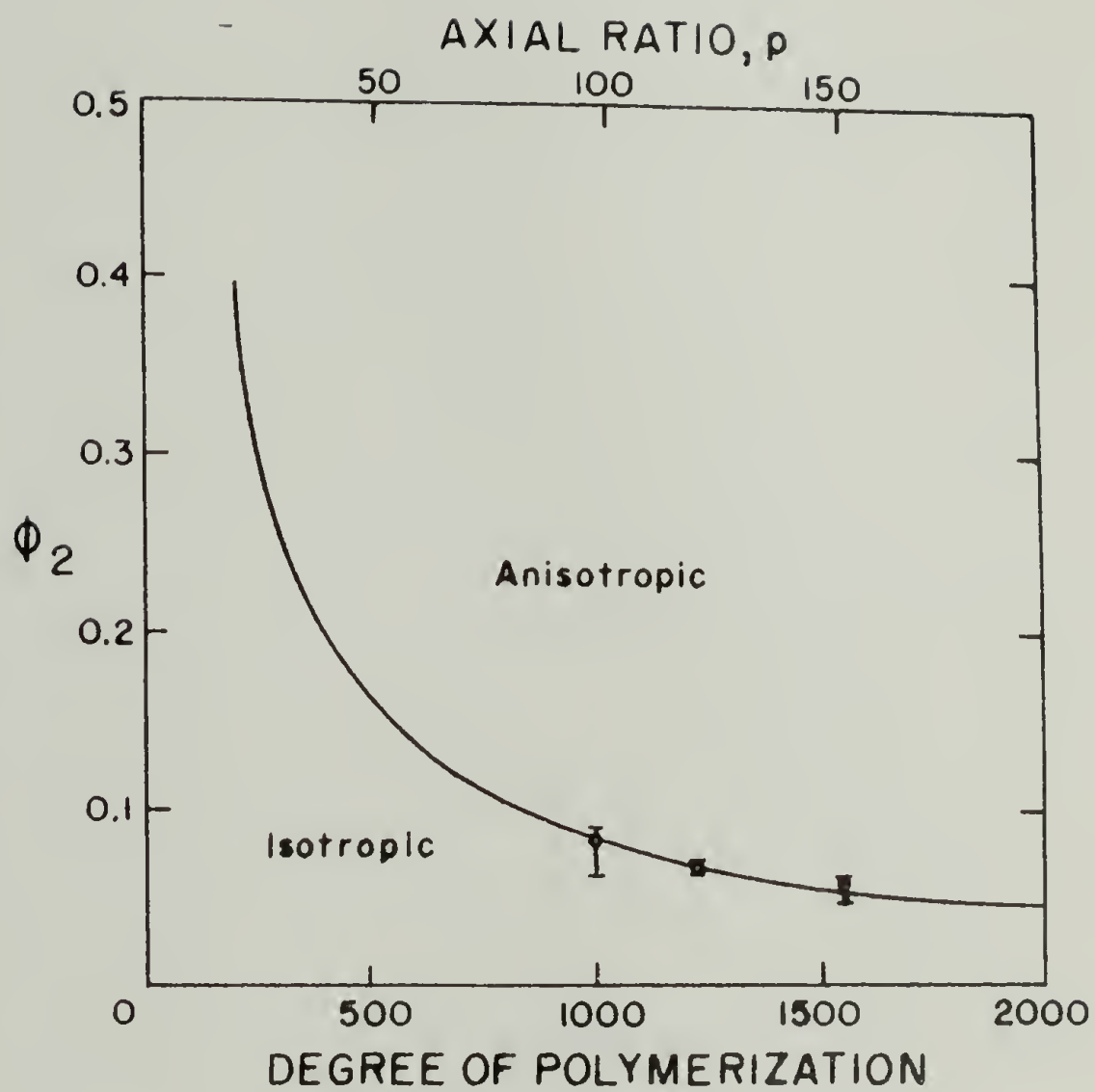


Figure 45. Volume Fraction of Solute at Isotropic-Anisotropic Transitions Versus Degree of Polymerization. Solid Line is Flory Theory.

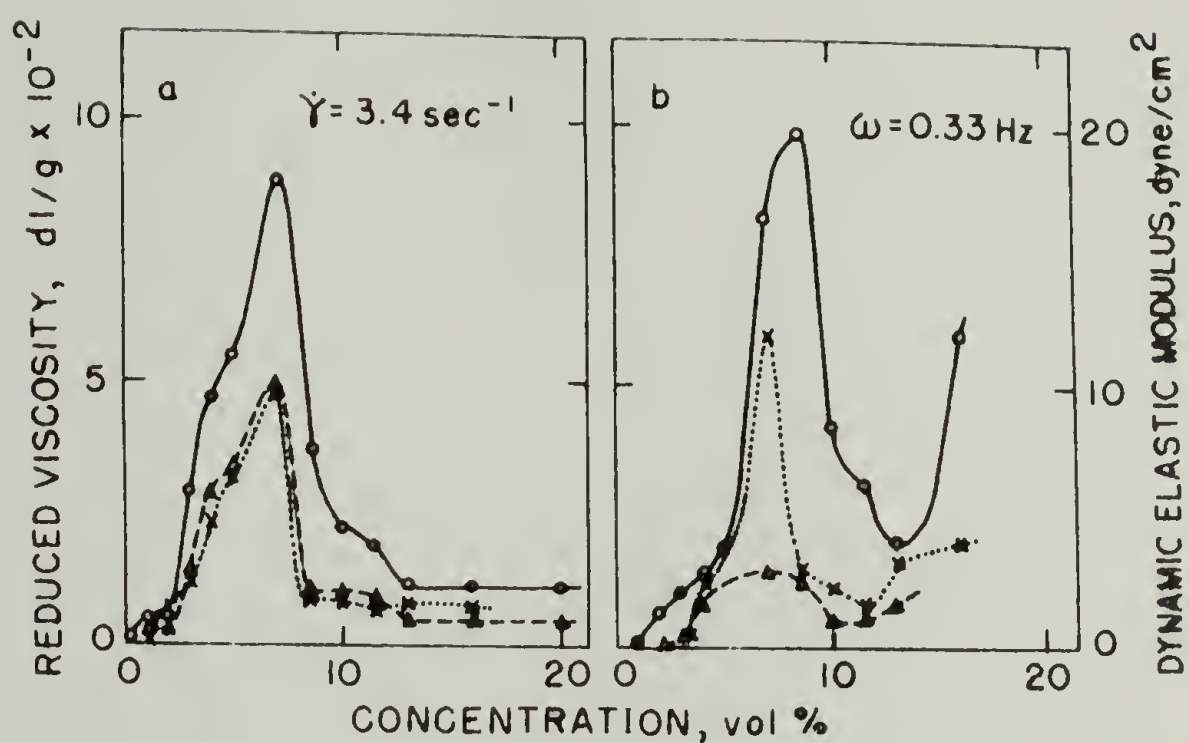


Figure 46. (a) Reduced Viscosity Measured at  $\dot{\gamma} = 3.4 \text{ sec}^{-1}$  Versus Polymer Concentration. (b) Dynamic Elastic Modulus Measured at  $\omega = .33 \text{ Hz}$  Versus Polymer Concentration. Full Line - PELG in 1,4 Dioxane; Dashed Line - PELG in CH<sub>2</sub>Br<sub>2</sub>; Dotted Line - PELG and PEDG in CH<sub>2</sub>Br<sub>2</sub>.

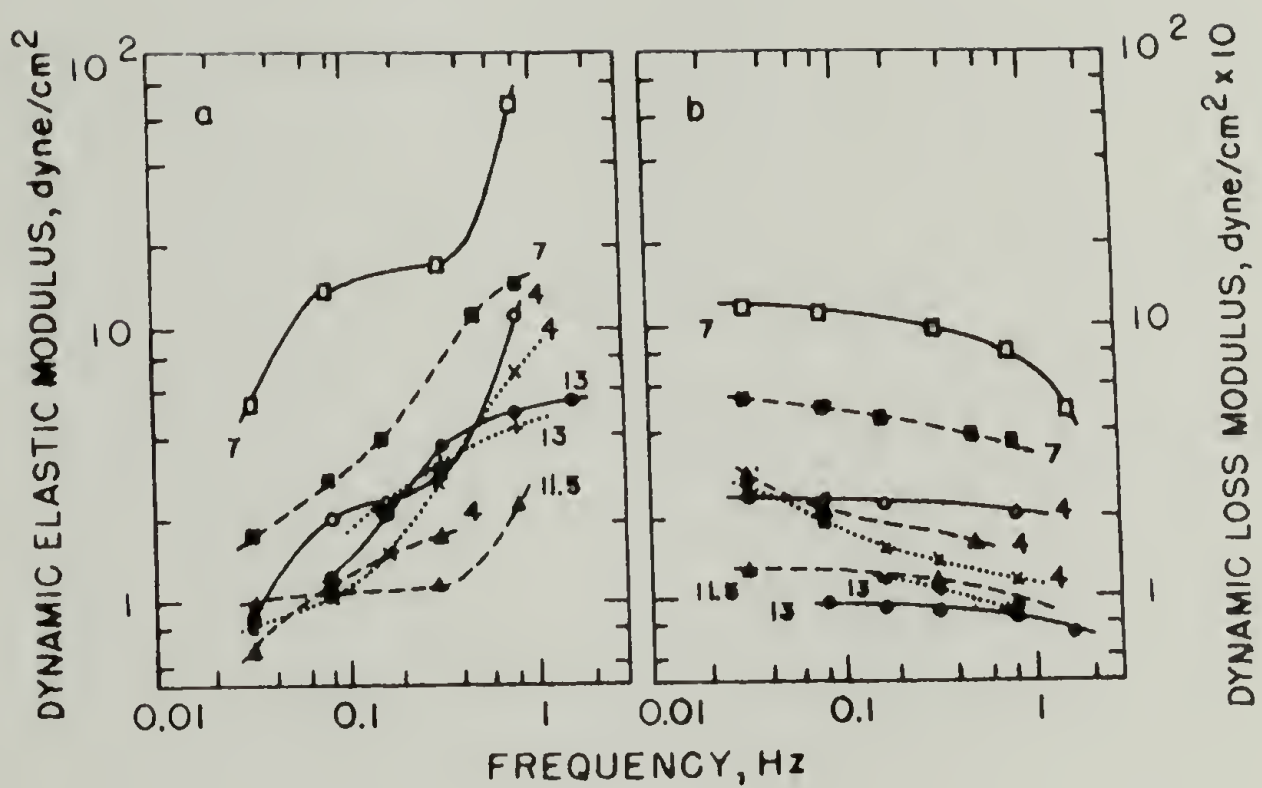


Figure 47. Dynamic Properties vs. Frequency Relationships. Measured at a Frequency of .33 Hz. Lines same as in Figure 46. Amplitude of the Oscillatory Motion of the Plate of the Rheometer was 0.93°. Numbers are Volume Concentration.

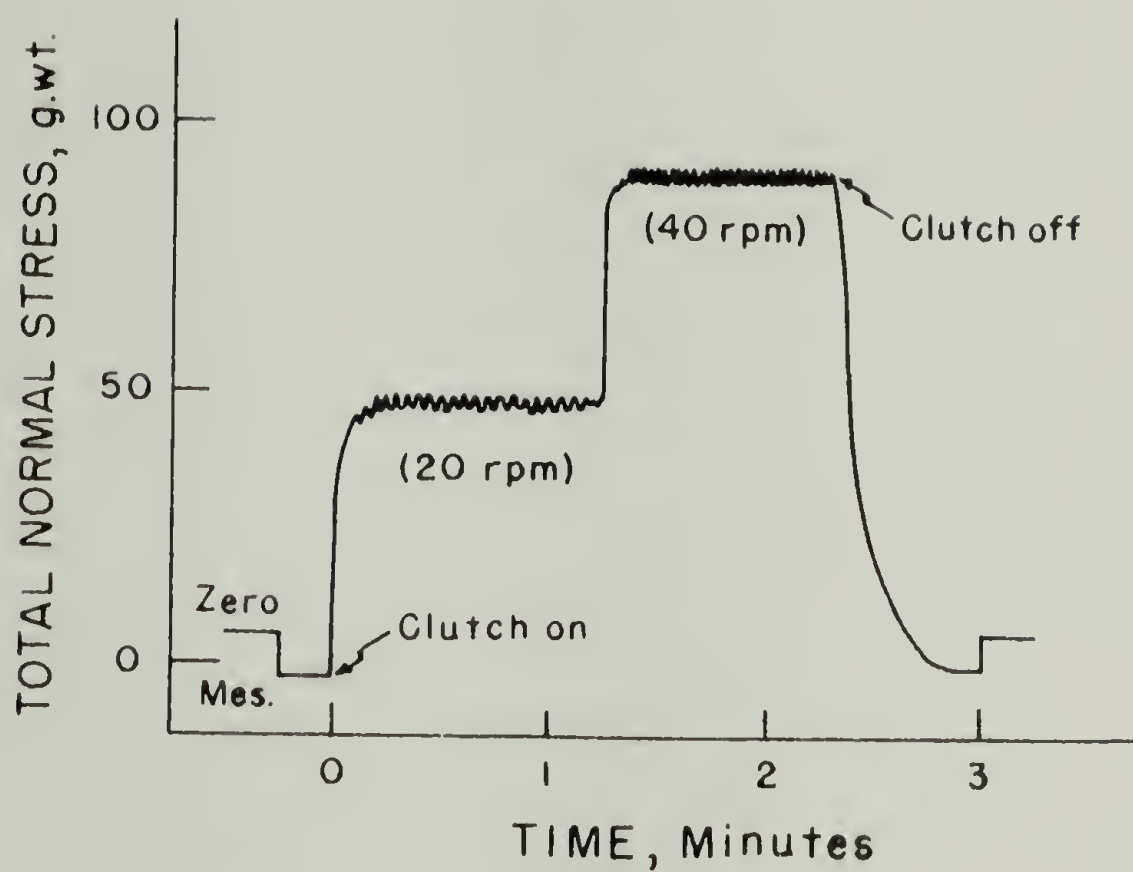


Figure 48. Typical Weissenberg Effect for 10 Vol. % of PBLG in Dioxane at 22°C. Cone Angle 1.76° and Diameter 6 cm.

$$\cot^2 \chi = \frac{F}{\pi R^2} \eta \dot{\gamma} \quad (25)$$

F = total normal stress

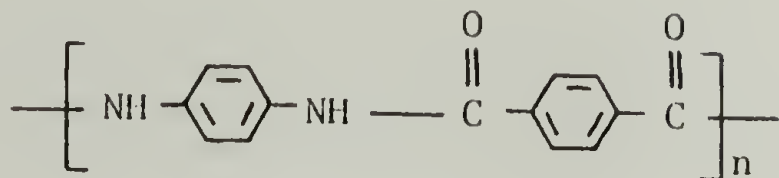
R = radius of plate and of cone

$\eta$  = solvent viscosity

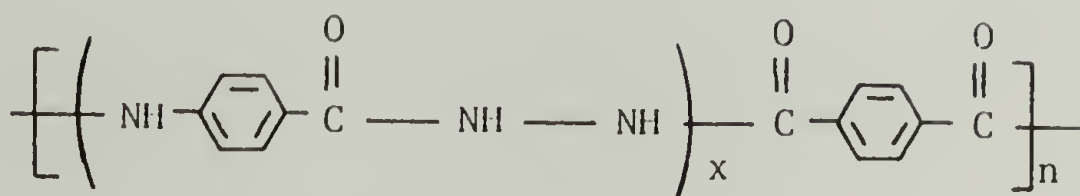
Scheraga's tables relating  $\chi$ ,  $\dot{\gamma}$  and  $\theta$  were then used by Iizuka in conjunction with Perrin's equation relating ellipsoid length and aspect ratio to  $\theta$  (both of these works are referenced above) to calculate particle length. The value obtained for isotropic solutions was longer than the known molecular length, and this value increased further in liquid crystalline solutions. From this Iizuka inferred the existence of well defined molecular clusters. Note, however, that the Perrin equation assumes non-interference of the ellipsoidal particles and may thus be suspect in this application.

The macromolecules which have been dealt with to this point have been amenable to modeling by rigid rods as a consequence of their secondary structure, i.e.,  $\alpha$ -helix for synthetic polypeptides, double helix for D.N.A., triple helix for collagen, micro-crystals for cellulose, etc. There exists an additional class of polymers which can be considered rod-like by virtue of their primary structure. Chain units include linear chain units (e.g.,  $\begin{array}{c} \text{H} \quad \text{H} \\ | \quad | \\ -\text{N} - \text{N}- \end{array}$ ), hindered chain bond rotations, backbone unsaturation, para-substituted cycloaliphatic and para substituted aromatic groups in the backbone. Most polymers studied among this group have resulted from commercial motivations which will be touched upon later. They have been predominantly the

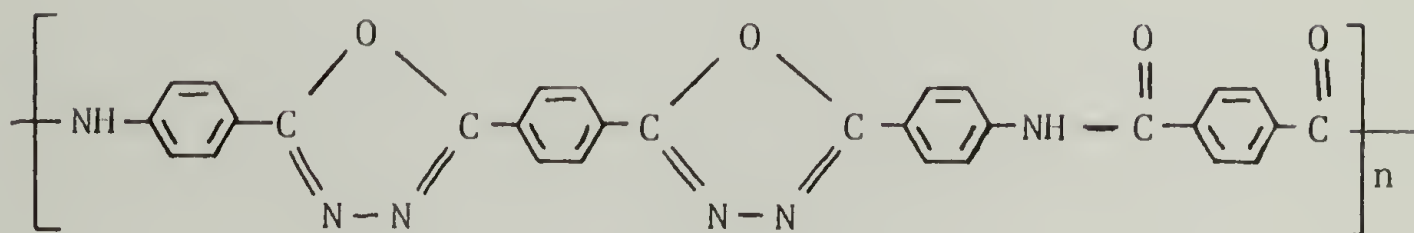
para aromatic polyamides. Examples are poly-parabenzamide (PBA), poly-para-phenylene terephthalamide (PPT)



para-polyamide hydrazides



and para 1,3,4 oxadiazole diamines



These polymers have little freedom of rotation because of the stiffness of the phenyl group, resonance effects enforcing the planarity of the peptide groups and the phenyl groups, and the absence of free rotation about the phenyl-carbonyl bond and the phenyl-nitrogen bond.

A limiting property of these polymers is that solution is achieved only by use of powerful and exotic solvents such as concentrated sulfuric acid, dimethyl sulfoxide (DMSO), or N,N-dimethylacetamide (DMAC) plus LiCl. Addition of up to 5% LiCl to DMAC improves solubility because of complex formation similar to that observed with low molecular weight model amides (93,94). Aromatic polyamides are often synthesized by solution polymerization in DMAC



and once removed from solution are difficult or impossible to redissolve.

The formation of anisotropic solutions has been observed for these rod-like polymers. Birefringence has been reported in concentrated spinning dopes and in fact is cited as a distinguishing feature of solutions of such polymers in patent claims (95,98). Nematic liquid crystalline order in a 10% solution of PPT was revealed by x-ray diffraction (96). Anisotropic solutions of PBA in DMAC at concentration just exceeding the critical value were found to undergo reversible nematic-isotropic transitions with temperature (97). A phase diagram of a ternary system of polymer-solvent-nonsolvent showing the stability range of the anisotropic phase was also presented.

The behavior of these stiff polyamides follows the pattern previously illustrated with viscosity increasing rapidly until the formation of the anisotropic phase and then decreasing. This behavior is also cited in a patent claim as a distinguishing feature of anisotropic spinning dopes (98); see Figure 49. Also reported in this patent are critical concentration versus aspect ratio (expressed in terms of inherent viscosity which is directly related to molecular weight); see Figure 50, and phase diagrams outlining the regions of existence of solid, isotropic fluid and anisotropic fluid as concentration of polymer and strength of sulfuric acid solvent were varied; see Figure 51.

Slight shear thinning was found for a solution of polyamide hydrazide of  $\overline{M}_w = 62,000$  in DMSO at a concentration of .05 g/dl but

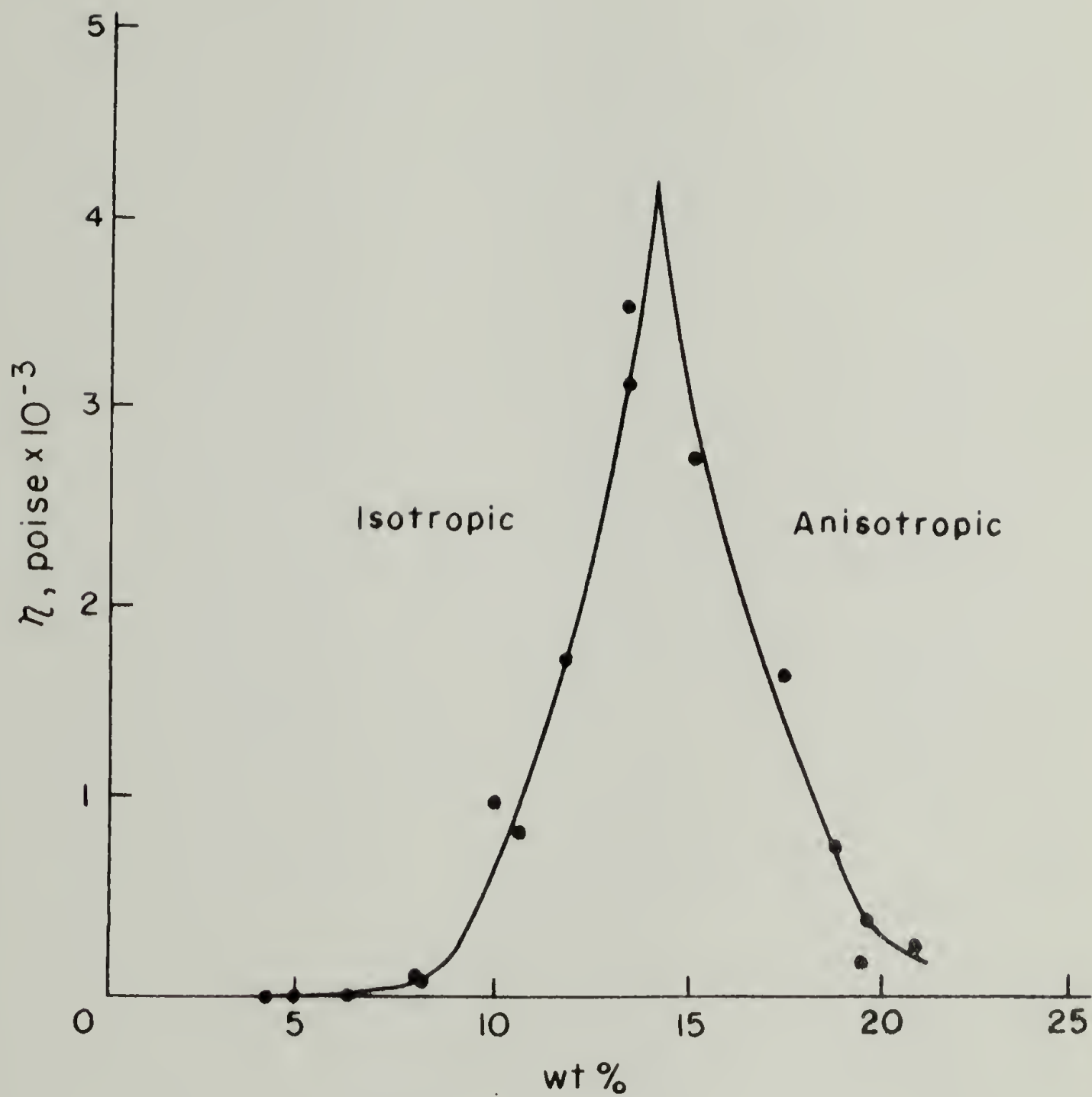


Figure 49. Viscosity Versus Concentration for Poly(p-Benzamide) in Hydrofluoric Acid.

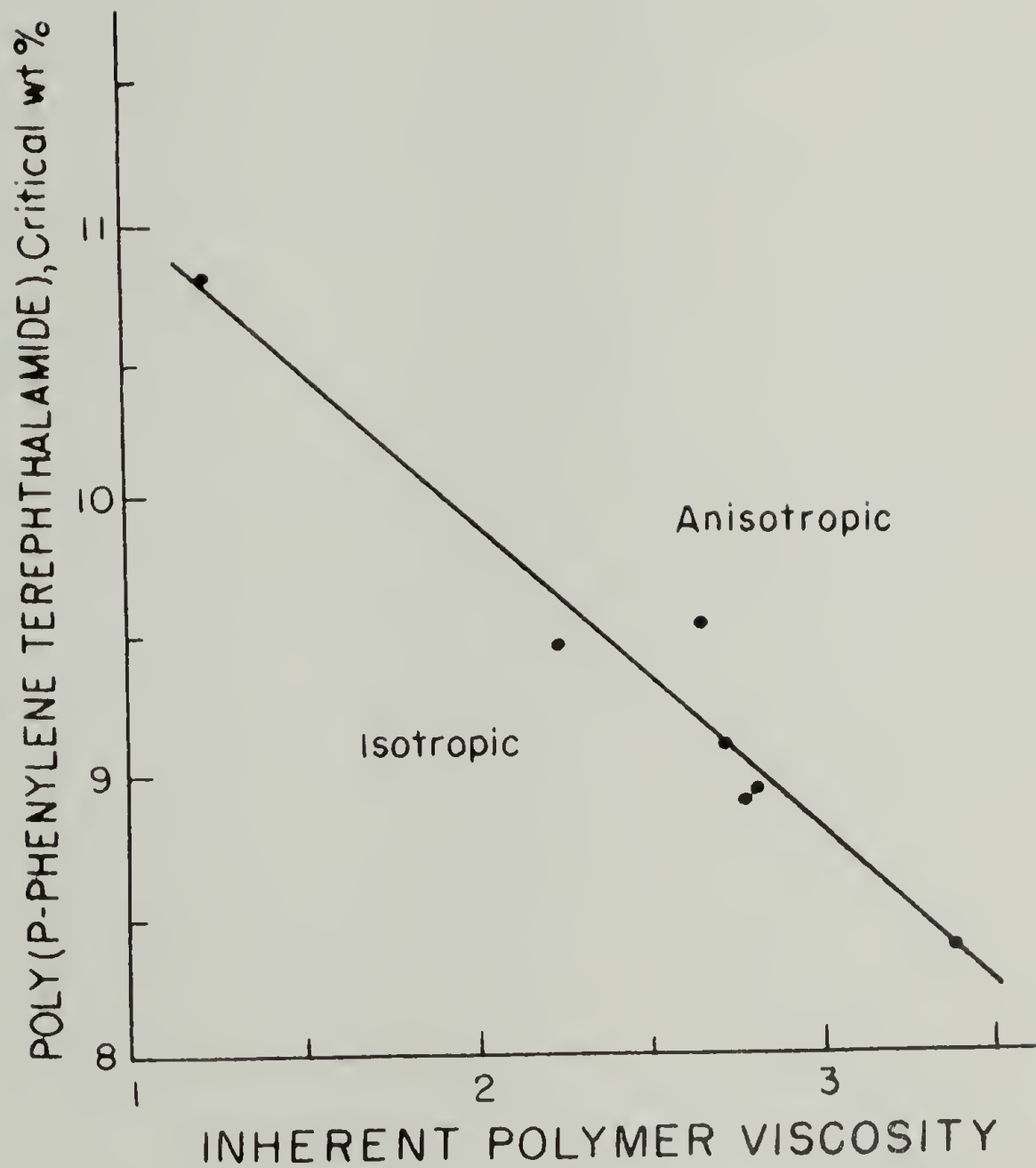


Figure 50. Critical Concentration for Formation of Anisotropic Phase Versus Molecular Weight (as Measured by Inherent Viscosity), for PPT.

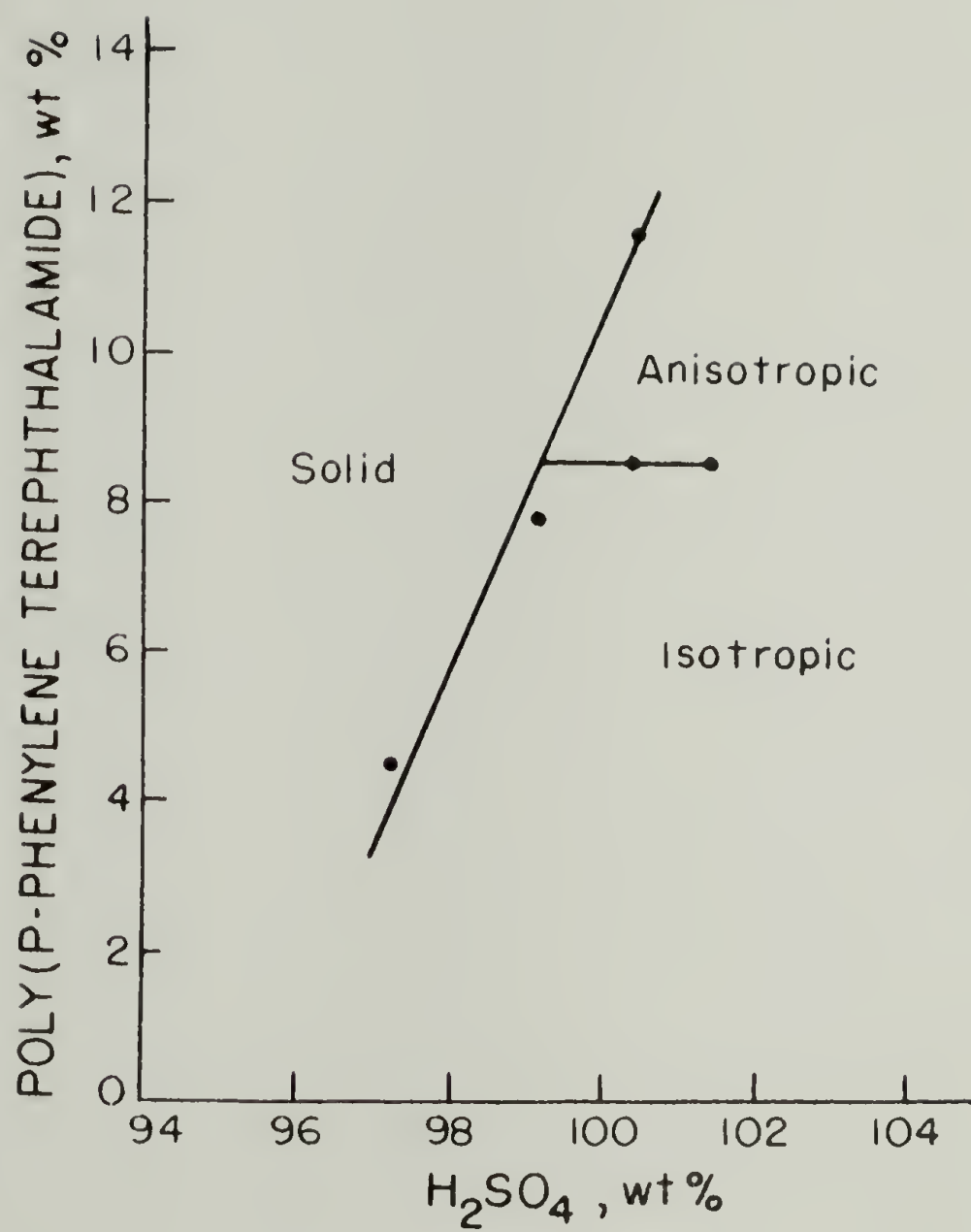


Figure 51. Phase Diagram of PPT in  $H_2SO_4$ .

not for a sample of  $\overline{M}_w = 44,000$  at a concentration of .10 g/dl (99). A study of poly-para-phenylene terephthalamide by Papkov et al. (100) resulted in the curves shown in Figure 52 which differ from results for other rod systems in exhibiting a sharp increase in viscosity after the expected viscosity peak at the critical concentration for anisotropic phase formation. This curve was interpreted using the authors' previously published results (101) in which the viscosity of the anisotropic phase decreased at first with increasing polymer concentration and then with a further 2-3% increase in concentration, increased so rapidly that it was almost impossible to obtain homogeneous solutions. The interpretation of Figure 52 is thus that a heterogeneous system is formed at the critical concentration in which the anisotropic phase is suspended in the isotropic phase. Further increase in concentration changes the volume ratio of the coexisting phases until a phase inversion occurs so that the anisotropic phase becomes the suspending medium, and "the viscosity of this phase is very high so that the aggregate viscosity increases sharply" (100). This interpretation is not in complete accord with the thinking of investigators of other rigid rod systems and may be based on behavior peculiar to the PPT-H<sub>2</sub>SO<sub>4</sub> systems. In this same work it was shown that viscosity of PPT solutions vary with concentration with a maximum at 98% H<sub>2</sub>SO<sub>4</sub> (this is the concentration of maximum density for aqueous sulphuric acid) for the case of isotropic solutions of 3% and 5% polymer. The isotropic solution of 7% polymer shows a minimum in viscosity at 98% H<sub>2</sub>SO<sub>4</sub>. For the case of an anisotropic solution of 11% polymer, the viscosity increased monotonically with

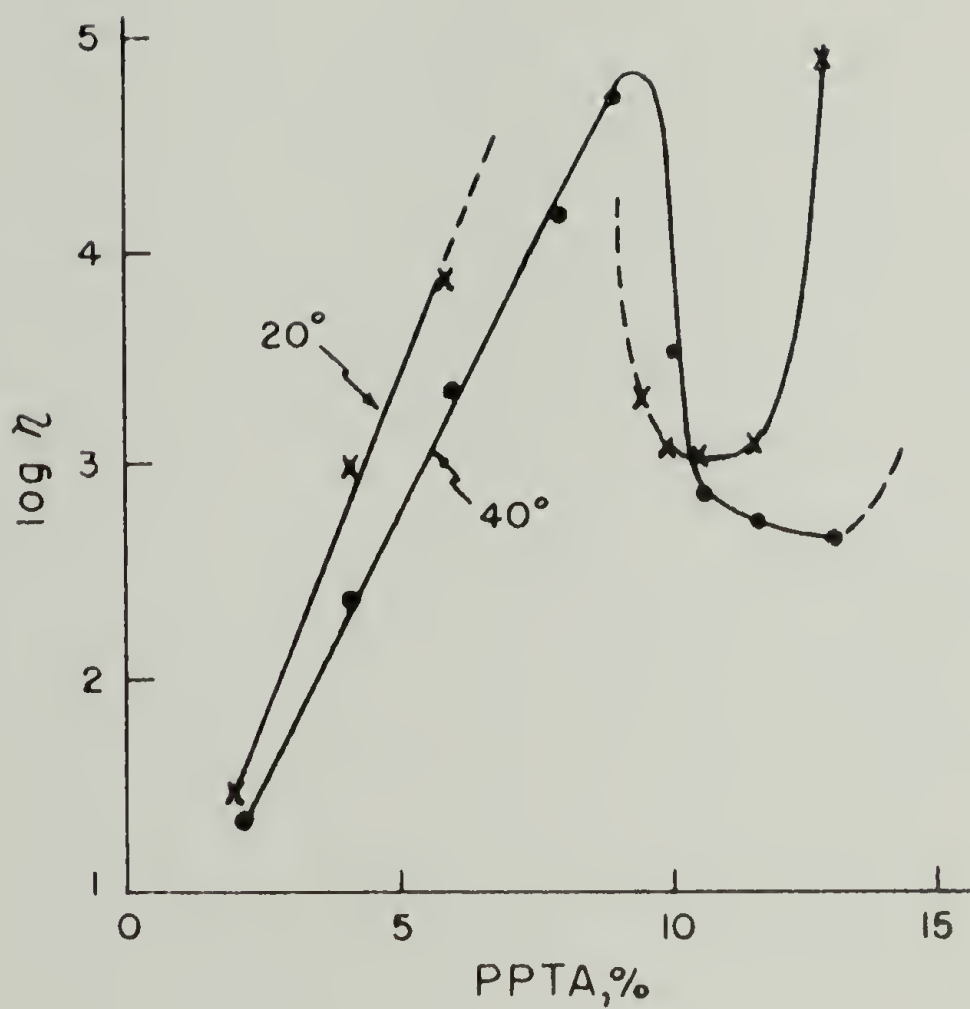


Figure 52. Viscosity vs. Concentration for PPTA at 20 and 40°C.  
 $\tau = 2 \times 10^3$  dyne/cm<sup>2</sup>,  $[\eta] = 3.1$ .

sulphuric acid concentration, and very rapidly for solvent exceeding 100%  $H_2SO_4$ . This complex behavior is summarized in Figure 53.

A detailed rheological investigation of PBA in DMAC was also conducted by Papkov (102). The polymers were of  $\overline{M}_w$  up to 69,000 and the solutions in a concentration range of .5-14 wt%. Solutions below the critical concentration showed a low shear Newtonian plateau and shear thinning. Solutions in the anisotropic state showed a yield stress; see Figure 54. The 3% solution is below and the >5% solutions are above the critical concentration. The yield stress was below  $10 \text{ dyne/cm}^2$  and tended to increase with solution concentration. The authors commented that the existence of a yield point in an unfilled fluid system is apparently typical of polymeric liquid crystals, citing the behavior of poly(alkyl acrylates) and poly(alkyl methacrylates) in which long side groups form a crystalline structure in the melt (103). The yield stress in anisotropic solutions of PBA is small in part because of its low concentration (compared to a melt) and the weakness of the resulting structures.

Viscosities in the quasi-Newtonian region of anisotropic solutions were taken as the zero shear values for comparisons with the measured  $\eta_0$  for the isotropic solutions. The behavior of  $\eta_0$  versus concentration is equivalent to that previously illustrated for other rod systems; see Figure 55. This figure shows clearly a decrease in critical concentration,  $C^*$  and an increase in low shear viscosity,  $\eta_0$ , with increasing rod length.  $\eta_{\text{max}}$  was found to vary with molecular weight to the 3.2 power which is close to 3.4 power encountered in many polymer melts. The product  $C^*\overline{M}$  was found to be

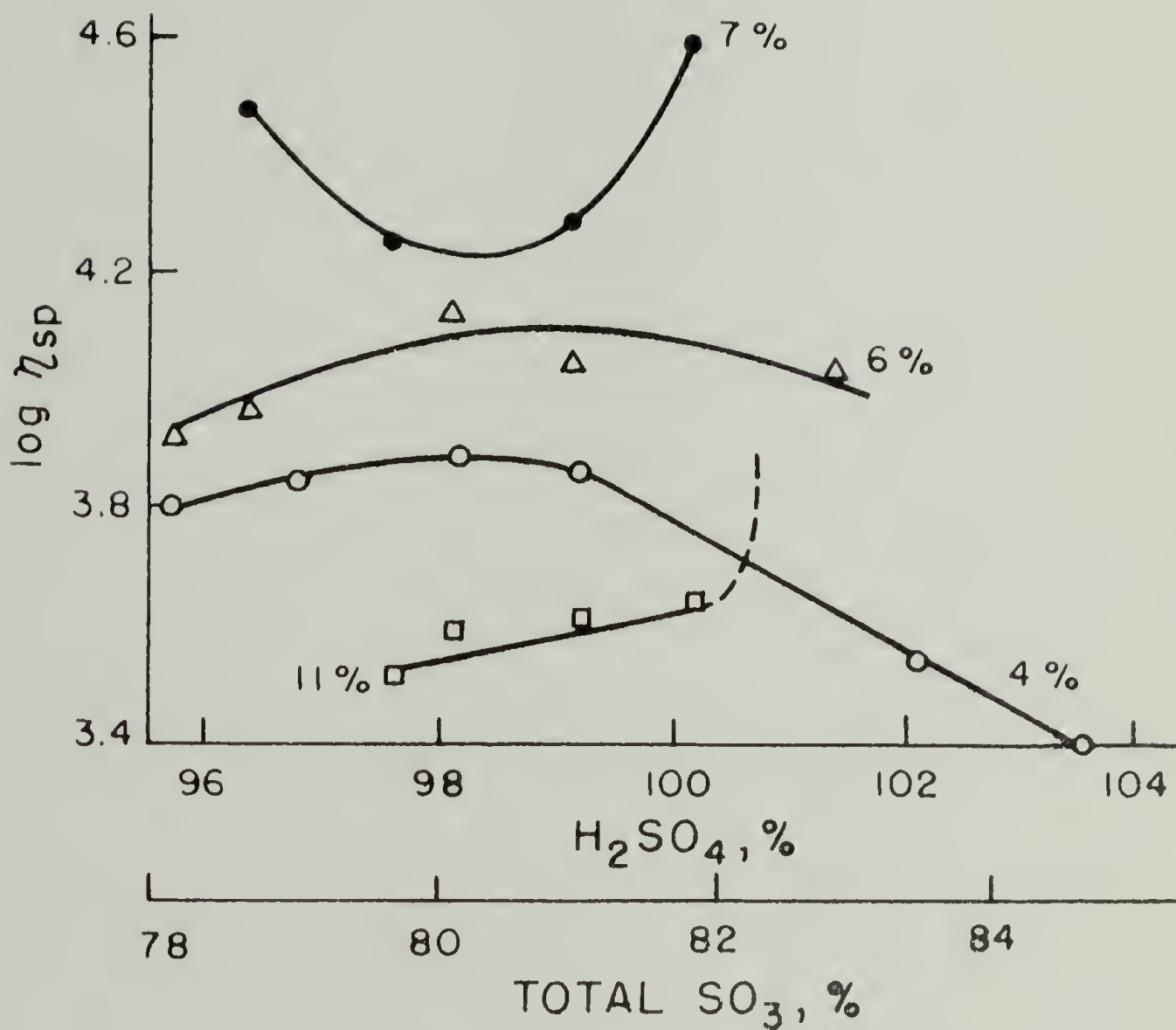


Figure 53. Relative Viscosity of PPTA Solutions of Varied Concentration as a Function of the Sulphuric Acid Content ( $[\eta] = 3.0$ ): (1) 4%, (2) 6%, (3) 7%, (4) 11%.



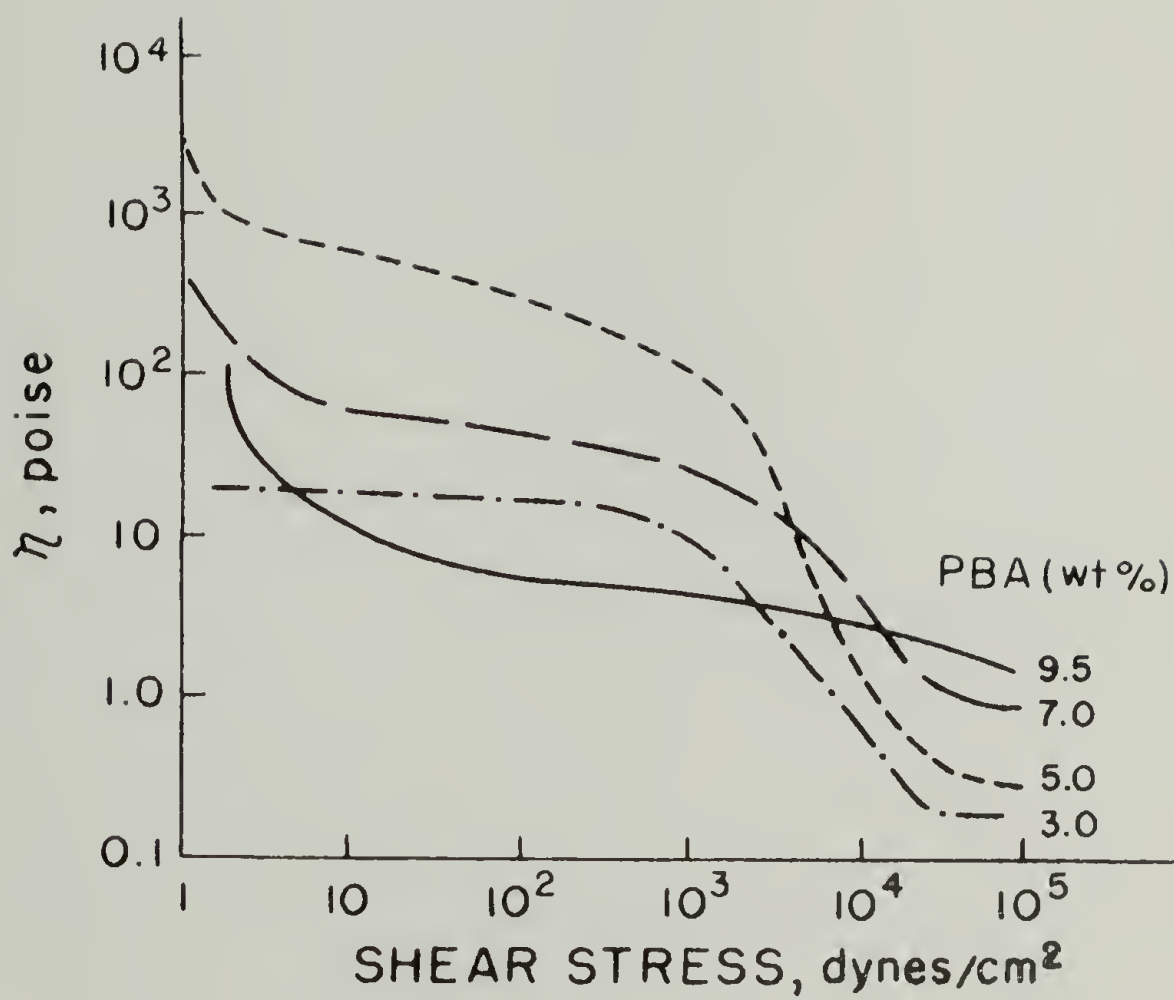


Figure 54. Viscosity vs. Shear Stress for Solutions of PBA in DMAC.

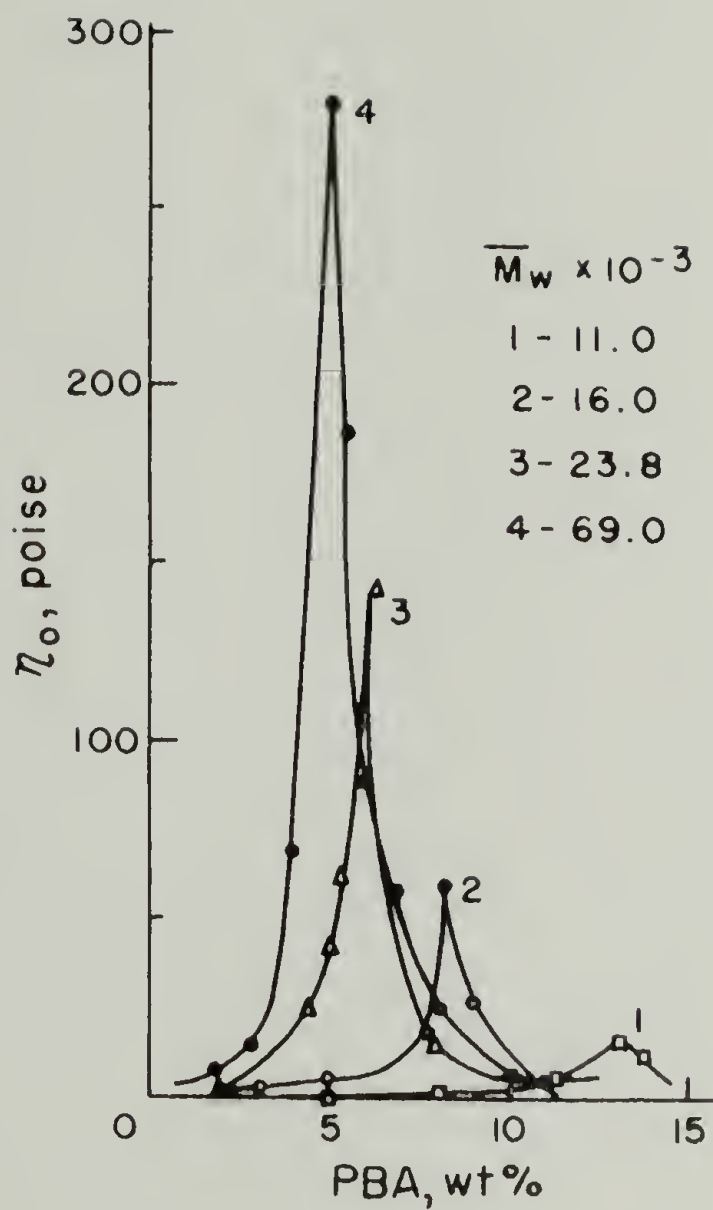


Figure 55. Concentration Dependence of Viscosity at 20°C for Solutions of PBA Samples.

constant and data for four different molecular weights were superimposable using  $\bar{C}\bar{M}$  and  $\eta_0/\eta_{\max}$  as reduced variables; see Figure 56.

The rod-like character of PBA was confirmed by the high exponent for  $\bar{M}$  in the Mark-Houwink equation:

$$[\eta] = 1.59 \times 10^{-8} \times \bar{M}^{1.85} \quad (26)$$

Polydispersities were not reported but assumed to be 2 which is the value expected for the most probable distribution of molecular weights obtained from polycondensation reactions. The authors speculated that the effect of polydispersity would be to widen the isotropic-anisotropic transition range. It was also supposed that monodisperse polymers should exhibit an extreme viscosity drop on crossing  $C^*$ . However, PBLG solutions, which are considered nearly monodisperse, exhibit a steep but not discontinuous viscosity decrease at  $C^*$  and viscosity decreases further as concentration is increased.

Viscosity versus shear rate data for solutions of differing concentration were superimposable using  $\log(\eta/\eta_0)$  and  $\log(\eta_0\dot{\gamma})$  as the reduced variables; see Figure 57. Here again the viscosity in the quasi-Newtonian region was taken as  $\eta_0$  for the anisotropic solutions. The data for isotropic solution at different concentrations superimposed well. Deviations from common behavior were observed for anisotropic solutions. The higher the shear rate, the lower the concentration at which the deviations occurred.

The viscosity versus temperature behavior was investigated within the constraints of the freezing and boiling points of the solvent. Between  $-20^\circ$  and  $40^\circ\text{C}$ , viscosity decreased with temperature

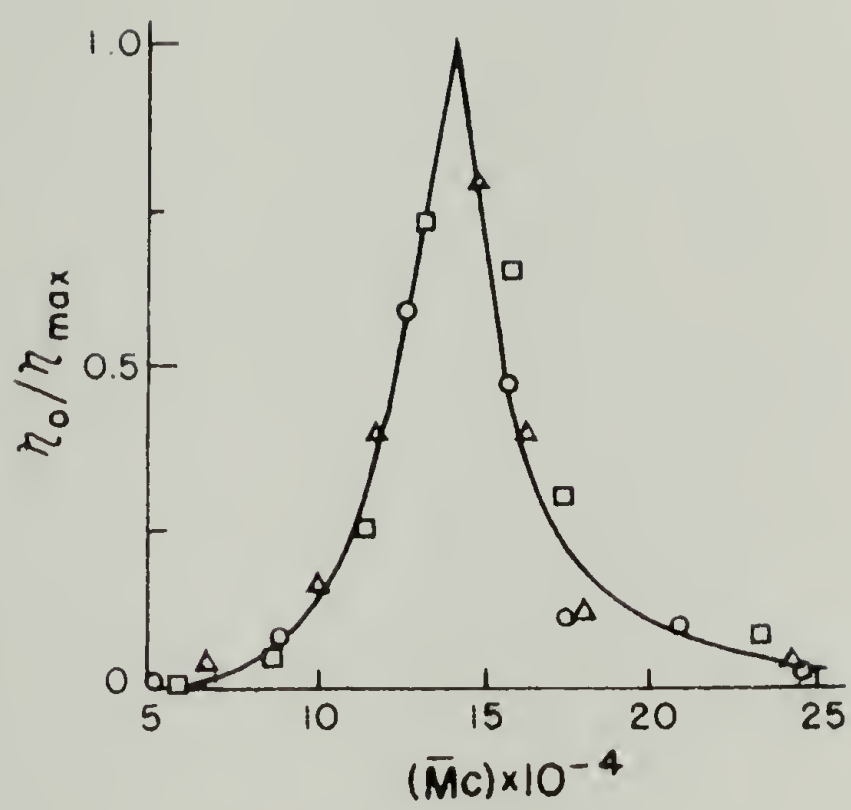


Figure 56. Reduced Viscosities for PBA in DMAC.

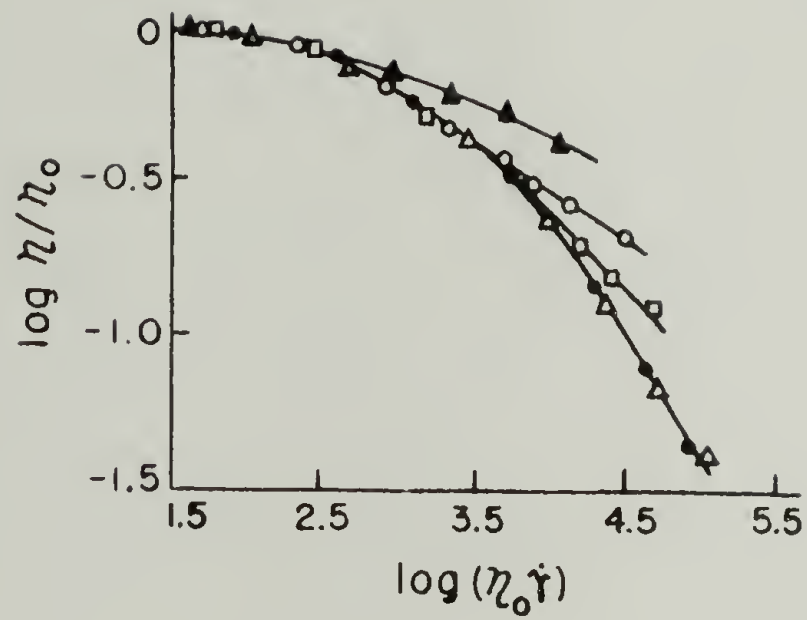


Figure 57. Flow Curves for PBA Solutions in Reduced Coordinates. Concentrations: ( $\Delta$ ) 3%; ( $\bullet$ ) 4%; ( $\square$ ) 5%; ( $\circ$ ) 7%; ( $\blacktriangle$ ) 9.5%.

exponentially consistent with a common flow mechanism. Above 40°C, however, the liquid crystal structure begins to disintegrate, leading to an increase in intermolecular interference and a viscosity increase; see Figure 58. It increased up to 130°C, where the isotropic solution reforms as indicated optically. The isothermal constant ( $C^*\bar{M}$ ) was almost invariant from -20° to +130°C.

Commercial aspects of anisotropic solutions. It is commonly known that the mechanical properties attained by polymers are generally but a small fraction of the theoretical ultimates (104). In the case of polyethylene, the Young's or tensile modulus as measured by x-ray diffraction of a crystal under stress is near 240 GPa or  $2.4 \times 10^{12}$  dyne/cm<sup>2</sup>, whereas the highest value attained to date is near 70 GPa (105). This discrepancy is due to nonideal morphologies which includes amorphous regions, chain folding, and crystalline regions with defects and with chains non-parallel to the stress direction. These deviations from the idealized continuous crystal (full chain extension and perfect alignment) allow failure through weak interchain forces rather than by bond rupture and full chain translation which would result in mechanical properties approaching the upper theoretical limits.

Two approaches to attaining more perfect morphologies suggest themselves; align and extend flexible chain polymers such as polyethylene by ultra-draw (105) or the use of rod-like polymers which are already extended so that the processing need only orient the chains in the stress direction. Since rod-like molecules in an anisotropic

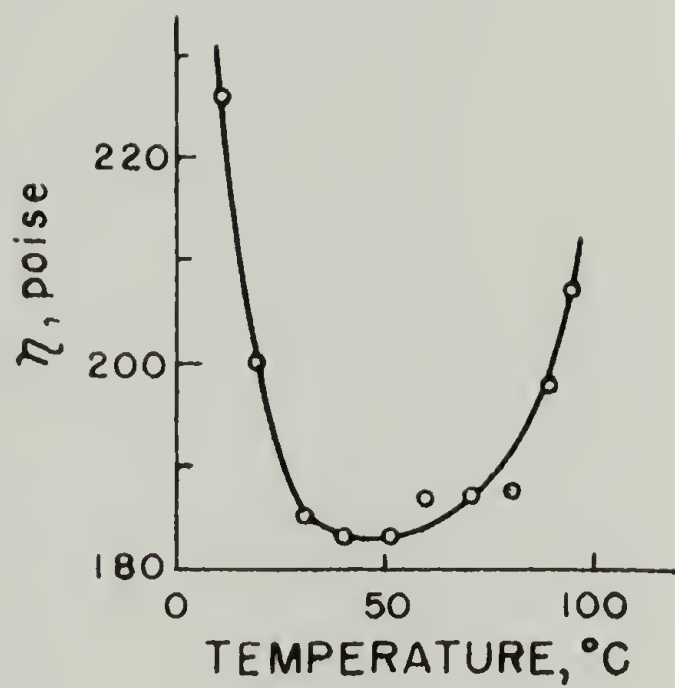


Figure 58. Viscosity-Temperature Behavior of a Concentrated Solution of PBA in DMAC.

solution are both already extended and highly oriented, the fabrication process need only control the direction in which the molecules are oriented. The end result of such a procedure would be a material which is exceedingly strong in the orientation direction yet weaker laterally, characteristics appropriate for fiber applications. Note also the further advantage that anisotropic solutions of rigid polymers have lower viscosities than isotropic solutions of lower concentration. They can, therefore, be spun at a rapid rate into a stronger fiber with less expenditures of energy.

Fibers have been spun from anisotropic solutions of PMLG (106). Since PMLG molecules are in helices rather than fully extended, these fibers do not, however, exhibit outstanding mechanical properties.

Fibers spun from anisotropic solutions of rigid para-substituted polyamides are examples of, and in fact dominate at present, the new class of ultra-high strength fibers, which exhibit moduli which approach the theoretical limits. Two examples of such fibers are Dupont's well known Kevlar, which may vary in composition including poly-p-phenyleneterephthalamide (PPT) (107) and Monsanto's X-500, which is poly(para-aminobenzhydride terephthalamide) (PABH-T) (107). Specific modulus, i.e., on a weight basis, of over 1000 grams/denier have been achieved. This is much higher than glass and steel and compares favorably with graphite due to the comparatively low density of these fibers (see Table 3).

The elongation-to-break of the materials with highest modulus is small compared to glass and steel and can be increased at some cost to modulus, by using the empirical expression (for PABH-T) (108).



$$E_i = 1000/\epsilon_b^{.58} \quad (27)$$

$E_i$  = initial modulus in g/den

$\epsilon_b$  = elongation to break in %

High tensile strength and modulus are associated with variations influenced by fiber perfection, which is controlled by spinning. A major stumbling block in the manufacture of these fibers is their previously-mentioned insolubility in all but the most powerful solvents. It has been reported (108) that random copolymers of para-substituted aromatic amides and hydrazides have a higher solubility in organic solvents with little decline in physical properties.

The ultimate properties are not exhibited by the as-spun fibers but are improved considerably by heat treatment or by hot drawing. Hot drawing of PABH-T can result in an increase in crystallinity as measured by x-ray from 30 to 90% and in density from 1.34 to 1.47 g/cc. The unit cell density is 1.51 g/cc (104). The modulus of PTA fibers is sensitive to chain orientation and is improved by the decrease in orientation angle resulting from heat treatment; see Figure 59 (98). The reason for this is probably that the anisotropic solutions from which these fibers are spun are not perfectly oriented, hence post extrusion treatment can enhance alignment. Papkov et al. (109) lend support to this speculation by observing that the strength of fibers spun from a solution of given concentration increased with molecular weight of the dissolved polymer. They attributed this to the fact that at a given concentration, a longer polymer would be farther from the critical concentration than a shorter one and would,

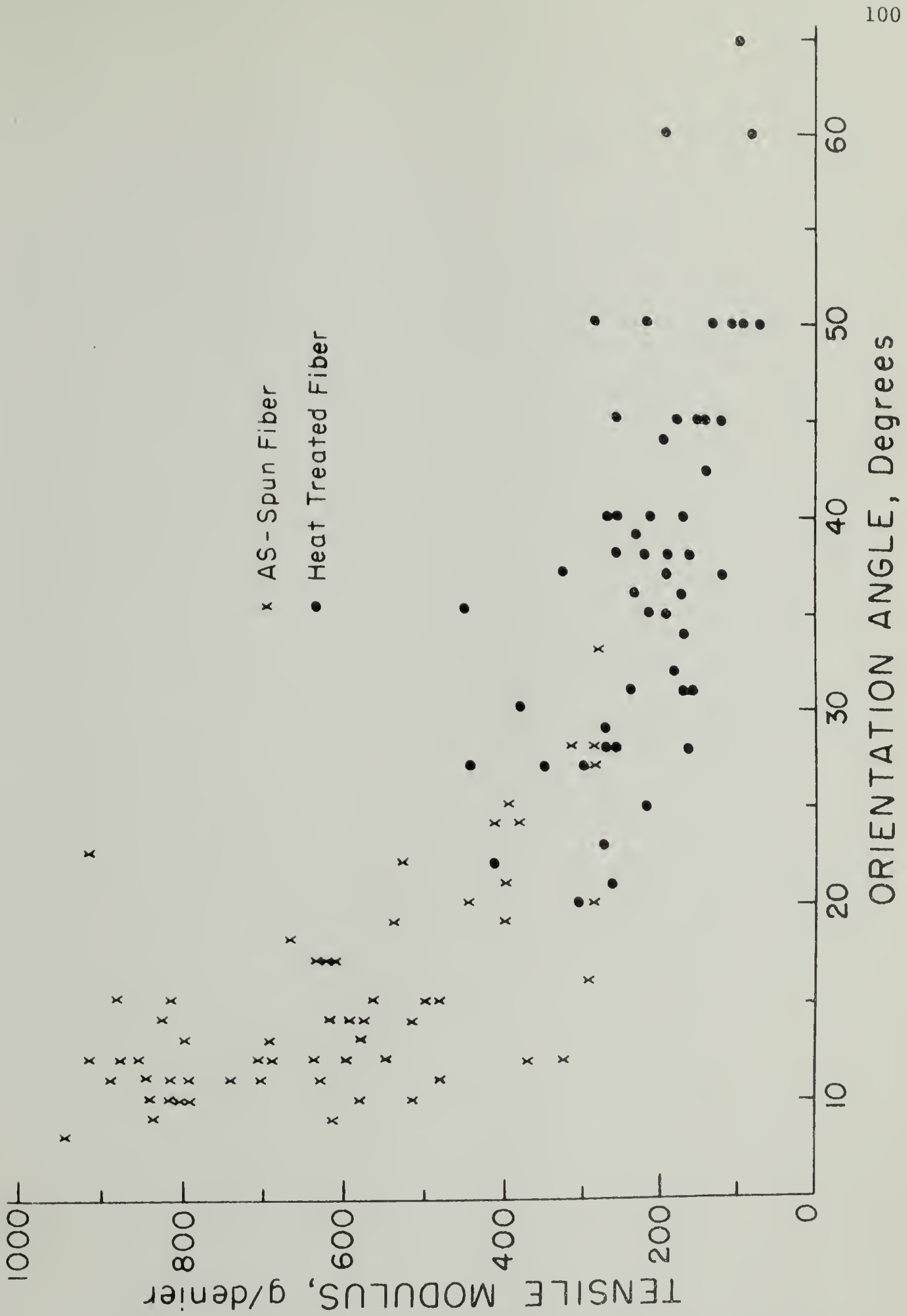


Figure 59. Correlation of Modulus and Orientation Angle for PTA Fibers.

therefore, give rise to a greater fraction of the solution being in the anisotropic state. Thus the following sequence would be expected for solutions of rigid polymers of increasing molecular weight at a given concentration:

1. For low molecular weight such that the concentration is below the A-point: the solution is isotropic and very viscous, difficult to spin, and produces a weak fiber.
2. For a molecular weight such that the given concentration coincides with the A-point: the solution is partially anisotropic and partially isotropic so the viscosity drops and the as-spun fiber is partially oriented.
3. For increasing molecular weight such that the given concentration approaches the B-point: the fraction of solution in the anisotropic phase approaches unity and the as-spun fiber increases in orientation since it is being spun from a solution of increasing order.
4. For yet higher molecular weights such that the concentration is above the B-point: the entire solution is anisotropic so that the effect of increase in molecular weight is to improve the ordering, hence the orientation of the as-spun fiber is increased.
5. For molecular weights so high that at the given concentration the solution is essentially completely ordered: the as-spun fibers should be almost perfectly oriented and would benefit little from post-extrusion treatment.

Because of the difficulty in dissolving high molecular weight parasubstituted aromatic polyamides, solutions of type 5 have not been achieved. In any case, polymers of lower molecular weight are used in commercial processes (e.g., DP of 100 for DuPont's Kevlar) since good mechanical properties are attained at relatively modest molecular weight for rigid polymers in contrast to folded chain polymers (108).

### Rod Systems in Bulk

Low molecular weight liquid crystals. The liquid crystal phenomena discussed above have been properties of "lyotropic" liquid crystals, i.e., phenomena which are produced in solutions by changes in solute concentration. Another class of liquid crystals is known as "thermotropic," i.e., those pure substances which are crystalline solids at low temperatures, undergo transitions to one or more mesophases at well-defined temperatures, and finally convert to an isotropic liquid. These materials are generally of low molecular weight so their aspect ratios are low. Although these are technically rod systems, the bias of this paper is towards macromolecules and the treatment of such short rods will be cursory. It is included to bring attention to parallels and discrepancies in the behavior of low molecular weight mesophases and their counterparts in the mesophases formed by solutions of rigid rods of much higher aspect ratio. It may be that some of the more subtle and unusual experiments which have been performed on the low molecular weight thermotropic mesophases will also be applicable to the high molecular weight lyotropic mesophases.

Early attempts to explain the behavior of nematic liquid crystals by Ornstein and Kast (110) and Tsvetkov and Marinin (111) involves the concept of "swarms" of perhaps  $10^4$  molecules which behave cooperatively. These swarms were thought of as either being mutually independent or capable of interaction, depending on the theory. This approach has been largely discarded (112) and a continuum mechanical approach adopted in which the orientation of the nematic liquid crystal at any point is represented vectorially. The degree of perfection for parallel alignment of molecules is represented by the Hermans-Stein order parameter;

$$S = \frac{3\langle \cos^2 \theta \rangle - 1}{2} \quad (27)$$

where  $\theta$  is the angle made by the long axis of a molecule with the aggregate nematic axis at that point.

A theory for the elastic properties of nematic liquid crystals (hydrostatics) was given first by Oseen (113) and extended by Frank (114). A review of the subject is given by Ericksen (115).

Hydrodynamic theories for nematic liquid crystals have been developed by Ericksen (116) and Leslie (117). The Leslie theory fails to reduce to the Oseen-Frank theory in the static case, but this deficiency was not considered important for nematic liquid crystals. A theory suitable for the discussion of the hydrodynamics of smectic and cholesteric liquid crystals is presented by Stephen (118). Also, Forster et al. (119) and Huang (120) present more general derivations of the Leslie-Ericksen theory. These theories

involve 5 independent coefficients with the dimensions of viscosities and two shear-torque coefficients. Measurements of viscosity and birefringence for various relative orientations of flow, velocity gradient, and magnetic field directions, while changing flow velocity and magnetic field strength, allow the evaluation of these coefficients (121). The coefficients can also be obtained from inelastic light scattering or the attenuation of ultrasonic shear waves (122) or by an optical method proposed by Wahl and Fischer (123,124), which utilized interference rings produced when a nematic liquid crystal is sheared between rotating parallel glass discs and viewed between cross-polars.

A test of the Leslie-Ericksen theory using elastic and viscosity coefficients obtained from a number of sources was performed by Tseng, Silver and Finlayson (125) for Poiseuille flow. The theory was found to agree with observations on p-azoxyanisole. The controversy as to whether the stress tensor should be asymmetric (Leslie-Ericksen theory) or symmetric (Forster et al.) was resolved in favor of the Leslie-Ericksen theory, thus p-azoxyanisole represents an established case for a fluid with an asymmetric stress tensor.

An observation made in the capillary viscometry of nematic mesophases is a dependence of viscosity on capillary diameter which would not occur for a fluid in the class of Noll simple fluids. Fishers and Frederickson (126) observed a significant change in the apparent viscosity with decreasing capillary diameter for capillaries treated to give perpendicular orientation at the surface of the capillary and very little effect of capillary diameter for capillaries

treated to give parallel orientation at the surface. By using a simple model in which a boundary layer near the wall exhibits the viscosity characteristic of orientation perpendicular to flow and the remainder of the fluid exhibits viscosity characteristic of orientation parallel to the flow (cf. (129)), they calculated boundary layers on the order of 1-10 microns, decreasing with increasing shear rate, and anticipated a value of 20 microns for the zero shear boundary layer, in accord with the 20 microns spoken of by Gray (127) for static orientation on a glass surface. The data can be superimposed by plotting viscosity against  $\frac{4Q}{\pi R}$  (where  $Q$  = volume flow rate and  $R$  = capillary radius) in accord with the prediction of Atkins' (128) application of the Ericksen-Leslie theory to Poiseuille flow and in conflict with the Noll theory of simple fluids which requires viscosity to be a function of  $\frac{4Q}{\pi R^3}$ , see Figure 60. Porter and Johnson (129) earlier reported an apparent adsorption layer of 3-6 micron thickness in concentric cylinder viscometry of nematic liquid crystals. The question of boundary layer effects in the viscometry of liquid crystals is discussed by Ericksen (130).

As discussed previously, isotropic solutions of rod-like macromolecules can undergo shear induced orientation by rotating at an angular velocity which changes during the course of the rotation, so that the molecule spends the largest fraction of its time oriented in the flow direction. This average flow orientation angle approaches  $45^\circ$  (midway between the flow direction and the velocity gradient), at low shear rates for the isotropic state. Nematic liquid crystals under shear also orient spontaneously in this plane; however, the flow

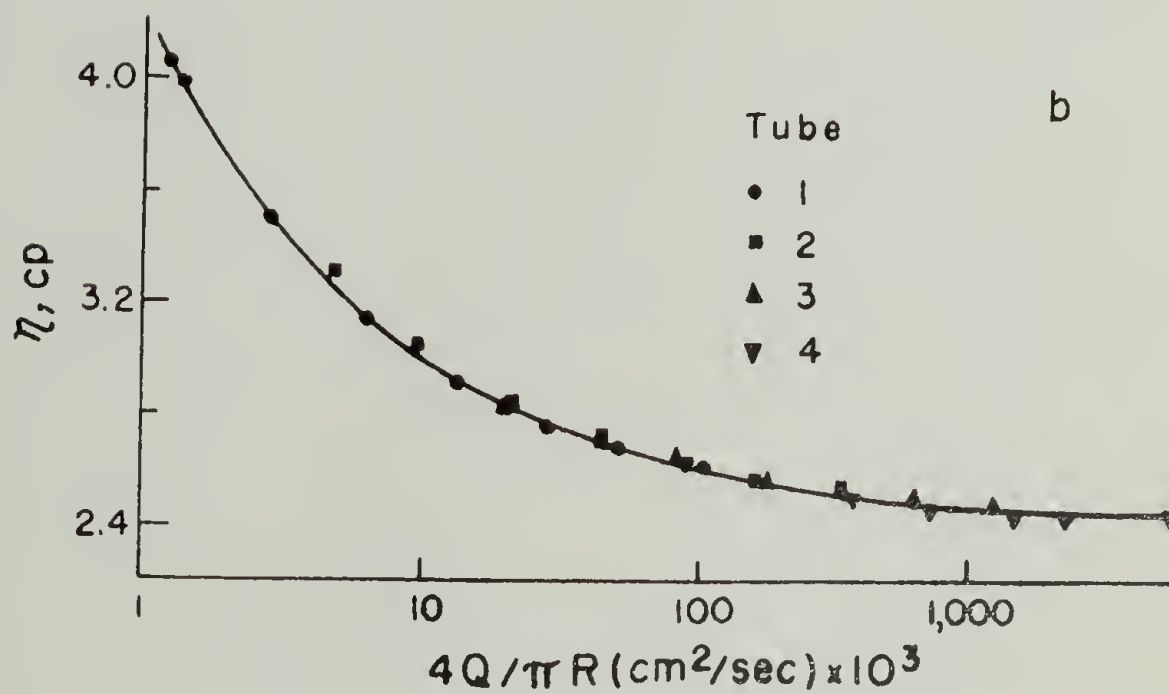
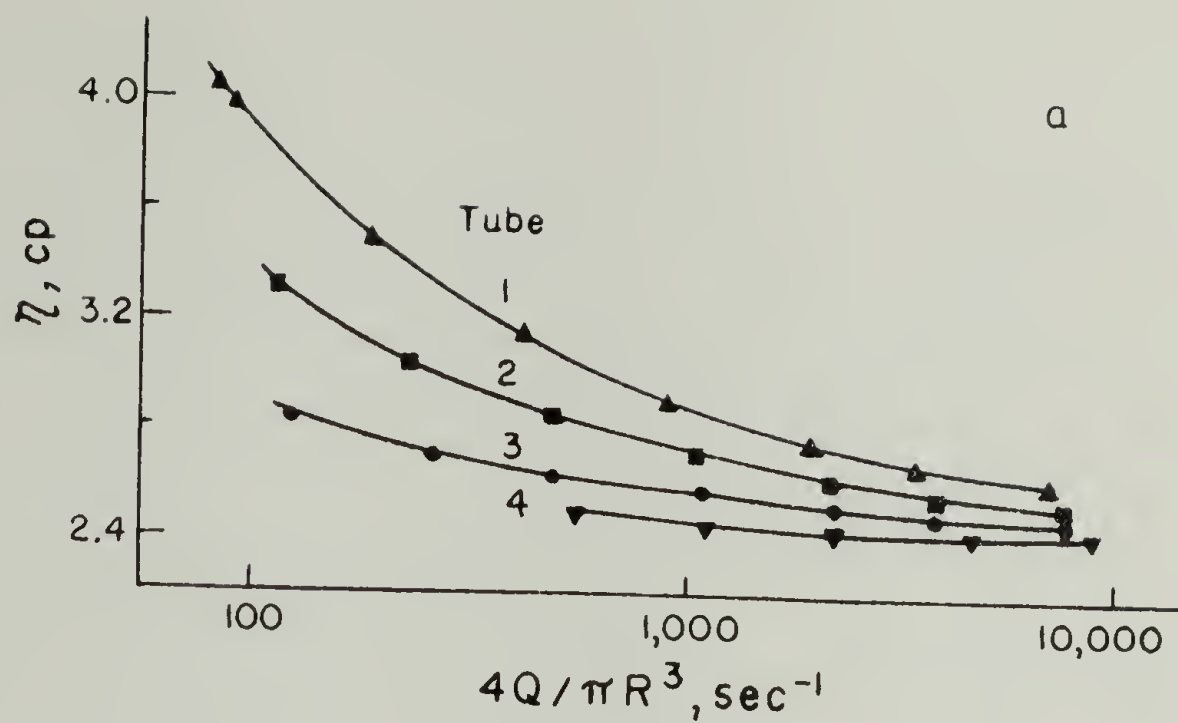


Figure 60. (a) Viscosity of Nematic p-Azoxyanisole at  $121.8^\circ\text{C}$ . Surface Treated to Produce a Perpendicular Orientation of Mesophase.  
 (b) Flow Data on Nematic p-Azoxyanisole at  $121.8^\circ\text{C}$ . Perpendicular Orientation at Interface.



alignment angle is smaller, being about  $10^0$  for p-azoxyanisole (131), the most widely studied thermotropic nematic.

A theory of flow alignment has been proposed by Helfrich (112) in which the nematic liquid is regarded as a gas of rigidly and equally oriented ellipsoids of revolution, and which gives results in good agreement with experiment. As a nematic is heated toward the nematic-isotropic-transition point, the order parameter decreases toward zero leading to pretransitional effects. The theory of Helfrich incorporates  $S$  and predicts that the flow alignment angle increases to  $45^\circ$ , the isotropic value, as  $S$  decreases to zero (132). This paper quoted a personal communication from Gähwiller reporting experiments which indicated that the flow alignment angle in a nematic increases substantially within the last  $10^\circ$  of the nematic-isotropic-transition point.

The flow mechanism of nematic liquid crystals in capillary flow, without wall effects, may be regarded as normal Poiseuille flow in which molecules in adjacent planes slip past one another. Nematic liquid crystals exhibit low viscosities on the order of the values for the corresponding isotropic melts. In contrast, viscosities for cholesteric and smetic thermotropic liquid crystals are strongly shear dependent and generally orders of magnitude greater than their corresponding isotropic liquids (133). Helfrich suggested that flow in cholesterics and smetic might occur by a plug flow mechanism ("permeation") in which a plug of fluid travels through an orientation pattern which is fixed with respect to the capillary (see Figure 61). Using parameters such as the pitch of the cholesteric super-

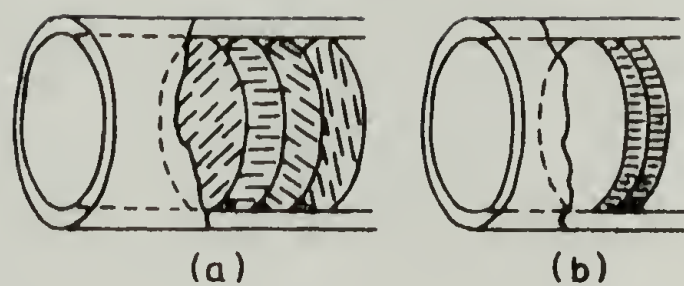


Figure 61. Envisaged Orientation Patterns in the (a) Cholesteric and (b) Smectic Case. The Dashes Represent the Rod-like Molecules with long Axes Perpendicular (a) and Parallel (b) to the Capillary Axis.

helix, he calculated an apparent viscosity which agreed with the values obtained from capillary flow. At extreme shear rates cholesterics are observed to flow almost as easily as the isotropic liquid, indicating that the flow mechanism has changed to one incorporating deformation of the alignment pattern and allowing orientation of molecules in the flow direction. An extensive review of rheology for low molecular weight liquid crystals is given in reference (134).

A fascinating study of the rheo-optics of cholesteric mesophases has been carried out by Erhardt, Pochan and Marsh (135) in which a mixture of cholesteryl oleyl carbonate and cholesteryl chloride was sheared between parallel rotating glass discs. In this geometry shear rate increases linearly from zero with distance from the center of the discs, thus at any given rotation speed, material held between the discs is subjected to a wide range of shear rates. Two shear induced textural changes were observed. In order of increasing shear rate, the textures observed were the Grandjean, the dynamic focal conic, and the homeotropic. The Grandjean texture showed non-Newtonian viscosity, the dynamic focal conic showed Newtonian viscosity over two decades of shear and the homeotropic phase showed both non-Newtonian viscosity and normal stresses. The proposed mechanism of the textural changes was that at low shear rates the Grandjean texture is adopted and the effect of increasing shear rate is to tilt the super-molecular helices (as indicated by a shift in spectral reflectivity). At higher shear rates the Grandjean texture is disrupted to form the dynamic focal conic in which super-molecular helices are preserved. This texture does not revert

to the Grandjean upon cessation of shear. However, addition of  $\approx 3\%$  polyisobutylene allows relaxation back to the Grandjean similar to raising the temperature or releasing the surface constraints (136). Finally, at a higher and critical shear rate, near  $10^3 \text{ sec}^{-1}$ , the super-molecular helices are broken down into smaller units which act like short rods of  $\leq 400\text{\AA}$  in length (decreasing in length with further increase in shear rate) and give rise to normal stresses. It would be interesting to test whether or not the parallels between thermotropic cholesteric liquid crystals and the lyotropic solutions of polypeptides discussed earlier would extend the exhibiting of such shear-induced texture changes.

Liquid crystal phenomena in bulk polymers. Stiff molecules of high molecular weight generally have melting points higher than their thermal decomposition temperatures. Thus thermotropic liquid crystals formed by polymers are few and literature on their rheology is virtually non-existent. However, familiarity with liquid crystal properties is helpful for the understanding of certain phenomena in bulk polymers.

An example of a polymer which appears to be liquid crystalline in the melt is the polyester made from the reaction of p-acetoxybenzoic acid with poly(ethylene terephthalate). The polymer is first fragmented and then a second polycondensation carried out with the elimination of acetic acid (137). This polymer is known as Polyester X7G as developed at Eastman Chemical Co. It is only one of a class of compositions described by patent (137). Even in the

absence of shear, the melt is anisotropic and has a hazy appearance (138). Detailed rheological information on this polymer is presented in (146). A mesomorphic melt is indicated by a low viscosity at relatively low temperature; see Figure 62. The effect of composition of the polyester on melt viscosity and the extent of non-Newtonian behavior is also discussed. Another unusual property of X7G is its self-reinforcing characteristic. That is, bars molded from X7G show much higher modulus, impact strength, and lower ultimate elongation and thermal expansion coefficient in the direction parallel to flow developed during molding than perpendicular to the flow. The degree of anisotropy was greater at reduced bar thickness and at reduced melt temperature (i.e., at greater stress to produce greater orientation) (139). This behavior is also consistent with the assertion that X7G forms a mesomorphic melt.

Another class of polyesters which is claimed to be thermotropic liquid crystals has surfaced recently in the patent literature (147). These patents, granted to DuPont, claim a class of polymers which can be prepared from appropriate monomers by melt polymerization under anhydrous conditions in an inert atmosphere. Monomers used for various compositions include several bivalent phenols and one or several aromatic and/or cycloaliphatic dicarboxylic acids. The resultant polymer chains are stiff as a result of their predominantly annular structure, and in fact homopolymers of unsubstituted ring structures melt at too high a temperature to be conveniently processed. For this reason several techniques for reducing the melting temperature without loss of the rigidity required for an anisotropic

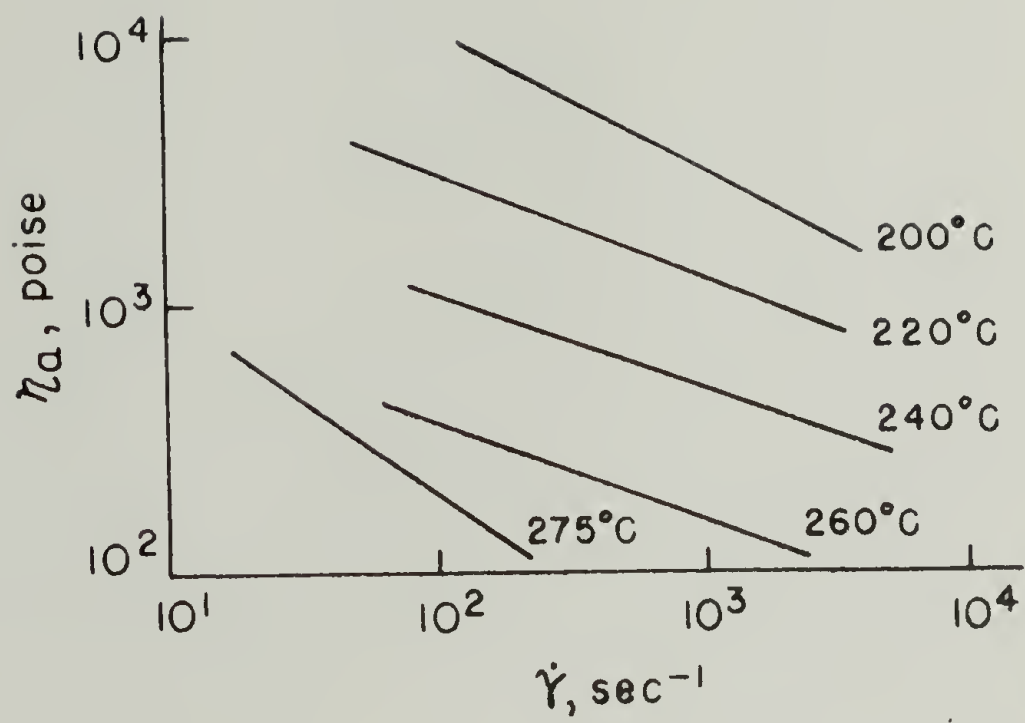


Figure 62. Apparent Melt Viscosity of Polyester X7G.

melt are cited.

- (1) limited substitution of annular groups with chlorine, bromine, or lower alkyl groups
- (2) limited copolymerization
- (3) introduction of limited flexibility by either bridges or aliphatic chains of limited length.

The existence of an anisotropic melt for these polyesters was indicated by transmission of light through cross-polars above the flow temperature of the polymer. Some compositions were found to melt to an isotropic melt at a higher temperature, others were found to be anisotropic up to the decomposition temperature. Another indication of an anisotropic melt was the observation of stir opalescence.

Important commercial advantages of spinning polyesters from anisotropic melts are enumerated in these patents.

- (1) They can be melt spun directly to an oriented fiber without a post-spinning drawing step. X-ray orientation angles as low as  $12^\circ$  were found in the as-spun fiber.
- (2) Spinning speed fluctuations which can cause a great change in the properties of P.E.T. fibers have little effect on the orientation of these polyesters.
- (3) These polyesters can be given a post-spinning heat treatment to increase the molecular weight without fear of the loss of orientation which occurs in drawn P.E.T. fibers.

Liquid crystalline order in melts of poly-diethylsiloxane

has been reported (140). N.M.R., dielectric, x-ray diffraction, and calorimetric data were used to identify a semi-ordered state which exists between 268° and 293°K. This state is a two phase system consisting of an amorphous phase coexisting with a one-dimensional ordered phase. The relative amounts of the two phases are temperature dependent with the amorphous phase predominating at higher temperatures.

Multiple post-melting transitions have been reported by Smit on the basis of heat capacity measurements on isotactic polypropylene (141). Through a variety of thermal and mechanical pre-treatments such as annealing and shear-crystallization, he identified transitions at 169°, 200°, 217°, 234°, 256°, 283° and possibly 308°C and observed a one-to-one correspondence with transitions observed in smectic anhydrous sodium soaps. The change in heat capacity with temperature indicates several post-melting transitions. No rheology was reported.

Melt transitions in isotactic and atactic polypropylene were also reported by Beck and Heltz (142), who suggested that liquid crystalline behavior in the melt may be responsible for the effect of temperature and time in the melt upon the crystallization kinetics as discussed by Collier and Neal (143). That is, regions of order may persist in the melt of polypropylene and may serve as nuclei for subsequent crystallization.

The concept of a micromosaic structure was invoked by Adrianova (144) to explain the remarkable effects of dissolution history (that is, polymer obtained by evaporating to dryness solutions of different concentrations and various solvents) and of small



quantities of oligomeric compounds on the melt viscosity of polypropylene and polystyrene. It was found that melt viscosity of polystyrene and polypropylene could be reduced by a factor of 15-20 in favorable cases; see Figure 63. This was interpreted on the basis of a micromosaic structure formed in the amorphous polymers which were then stable for long periods of time at temperatures more than 100°C above the glass transition temperature.

A similar effect was reported by Shih (149) upon addition of small quantities (.04-10 wt%) of EPDM (ethylene, propylene, 1,4 hexanediene) terpolymer to Viton A fluoroelastomer. Although the melt viscosities of the polymers as measured by capillary viscometer were 126,000 and 78,000 poise, respectively at 160° and 35 sec<sup>-1</sup>, that of the blends was 30,000 poise. By studying the effect of extrusion time, capillary diameter, capillary aspect ratio, and extrusion of pure polymer after a blend without cleaning the rheometer barrel, Shih concluded that the phenomenon was not due to a structural heterogeneity. It was suspected that the EPDM may have migrated to the capillary wall, resulting in slippage at the wall and thus a lower apparent viscosity.

The synthesis of a class of comb-like polymers with pendant mesogenic groups containing phenyl rings has been reported (148). The range of temperatures over which mesomorphic behavior was observed increased with increasing length of alkyl chain, being 165°-220°C for the polymer of p-methacryloyl oxyphenol ester of p-n-cetyl oxybenzoic acid.

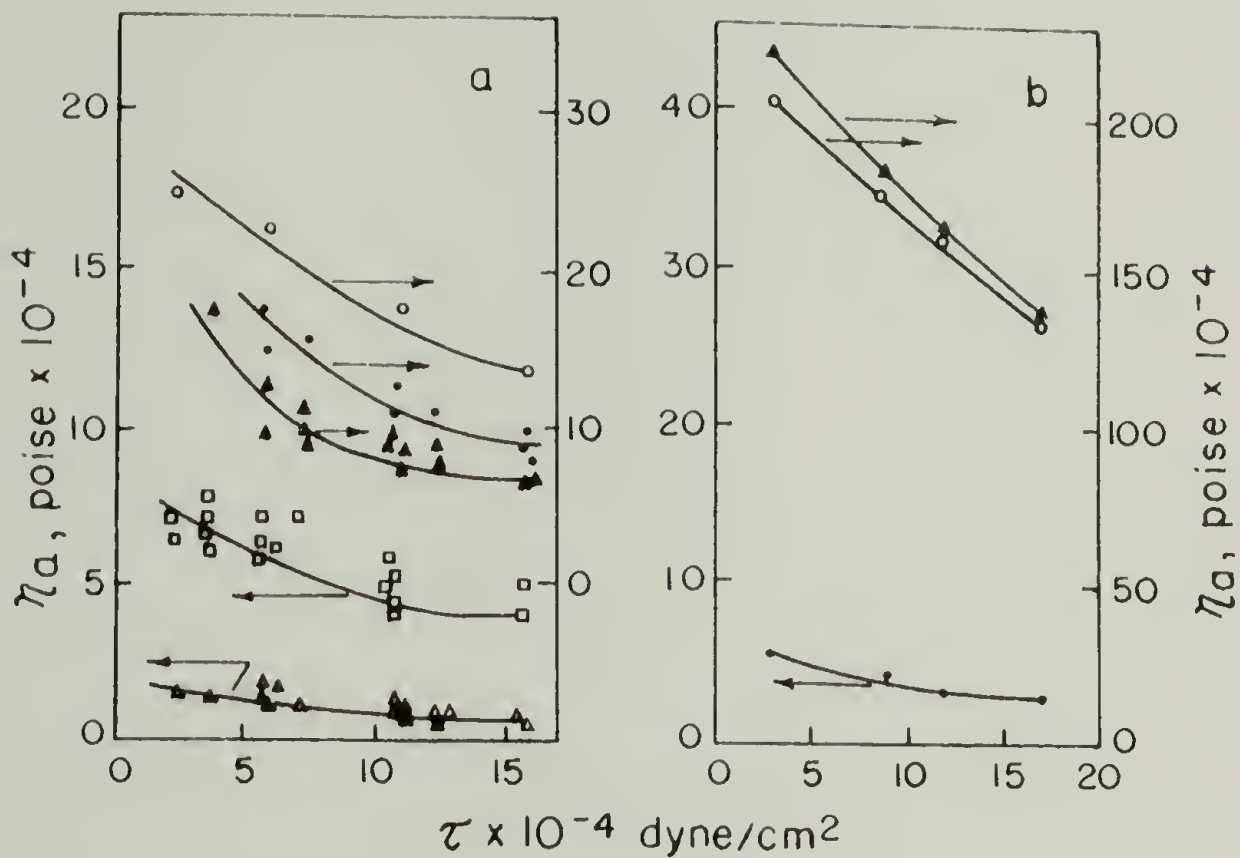


Figure 63. (a) Flow Curves for Polystyrene Melts of Different Histories at 190°C: (○), Original Sample; (●) Samples Prepared from Cyclohexane; (▲) Samples Prepared from Toluene and then again from Cyclohexane; (□), Samples Prepared from Toluene; (Δ), Samples Prepared from p-Xylene.

(b) Comparison of the Flow Curves of Melts of Original Polypropylene (○) and Samples Modified by Introducing 0.1% of Polyethylsiloxane Fluid PES-S, Introduced by Mechanical Mixing (▲) or by Codissolution in a Single Solvent (●). Temperature 194°C.

TABLE 1  
 PARTICLE LENGTHS OF POLY- $\gamma$ -BENZYL-L-GLUTAMATES  
 Particle Length,  $\text{\AA}$

$M_w$	$[\eta]_0$	Theoretical	From $[\eta]_0$	From Light Scattering
21,400	0.107	150	170	--
66,500	0.451	510	470	--
130,000	1.32	890	920	910
208,000	3.27	1420	1510	1410
358,000	7.20	2450	2450	2030

TABLE 2  
 SOME POLYPEPTIDES WHICH FORM LIQUID  
 CRYSTALS IN SUITABLE SOLVENTS

Polypeptide	$\left[ \text{NH} - \text{CHR} - \text{CO} \right]_n$	R
Poly-L-Gluatamic Acid		$-\text{CH}_2\text{CH}_2\text{COOH}$
PLGA Esters:		
γ-Methyl		$-\text{CH}_2\text{CH}_2\text{COOCH}_3$
γ-Ethyl		$-\text{CH}_2\text{CH}_2\text{COOCH}_2\text{CH}_3$
γ-Benzyl		$-\text{CH}_2\text{CH}_2\text{COOCH}_2\text{C}_6\text{H}_5$
(L+D Isomers)		
Poly-β-Benzyl-L-Aspartate		$-\text{CH}_2\text{COOCH}_2\text{C}_6\text{H}_5$
Poly-ε-Carbobenzyloxy-L-Lysine		$-(\text{CH}_2)_4\text{NHCOOCH}_2\text{C}_6\text{H}_5$

TABLE 3

## MECHANICAL PROPERTIES OF ORGANIC AND INORGANIC FIBERS

Fiber Material	Density g/cc.	GPa or $\frac{\text{dyne}}{\text{cm}^2} \times 10^{-10}$	Young's Modulus	Tensile Strength GPa	Specific Modulus $\frac{\text{GPa} \cdot \text{cc}}{\text{g}}$	Specific Strength $\frac{\text{GPa} \cdot \text{cc}}{\text{g}}$
Aromatic Amide	1.47	131	2.7	89.1	1.8	
Polyethylene (145)	.97	70.0	.48	72.2	.5	
Quartz	2.19	73.1	3.57	33.4	1.6	
Boron	2.30	400.2	2.76	174.0	1.2	
Beryllium	1.80	303.6	1.31	168.7	.7	
High Carbon Steel	7.81	207.0	4.14	26.5	.5	
Titanium	4.71	103.5	1.86	22.0	.4	
S-Glass	2.49	85.6	4.5	34.4	1.8	

C H A P T E R   I I  
RHEOLOGY OF CONCENTRATED SOLUTIONS OF  
POLY- $\gamma$ -BENZYL-GLUTAMATE

Abstract

Steady shear viscosity, dynamic viscosity, dynamic modulus, and normal force were measured via rotational rheometry for concentrated solutions of racemic mixtures of PBLG and PBDG in m-cresol. A transition from non-liquid crystalline to liquid crystalline order with increase in concentration was indicated by optical anisotropy and maxima in all four material functions. This occurred at a critical concentration higher than the Flory prediction. Some of the liquid crystalline solutions exhibited negative first normal stress differences over a well defined range of concentration and shear stress which was not due to inertial effects.

Introduction

It has been known for some time that solutions of rigid rod-like particles form anisotropic, i.e., liquid crystalline, solutions if the concentration is sufficiently high. Well-established theories (150-155) predict that, as the concentration of a dilute (isotropic) solution is increased, a phase transition occurs which results in the formation of an anisotropic phase. As concentration is increased fur-

ther, the fraction of anisotropic phase increases at the expense of the isotropic phase, without, however, changing the concentrations within each phase until the solution becomes fully liquid crystalline. This phenomenon has been demonstrated for systems of a variety of rod-like particles (156-159).

One class of rod-like molecules which has received considerable attention is the synthetic polypeptide, poly- $\gamma$ -benzyl-glutamate, usually the L enantiomer (PBLG). This polypeptide is obtainable in narrow molecular weight distributions, and in appropriate solvents forms a helix which behaves in solution like a rigid rod (160). When a single enantiomer is dissolved in an appropriate solvent, the helices all have the same optical rotatory sense, resulting in a cholesteric liquid crystal. However, for equimolar mixtures of both L and D enantiomers, a nematic liquid crystal is obtained (161). The early developments in this field have been reviewed (162). The rheology of concentrated solutions of this polymer was studied by Hermans (163) and later by Iizuka (164). Hermans studied several molecular weights of PBLG in m-cresol by capillary flow measurements. Iizuka used solutions of PBLG in  $\text{CH}_2\text{Br}_2$  and in dioxane, and made steady shear and oscillatory measurements using a cone-and-plate rheometer.

The present work is an extension of previous studies with distinctions in the following respects: (1) an equimolar mixture of PBLG and PBDG was used rather than a single enantiomer; (2) a wider range of homogeneous shear rates was accessible through the use of a variety of cones with different radii and cone angle for steady shear in the cone-plate geometry; (3) measurements of dynamic viscoelastic proper-

ties were made using the "eccentric rotating disc" geometry. This permits decoupling the viscous and elastic response of the system without the need for mechanical oscillation and the necessity of making precise phase angle measurements. This technique has been shown to give results equivalent to those from oscillatory shear for a variety of polymer solutions and melts (165).

### Experimental

PBLG of molecular weight 350,000 and low dispersity was obtained from Biopolymer Corp. of Moreland Hills, Ohio, and PBDG of molecular weight 320,000 and low dispersity was obtained from Pilot Chemical Corp. of Watertown, Massachusetts. All solutions contained equal weights of both enantiomers; this will henceforth be indicated by use of the acronym "PBG."

The (helicogenic) solvent selected was m-cresol in order to minimize concentration changes during measurement due to solvent evaporation. The m-cresol was distilled prior to use. Solutions from 3-10 wt. % were made by successive evaporation of a dilute solution in a vacuum evaporator at 80°C. Solutions from 25-11 wt. % were made by successive dilutions of a 25 wt. % solution which was obtained by introducing weighed amounts of PBG and m-cresol into a sealed container. A homogeneous solution was obtained in about two weeks.

Due to the high cost of the PBG and the high concentrations required, fresh solutions were not made up for each of the rheological measurements. Thus each solution was re-used several times. Importantly it has been shown that shear stresses higher than those achieved



in this study neither disrupt the helical structure of PBG of comparable molecular weight dissolved in m-cresol, nor cause mechanochemical degradation (166). The solutions were observed to darken with time but this was presumed to be due to oxidation of the solvent, which normally darkens on standing. In fact, the ease with which m-cresol oxidizes may be a desirable property for inhibiting solute oxidation. After rheological measurements were completed aliquots of each solution were retained and the polymer recovered by dissolving in methylene chloride followed by precipitation with methanol. The recovered PBG was then dissolved in dichloroacetic acid (a non-helicogenic solvent) to  $.0467 \pm .00002$  wt%. Flow times through a Ubelhode viscometer were compared to that for a solution of fresh polymer. In all cases the flow times were found to be identical, indicating that no degradation had occurred.

Steady shear viscosity and total normal thrust measurements were made on a Rheometrics RMS-7200 mechanical spectrometer. Shear rates in the range of  $0.25-10,000 \text{ sec}^{-1}$  were accessible through the use of cone and plate geometries of the following radii (in cm) and cone angles (in rad) respectively; 5.00, .04; 2.50, .04; 2.50, .1; 1.25, .1; 1.25, .01. All data reported herein represented the averages of many measurements. Precision within runs was ~5% for both viscosity and normal force, however, run-to-run reproducibility was no better than 20% in some cases. This scatter was not due to instrument instability but to some unknown phenomenon, possibly occurring at the platen surface.

An effort was made to obtain data at each shear rate using as

wide a variation in geometry as possible. The data at intermediate shear rates were measured over the overlapping ranges for at least two different cones with data at extremely low and high shear rates measured with one cone only. Data at shear rates  $>1000 \text{ sec}^{-1}$  are not from steady state measurements due to sample exuding from the gap at longer times. Reported values were extrapolated to time of initiation of shear. All data were taken with both clockwise and counterclockwise rotation, which gave identical results.

Dynamic viscosities and moduli were measured in the same instrument using the eccentric rotating disc mode over a rotation speed range of .01-62.5 rad/sec. Each reported point represents an average of many measurements generally made with plates of different radii and plate separation. To test whether results were in the linear viscoelastic region, each measurement was made at five different strains ranging from .15-.75 at low rotation speeds to .03-.15 at high rotation speeds. This procedure reduced the rather large scatter of data which amounted to about 30% of the mean values reported.

All measurements were made at an ambient temperature of  $24 \pm 0.5^\circ\text{C}$ . Shear heating as measured by a thermocouple imbedded in one platen was negligible.

## Results

Birefringence. Examination of the PBG solutions in m-cresol by polarizing microscope indicated that solutions of 8.1 wt% and below were optically isotropic and solutions of 9.9% and above were optically anisotropic. This result may be compared with conditions

expected to produce anisotropy by theory. For example, PBG of molecular weight 335,000 corresponds to 1506 residues. Since the diameter of the  $\alpha$ -helix is  $15\text{\AA}$  and the length of the helix is  $1.5\text{\AA}$  per residue, the axial ratio would be 150 (167). The appropriate equation given by Flory (152)

$$\phi_2^* = \frac{8}{p} \left( 1 - \frac{2}{p} \right)$$

yields a critical volume fraction for formation of an anisotropic phase of .053. This corresponds to a concentration of 6.9 wt% for PBG in m-cresol. Thus the Flory theory appears to slightly underestimate the critical concentration for formation of the anisotropic phase. An error in this direction would be expected if the helices are not perfectly rigid (155).

Steady shear and dynamic viscosities. Steady shear viscosity measurements were made over a wide range of shear rates for all concentrations. In all cases a low shear limiting viscosity was obtained but in no case could a high shear limiting viscosity be observed. Plotting the low shear limiting viscosity reveals a rapid increase with concentration to a maximum at 11.0 wt%, followed by an equally rapid decrease to a minimum at 22 wt%; see Figure 64. At yet higher concentrations there is the suggestion of further gradual increase in viscosity. The shoulder which appears on the low concentration side of the viscosity maximum is unlikely to be due to experimental error. Moreover, a comparable feature has been reported by Iizuka (164).

Steady shear viscosity measurements for the three lowest

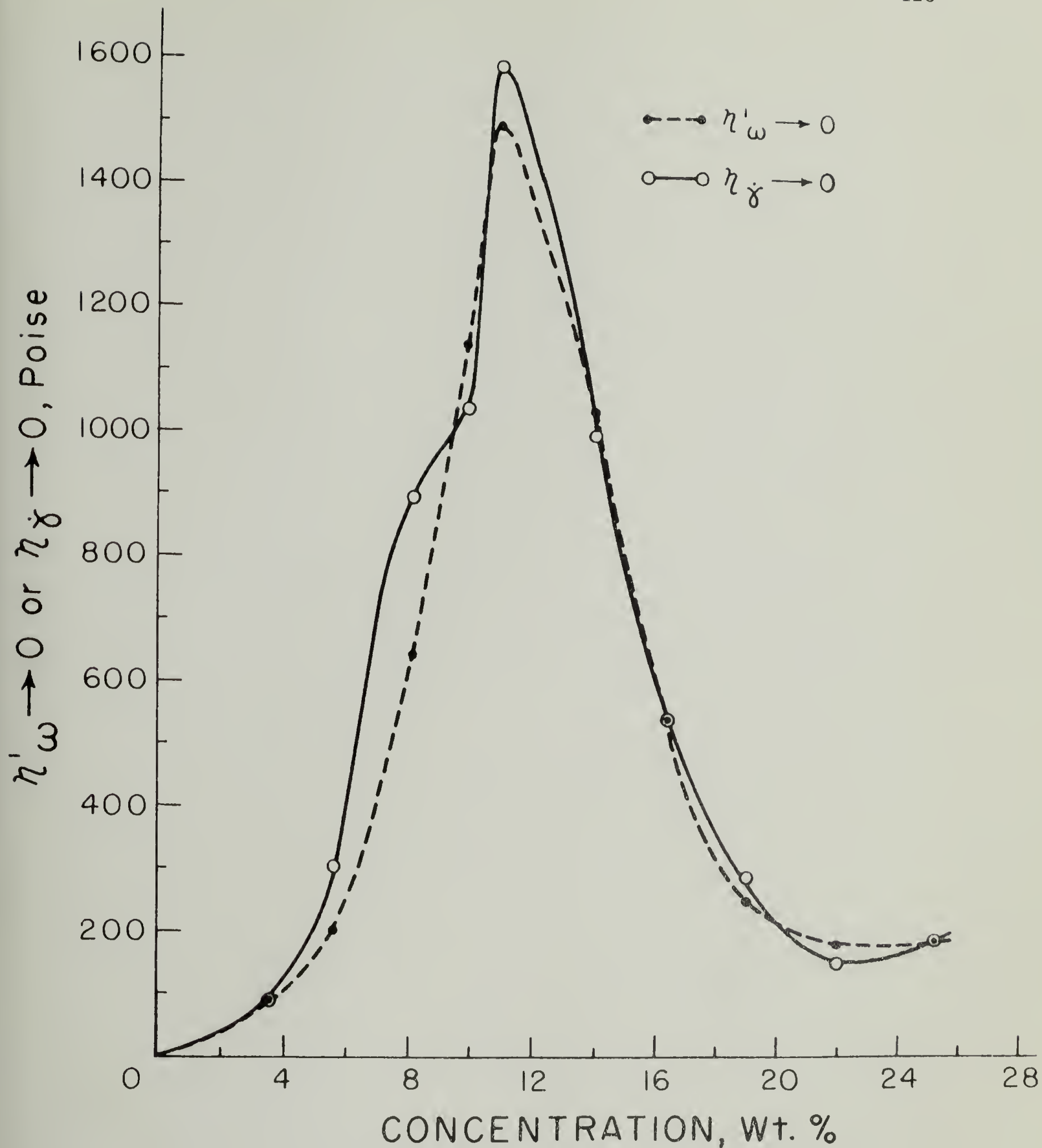


Figure 64. Low Shear Limit of Steady Shear Viscosity and Low Frequency Limit of Dynamic Viscosity Versus Concentration for 335,000 M.W. PBG.

concentration solutions did not extend to a shear rate high enough to obtain an unambiguous power law index (i.e., the exponent  $n$  such that  $\tau_{12} \propto \dot{\gamma}^n$ ), but an estimate of  $n = .12$  can be made; see Figure 65. The solutions of concentration 9.9 wt% and above all gave measurements in the power law region; in some cases  $\log \eta$  vs.  $\log \dot{\gamma}$  was linear for up to four decades of shear rate; see Figure 66. The power law index obtained for these solutions were in the range  $n = .45-.5$ .

It can be seen in Figures 65 and 66 that the flow curves for the different solutions intersect, implying that the concentration at which the viscosity reaches a maximum depends on the shear rate. Indeed, it would be expected that the effect of shear orientation would be to ease the formation of the anisotropic phase. This behavior is seen explicitly in Figure 67, which shows that the concentration of maximum viscosity decreases with shear rate, in agreement with the observation of Hermans (163).

Dynamic viscosity measurements were made for all concentrations over a frequency range of three decades in most cases; see Figures 68 and 69. Clear low frequency limiting values were indicated in most cases, which agree well with the low shear limit of  $\eta$  (see Figure 64). The maximum value of  $\eta'_{\omega \rightarrow 0}$  was observed at the same concentration as the maximum value of  $\eta_{\dot{\gamma} \rightarrow 0}$ . However, the shoulder on the low concentration side of the viscosity maximum was clearly absent. Also, it is not clear whether the dynamic viscosity would have increased gradually with further concentration, or had reached a limiting value.

The curves of  $\log \eta'$  vs.  $\log \omega$  for various concentrations; see

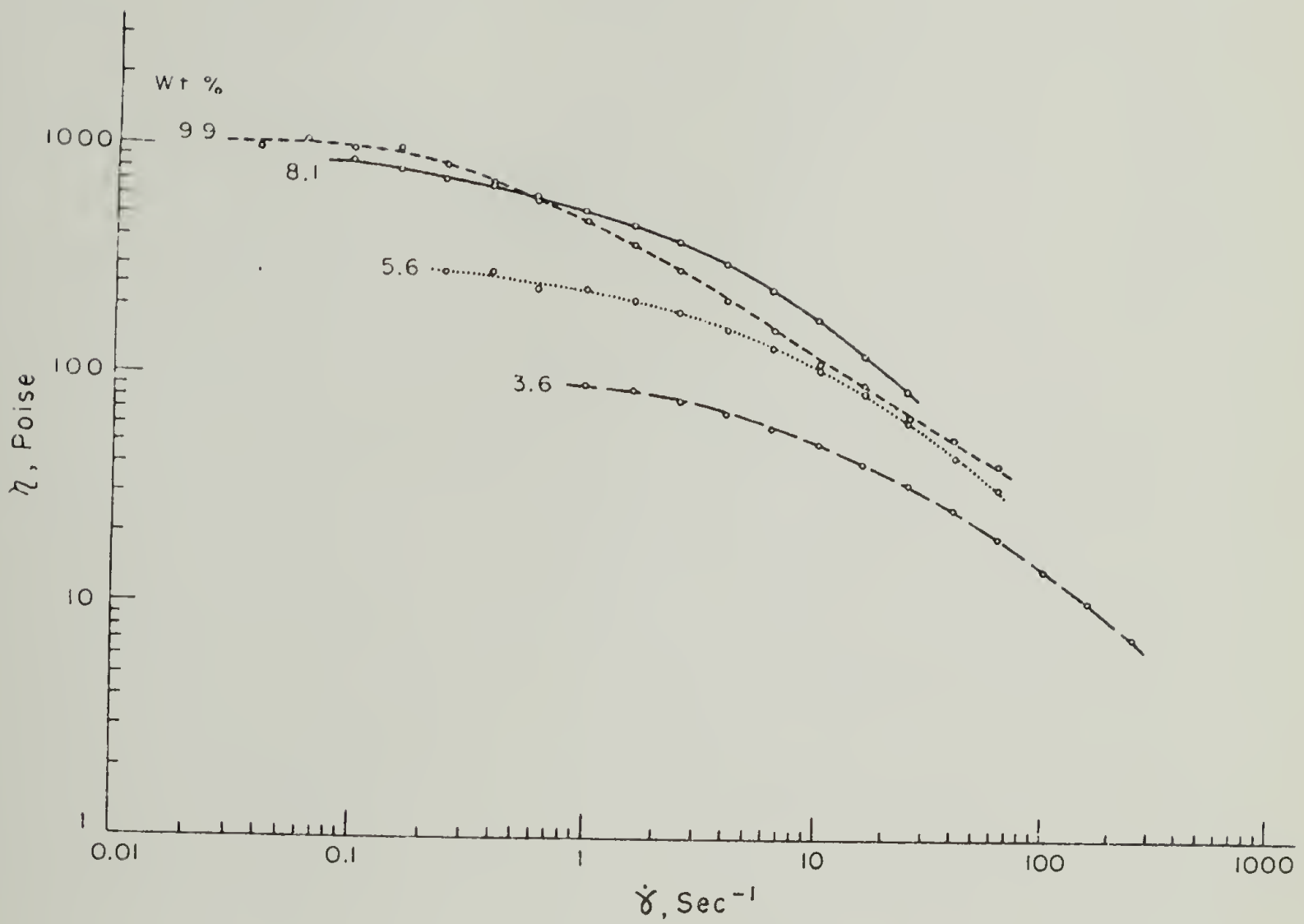


Figure 65. Steady Shear Viscosity Versus Shear Rate for 335,000 M.W. PBG Solutions.

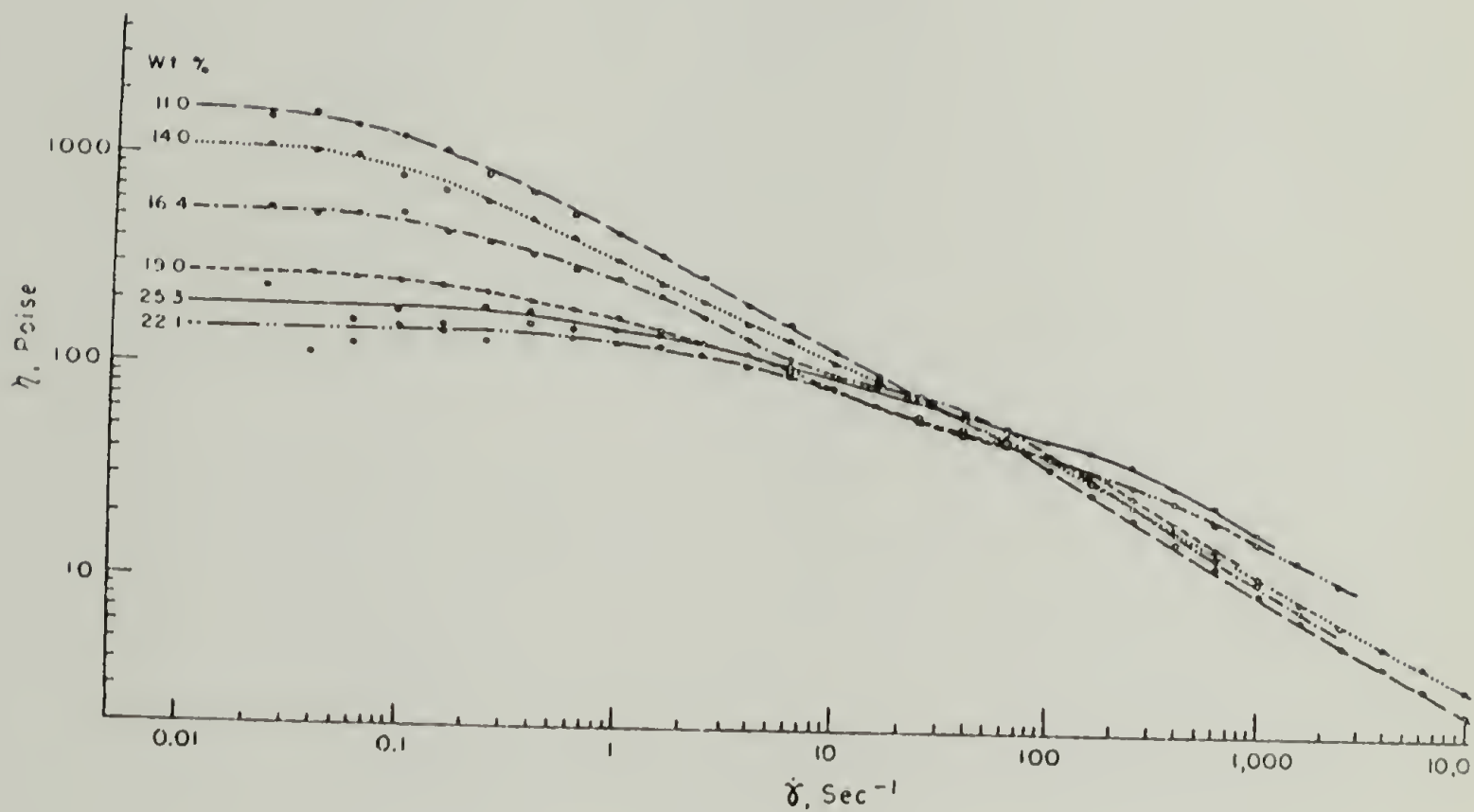


Figure 66. Steady Shear Viscosity Versus Shear Rate for 335,000 M.W. PBG Solutions.

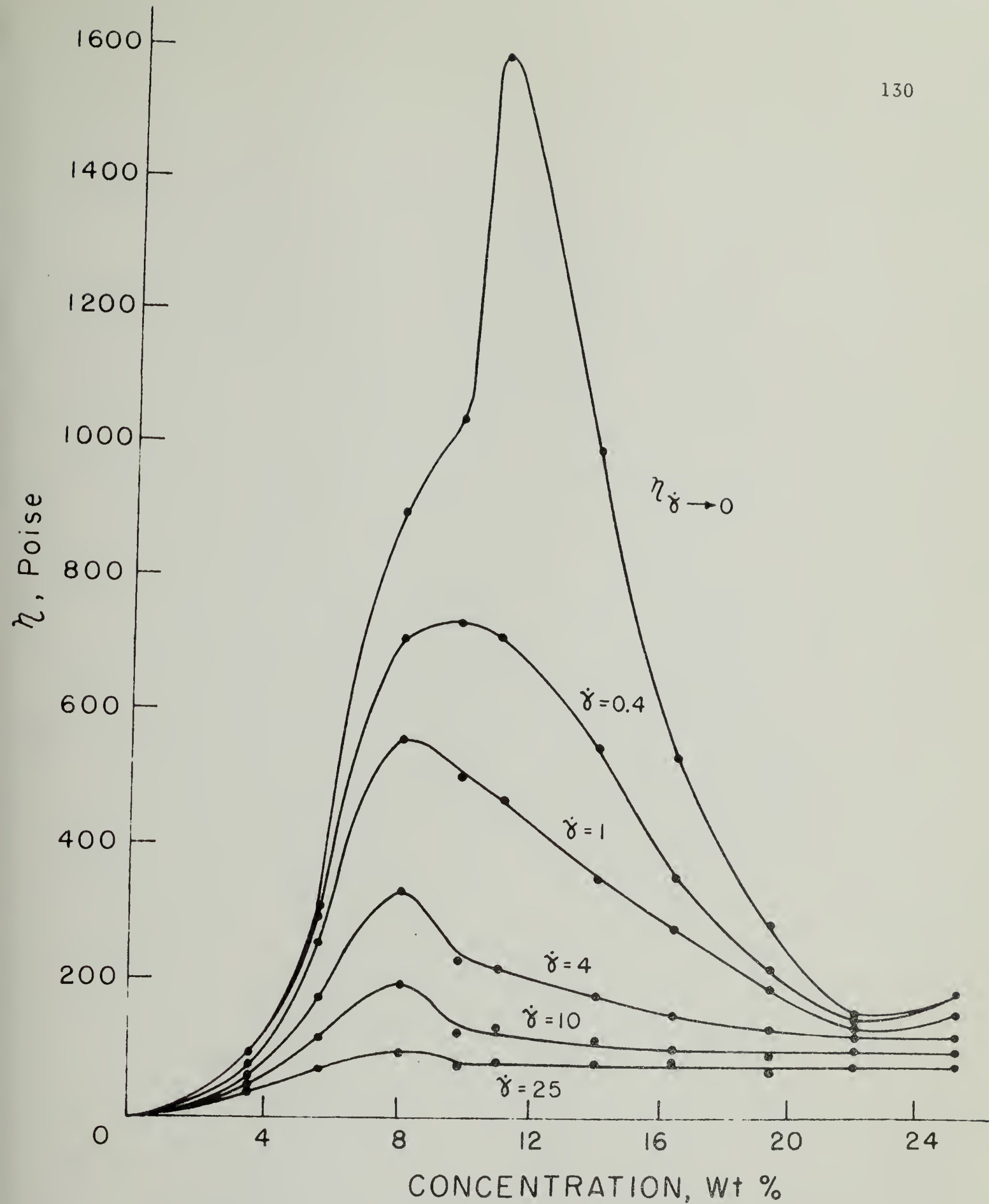


Figure 67. Concentration Dependence of Steady Shear Viscosity at Several Shear Rates for 335,000 M.W. PBG.



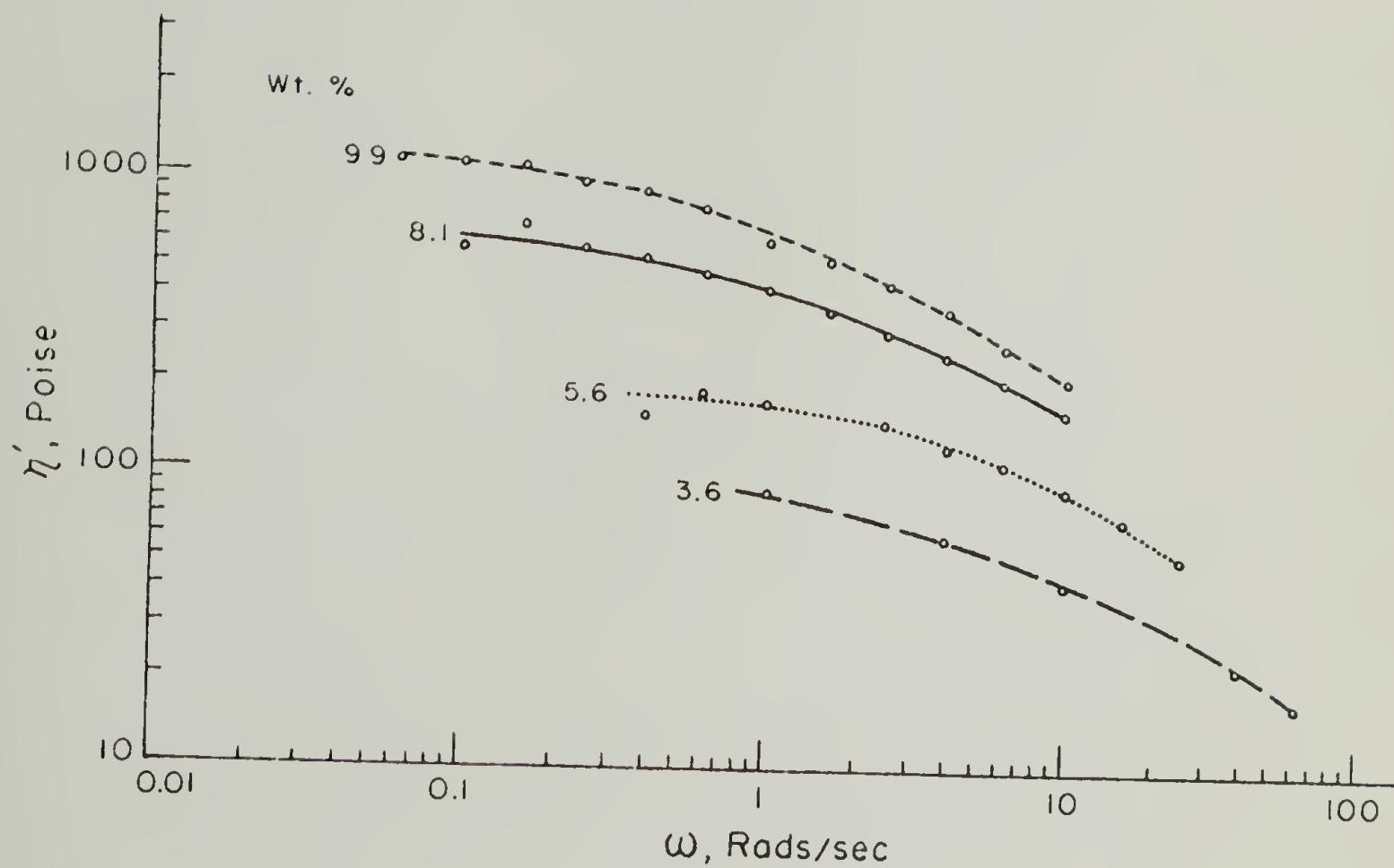


Figure 68. Dynamic Viscosity Versus Frequency for 335,000 M.W. PBG Solutions.

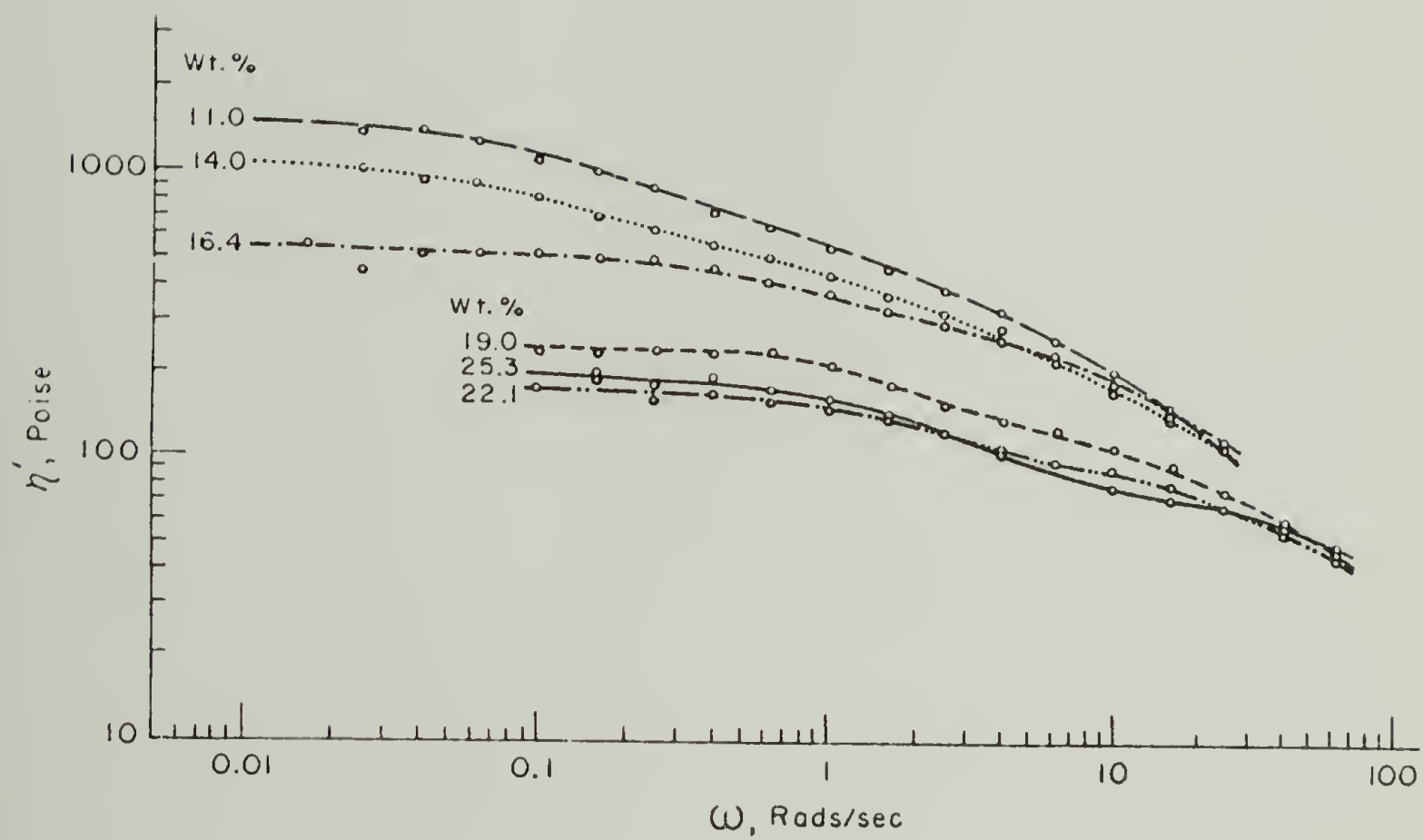


Figure 69. Dynamic Viscosity Versus Frequency for 335,000 M.W. PBG Solutions.

Figures 68 and 69, generally did not cross, indicating that the peak in  $\eta'$  vs.  $C$  would not be shifted to lower concentration by an increase in frequency of measurement. Thus, unlike steady shear, dynamic shear does not appear to drive the thermodynamic transition to the anisotropic phase to a lower concentration.

It is also suggested in Figure 69 that  $\log \eta'$  vs.  $\log \omega$  converge to a common curve at high  $\omega$  for all concentrations above that at which the viscosity peak was observed. This behavior is in contrast to that of the same solutions in steady shear for which curves of  $\log \eta$  vs.  $\log \dot{\gamma}$  all intersect at approximately the same point; see Figure 66. It is of note that the curves of  $\log \eta$  vs.  $\log \dot{\gamma}$  change order at this intersection point; i.e., viscosity decreases with concentration for solutions between 11.0-25.3 wt% at lower shear rates and increases with concentration at higher shear rates.

The plateaus which occur in curves of  $\log \eta'$  vs.  $\log \omega$  and to a lesser extent in  $\log \eta$  vs.  $\log \dot{\gamma}$  were experimentally significant and reproducible. They may have been a consequence of the use of a mixture of two polymers (PBLG and PBDG) of slightly different M.W. as the solute.

It is worthwhile to contrast the behavior of solutions on either side of the viscosity-concentration maximum with increasing deformation rate (i.e., shear rate or frequency). The steady shear viscosities of the non-liquid crystalline solutions (those below the viscosity maximum) was much more dependent on shear rate than those of the liquid crystalline solutions (those above the viscosity maximum), as is indicated by the difference in power law exponents; see

Figures 65 and 66. The dependence of dynamic viscosity on frequency was also slightly greater for the non-liquid crystalline solutions, though this difference is less evident due to the curvature of the graphs and the restricted range of measurements; see Figures 68 and 69. A more easily seen difference in the dynamic viscosity behaviors is that  $\log \eta'$  vs.  $\log \omega$  tends to converge to a common curve for the liquid crystalline solutions (see Figure 69) but not for the non-liquid crystalline solutions (see Figure 68).

Dynamic modulus. Dynamic modulus,  $G'$ , measurements were made for all solutions over a range of about two decades of frequency,  $\omega$ , see Figures 70 and 71.  $\log G'$  vs.  $\log \omega$  increases linearly with a slope of slightly less than one for most concentrations. However,  $\log G'$  vs.  $\log \omega$  for the 9.9 wt% solution is curved and intersects the curve for 11.0 wt% at a frequency of 1 rad/sec. This means that for frequencies greater than 1 rad/sec the maximum modulus occurred at 9.9 wt% whereas for frequencies less than 1 rad/sec the maximum modulus occurred at 11.0 wt%.  $G'$  at a frequency of 4 rad/sec is plotted against concentration in Figure 72. It is quite similar in appearance to  $\eta_{\dot{\gamma} \rightarrow 0}$  vs.  $C$  and  $\eta'_{\omega \rightarrow 0}$  vs.  $C$ . (see Figure 64). There is a suggestion of a shoulder on the high concentration side of the maximum, possibly due to the coexistence of an isotropic phase and an anisotropic phase at these concentrations. This would correspond to a concentration between Robinson's A-point and B-point (159). This curve of  $G'$  vs.  $C$  differs from those obtained by Iizuka (164) for PELG in dioxane of  $\text{CH}_2\text{Br}_2$  in that  $G'$  does not appear to increase

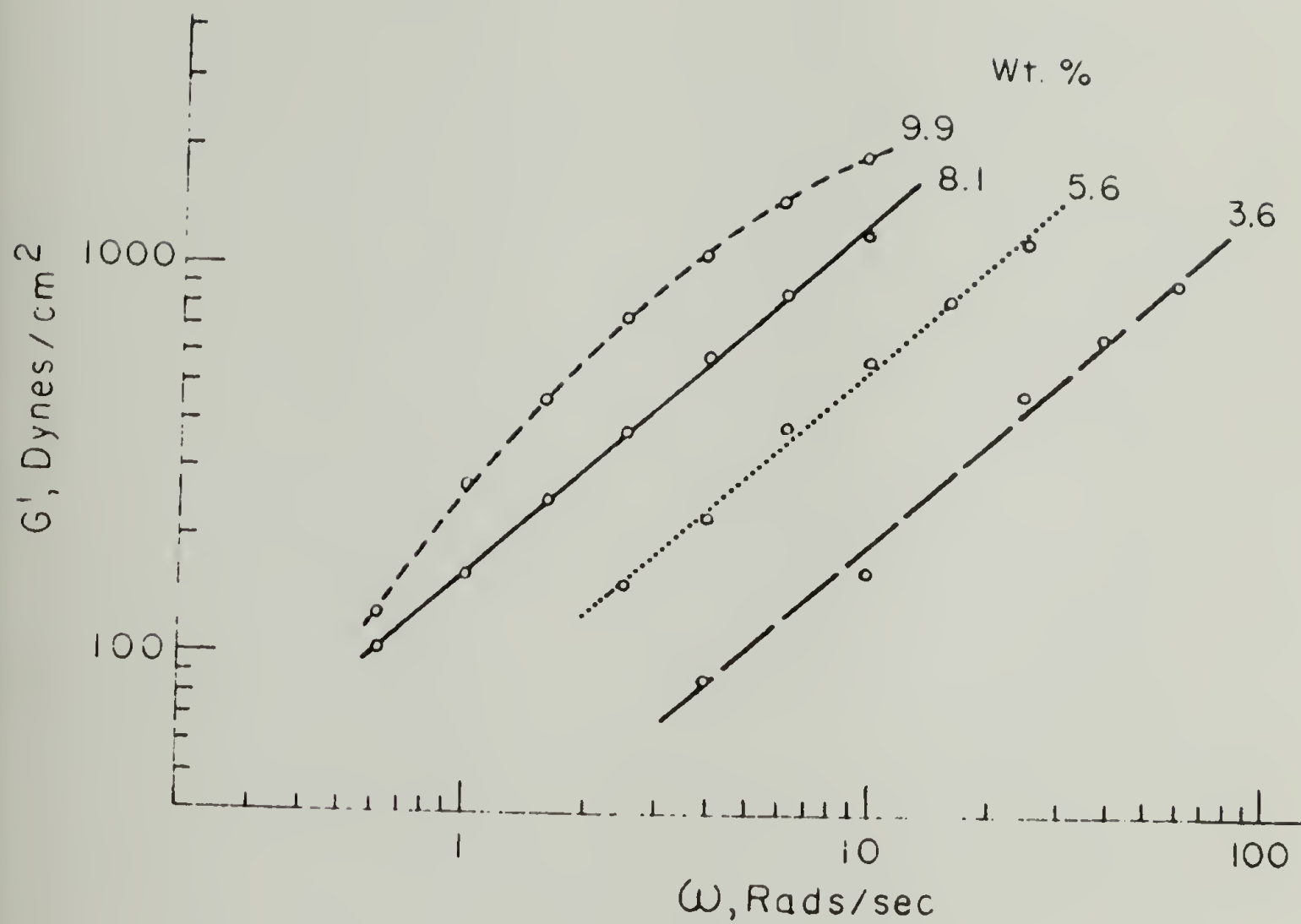


Figure 70. Dynamic Modulus Versus Frequency for 335,000 M.W. PBG Solutions.

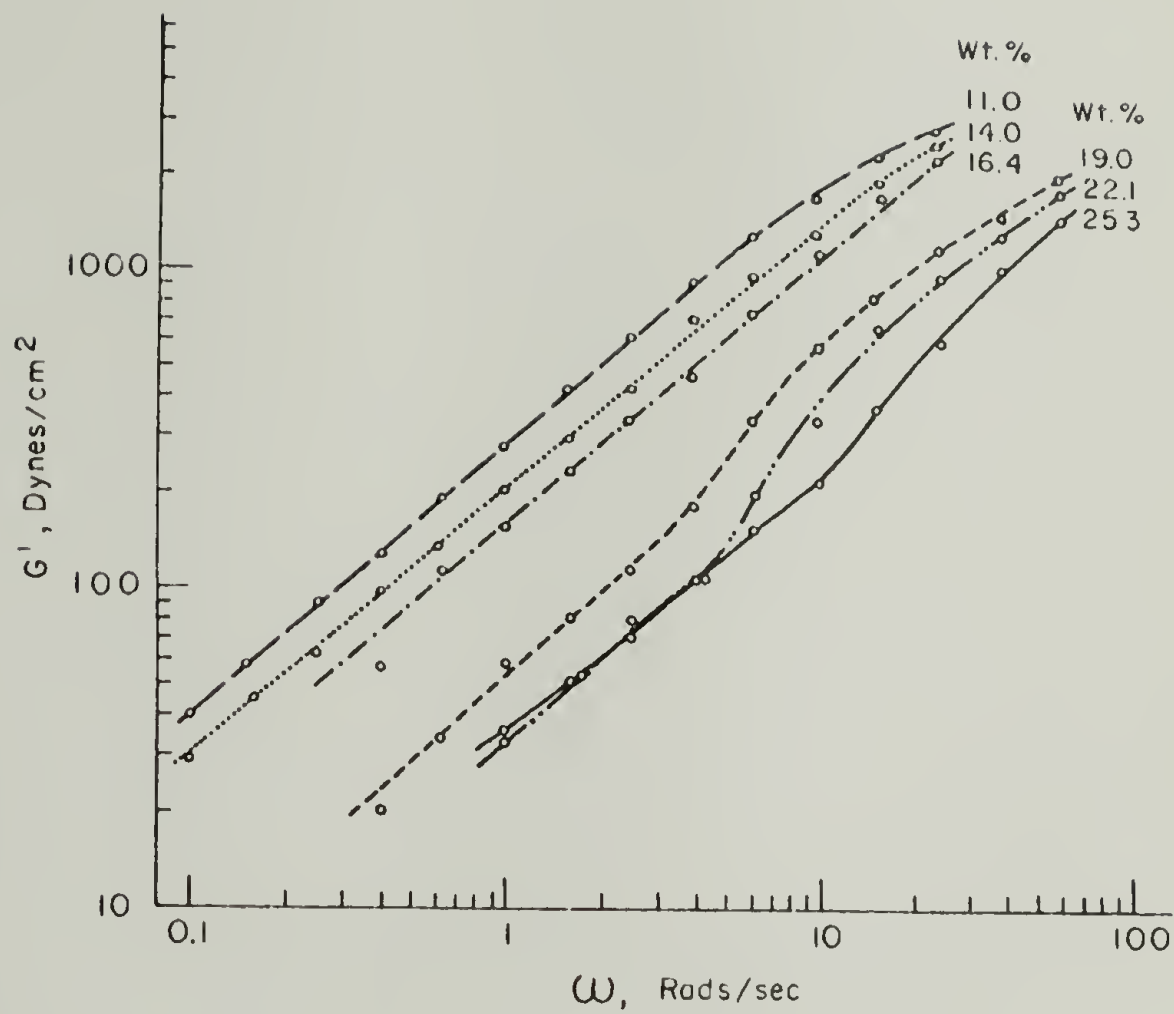


Figure 71. Dynamic modulus versus frequency for 335,000 M.W. PBG solutions.

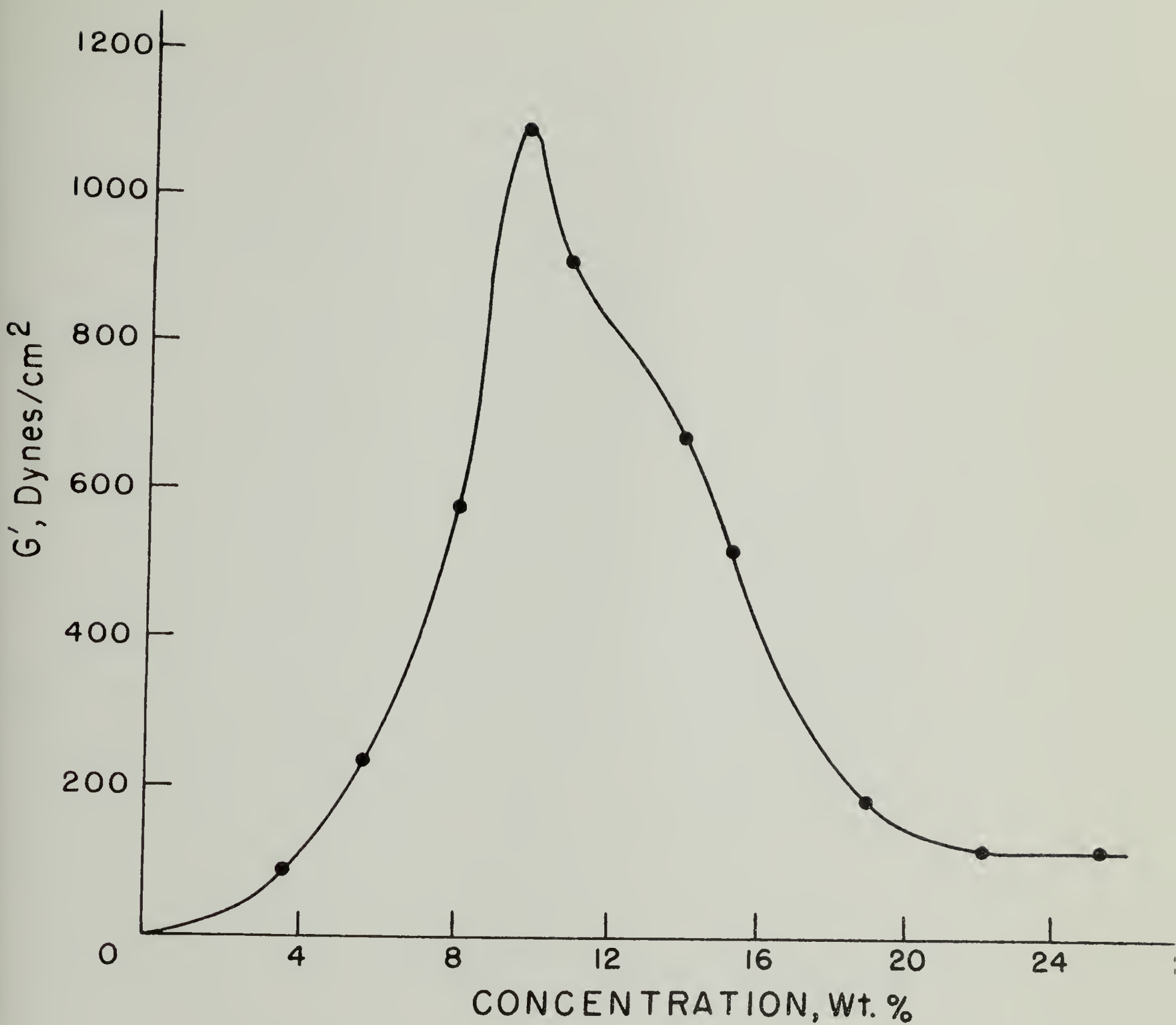


Figure 72. Dynamic Modulus at  $\omega = 4$  rad/sec Versus Concentration for 335,000 M.W. PBC.

sharply again at the highest concentrations, where the solutions were fully liquid crystalline.

Referring again to Figure 71, we observe that the curve of  $\log G$  vs.  $\log \omega$  deviates from linearity for the three highest concentrations at higher frequencies. The onset of these deviations appears to be at frequencies such that  $G'$  was approximately constant at 100-200 dyne/cm<sup>2</sup>.

It is significant that the slope of  $\log G'$  vs.  $\log \omega$  is similar for both liquid crystalline and non-liquid crystalline solutions, whereas  $\log \eta$  vs.  $\log \dot{\gamma}$  and  $\log \eta'$  vs.  $\log \omega$  were quite different (see Figures 65, 66, 68 and 69). The value of this slope (slightly less than one) is in contrast to the Kirkwood-Auer (168) prediction of a slope of two at low frequencies, increasing to an asymptotic value at high frequency. Of course, the K-A theory was derived for dilute solutions of rigid rods and cannot be applied to concentrated solutions. Predictions of the dynamic elastic behavior of liquid crystalline or concentrated solutions of rigid rods are lacking.

First normal stress difference. The first normal stress difference  $\tau_{11} - \tau_{22}$  was measured via total normal thrust for flow in a cone-and-plate geometry for all solutions over a wide range of shear rates.

The four least concentrated solutions were investigated prior to improvements in instrumentation which greatly extended the accessible shear rate range. All results are shown in Figure 73. The plots of  $\log \tau_{11} - \tau_{22}$  vs.  $\log \dot{\gamma}$  are convex and parallel. The maximum



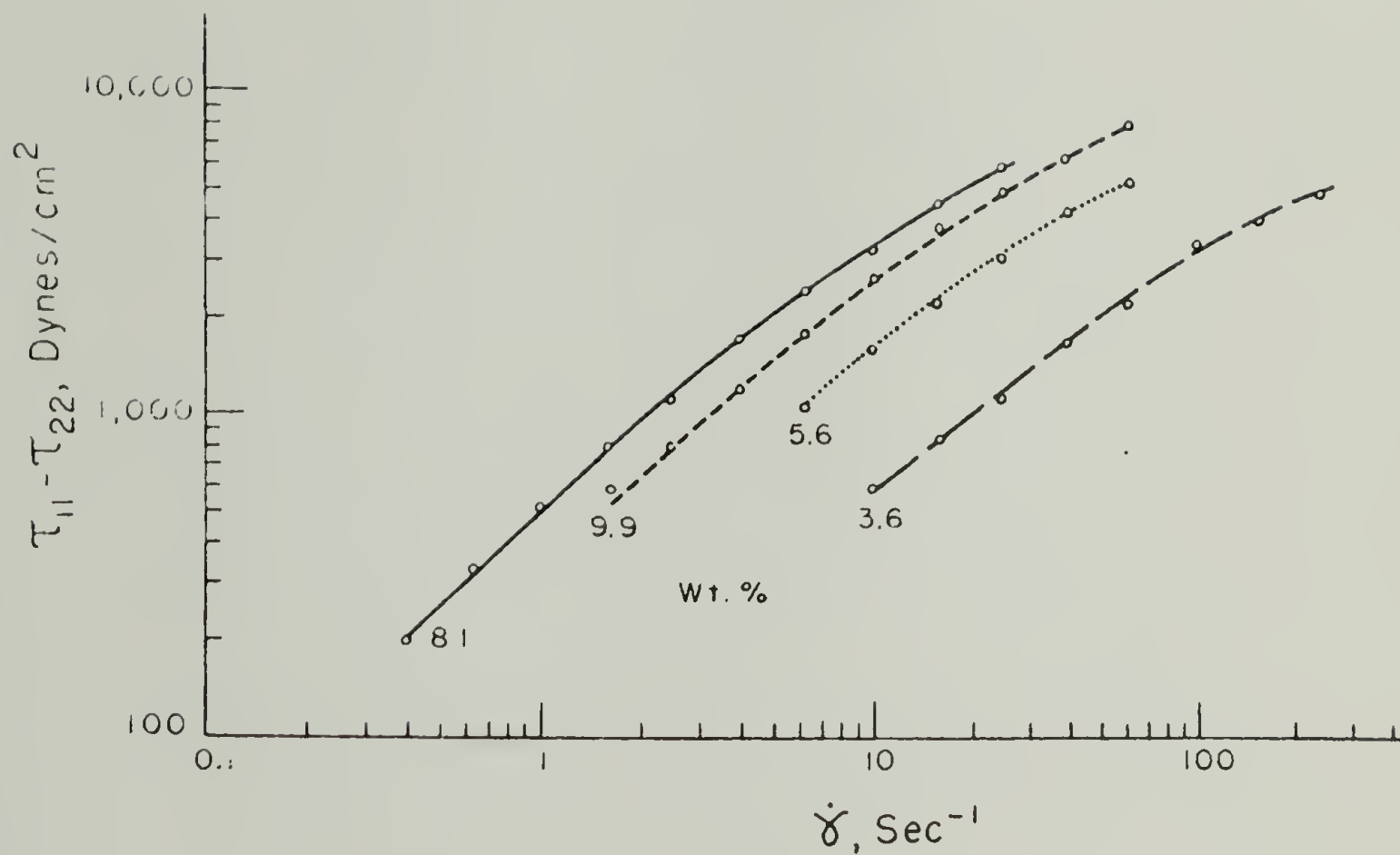


Figure 73. First Normal Stress Difference Versus Shear Rate for 335,000 M.W. PBG Solutions.

value of  $\tau_{11} - \tau_{22}$  was exhibited by the 8.1 wt% solution over the entire range of shear rate.  $\log \tau_{11} - \tau_{22}$  vs.  $\log \dot{\gamma}$  for the 11.0 wt% solution is shown in Figure 74. This curve has quite a peculiar appearance, with an inflection point at  $1 \text{ sec}^{-1}$  followed by a convex region, another inflection point at  $70 \text{ sec}^{-1}$  and finally a long linear region with slope of .6. It is possible, but not likely, that the four least concentrated solutions would have behaved similarly if a greater range of shear rate had been accessible and that those measurements which could be made fell fortuitously in the convex region.

$\tau_{11} - \tau_{22}$  for the 14.0 wt% solution is presented in Figure 75. The appearance of this curve is peculiar indeed, with  $\tau_{11} - \tau_{22}$  increasing with  $\dot{\gamma}$  for low shear rate, reaching a maximum at  $\dot{\gamma} \approx .2 \text{ sec}^{-1}$ , abruptly becoming negative at  $\dot{\gamma} \approx .6 \text{ sec}^{-1}$ , reaching a maximum negative value at  $\dot{\gamma} \approx 3 \text{ sec}^{-1}$ , and abruptly becoming positive again at  $\dot{\gamma} \approx 5 \text{ sec}^{-1}$ , then increasing to a linear region with slope of approximately 0.7. This remarkable behavior was also observed for solutions of concentrations 16.4, 19.0 and 22.1 wt%; see Figures 76, 77, and 78. The solution of concentration 25.3 wt% did not exhibit any unusual (negative) normal stress behavior; see Figure 79.

It can be observed in Figures 75 through 78 that the shear rates at which the reversals in sign of  $\tau_{11} - \tau_{22}$  occurred were concentration dependent. The shear stress to which the fluids were being subjected at these reversal points is shown in Figure 80 as a function of concentration. The experimental points frame an area in which negative first normal stress differences were observed. The dashed extrapolations intersect at a concentration of 11 wt%,

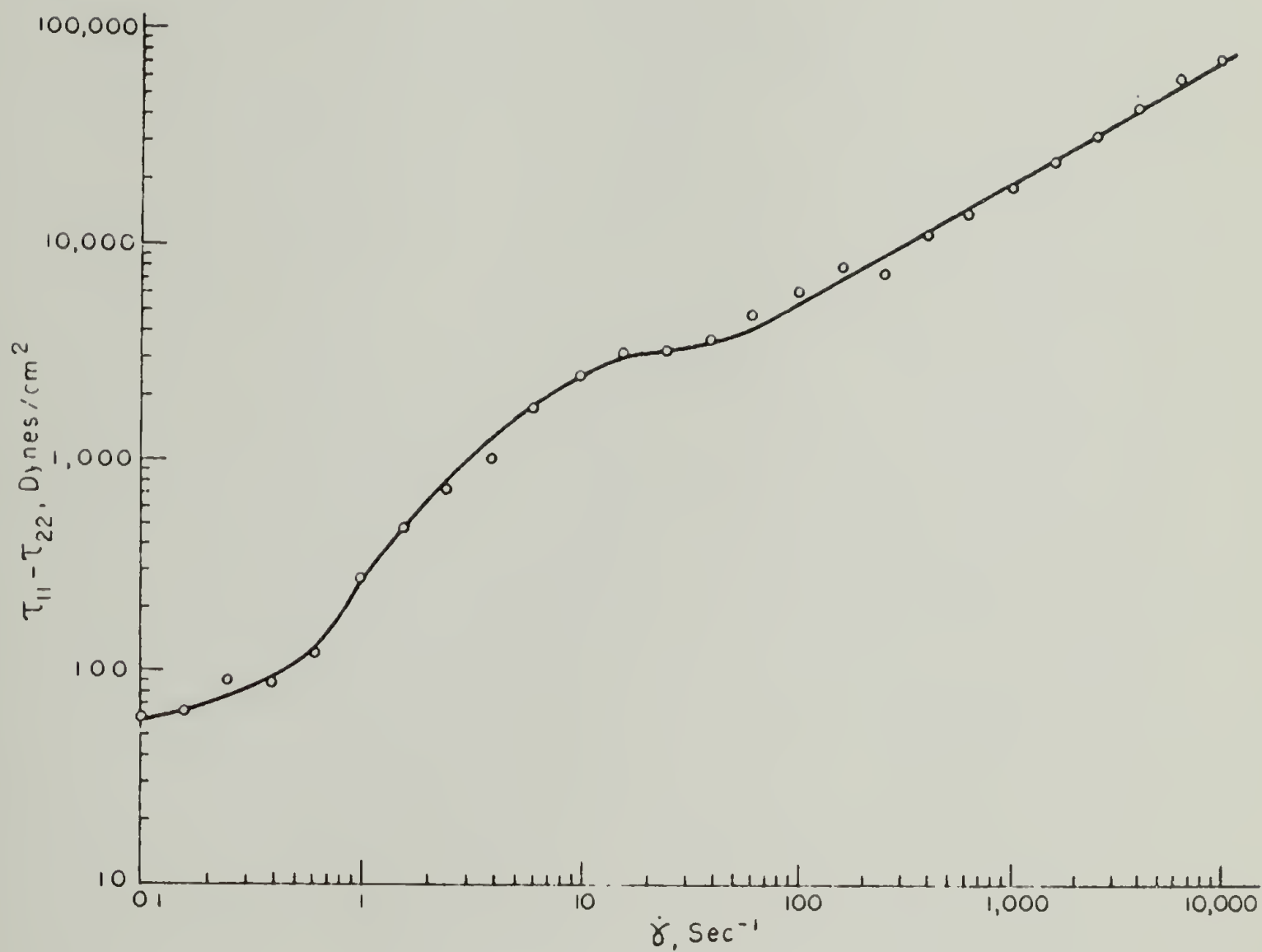


Figure 74. First Normal Stress Difference Versus Shear Rate for 335,000 M.W. PBG (11.0 wt%).

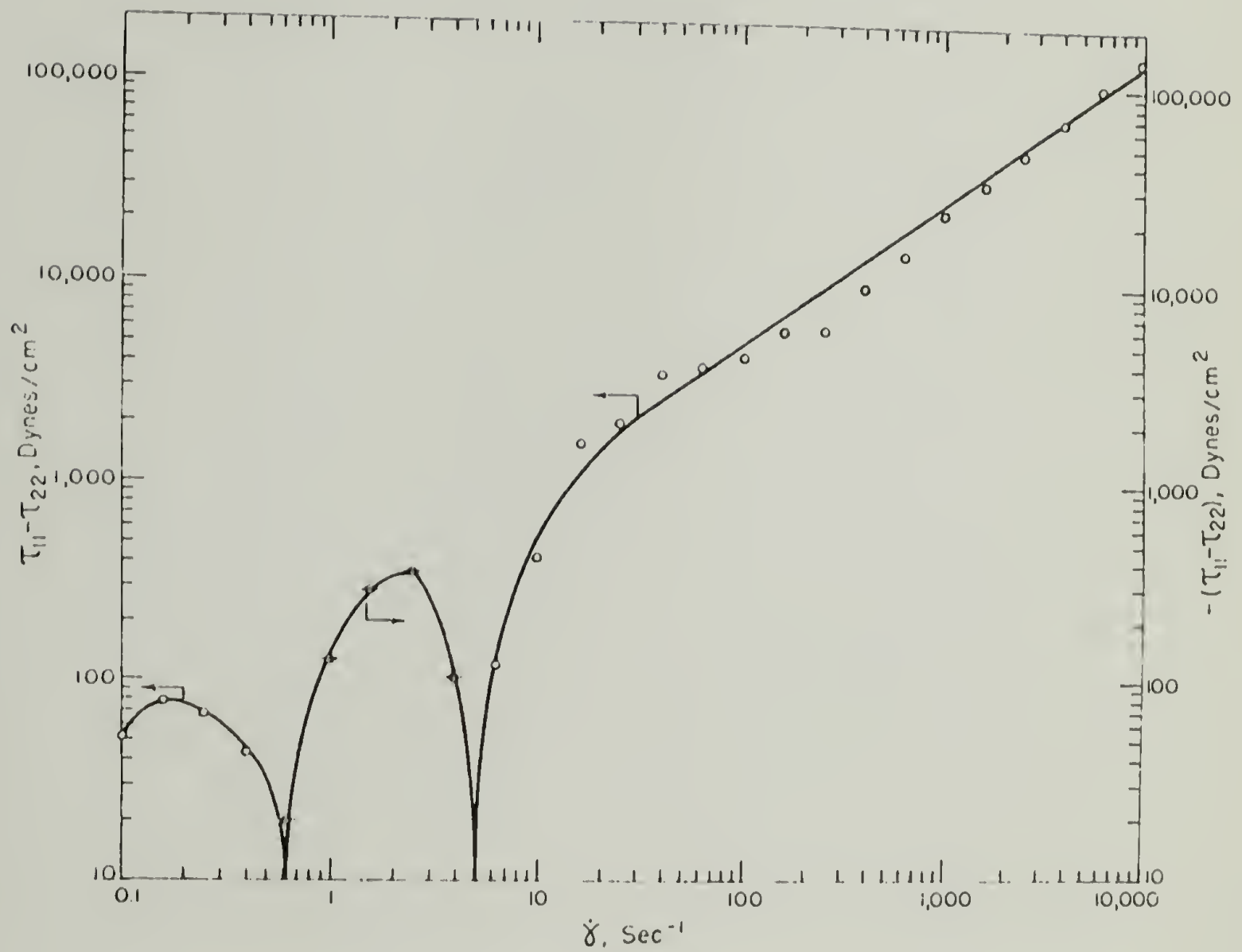


Figure 75. First Normal Stress Difference Versus Shear Rate for 335,000 M.W. PBG (14.0 wt%).

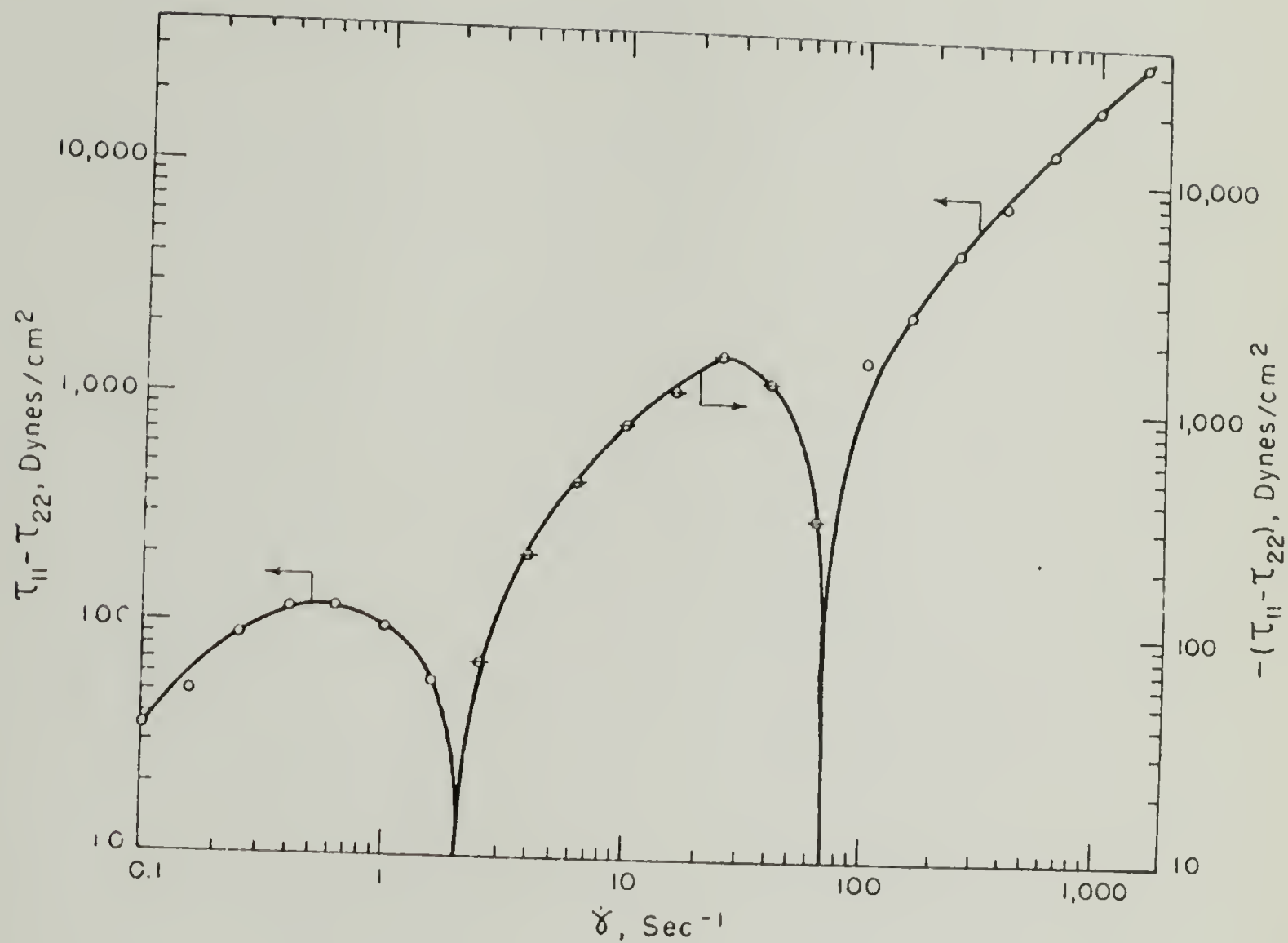


Figure 76. First Normal Stress Difference Versus Shear Rate for 335,000 M.W. PBG (16.4 wt%).

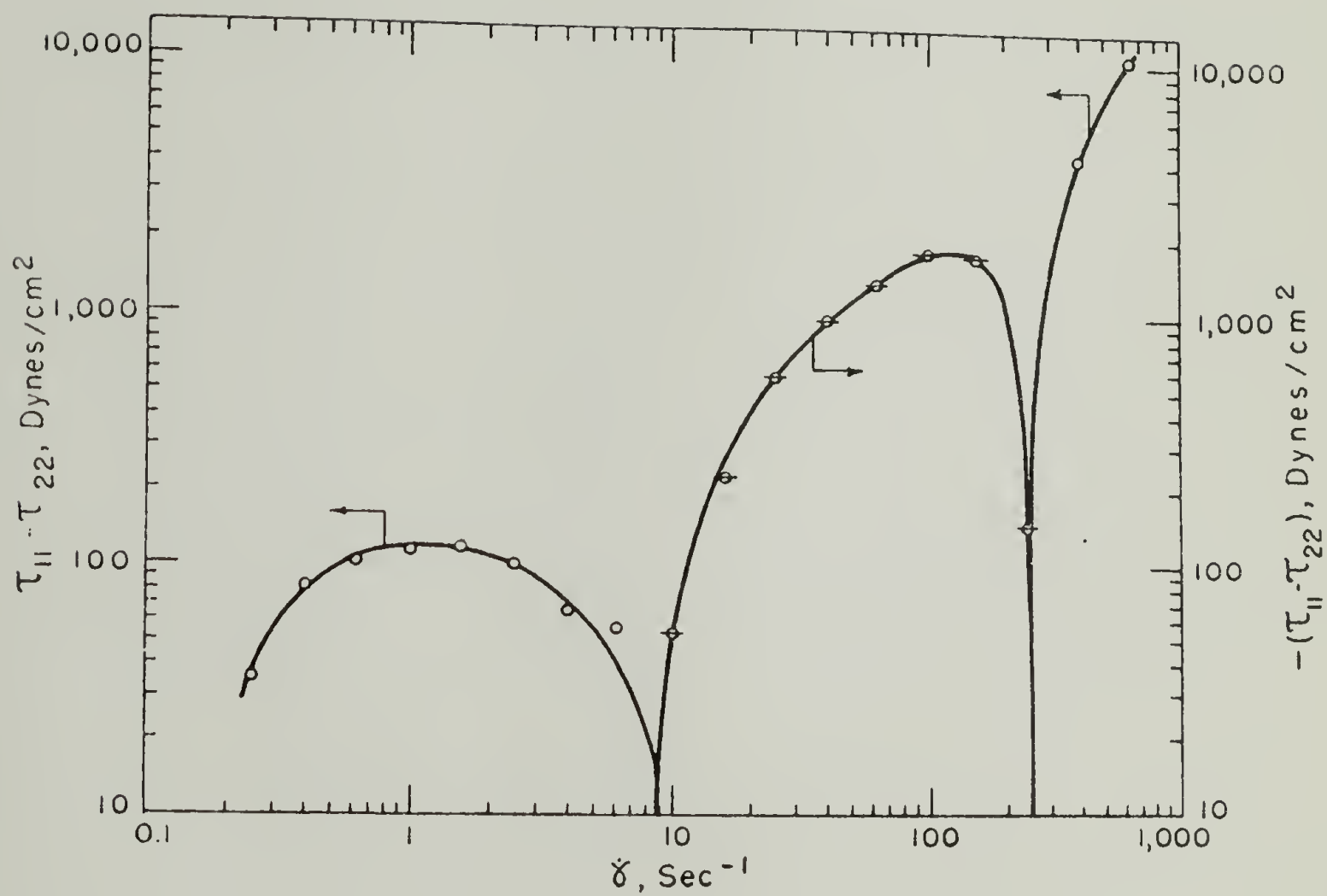


Figure 77. First Normal Stress Difference Versus Shear Rate for 335,000 M.W. PBG (19.0 wt%).

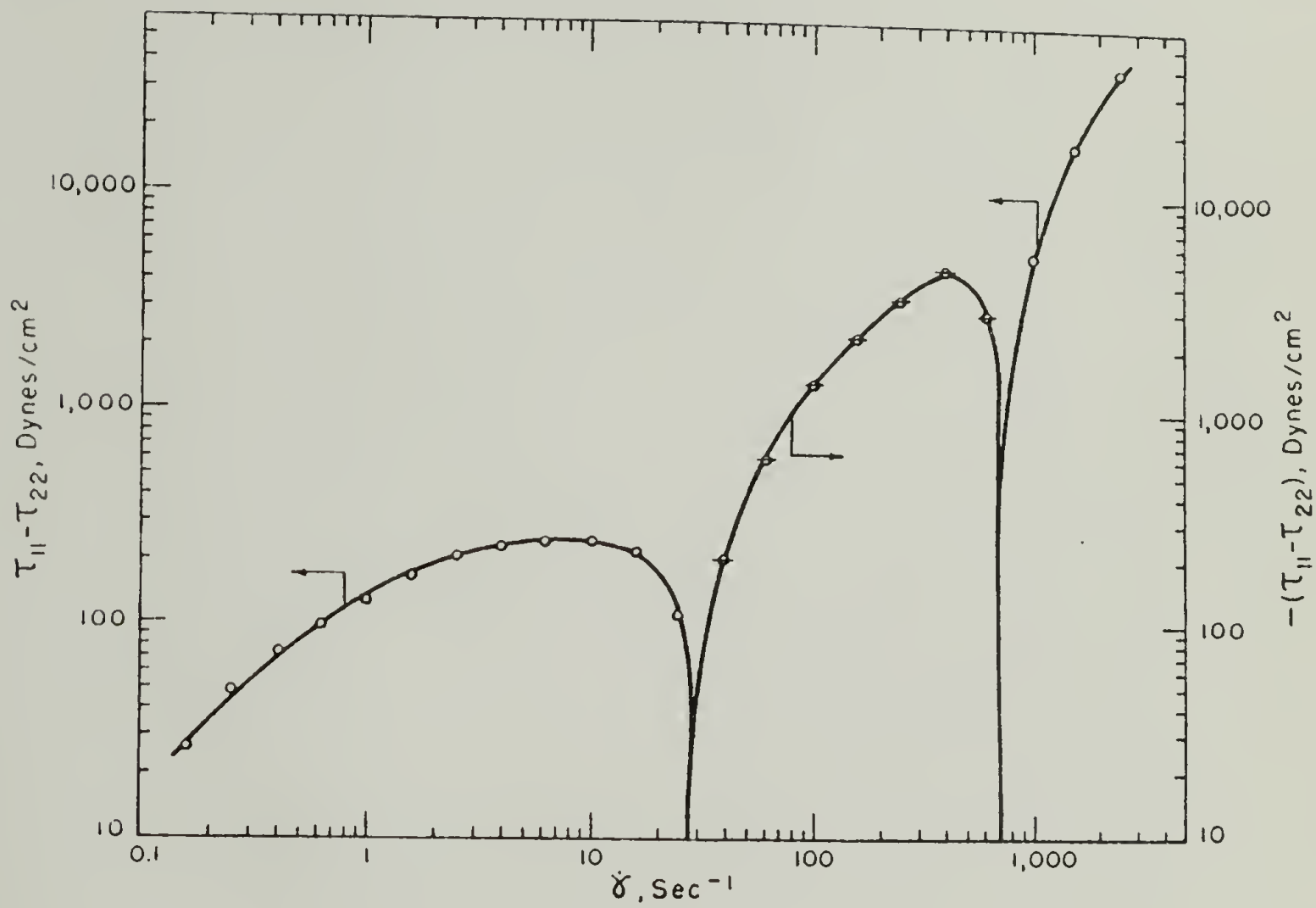


Figure 78. First Normal Stress Difference Versus Shear Rate for 335,000 M.W. PBG (22.1 wt%).

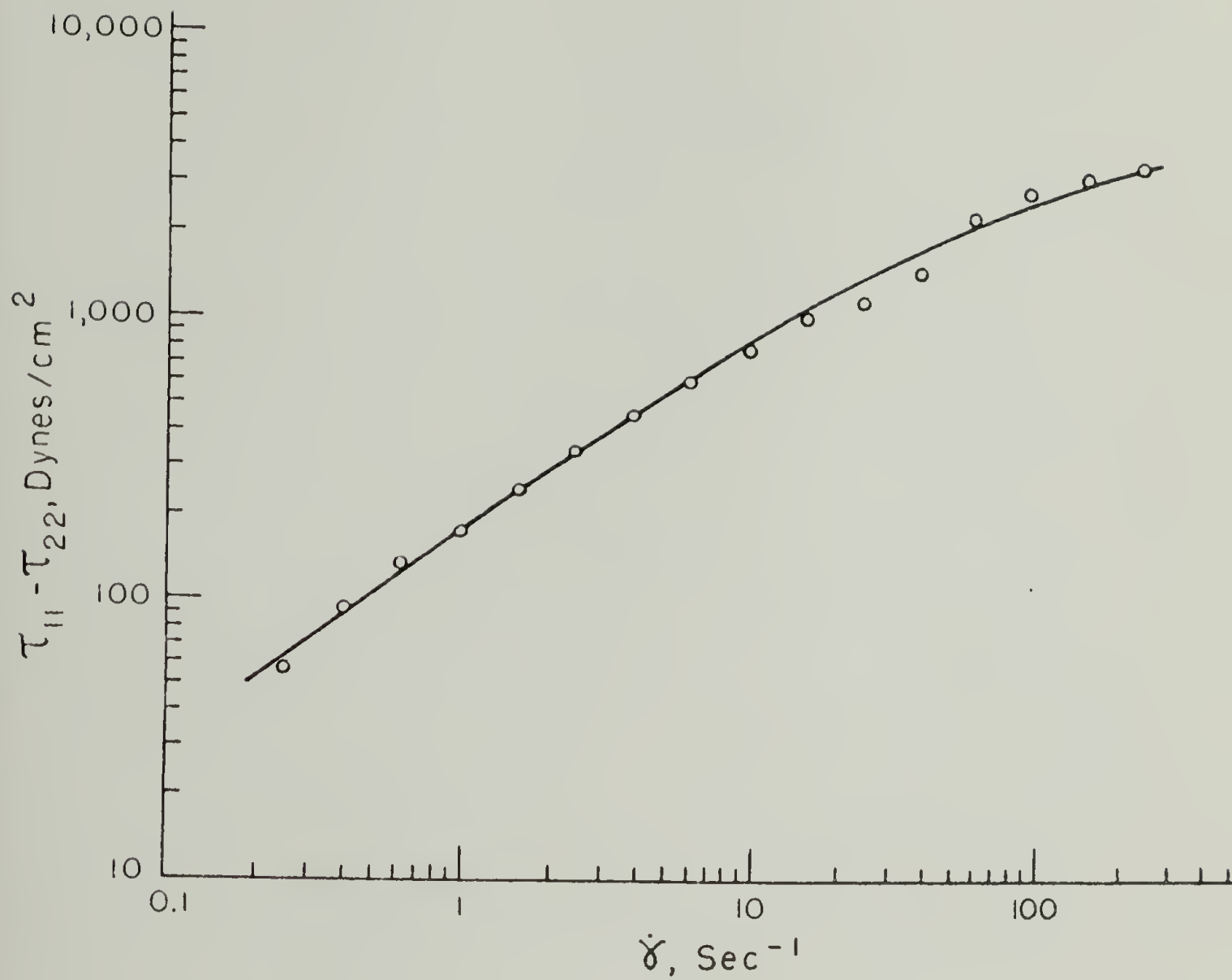


Figure 79. First Normal Stress Difference Versus Shear Rate for 335,000 M.W. PBG (25.3 wt%).



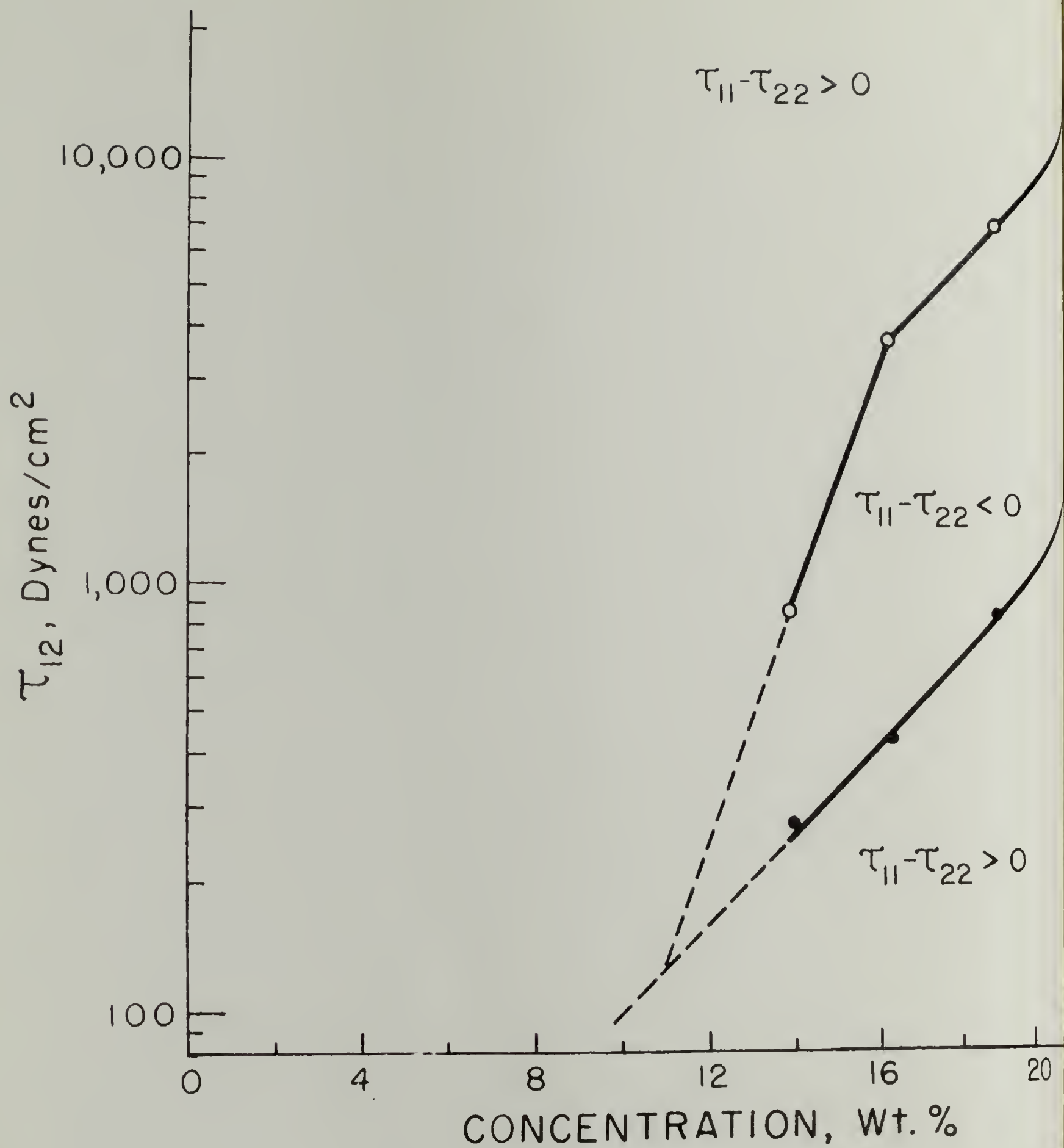


Figure 80. Shear Stress at Points of Change in Sign of First Normal Stress Difference Versus Concentration for 335,000 M.W. PBG.

consistent with the positive  $\tau_{11} - \tau_{22}$  measured at all shear rates for the 11.0 wt% solution.

An effort was made to exclude the possibility that these unusual (negative) normal stress observations were the result of artifact. It has been known for some time that inertial forces, which are neglected in the conventional analysis relating first normal stress difference to total normal thrust in cone-and-plate flow, can make a negative contribution to the normal thrust (169). The inertial contribution can in fact produce a spurious sign reversal in  $\tau_{11} - \tau_{22}$  for certain polymer solutions, which is eliminated when a correction is applied; see Figure 81. This correction was applied to all normal thrust data and found to be much smaller than the measured normal thrust in all of our observations of PBG in m-cresol. Since the only material property which influences the magnitude of the inertial correction is density, inertial effects cannot be responsible for the negative first normal stress difference observed here.

Another precaution which was taken to preclude artifact was the use of a variety of cones of different radii and cone angles. It would be expected that any contribution due to edge effects or secondary flow would be of very different magnitude for different cones and would have been immediately obvious.

Finally, it should be noted that both total normal thrust (from which  $\tau_{11} - \tau_{22}$  is calculated) and torque (from which  $\eta$  is calculated) were measured simultaneously, both on the bottom plate below the rotating cone. Therefore, it would be expected that any gross

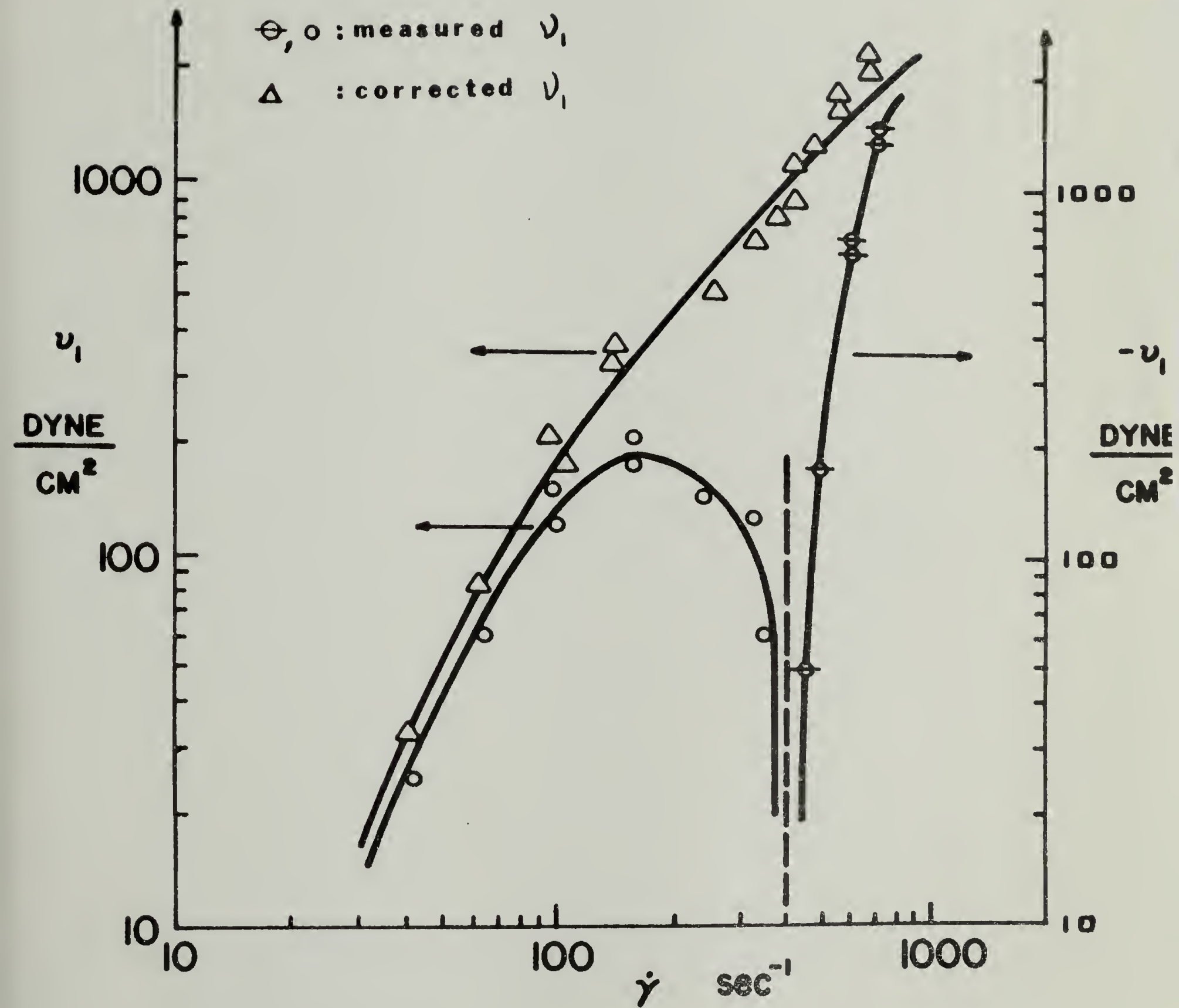


Figure 81. First Normal Stress Difference Versus Shear Rate for 2% Aqueous Polyacrylamide Solution ( $\bar{M}_n = 1.56 \times 10^6$ ).

departure from the simple laminar flow field assumed by conventional analyses of cone-and-plate flow would also have been manifested in the apparent viscosity behavior as a discontinuity or change in slope.

A possible rationalization of a negative normal thrust can be found in postulating a dilatometric effect, i.e., a reduction of sample volume upon shearing. Efforts to correlate the shape of the free surface at the edge of the cone with negative normal thrust observations were frustrated by changes in shape caused by incipient secondary flow or the fluid being forced out by centrifugal force. Another pertinent observation is that normal thrust values (both positive and negative) were established almost immediately upon initiation of shear and were time-independent for the duration of the measurement (up to 15 minutes). The same normal thrust values were obtained for both clockwise and counterclockwise rotation. Decay of the normal thrust upon cessation of shear was very rapid. All of these observations argue against the negative normal thrust's being a dilatometric effect.

### Discussion

In the course of the exposition of the experimental results we have had occasion to use the terms "liquid crystalline" and "non-liquid crystalline" to describe solutions of different concentrations. Strictly speaking, the term "liquid crystalline" should be applied to any fluid which exhibits long range order, e.g., a solution of rod-like molecules at the A-point (at which the anisotropic phase first emerges). Previous workers have identified the concentration of

maximum viscosity with the A-point (170) and have accordingly labelled solutions of higher concentrations as liquid crystalline and those of lower concentration as non-liquid crystalline.

It is unlikely, however, that the formation of a small fraction of an anisotropic phase at the A-point would be reflected in an immediate and drastic change in the macroscopic properties of the solution as a whole. It is more likely that the anisotropic phase must comprise a substantial fraction of the solution; this would correspond to a concentration somewhere between the A-point and the B-point (that at which the solution becomes wholly anisotropic). It would not be unexpected that different material properties of the solution would be sensitive to the presence of an anisotropic phase to varying degrees. Thus, depending on which property one were to observe, the solutions would appear to become liquid crystalline at different concentrations. As shown in Table 4, liquid crystalline order was manifested at different concentrations by various properties, corresponding to different ratios of anisotropic phase to isotropic phase. The Flory prediction of the critical concentration for formation of an anisotropic phase is in fact lower than the indications of any of the observed properties. It is interesting that birefringence, which would be expected to be the most sensitive to the presence of a small amount of anisotropic phase coexisting with a large amount of isotropic phase, gave a higher estimate for the critical concentration than first normal stress differences.

The steady shear viscosity measurements presented here are in qualitative agreement with those of previous workers (163,164) in that

viscosity increased sharply with concentration to a maximum value after which it dropped sharply, and also in that solutions beyond the viscosity maximum were partially or fully liquid crystalline. We feel, however, that the viscosity peak does not uniquely mark the emergence of the anisotropic phase, but that some of this phase is present before the maximum viscosity is achieved. The magnitude of the viscosities observed were similar to those previously reported but detailed comparisons were impossible since previous investigations had used systems with slight differences (e.g., solvent, molecular weight of PBLG). In particular, no previous reports of the rheological behavior of equimolar mixtures of PBLG and PBDG are available.

It would be anticipated that concentrated solutions of an equimolar mixture of PBLG and PBDG (which form nematic liquid crystals (159)) would exhibit different rheological properties than concentrated solutions of a single enantiomer (which forms cholesteric liquid crystals). Cholesteric liquid crystals are generally considered to be special cases of nematics in which adjacent molecular layers are slightly displaced leading to a helical superstructure with its screw axis perpendicular to the molecular layers (171). Experiments on low molecular weight thermotropic liquid crystals indicate that the viscosity changes at the nematic→isotropic liquid and cholesteric→isotropic liquid transitions are markedly different (172). Nematics generally have lower viscosities than their isotropic liquids since their molecules are readily oriented in the direction of flow measurements. Cholesterics generally have higher viscosities than their corresponding isotropic liquids. This behavior may be understood by

reference to results obtained by Pochan and Marsh (173) who observed that mixtures of cholesteryl chloride and cholesteryl oleyl carbonate were found to exhibit the Grandjean texture at low shear rate (helical screw axes perpendicular to direction of shear). The effect of increased shear was to tilt the helical screw axes to a direction parallel to the direction of shear (dynamic focal conic texture), meaning that the molecules themselves would be oriented perpendicular to the direction of shear.

Another difference in the rheological behavior of thermotropic cholesterics and nematics is the observation that nematics are Newtonian whereas cholesterics are non-Newtonian (172). Thus, the presence of cholesteric superstructure has a significant effect on the rheology of thermotropic liquid crystals.

For this reason it is interesting that both nematic and cholesteric solutions of helical polypeptides behave so similarly. The viscosity-concentration behavior of PBLG in *m*-cresol reported by Hermans (163) is very similar to that of our racemic mixtures and also for solutions of non-chiral rod-like macromolecules (174,175). A direct comparison of PBLG in  $\text{CH}_2\text{Br}_2$  with a mixture of PBLG and PBDG in the same solvent revealed very similar viscosity behavior (164).

Our observation was that for concentrations up to 25.2 wt%, the liquid crystalline solutions were lower in viscosity than the non-liquid crystalline solutions at the highest concentration. It may be argued that since the cholesteric superstructure in solutions of a single enantiomer would be quite weak (probably much weaker than that in thermotropic cholesterics), and easily disrupted by shear,

rheological measurements on such solutions were in fact made on nematic liquid crystals. Such a shear-induced cholesteric→nematic transition process would be analogous to the "unwinding" of a cholesteric in a magnetic field (176). Such an argument would be strengthened by the observation of yield stresses in solutions of a single enantiomer (nominally cholesteric) and not in solutions of mixtures of both enantiomers (nematic).

The observation of normal stresses for liquid crystals has been infrequently reported. Erhardt, Pochan, and Richards (177) have reported normal stress measurements on mixtures of cholesteryl chloride and cholesteryl oleyl carbonate. They observed behavior consistent with that of a second order fluid, i.e., that

$$\lim_{\omega \rightarrow 0} G'/\omega^2 = \lim_{\dot{\gamma} \rightarrow 0} \frac{\tau_{11} - \tau_{22}}{2\dot{\gamma}^2} \quad (178).$$

Normal stress measurements on concentrated solutions of helical polypeptides including PBLG were conducted by Iizuka (165,179). However, the results were not reported but used to calculate extinction angles from which the rotary diffusion constant was deduced and thence an apparent particle size for molecular clusters from tables given by Scheraga (180). Therefore, our report of negative normal forces appears to be unprecedented in the liquid crystal literature and in fact may be rare in the rheological literature. Coleman and Markovitz (178) demonstrated that for a second order fluid in slow Couette flow the viscoelastic contribution to normal thrust must have a sign opposite to the inertial contribution on thermodynamic grounds.



Walters (181) reports that measurements of first normal stress difference have invariably led to a positive quantity except for one which was later found to be in error. Adams and Lodge (182) reported the possible observation of a negative value for  $\tau_{11} - \tau_{22}$  for solutions of polyisobutylene in decalin. This result was obtained by a combination of  $\tau_{11} + \tau_{22} - 2\tau_{33}$  (obtained from radial variation in normal stress in a cone-and-plate) with measurements of  $\tau_{22} - \tau_{33}$  which were of uncertain accuracy. However, in a discussion of this point, Adams and Lodge concluded that negative values of  $\tau_{11} - \tau_{22}$  would be curious but not impossible.

Other observations of negative normal stress have been reported. In a study of rheological properties of aqueous lecithin solutions Duke and Chapoy (183) observed a positive normal thrust in steady shear cone-and-plate flow, but upon reversing the direction of rotation, the normal thrust became negative and then increased to the positive steady state value. This effect was attributed to incomplete normal stress relaxation upon cessation of flow.

Time dependent negative normal thrust observations were reported by Huang (184) on melts of an SBS copolymer. In this case a negative normal thrust was generated upon initiation of shear but decayed to zero after about 75 seconds. This effect was thought to be due to a small volume decrease caused by shearing.

In a personal communication Iizuka (185) reported the observation of negative normal stress in solutions of PBLG in  $\text{CH}_2\text{Br}_2$  of concentration 10 vol % or greater. This is in agreement with our observation of negative normal thrust only in liquid crystalline

solutions of PBG in m-cresol. This effect was ascribed by Iizuka to the adhesive force of the solution.

Our observations differ from those referred to above in that the negative normal thrust was not time dependent, nor did it appear only upon sudden reversal of the direction of rotation.

### Conclusion

At this point a theory for the rheological properties of liquid crystalline solutions of rigid rod-like molecules is lacking. Progress has been made in the flow properties of thermotropic (bulk) liquid crystals from a continuum approach (186) and dilute solution theories of rigid rod-like molecules are very successful (168,187). However, neither of these could be expected to apply to this work.

Therefore, we have merely described our observations in the thought that they will stimulate progress towards an understanding and perhaps a theory for the rheology of such fluids.

TABLE 4  
 INDICATION OF LIQUID CRYSTALLINE ORDER OF  
 335,000 M.W. PBG

Indication of Liquid Crystal Order	Concentration wt%
Optical anisotropy (birefringence)	9.9
Maximum in $\eta_{\gamma \rightarrow 0}$ vs. C	11.0
Maximum in $\eta_{\omega \rightarrow 0}$ vs. C	11.0
Maximum in $G'$ vs. C	9.9
Maximum in $\tau_{11} - \tau_{22}$ vs. C	8.1
Flory theory	8.2

## C H A P T E R   I I I

### RHEOLOGY OF CONCENTRATED SOLUTIONS OF PBLG AND PCBZL

#### Abstract

Rheological studies were carried out on concentrated m-cresol solutions of two helical synthetic polypeptides; poly- $\gamma$ -benzyl-L-glutamate (PBLG, M.W. = 150,000) and poly- $\epsilon$ -carbobenzyloxy-L-lysine (PCBZL, M.W. = 200,000). Steady shear measurements were made over a range of  $.01$ - $16,000 \text{ sec}^{-1}$  to obtain steady shear viscosity and first normal stress difference. Dynamic viscosity and dynamic storage modulus were measured both by oscillatory shear between cone-and-plate and also by eccentric rotating disc measurements over frequency ranges of  $.1$ - $400$  and  $.1$ - $63 \text{ rad/sec}$ , respectively. The concentration ranges were such that both liquid crystalline and isotropic solutions were investigated. The previously reported observations of an apparent negative first normal stress difference within a defined range of shear rate for liquid crystalline solutions were confirmed for the PBLG and PCBZL solutions. At high shear rates the peaks in steady shear viscosity vs. concentration were profoundly suppressed but peaks in first normal stress difference versus concentration were not. The observation of liquid crystalline order in PCBZL/m-cresol solutions at room temperature constitutes evidence that the inverse coil-helix transition temperature is lower in concentrated solutions

than in dilute solutions. The critical concentration for formation of the liquid crystalline phase was higher for PCBZL than for PBLG, despite a higher axial ratio, due to helix flexibility.

### Introduction

The occurrence of a transition from an isotropic to a liquid crystalline solution at a critical concentration of rod-like molecules is well known (188-191). The rheology of such systems is also of interest. The viscosity behavior, i.e., a peak in viscosity at the critical concentration, has been well documented (192,193), but the literature is less informative on the dynamic and normal stress behavior (194) due to the greater demands imposed on instrumentation.

In Chapter II (195) which deals with the behavior of four material functions ( $\eta$ ,  $\eta'$ ,  $N_1$ ,  $G'$ ) of both isotropic and liquid crystalline solutions of an equimolar mixture of the L and D enantiomers of poly- $\gamma$ -benzyl-glutamate (PBLG and PBDG), we observed a variety of rheological phenomena. Particularly striking was the occurrence of negative (as well as positive) values for the first normal stress difference over well-defined ranges of shear rate, which remained negative even after correction for the negative inertial contribution. In order to study these rheological phenomena further, two new samples of helical synthetic polypeptides were obtained. Also, improvements in instrumentation gave the capability of performing oscillatory measurements of dynamic viscoelasticity to supplement the eccentric rotating disc technique utilized in the previous study.

In Chapter IV we describe a rheo-optical study of the same solutions which correlates information about molecular organization obtained by polarized light photomicrographs taken during shear with some of the striking rheological phenomena described here.

### Experimental

Two samples of synthetic helical polypeptides were obtained from Sigma Chemical Co., St. Louis, MO. These were poly- $\gamma$ -benzyl-L-glutamate (PBLG, M.W. = 150,000), and poly- $\epsilon$ -carbobenzoxy-L-lysine (PCBZL, M.W. = 200,000). Chemical structures are shown in Figure 82. These polymers were dissolved in *m*-cresol at concentrations sufficiently high to produce birefringent solutions. Due to the high cost of the polymer and the high concentrations required, it was found necessary to re-use the solutions after each measurement. Thus, solutions of lower concentration were produced by subsequent dilution after completion of all measurements at higher concentrations. Solutions were refrigerated when not in use.

Steady shear measurements were performed on a cone-and-plate rheometer (Rheometrics, Inc., Union, N.J. RMS-7200). In the interest of precision and in order to obtain as wide a range of shear rate as possible, a variety of cone-and-plate combinations of different diameter and cone angle was used (100 mm, .04 rad; 50 mm, .1 rad; 50 mm, .04 rad; 50 mm, .01 rad; 25 mm, .01 rad). For each cone-and-plate combination, measurements were made both in order of increasing and decreasing shear rate. Thus, except for extremely low shear rates which were accessible only with the 100 mm cone-and-plate,

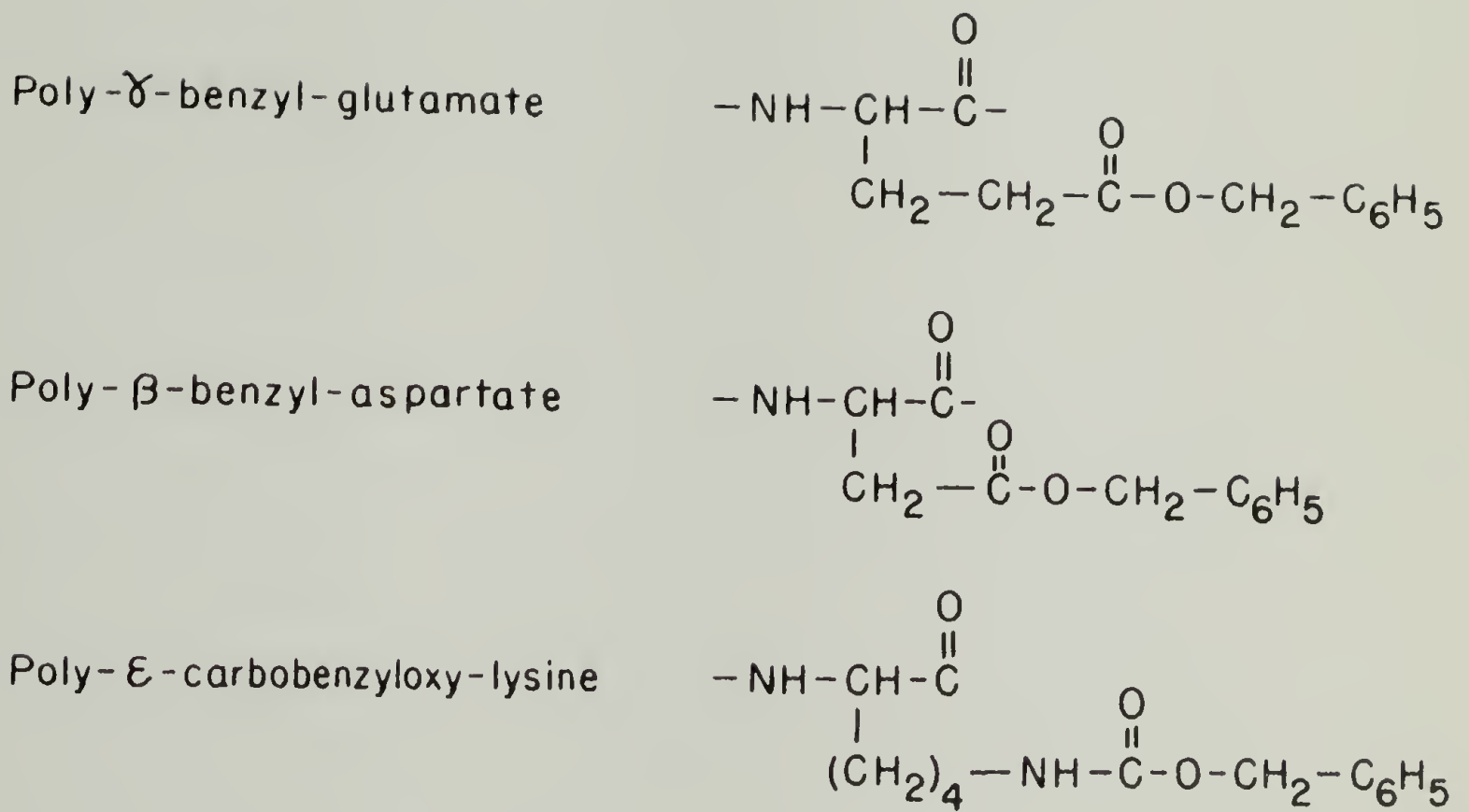


Figure 82. Chemical Structures of Poly- $\gamma$ -Benzyl-Glutamate, Poly- $\epsilon$ -Carbobenzyloxy-L-Lysine, Poly- $\beta$ -Benzyl-Aspartate.

every datum point on the figures represents the mean of at least four separate measurements on at least two different cone-and-plate combinations. Steady state measurements could not be made at shear rates greater than  $1000 \text{ sec}^{-1}$  due to the sample being forced out of the gap by centrifugal force; hence these measurements were obtained by extrapolating the torque and normal force traces on the strip chart to the time of initiation of shear. Normal force data were corrected for inertial contributions (196), which in general amounted to 10% or less. In most cases the agreement in measurements made in overlapping regions of shear rate accessible by various cone-and-plate combinations was quite good. An exception was normal force measurements made with the 50 mm, .01 rad and 25 mm, .01 rad cone-and-plate combinations. A minor but not insignificant shift was observed to bring these measurements into line with those made with the other three cone-and-plate combinations (which were in very good agreement in all cases). It was felt that this error was due to surface tension since the sample volumes given with this shallow cone angle were thin at the periphery (.25 mm and .125 mm respectively). No essential conclusion of this chapter would have been changed had this empirical correction been omitted.

Dynamic measurements were also made in the Rheometrics Mechanical Spectrometer, via both the eccentric rotating disc (E.R.D.) mode and oscillatory shear between cone-and-plate. Oscillatory measurements were made over a frequency range of 0.1-400 rad/sec using the same cone-and-plate combinations previously enumerated. The strain amplitude was varied to insure that the measured dynamic



viscosity  $\eta'$  and dynamic storage modulus  $G'$  were strain-independent. E.R.D. measurements were made at several fixed plate separations (.7, 1, 1.5 mm) and strain amplitudes over a frequency range of .1-63 rad/sec. Thus every datum in the case of the oscillatory and E.R.D. measurements represents the mean of approximately fifteen separate measurements. E.R.D. and oscillatory shear have been found to give identical results for a wide range of fluids (197). However, this is the first such comparison for anisotropic fluids.

In most cases, oscillatory measurements were performed on the identical samples used for steady shear measurements. That is, steady shear tests were interrupted at an intermediate shear rate, oscillatory measurements were performed, and then steady shear measurements were resumed.

### Results

Steady shear viscosity. Figures 83-86 show steady shear viscosity versus shear rate for solutions of PBLG and PCBZL in m-cresol ranging in concentration from 6.1-25.4 wt% and from 13.9-33.4 wt%, respectively. In all cases a well-defined low-shear Newtonian plateau is evident. The 33.4 wt% PCBZL/m-cresol solution indicated with filled circles in Figure 85 exhibits an unusual feature in a second Newtonian plateau between approximately .1-10  $\text{sec}^{-1}$ . The weak forces involved in measuring viscosities at low shear rates (and the lack of corroboration with other cone-and-plate combinations at these low shear rates) lead to rather low precision. Consequently, it is possible that the first Newtonian plateau between .04-.16  $\text{sec}^{-1}$  is an

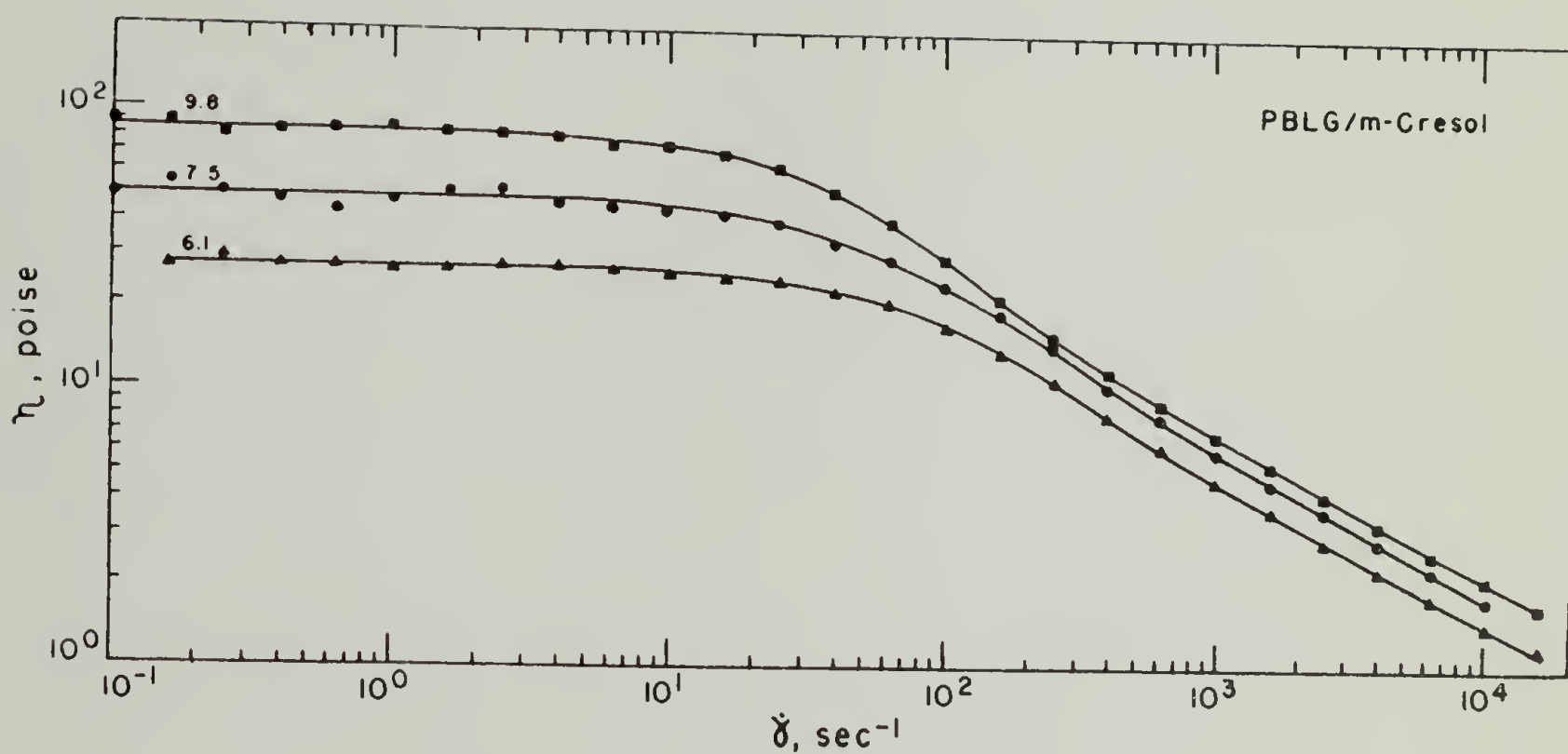


Figure 83. Steady Shear Viscosity vs. Shear Rate for 150,000 M.W. PBLG Solutions.

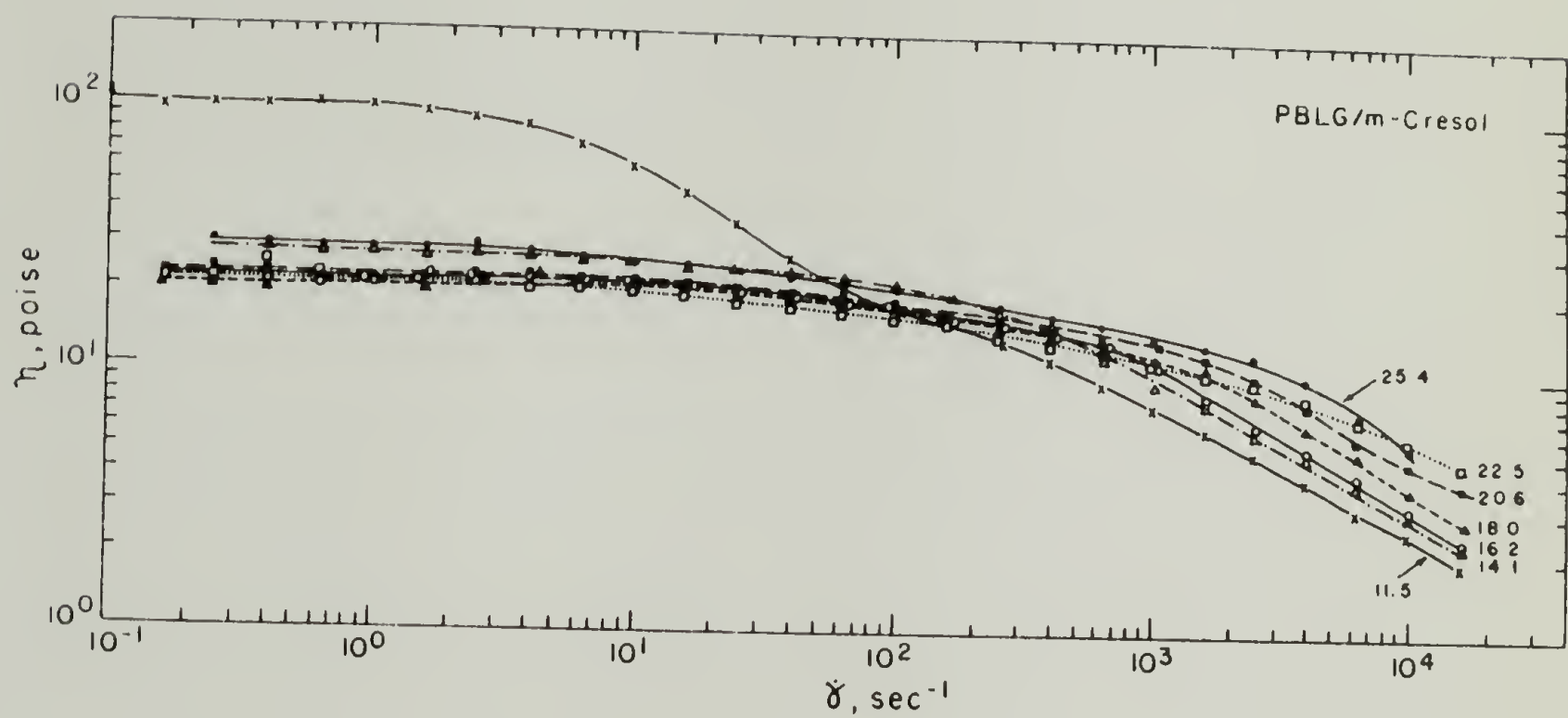


Figure 84. Steady Shear Viscosity vs. Shear Rate for 150,000 M.W. PBLG Solutions.

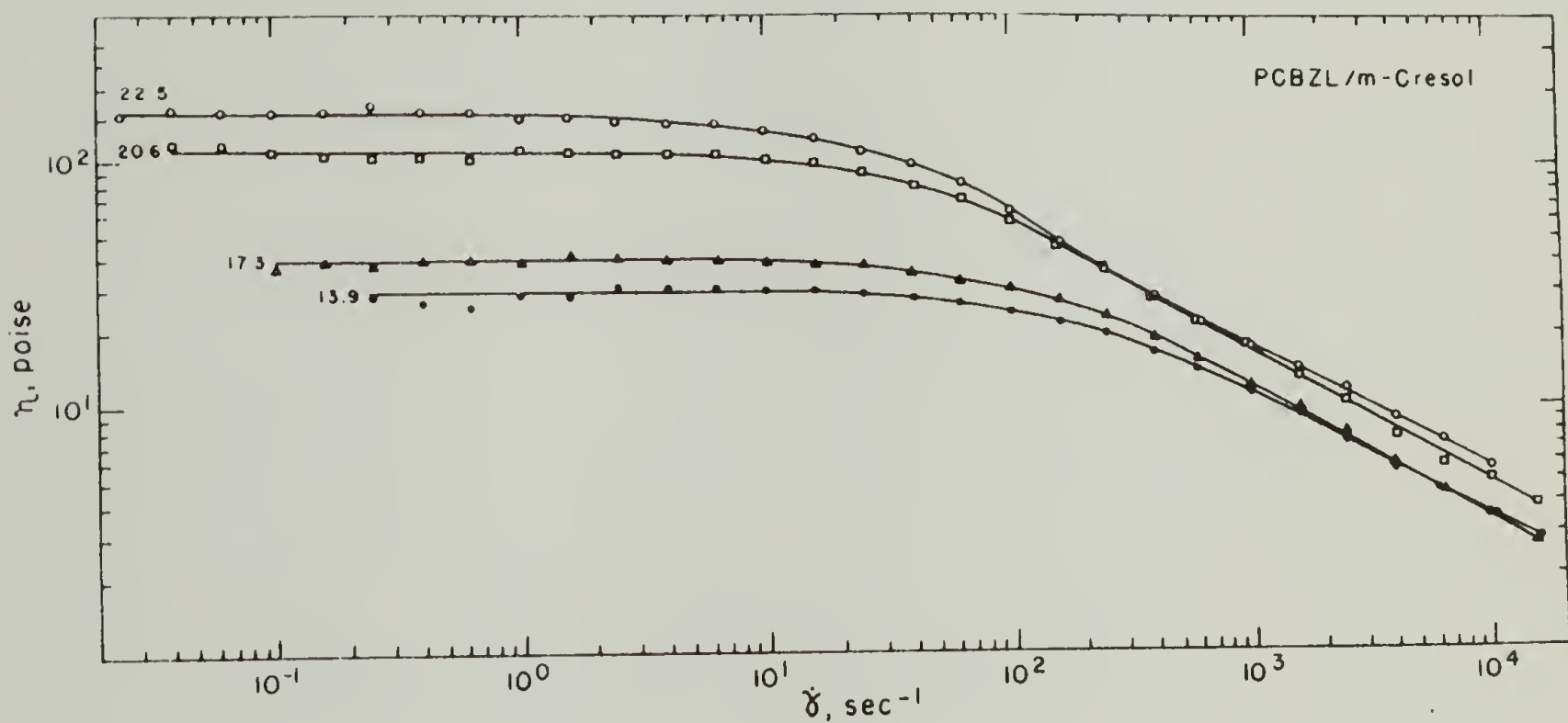


Figure 85. Steady Shear Viscosity vs. Shear Rate for 200,000 M.W. PCBZL Solutions.

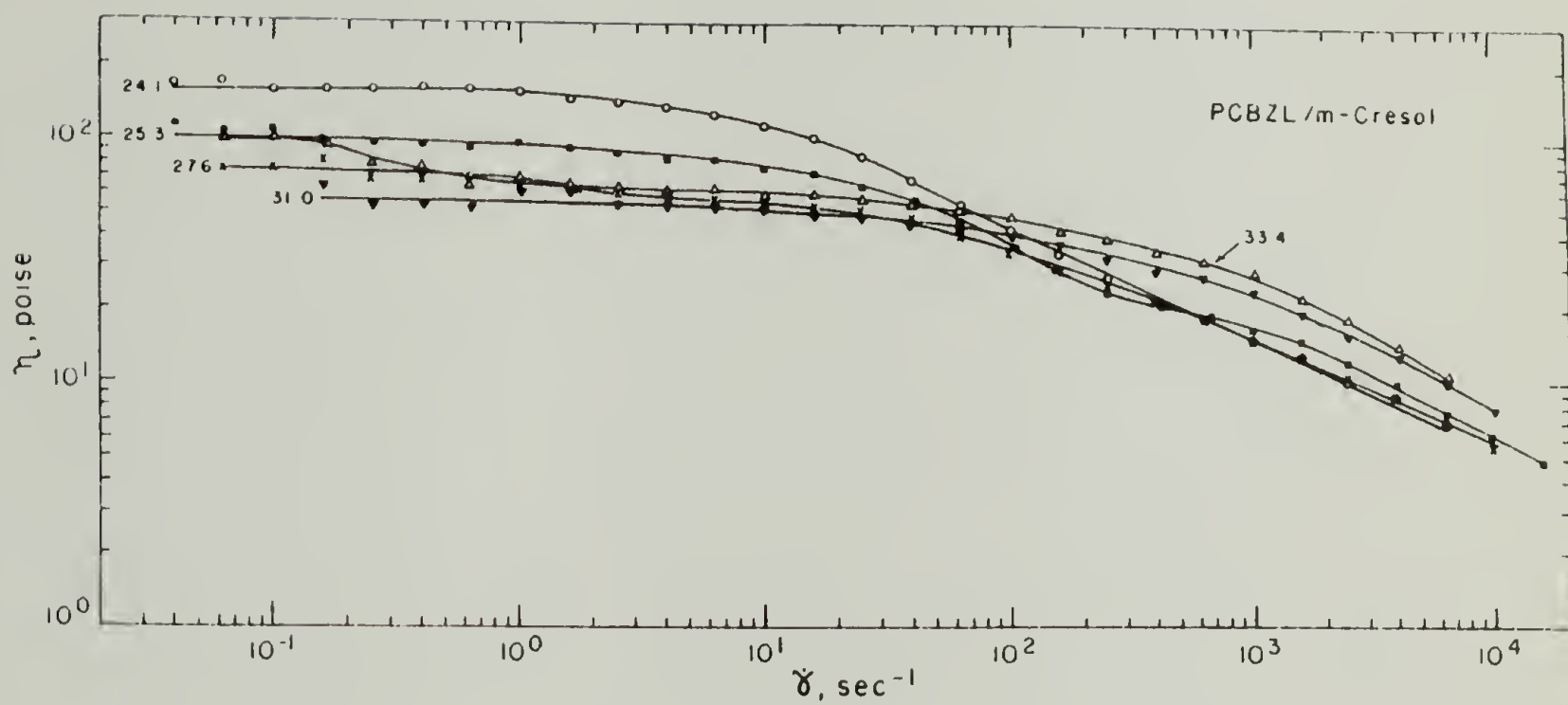


Figure 86. Steady Shear Viscosity vs. Shear Rate for 200,000 M.W. PCBZL Solutions.

artifact due to a coincidence of errors. However, none of the other flow curves exhibit similar features, moreover the dynamic viscosity behavior of this solution also reveals two Newtonian plateaus as will be shown below (Figure 114). Therefore, we are inclined to accept this behavior as genuine; it is certainly not out of keeping with the remarkable variety of rheological phenomena exhibited by these solutions in general.

Figures 84 and 86 show  $\eta_{\dot{\gamma} \rightarrow 0}$  generally decreasing with concentration contrary to the usual experience with polymer solutions. Figures 83 and 85 show  $\eta_{\dot{\gamma} \rightarrow 0}$  increasing with concentration as expected. When  $\eta_{\dot{\gamma} \rightarrow 0}$  is plotted explicitly as a function of concentration, Figures 87 and 88 result. It is evident that  $\eta_{\dot{\gamma} \rightarrow 0}$  rises very steeply with concentration to a maximum and then falls equally steeply to a minimum, whereupon it starts to climb again. The concentration at which the peak occurs in  $\eta_{\dot{\gamma} \rightarrow 0}$  has generally been identified with the critical concentration for the formation of anisotropic solutions,  $C^*$ , since it agrees approximately with the observation of birefringence at rest. In solutions below this concentration there is sufficient room for the rod-like molecules to tumble and therefore occupy a large hydrodynamic volume, leading to a high viscosity. Beyond the critical concentration, volume filling considerations require that the molecules align to high degree of local order, leading to phase separation into an anisotropic high concentration phase and an isotropic low concentration phase (198-200). Since the molecules can no longer tumble freely in the anisotropic phase, the hydrodynamic volume occupied is much smaller so the molecules can

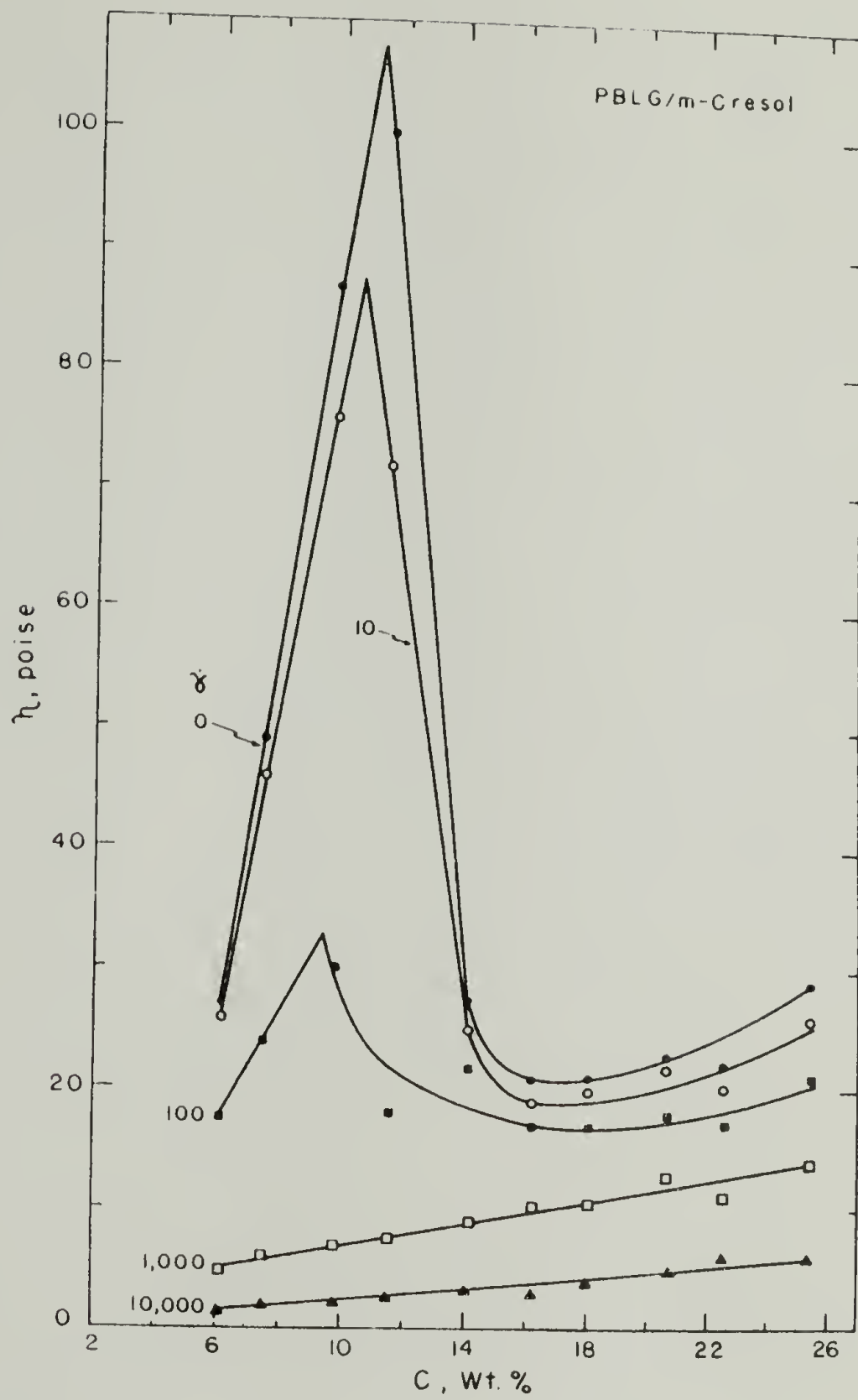


Figure 87. Steady Shear Viscosity at Various Shear Rates vs. Concentration for 150,000 M.W. PBLG Solutions.

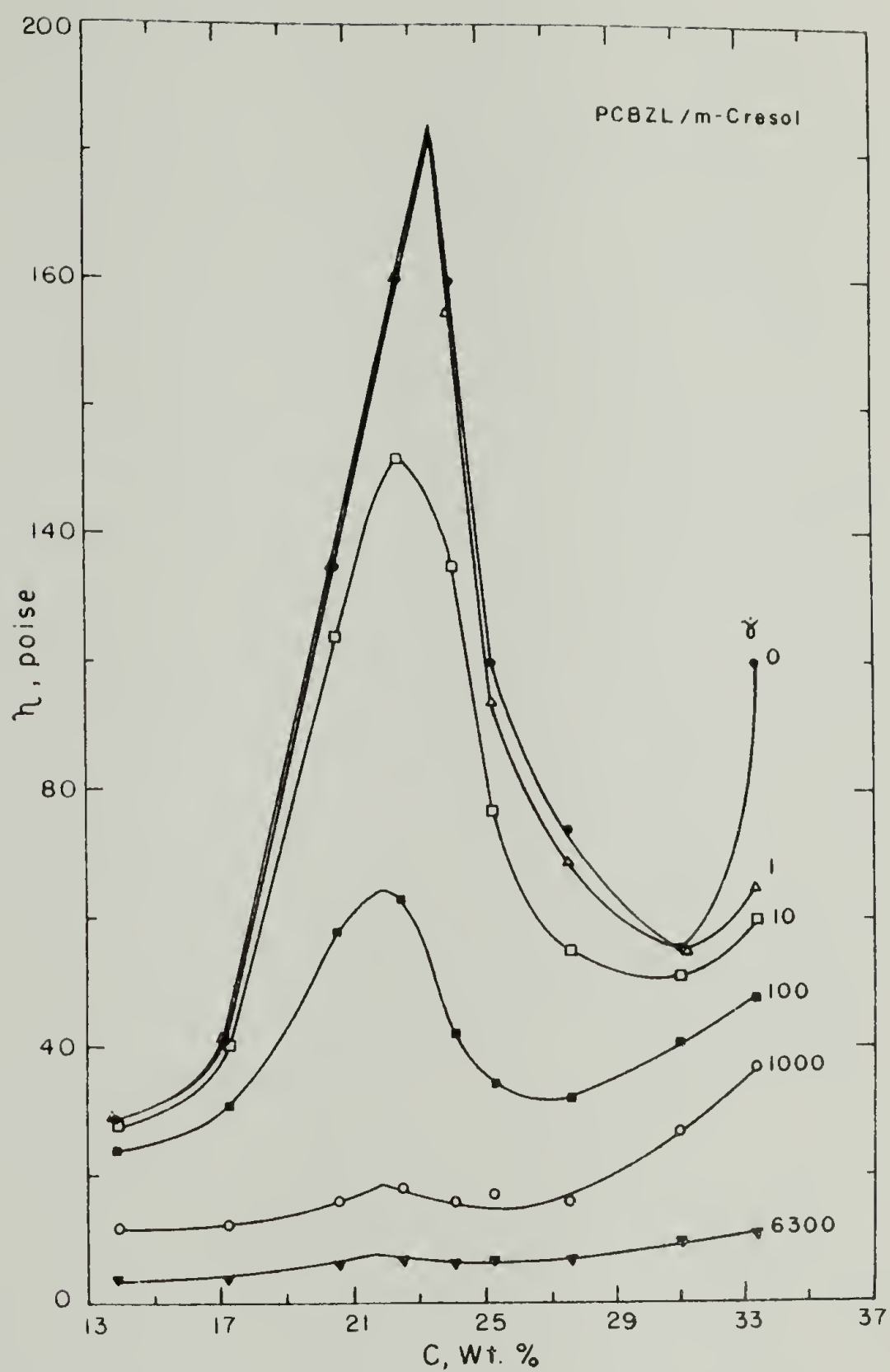


Figure 88. Steady Shear Viscosity at Various Shear Rates vs. Concentration for 200,000 M.W. PCBZL Solutions.



slip past each other with relative ease. As concentration is increased past the critical point, the amount of the low viscosity anisotropic phase increases at the expense of the high viscosity isotropic phase, leading to a steep decrease in the overall viscosity. When the concentration of the solution as a whole equals that of the anisotropic phase, the entire solution is anisotropic. Further increase in concentration increases the local order, thereby further reducing the hydrodynamic volume per molecule and therefore the viscosity. A point of diminishing returns is reached beyond which further increases in concentration cannot increase the local order sufficiently to offset the increased numbers of molecules, leading to a renewed viscosity increase at the highest concentrations.

There are two factors at work which reduce the effective hydrodynamic volume per molecule which in turn leads to a lower viscosity. The first is the local order due to volume-filling considerations, which leads to the maximum and minimum in  $\eta_{\dot{\gamma} \rightarrow 0}$  vs.  $C$ , seen in Figures 87 and 88. The second is shear-induced orientation. The relative effectiveness of these two influences can be seen in the shear thinning behavior (Figures 83-86). Since the liquid crystalline solutions are already highly ordered at rest, the effect of shear orientation is not felt until rather high shear rates. In the isotropic solutions a change in viscosity occurs when shearing forces can significantly affect the Brownian tumbling of the molecules. This behavior is apparent in Figures 84 and 86. Solutions with concentrations  $>C^*$  (i.e., above the peak in  $\eta_{\dot{\gamma} \rightarrow 0}$  vs.  $C$ ) are much less shear-thinning. The combined effects of the volume-filling

orientation, the shear-induced orientation (which together determine the "viscosity increment per molecule"), and the total number of solute molecules are such that the curves of  $\eta$  vs.  $\dot{\gamma}$  for concentrations greater than  $C_{\eta}^*$  intersect more or less at a specific velocity and shear rate. These are  $\sim 18$  poise at  $\sim 160 \text{ sec}^{-1}$  for PBLG and  $\sim 40$  poise at  $\sim 100 \text{ sec}^{-1}$  for PCBZL. At shear rates beyond this intersection point, flow curves for all concentrations are parallel and ranked in order of concentration, the most concentrated solutions having the highest apparent viscosity at a given shear rate. This observation suggests that at high shear rates the shear-induced orientation dominates that induced by volume-filling requirements.

Additional information can be extracted by plotting  $\eta$  vs.  $C$  at a variety of shear rates (Figures 87 and 88). It can be seen that the volume-filling effect which is so striking in the low-shear limiting values of viscosity is significantly suppressed at higher shear rates. This behavior is more striking for the PBLG solutions; no trace of the viscosity peak is left by  $1000 \text{ sec}^{-1}$  and viscosity increases linearly with concentration. In the case of the PCBZL solutions the viscosity peak is also greatly suppressed, but is evident even at shear rates as high as  $6300 \text{ sec}^{-1}$ . From these observations one might conclude that at shear rates on the order of  $1000 \text{ sec}^{-1}$  the structure, and hence the rheology, of the fluids is completely determined by shear-induced orientation in the case of the PBLG solutions and modified only slightly by volume-filling considerations in the case of the PCBZL solutions. This obvious and appealingly simple conclusion is completely erroneous, as will be shown in

the results of normal stress measurements.

Another significant observation which may be made from Figures 87 and 88 is the effect of shear rate on the concentrations at which the apparent viscosity at a given shear rate is maximum ( $C_{\eta}^*$ ). The trend is for  $C_{\eta}^*$  to decrease with increasing shear rate. This may be rationalized on the basis of an increase in stiffness of the imperfectly rigid helices due to the effect of the shear field, leading to an increase in the effective axial ratio of the rod-like molecules and hence a decrease in the critical concentration for the formation of the anisotropic phase (201). Inconsistent with this explanation, however, is the observation that the effect is more pronounced for the PBLG solutions ( $C_{\eta}^*$  dropping from 11.2 wt% at  $\dot{\gamma} \rightarrow 0$  to 9.4 wt% at  $\dot{\gamma} = 100 \text{ sec}^{-1}$  for PBLG, and only dropping from 23.6 wt% at  $\dot{\gamma} \rightarrow 0$  to 21.7 wt% at  $\dot{\gamma} = 6300$  for PCBZL). PCBZL helices are expected to be less rigid than PBLG for reasons given later and also in this case the nominal axial ratio of PCBZL is greater than PBLG (85 and 68.5, respectively) for the molecular weights of the particular samples. Both of these factors would make shearing forces more effective in stiffening the PCBZL molecules.

A final observation of possible significance is that the concentration at which the viscosity reaches a minimum is unaffected by shear for PBLG but strongly affected by shear for PCBZL. Recalling that this minimum represents essentially the point at which further increase in concentration has little effect on the degree of local order, it is not unexpected that a very stiff helix would be unaffected. Conversely, a somewhat less rigid helix would reach the

point of diminishing returns at a higher concentration and the effect of shear-stiffening would indeed be a shift of the minimum in the observed direction.

First normal stress difference. First normal stress difference versus shear rate for the lower concentration PBLG and PCBZL solutions are shown in Figures 89 and 90. Solutions of concentration below  $C_{\eta}^*$  are quite well-behaved. In all cases the curves of  $\log N_1$  vs.  $\log \dot{\gamma}$  consist of two linear regions. For the PBLG solutions (Figure 89) the steeper initial portions have slopes of 1.6-1.7 and the shallower portions have slopes of .6-.7. Extending the linear regions (not shown on the figure) results in break points which occur at a value of  $N_1$  of approximately 3000 dyne/cm<sup>2</sup> independent of concentration, but at shear rates decreasing with concentration (125 sec<sup>-1</sup> for 6.1%, 84 sec<sup>-1</sup> for 7.6%, and 44 sec<sup>-1</sup> for 9.8%). For the PCBZL solutions the initial slopes are also 1.6-1.7 but the second linear region is slightly steeper with slopes of .7-.8 (Figure 90). Extending the linear regions (not shown on the figure) gives break points at a value of  $N_1$  of approximately 6500 dyne/cm<sup>2</sup> independent of concentration and at shear rates decreasing with concentration, as for PBLG (240 sec<sup>-1</sup> for 13.8%, 220 sec<sup>-1</sup> for 17.3%, 74 sec<sup>-1</sup> for 20.6%, 46 sec<sup>-1</sup> for 22.5%).

The concentrations above  $C_{\eta}^*$  exhibit more complex behavior. The initial slopes are much shallower, being 1.0 for 11.5% PBLG (Figure 89), 1.1 for 24.1% PCBZL and 1.0 for 25.3% PCBZL (Figure 90). At higher shear rates the curves do not exhibit a second linear region,

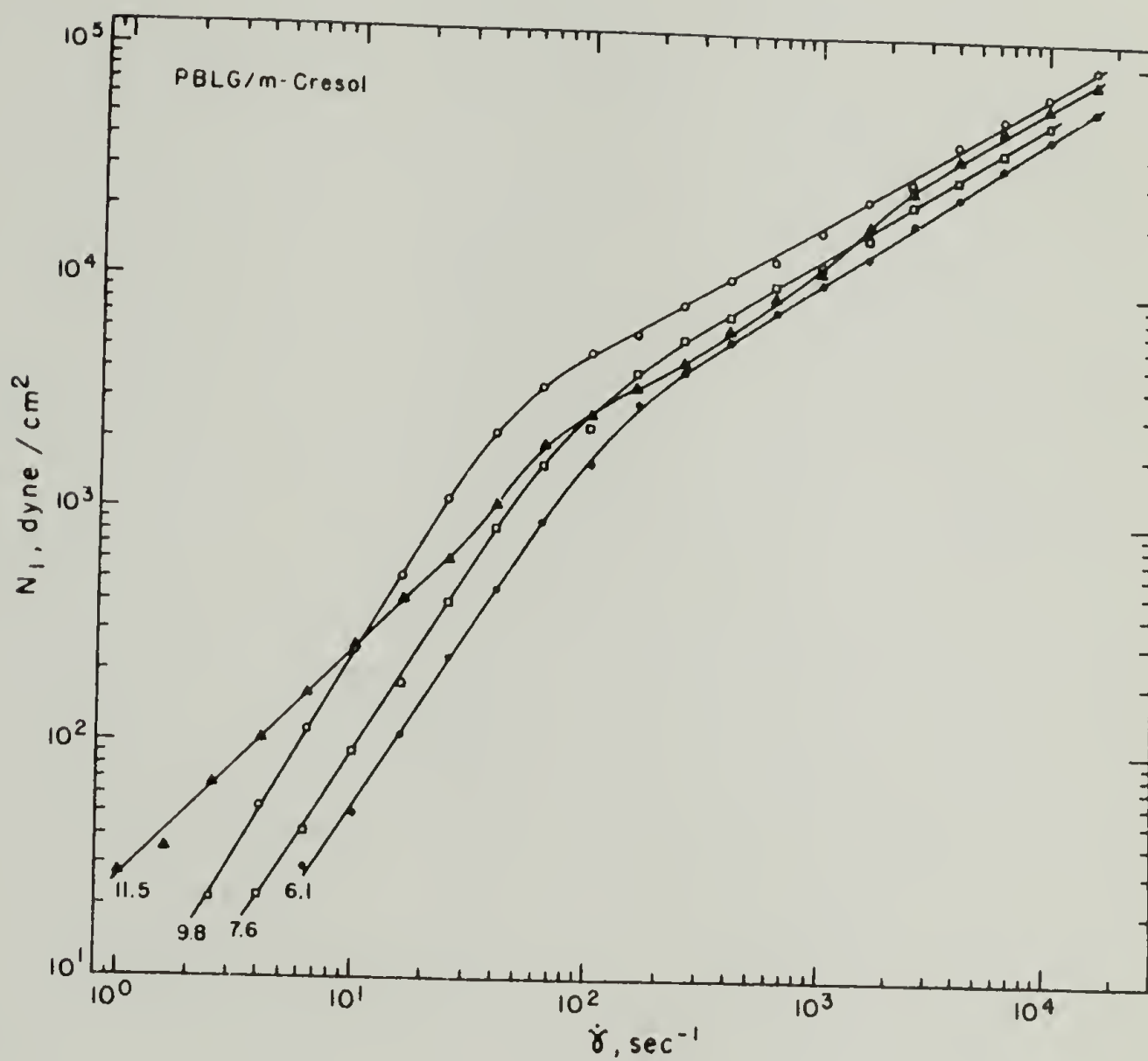


Figure 89. First Normal Stress Difference Versus Shear Rate for 150,000 M.W. PBLG Solutions.

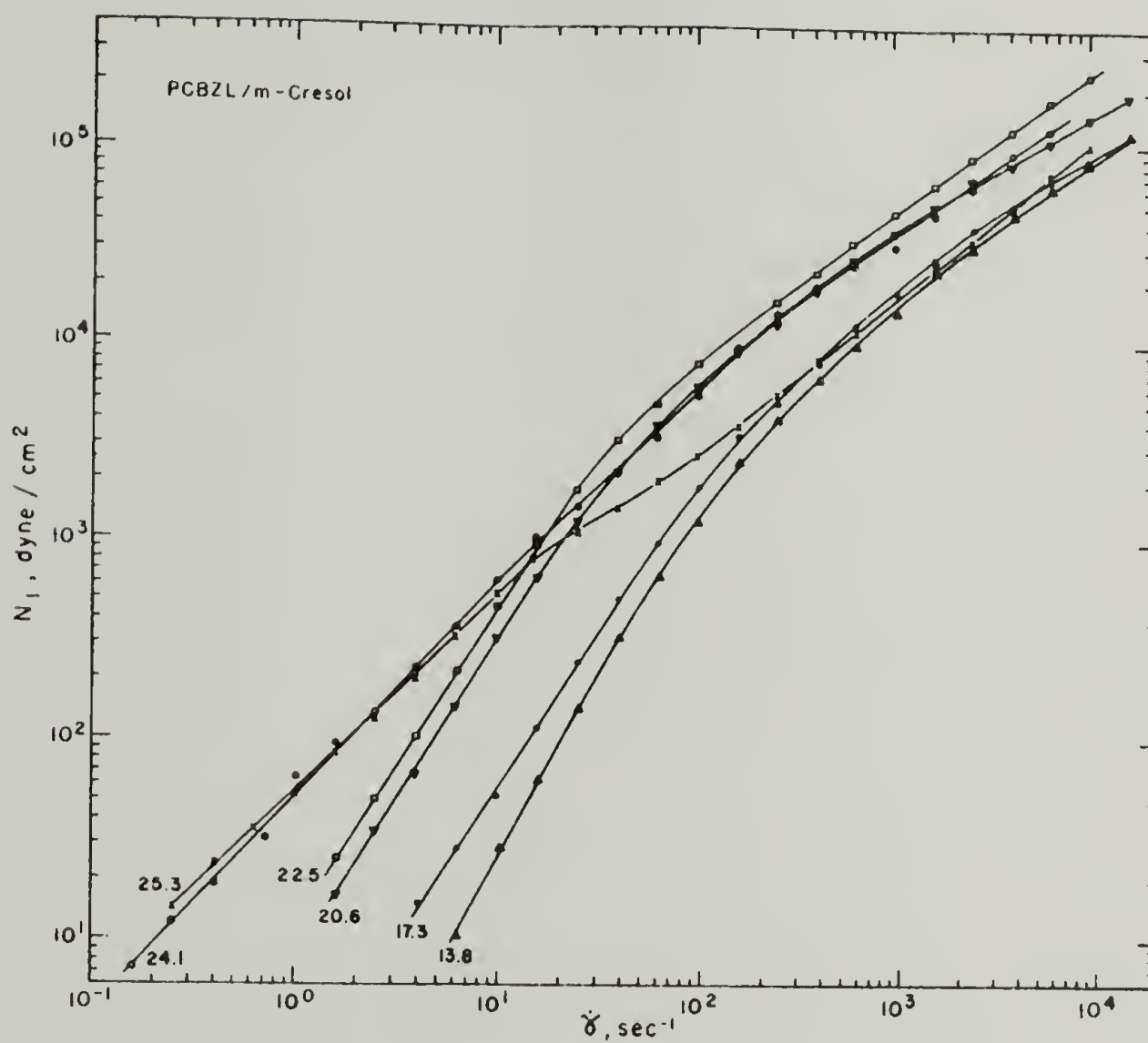


Figure 90. First Normal Stress Difference Versus Shear Rate for 200,000 M.W. PCBZL Solutions.

but rather a convex portion followed by a concave portion. This behavior can be seen most clearly in the 11.5% PBLG (Figure 89).

Further increase in concentration leads to the abrupt onset of a negative normal stress, as previously reported in Chapter II. See Figures 91-96 for PBLG solutions and Figures 97-99 for PCBZL solutions (note that circled points indicate negative values). In all cases  $N_1$  rises rather slowly with  $\dot{\gamma}$ , with an initial slope on the order of .8-1.1, to a maximum. Further increase in shear rate results in a steep decrease in  $N_1$  to negative values, then a sharp negative maximum, and finally another sign change with steeply increasing positive values. In those instances where a sufficient number of points are available in the second region of positive  $N_1$  (e.g., Figures 91, 92, 97, and 98), it appears that  $\log N_1$  rises linearly with  $\log \dot{\gamma}$  with a slope of approximately 1.0-1.4 when well past the sign change.

Before systematically exploring the behavior of the negative normal stress effect, a few words on the reliability of the normal force data are in order. Our first thought after making the first observations of the negative normal stress effect was that it was due to inertial effects; however, corrections for inertia made in accordance with (196) proved to be only 10% or less of the observed negative values. Another possible origin of this anomalous phenomenon is a secondary flow phenomenon. There can be little doubt that the assumption of laminar homogeneous shear flow implicit in the equations relating the measured total normal thrust to the material function  $N_1$  is violated at high shear rates. This can be seen in roughness at the free surface and is also predicted by some theories

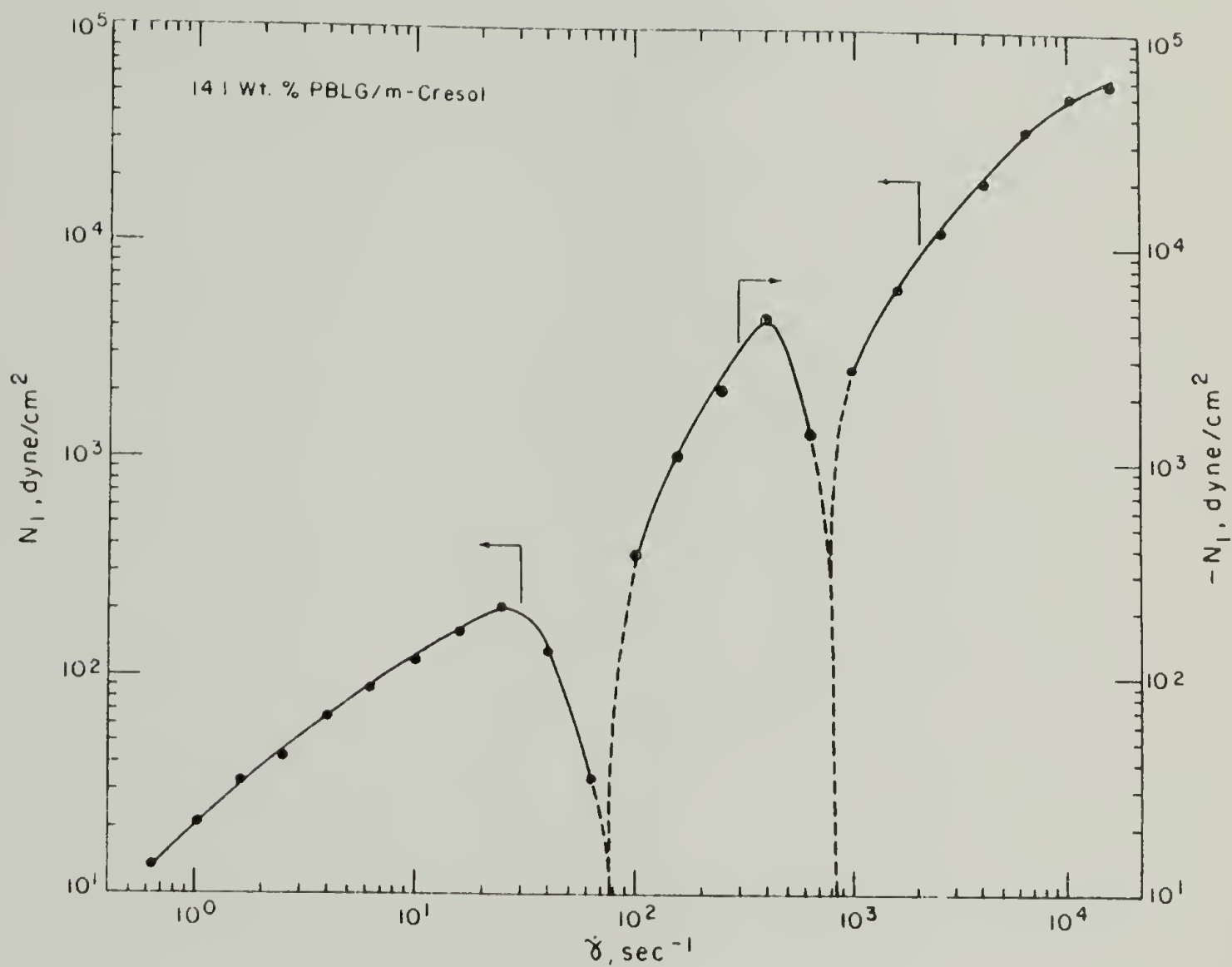


Figure 91. First Normal Stress Difference Versus Shear Rate for 14.1 wt% 150,000 M.W. PBLG Solution.



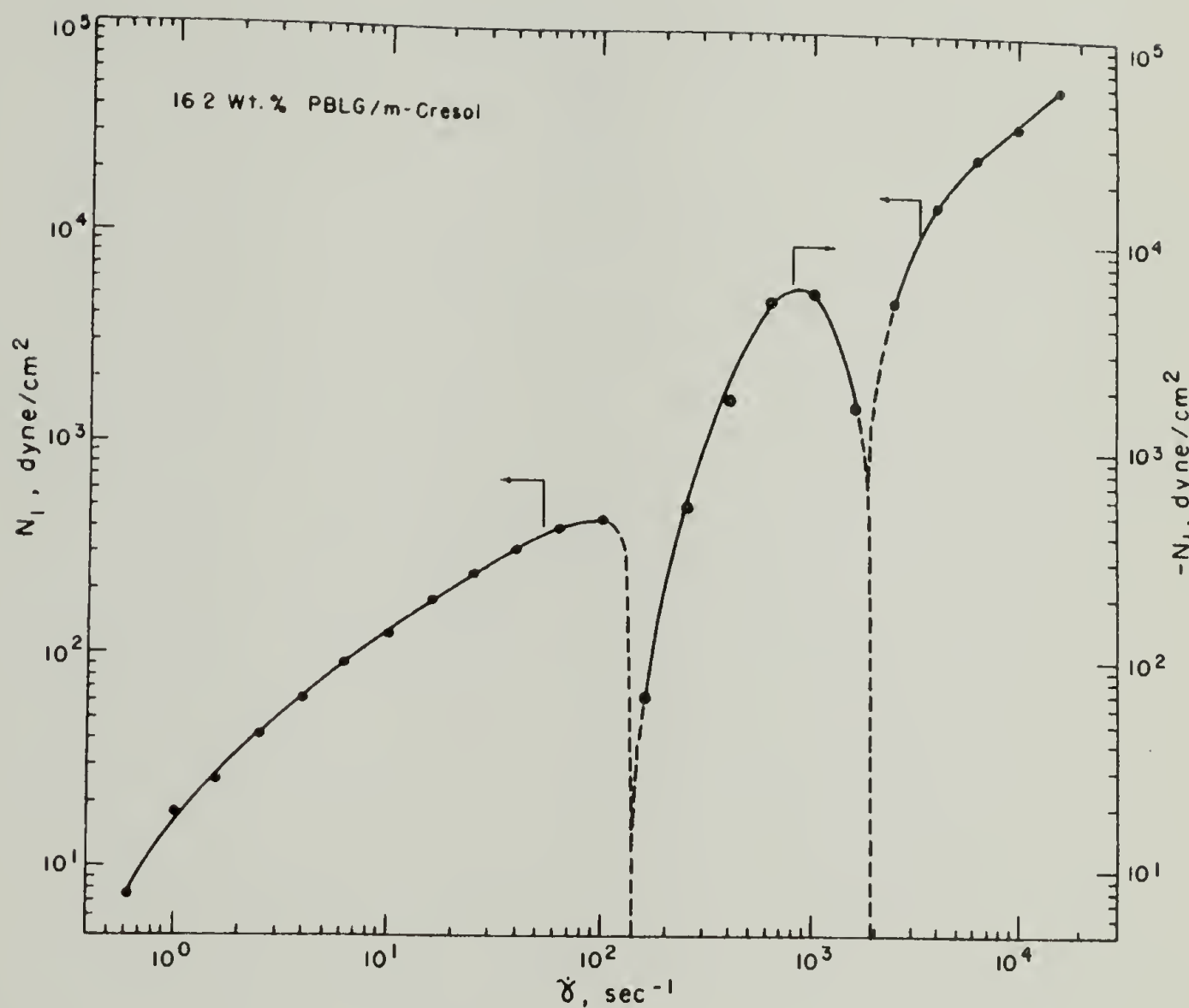


Figure 92. First Normal Stress Difference Versus Shear Rate for 16.2 wt% 150,000 M.W. PBLG Solution.

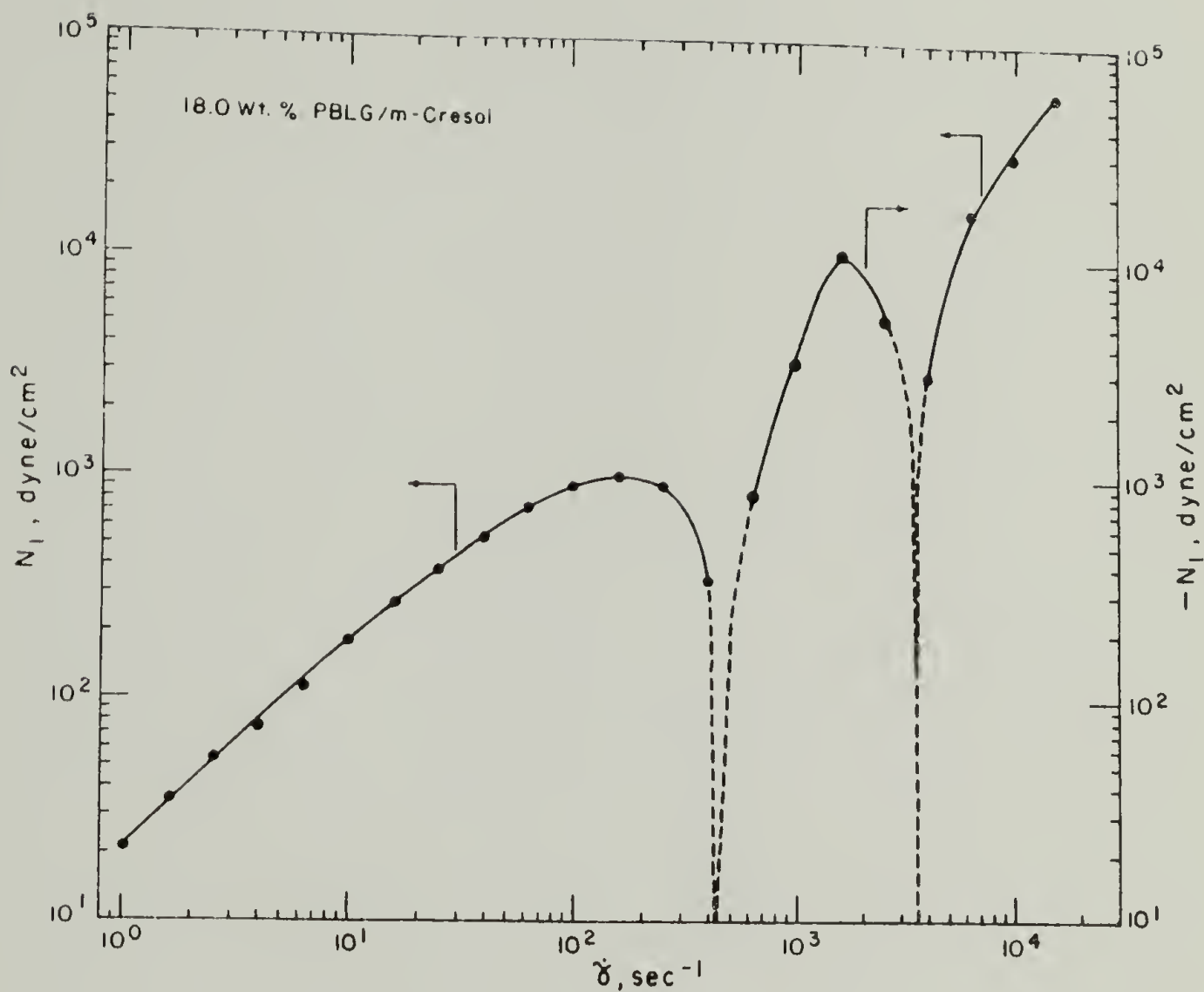


Figure 93. First Normal Stress Difference Versus Shear Rate for 18.0 wt% 150,000 M.W. PBLG Solution.

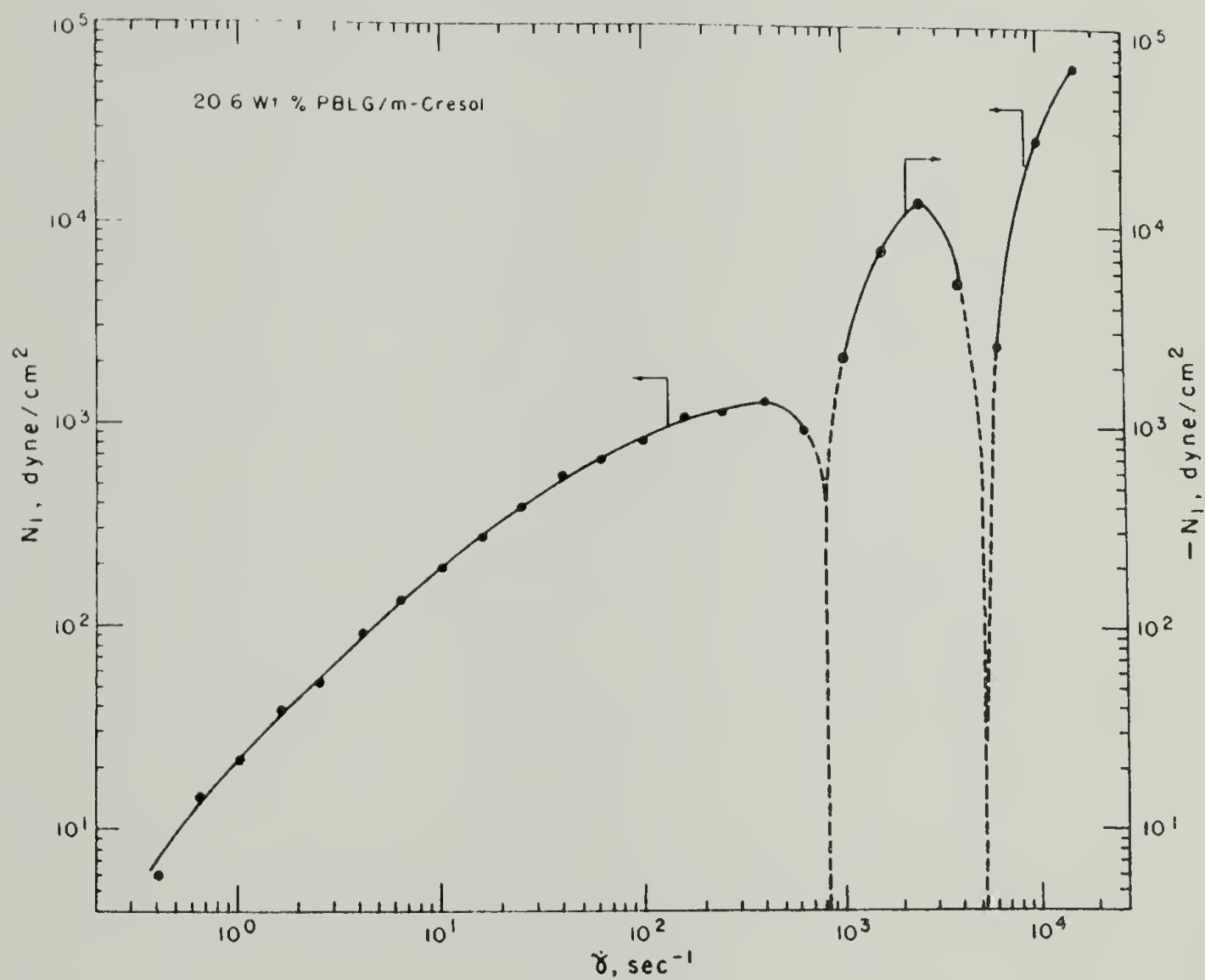


Figure 94. First Normal Stress Difference Versus Shear Rate for 20.6 wt% 150,000 M.W. PBLG Solution.

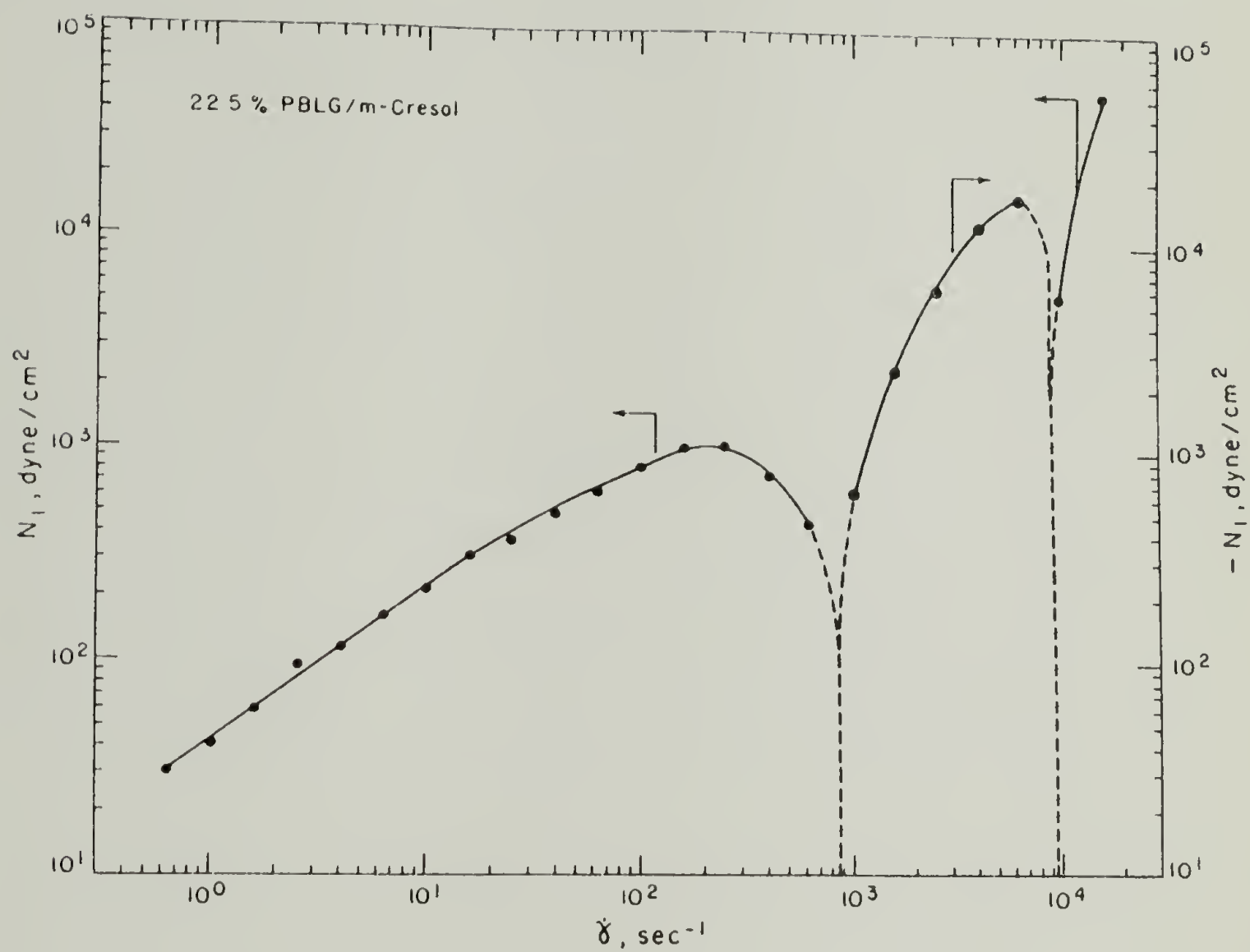


Figure 95. First Normal Stress Difference Versus Shear Rate for 22.5 wt% 150,000 M.W. PBLG Solution.

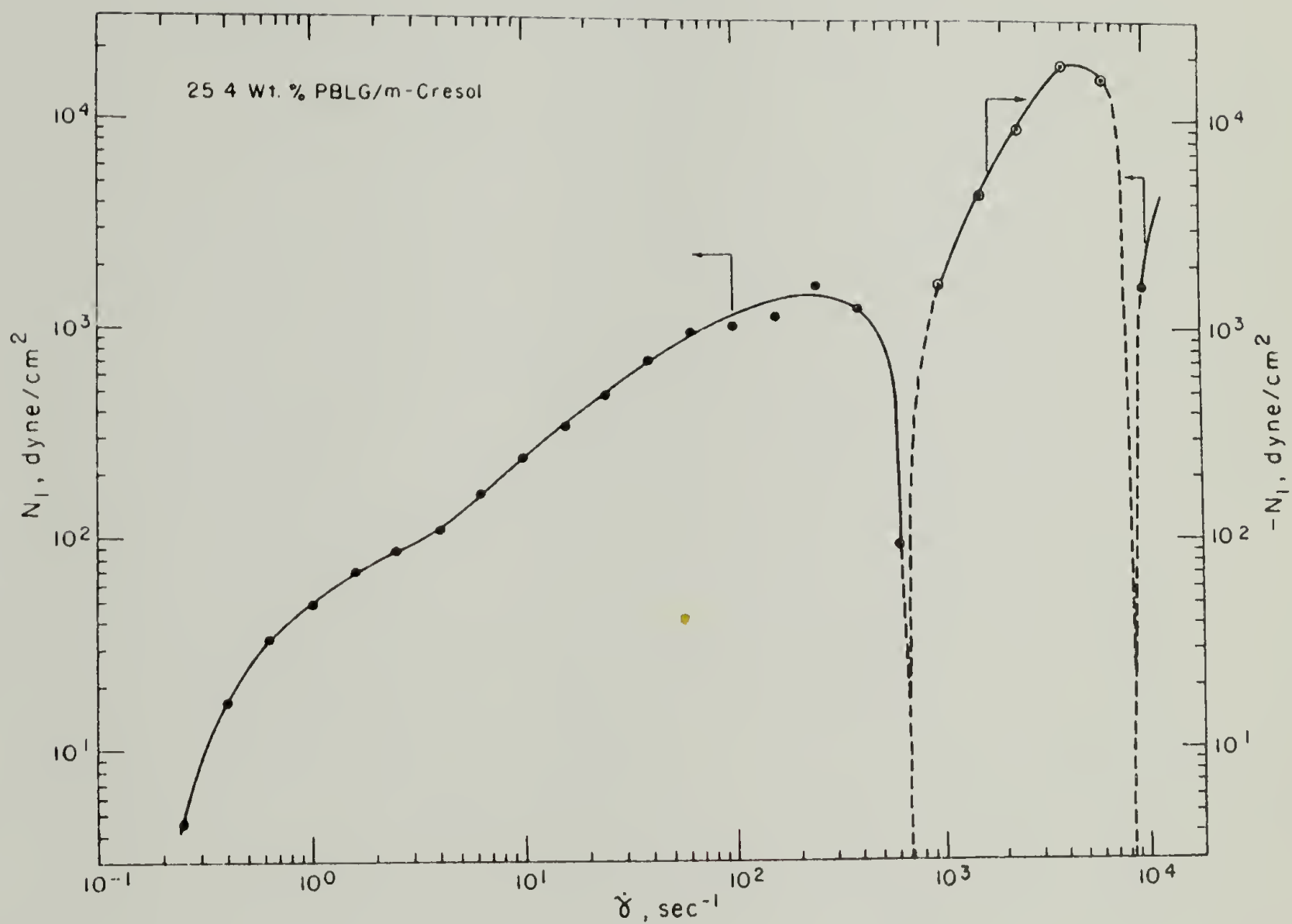


Figure 96. First Normal Stress Difference Versus Shear Rate for 25.4 wt% 150,000 M.W. PBLG Solution.

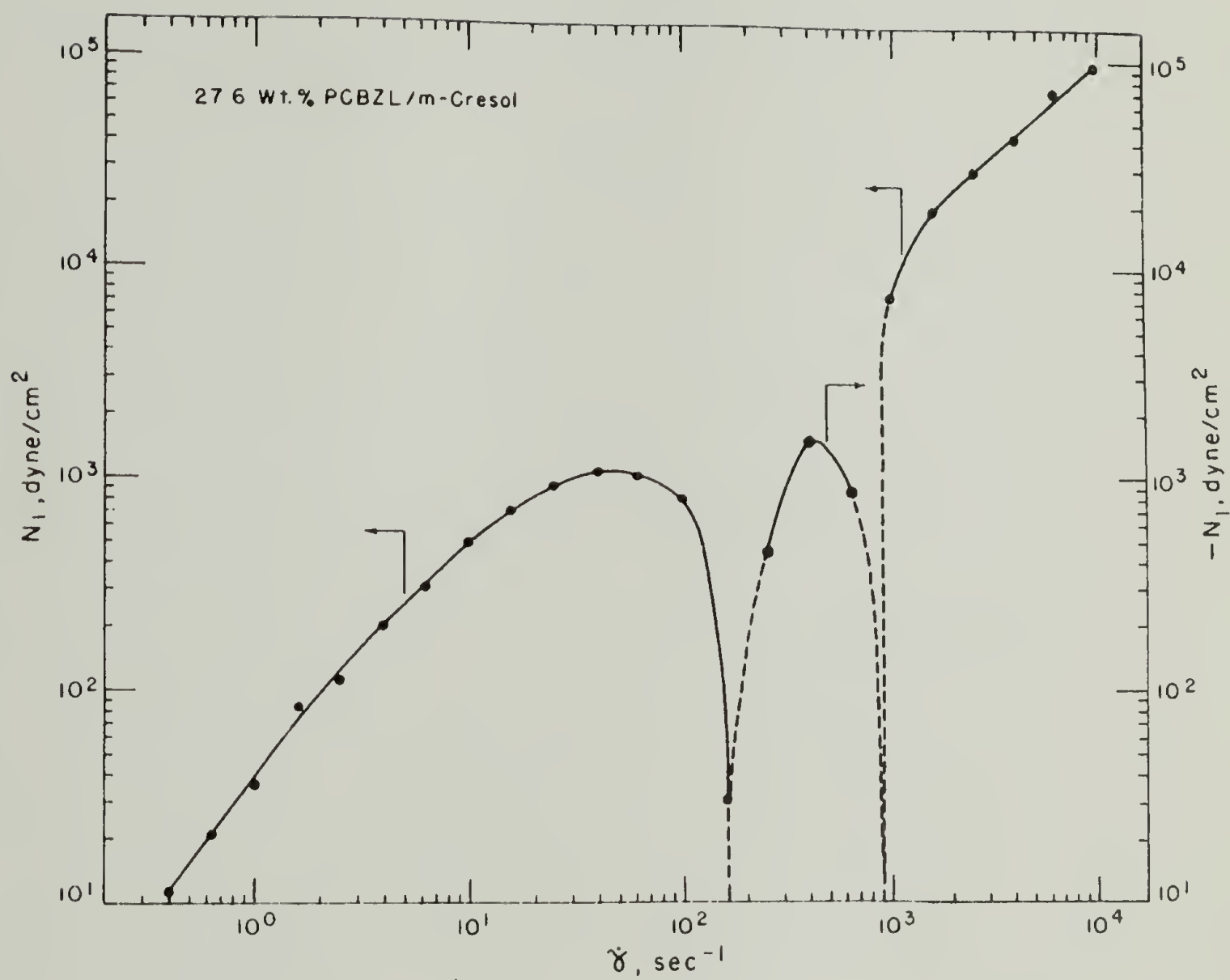


Figure 97. First Normal Stress Difference Versus Shear Rate for 27.6 wt% 200,000 M.W. PCBZL Solution.

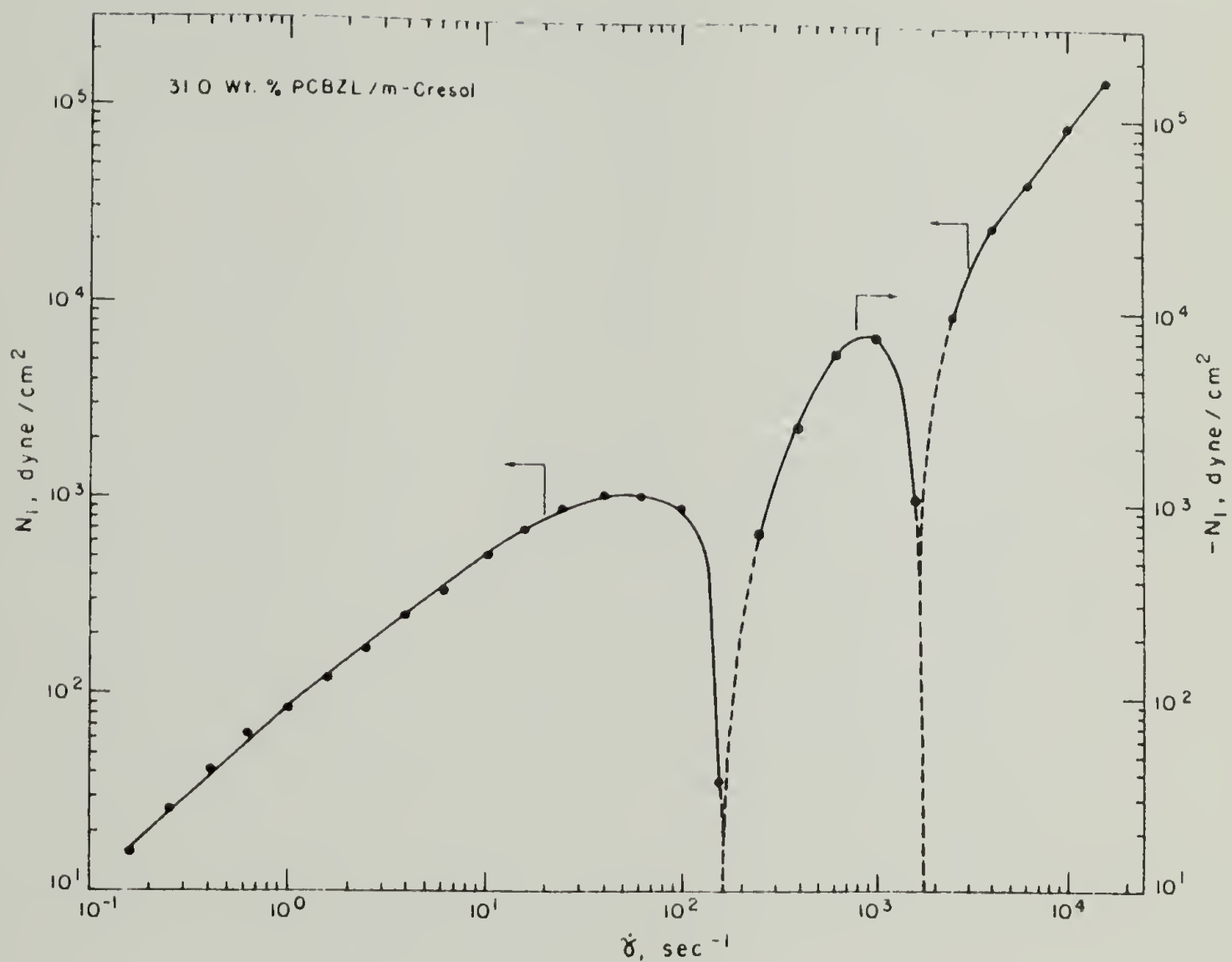


Figure 98. First Normal Stress Difference Versus Shear Rate for 31.0 wt% 200,000 M.W. PCBZL Solution.

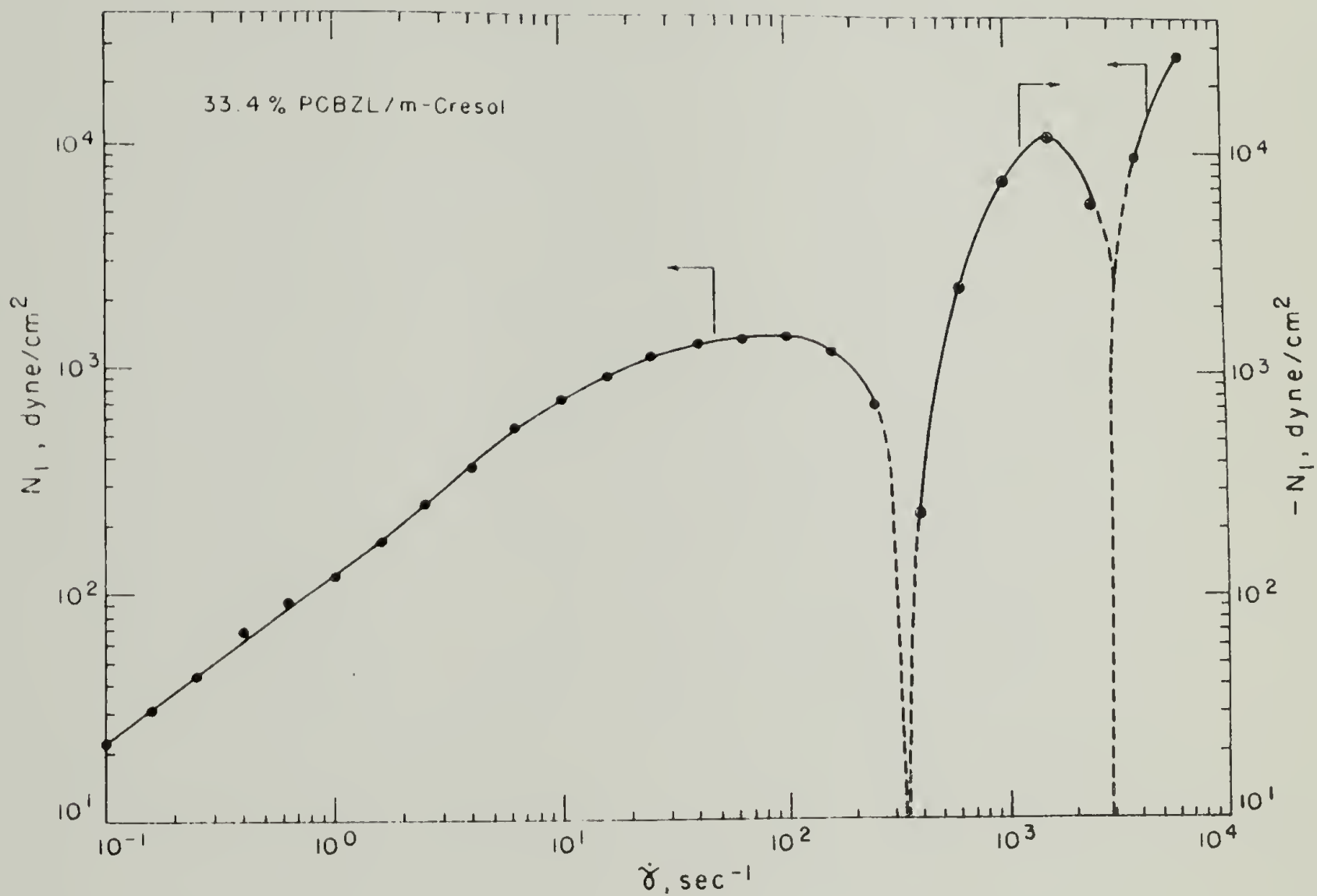


Figure 99. First Normal Stress Difference Versus Shear Rate for 33.4 wt% 200,000 M.W. PCBZL Solution.



(202). Since secondary flow phenomena are sensitive to boundary conditions, the influence of boundary conditions on the negative normal stress phenomenon was ascertained. The three geometries chosen give identical sample volumes (50 mm, .04 rad cone-and-plate) with different conditions at the edges of the cones: 50 mm, .04 rad cone with 50 mm plate; 50 mm, .04 rad cone with 100 mm plate ("infinite sea"); and concentric cylinders with a 50 mm inner cylinder machined to a .04 rad cone on the bottom surface. The experiment was performed on two different solutions chosen to give a positive-negative and a negative-positive transition over the shear rate range accessible via all three geometries. The results are shown in Figures 100 and 101. (Again, circled points indicate negative values of  $N_1$ .) It is evident that although the shear rates at which the sign changes occur are somewhat affected, the phenomenon most certainly occurs in all three geometries. It is still possible that some sort of bizarre secondary flow phenomenon is responsible and which is not greatly affected by edge conditions. If so, one would expect that material functions  $\eta$  and  $N_1$  calculated on the basis of the torque and normal thrust responses of this secondary flow (rather than the assumed laminar flow) would depend very strongly on the geometry of the actual sample volume. This expectation is tested in Figure 102. The agreement in  $\eta$  between the two sample geometries is excellent, agreement in  $N_1$  is quite good. Another noteworthy point revealed in Figures 101 and 102 is that negative normal stresses were observed at shear rates as low as  $1-10 \text{ sec}^{-1}$ , which is well within the range in which rheological measurements are routinely made without consideration of

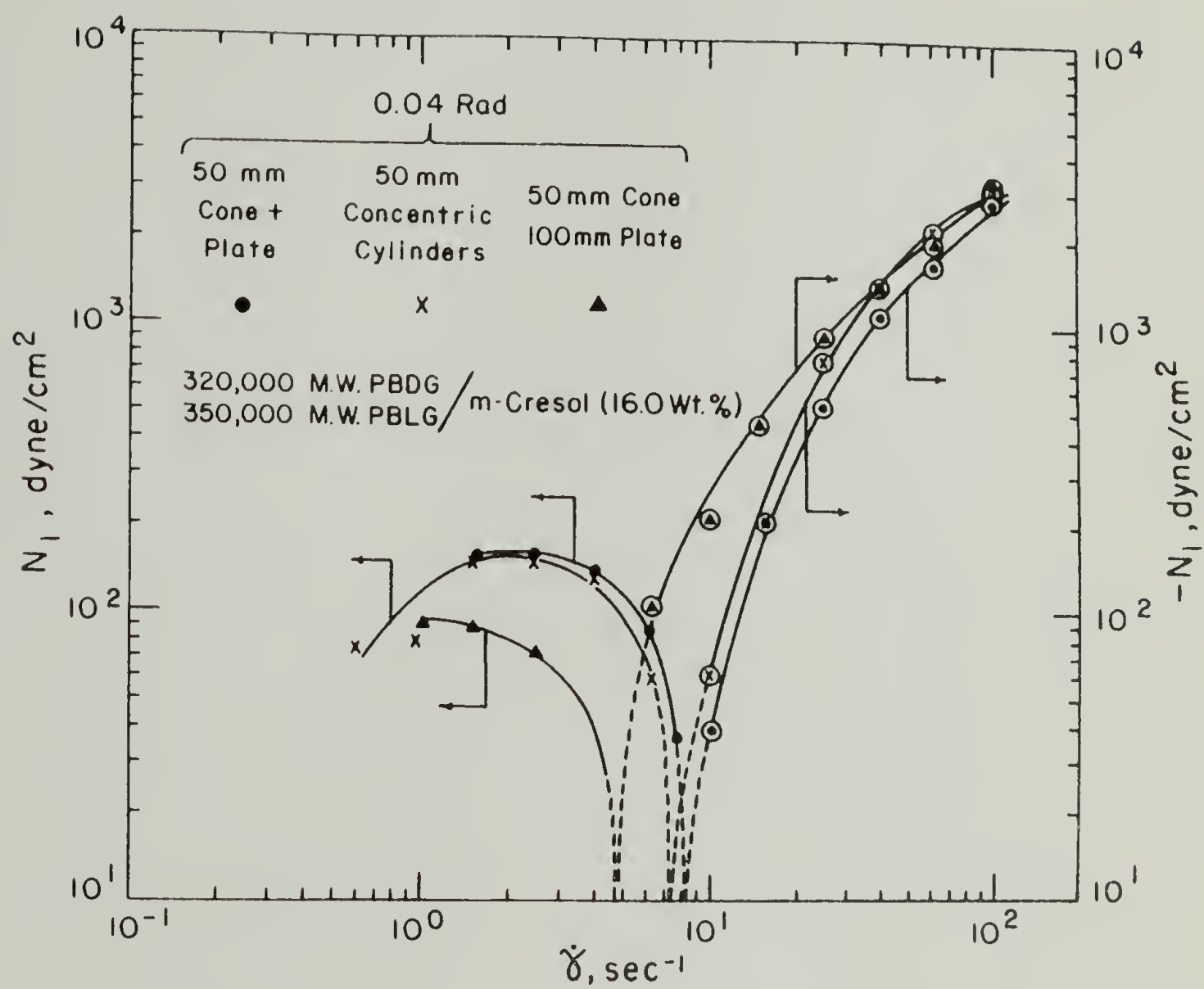


Figure 100. First Normal Stress Difference Versus Shear Rate for 16.0 wt% 335,000 M.W. PBG Solution for Three Different Edge Conditions.

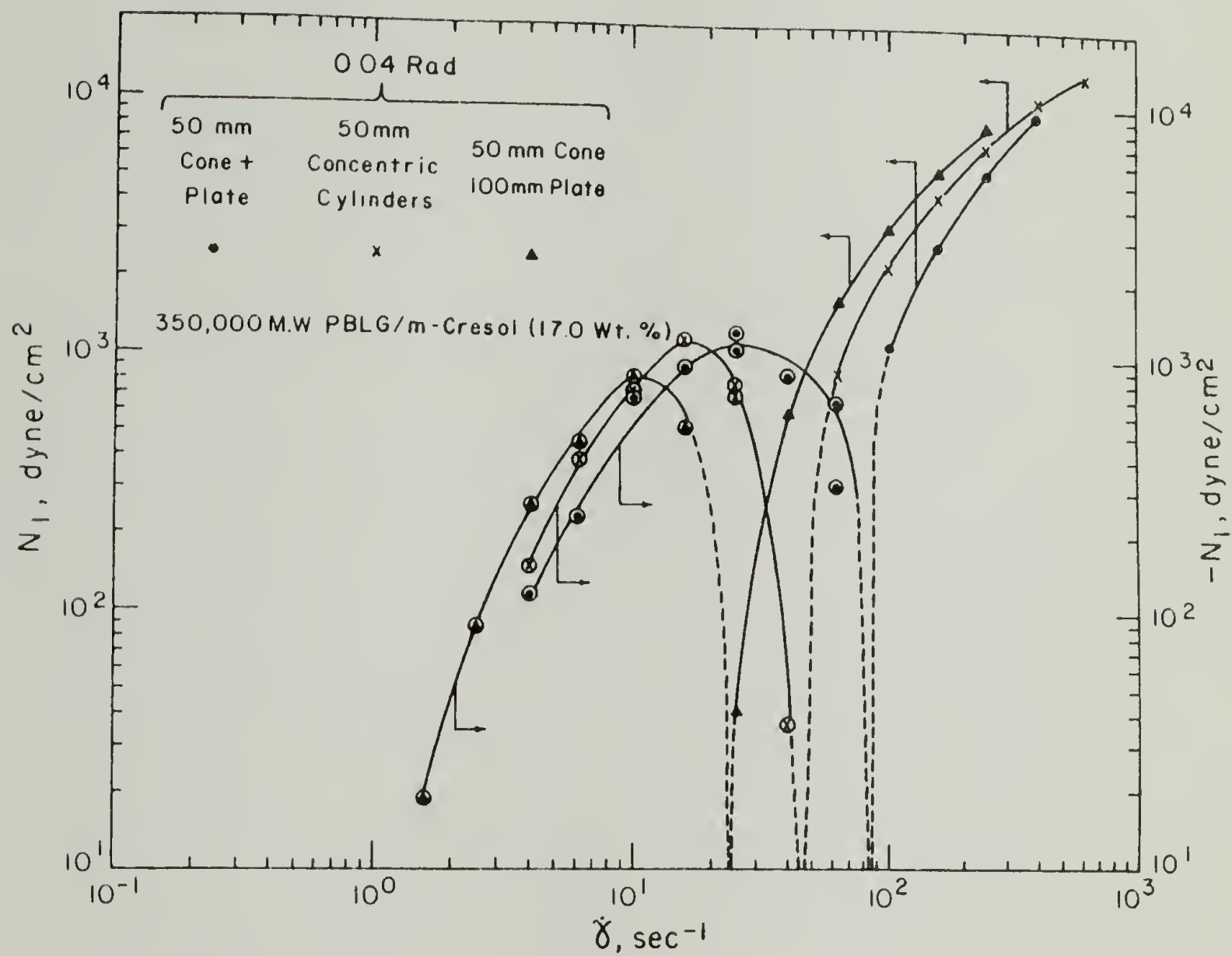


Figure 101. First Normal Stress Difference Versus Shear Rate for 17.0 wt% 350,000 M.W. PBLG Solution for Three Different Edge Conditions.

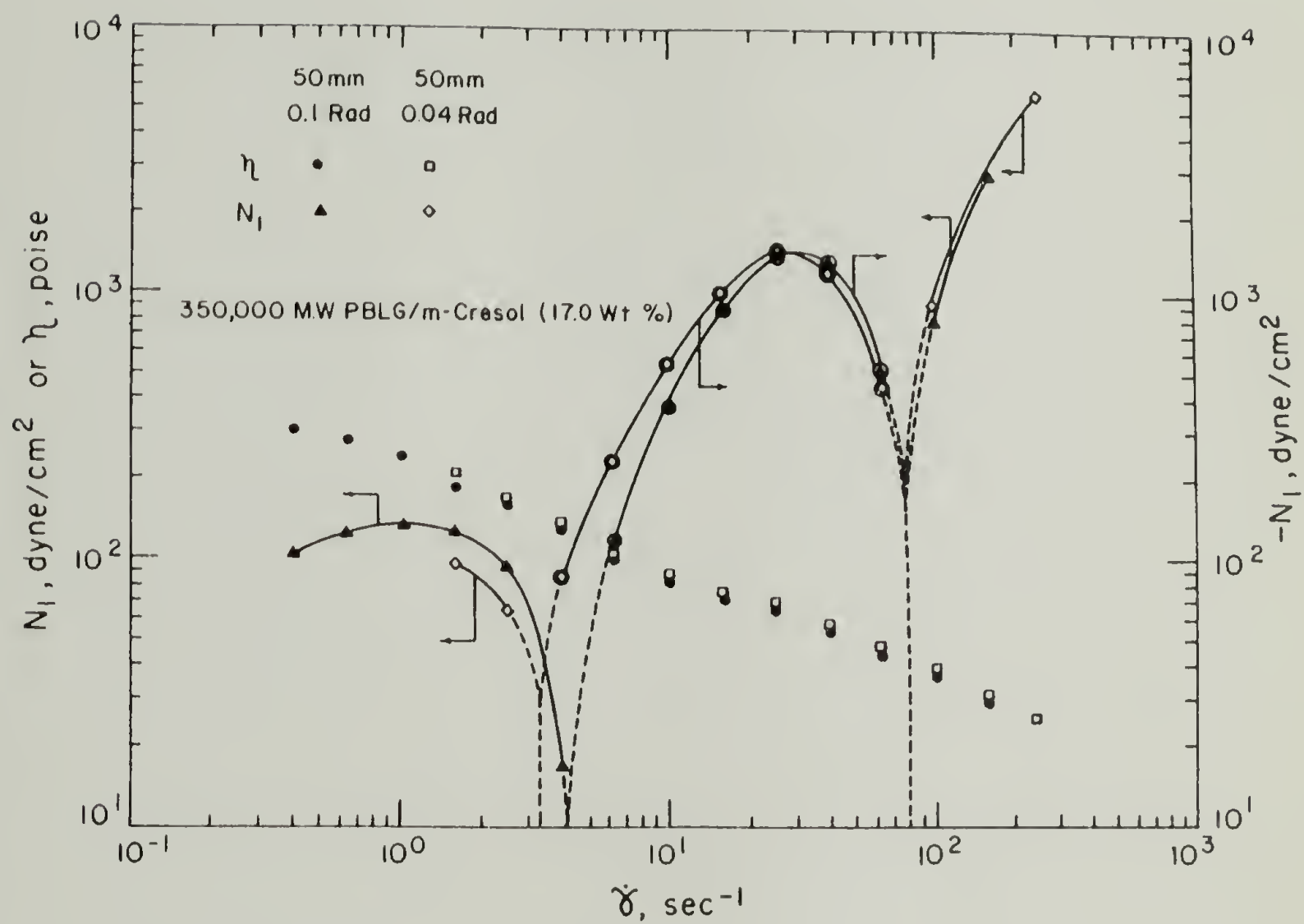


Figure 102. First Normal Stress Difference Versus Shear Rate for 17.0 wt% 350,000 M.W. PBLG Solution for Two Different Sample Geometries.

possible secondary flow effects. Finally, genuine (non-inertial) negative normal stresses have not been observed on any system in this laboratory (e.g., solutions of flexible polymers, isotropic solutions of stiff polymers, polymer melts, low M.W. fluids) apart from the liquid crystalline solutions of stiff polymers at issue here. The negative normal force measurements were steady state and were checked for stability over time periods up to 15 minutes. The measurements were independent of prior shear history. These points together constitute a strong argument against experimental artifact and suggest that the negative values of  $N_1$  truly reflect material functions of the solutions.

Since normal force measurements are more difficult than torque measurements in a cone-and-plate rheometer, the shear rates accessible with each cone were limited and therefore the degree of redundancy in the  $N_1$  data is not as great as for the  $\eta$  data. The agreement shown in Figure 102 is typical of data taken with the .1 and .04 rad cones, however surface tension effects caused some uncertainty in the measurements made with the .01 rad cones. The data shown in Figures 91-99 represent the averages of all available data. We would estimate the accuracy of the normal stress measurements to be ~20% in the first positive and the negative regions, and ~50% in the second positive region (bear in mind that the total range of normal stress measurements is 4 orders of magnitude). The accuracy of the critical shear rate at the changes in sign of  $N_1$  is ~30%. These inaccuracies lead to a fair amount of scatter in some of the figures which follow; however, even errors much larger than these estimates would not have changed

any of the important qualitative conclusions which will be drawn.

If the three regimes of normal stress behavior (positive-negative-positive) are due to shear-induced changes in the super-molecular organization of the molecules similar to those known in low M.W. thermotropic liquid crystals (203,204) one would anticipate that the shear stress required to produce these re-organizations might depend on factors which influence the molecular organization at rest, viz., temperature for thermotropic mesophases, temperature and concentration for lyotropic mesophases. Plotting the shear stress present in the fluids at the changes in sign of  $N_1$  versus concentration produces the gratifyingly systematic variation shown in Figure 103. The shear stress at the positive-negative transition climbs slowly with concentration and that at the negative-positive transition climbs much more rapidly, for both PBLG and PCBZL. In fact, the rate of variation is virtually the same for both polymer systems. Indeed, the lines frame a window on the shear-stress-concentration map within which negative normal stresses can be expected to occur. Extensions of the lines to below the lowest concentration at which observations of negative  $N_1$  were made intersect at concentrations above  $C_{\eta}^*$  for both PBLG and PCBZL. No negative normal stresses would be expected below the concentration at which the windows disappear, indicating that this phenomenon is characteristic only of the liquid crystalline solutions.

If the normal force behavior originates in the effect of shearing on the patterns of super-molecular organization ("textures"), one might anticipate that the magnitude of the normal stresses produced by deforming these structures would also depend on concentration. Figure

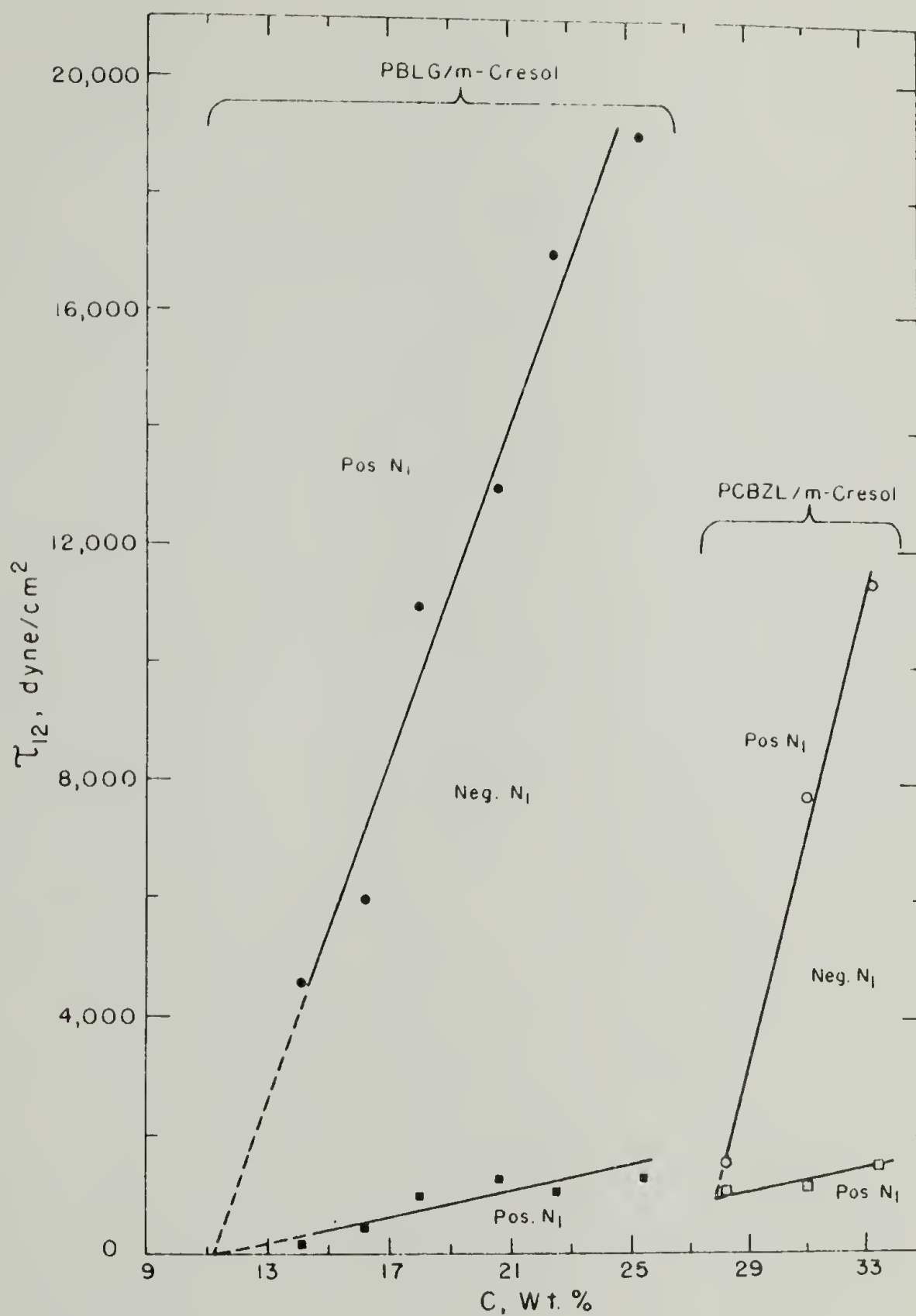


Figure 103. Shear Stress at Points of Change in Sign of First Normal Stress Difference vs. Concentration for 150,000 M.W. PBLG and 200,000 M.W. PCBZL Solutions.

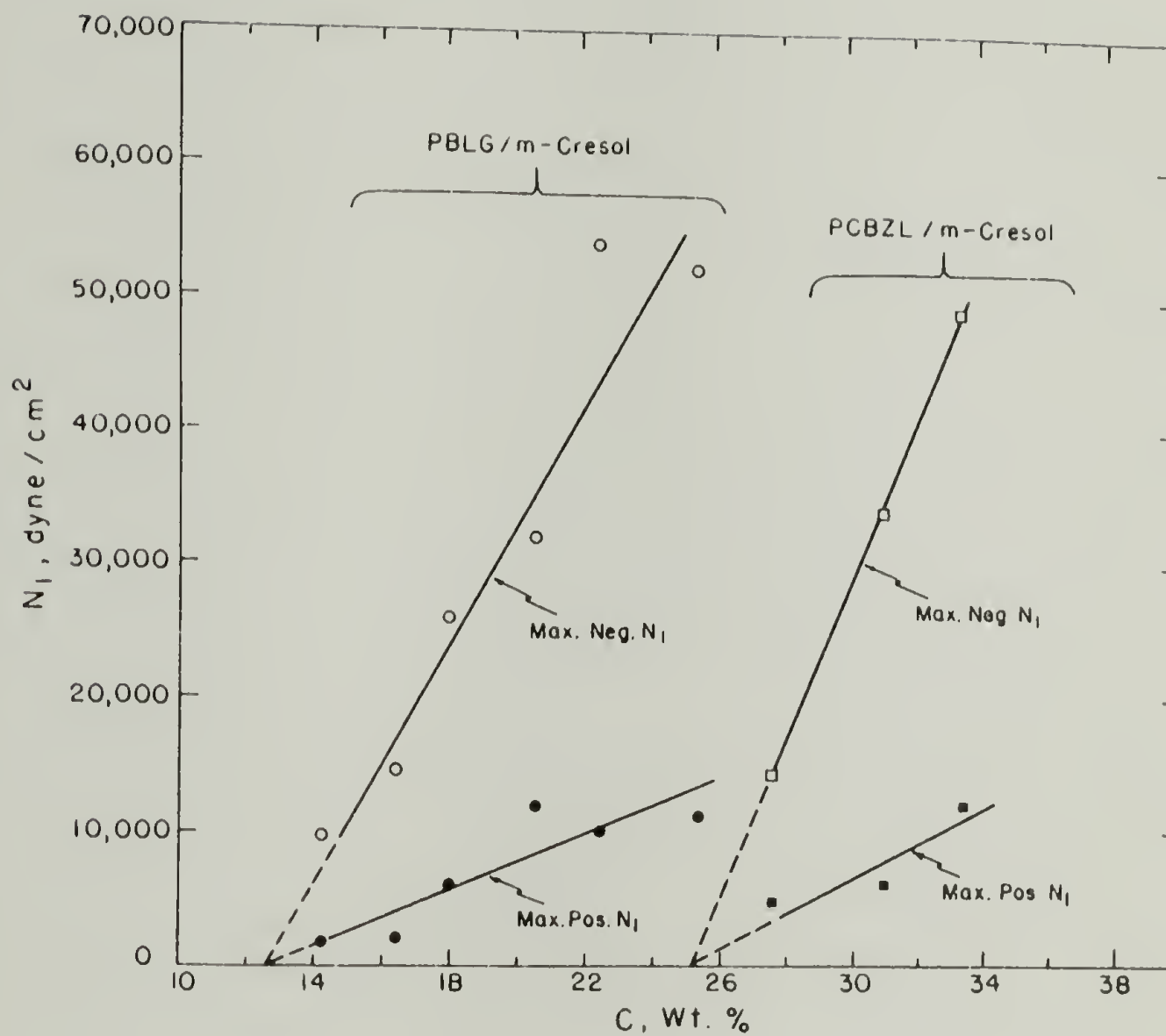


Figure 104. Maximum Positive and Negative Values of First Normal Stress Difference vs. Concentration for 150,000 M.W. PBLG and 200,000 M.W. PCBZL Solutions.



104 shows the magnitudes of the positive and negative maxima in  $N_1$  plotted against concentration. The positive maximum climbs rather slowly with concentration and the negative maximum climbs rather more quickly for both PBLG and PCBZL. The variation for PCBZL seems slightly more rapid than for PBLG but the scatter of the data is such that it is hard to make this assertion with confidence. Both lines extrapolate to  $N_1 = 0$  at the same concentration, which is above  $C_\eta^*$ , for both PBLG and PCBZL. This indicates that the mechanisms responsible for both the first positive and the negative region of normal stress diminish in effect as concentration is reduced toward  $C_\eta^*$  and disappear entirely before  $C_\eta^*$  is reached, leaving only the mechanism responsible for the second positive region, both for the PBLG and PCBZL solutions.

It might be presumed that the mechanism responsible for the second positive region of normal stress at high shear rates is also active in the isotropic solutions below  $C_\eta^*$ . This point of view is supported by the observations in Figures 87 and 88 that at high shear rates, there is very little going on at  $C_\eta^*$  for PCBZL and nothing at all for PBLG, as far as  $\eta$  is concerned. It appears that shear-induced orientation is the dominant factor and that space-filling considerations have little effect on determining the structure of the fluid at high shear rates, regardless of the concentration. This concept is tested in Figures 105 and 106 by plotting  $N_1$  vs.  $C$  at a low shear rate chosen so that it is in the first region of positive  $N_1$  for all concentrations and at a high shear rate chosen so that it is in the second positive region for all concentrations (of course  $N_1$  is

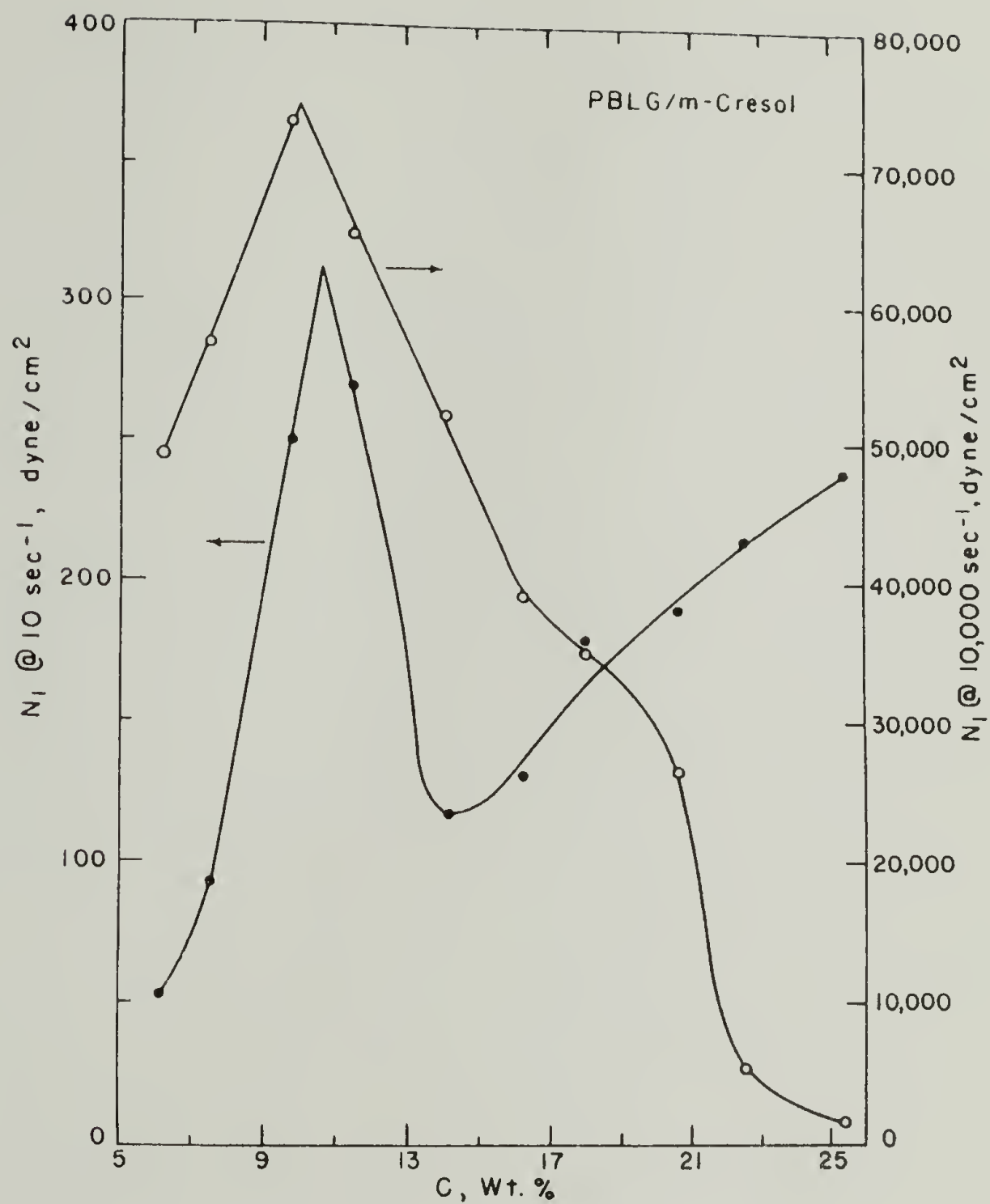


Figure 105. First Normal Stress Difference vs. Concentration at One Low and One Very High Shear Rate for 150,000 M.W. PBLG Solutions.

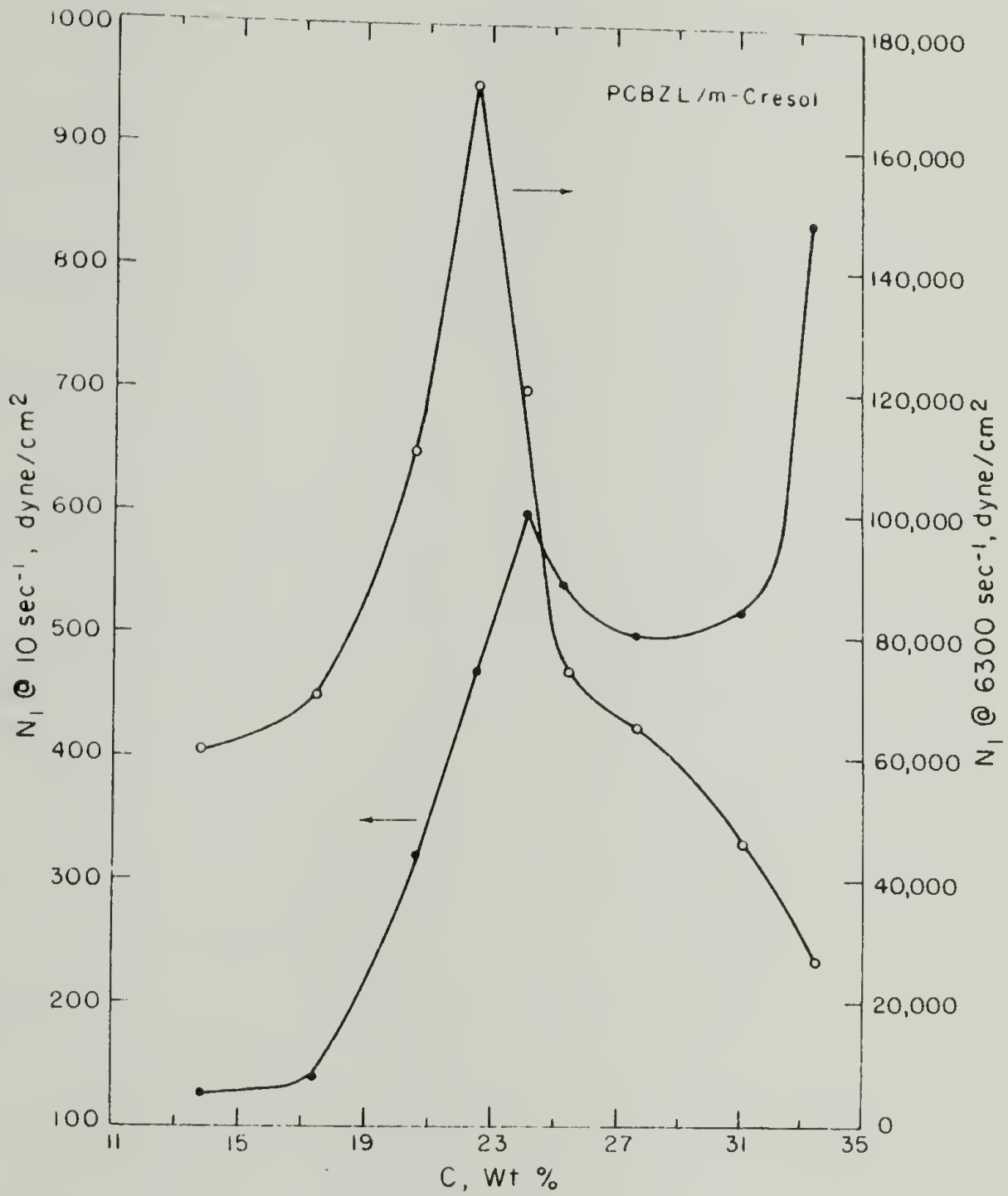


Figure 106. First Normal Stress Difference vs. Concentration at One Low and One Very High Shear Rate for 200,000 M.W. PCBZL Solutions.

positive at all shear rates for  $C$  less than  $C_{\eta}^*$ ). The curves of  $N_1$  vs.  $C$  at low shear rate appear very similar to  $\eta_{\dot{\gamma} \rightarrow 0}$  vs.  $C$  for both PBLG and PCBZL. The maxima agree with  $C_{\eta}^*$  for both polymer systems. The curves of  $N_1$  vs.  $C$  at high shear rate astonishingly show that the maximum in  $N_1$  vs.  $C$  is not suppressed for either polymer at high shear rates (although it is shifted to lower concentration, as is  $C_{\eta}^*$ ). The inescapable conclusion is that the mechanism responsible for the normal stress at high shear in the liquid crystalline solutions is not the same as that responsible for normal stress in the isotropic solutions. Furthermore, it is apparent that some sort of a structure which exists in the liquid crystalline solutions persists despite the high shear stresses which obtain at these high shear rates. The difference in behavior between  $\eta$  vs.  $C$  and  $N_1$  vs.  $C$  as shear rate is varied indicates that the mechanisms responsible for the occurrence of shear stress and normal stress are decoupled to a remarkable extent for both PBLG and PCBZL solutions over the entire concentration range.

Dynamic viscosity. Dynamic viscosity  $\eta'$  versus frequency  $\omega$  measured via oscillatory shear for the PBLG solutions is shown in Figures 107 and 108. The lower concentration solutions all exhibit similar behavior with well-defined low frequency limiting values and "power-law" behavior for the frequency dependence of  $\eta'$  at higher frequencies. The slopes within the power-law region seem to decrease as concentration is increased;  $-.55$  for 6.1%,  $-.52$  for 7.5%, approx.  $-.50$  for 9.8%,  $-.42$  for 11.5%. Extensions of the linear portions (not shown on the Figures) intersect at break points which decrease in frequency as

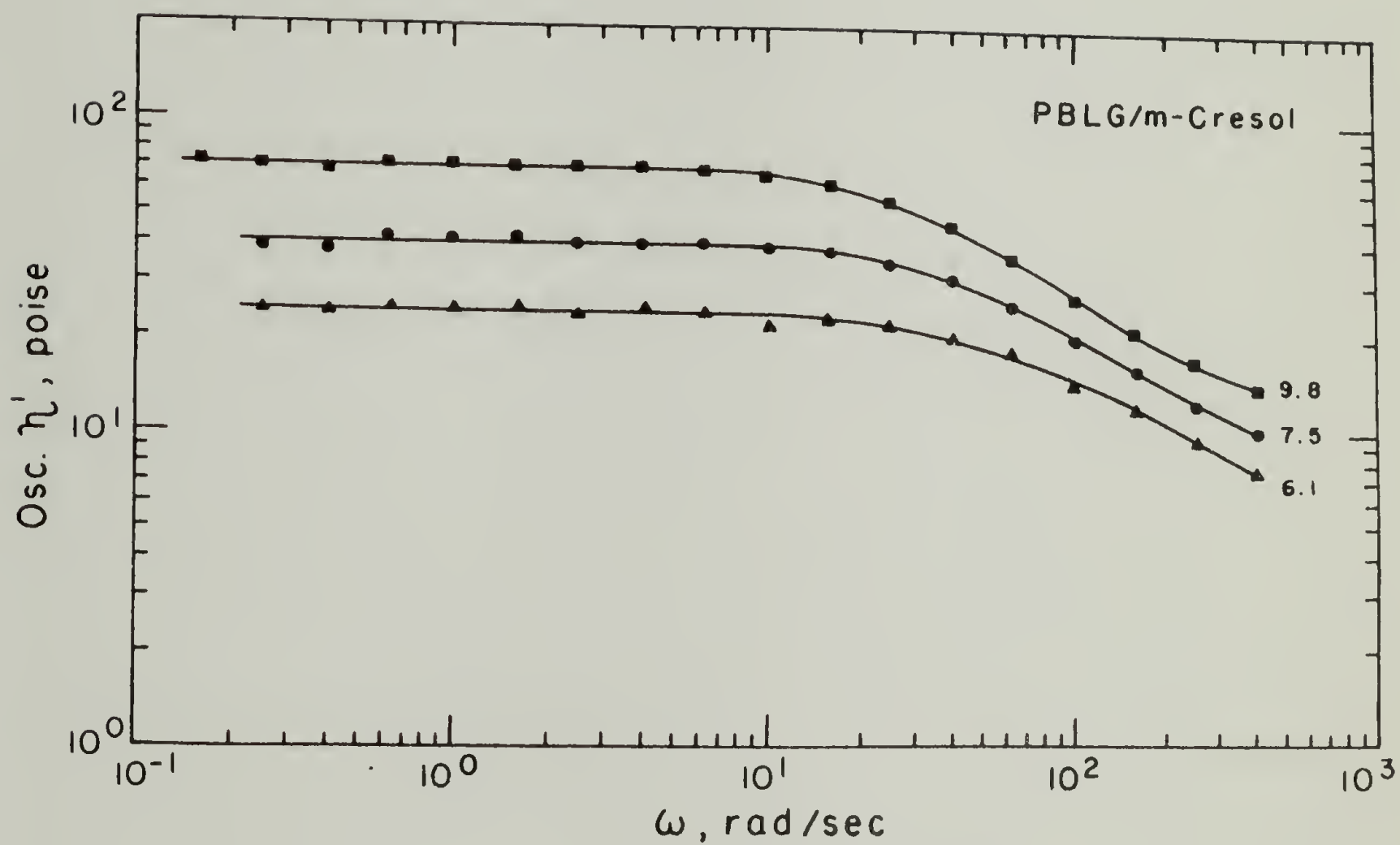


Figure 107. Dynamic Viscosity vs. Frequency (Oscillatory Shear) for 150,000 M.W. PBLG Solutions.

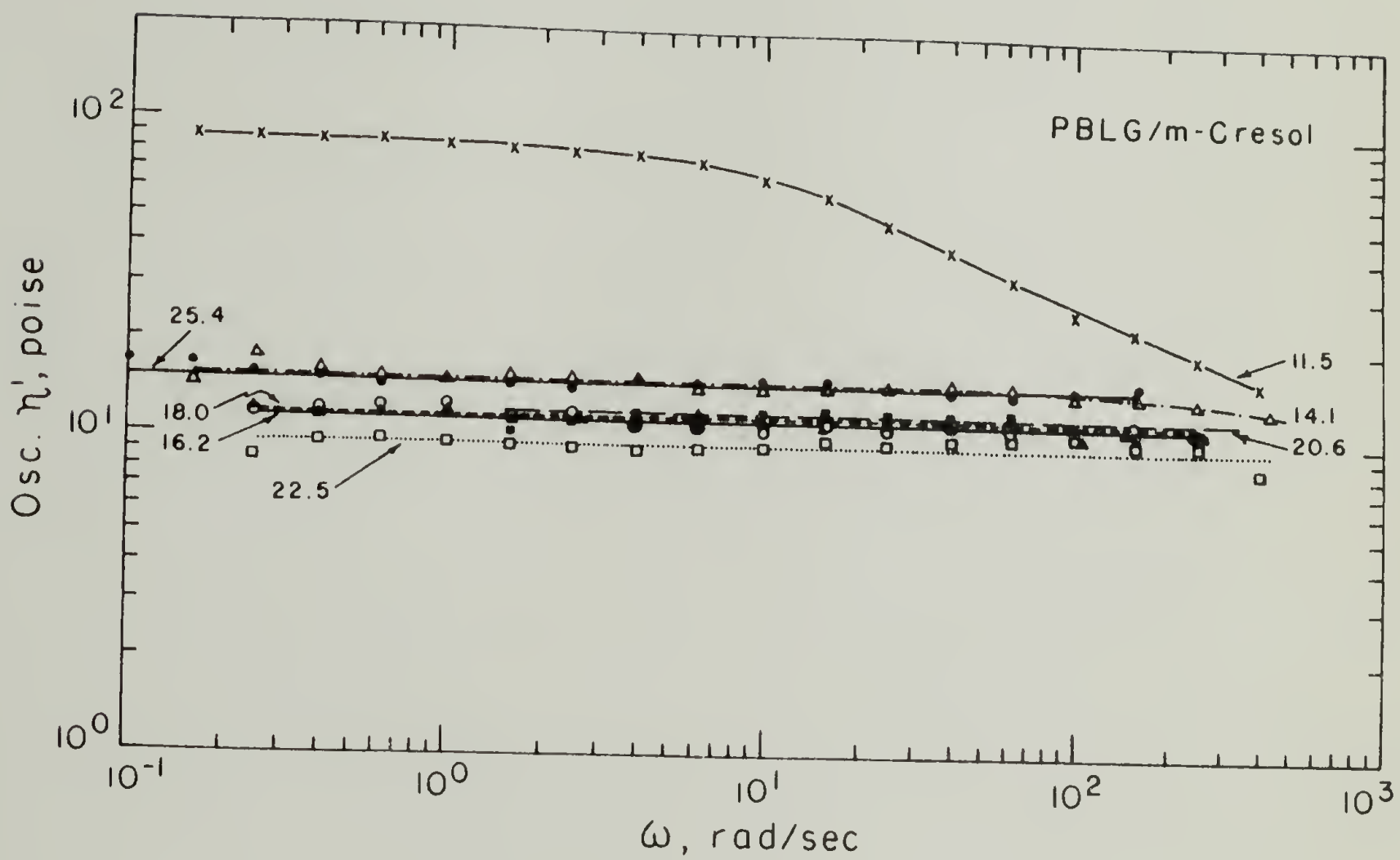


Figure 108. Dynamic Viscosity vs. Frequency (Oscillatory Shear) for 150,000 M.W. PBLG Solutions.

concentration is increased; 56 rad/sec for 6.1%, 30 rad/sec for 7.5%, 19 rad/sec for 9.8%, 7.6 rad/sec for 11.5%. The behavior of the solutions of 14.1% and higher is radically different;  $\eta'$  being independent of  $\omega$  over the entire accessible range of frequency. It is noteworthy that another radical difference in behavior has already been pointed out between PBLG solutions of 11.5 and 14.1%, that is, the latter is the least concentrated which exhibits the negative normal stress effect.

$\eta'$  vs.  $\omega$  as measured by the E.R.D. technique is shown for the PBLG solutions in Figure 109. The range of accessible frequency for these low viscosity solutions is much more limited than for oscillatory shear. The quantitative agreement between the two methods is fair-to-good. The important result of the E.R.D. measurements is confirmation that  $\eta'$  is frequency dependent for solutions of 11.5% or less, and Newtonian for solutions of 14.1% or higher.

The limiting low frequency values  $\eta'_{\omega \rightarrow 0}$  as measured by both techniques is plotted against concentration in Figure 110 (also shown is  $\eta_{\dot{\gamma} \rightarrow 0}$  which should be equal to  $\eta'_{\omega \rightarrow 0}$  for any fluid (205)). At the highest concentrations the agreement among the three values is less than excellent. As  $C_{\eta}^*$  is approached, the agreement between  $\eta_{\dot{\gamma} \rightarrow 0}$  and E.R.D.  $\eta'_{\omega \rightarrow 0}$  improves somewhat but osc  $\eta'_{\omega \rightarrow 0}$  remains low throughout the entire concentration range. As shown in Figure 111, the spread between  $\eta$ , E.R.D.  $\eta'$  and osc.  $\eta'$  is on the order of 10% for a Newtonian viscosity standard (note that the oscillatory measurements are reliable all the way to 400 rad/sec). This would indicate that the disagreement seen in Figure 110 is characteristic of the fluid rather than the

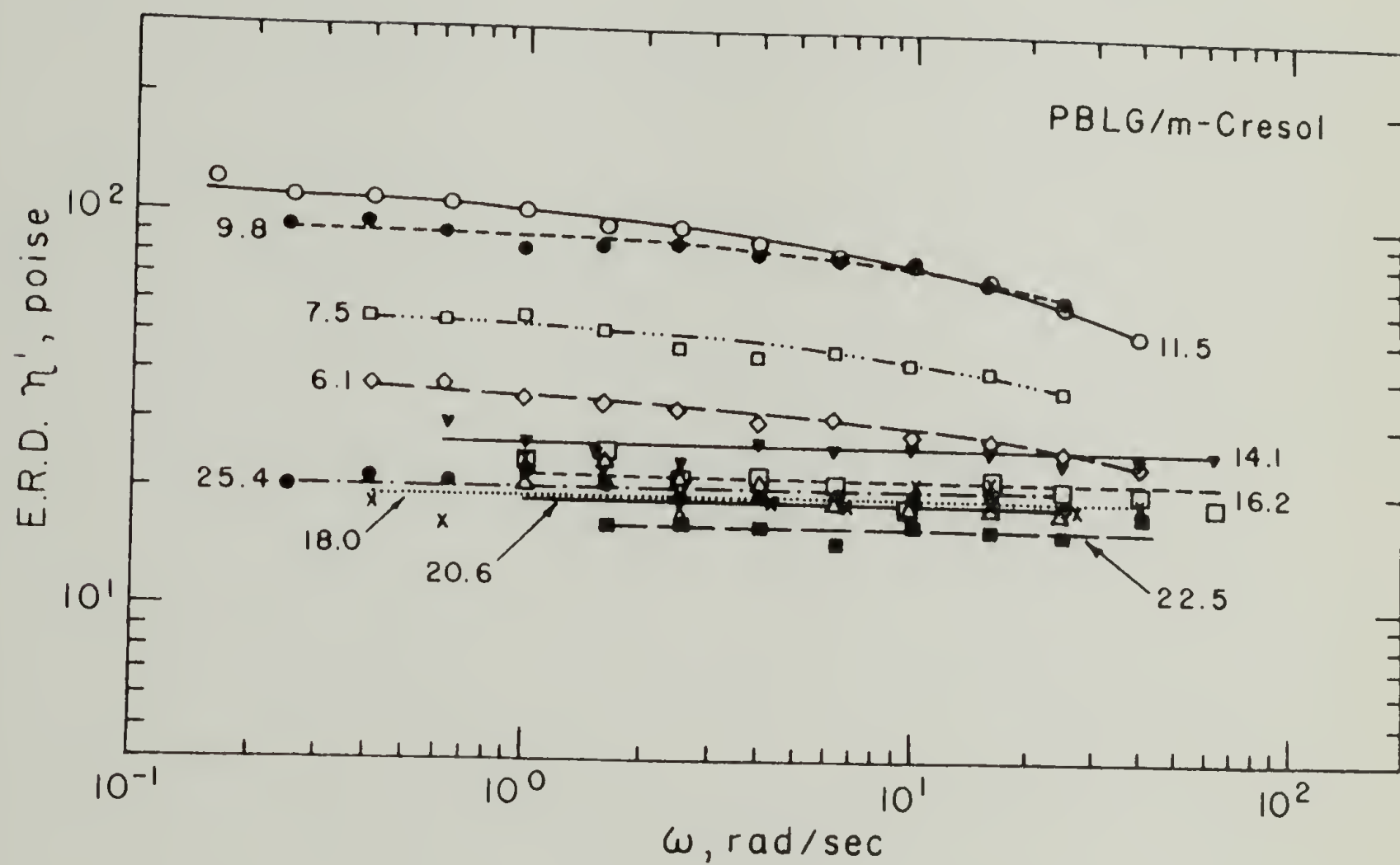


Figure 109. Dynamic Viscosity vs. Frequency (Eccentric Rotating Disc) for 150,000 M.W. PBLG Solutions.



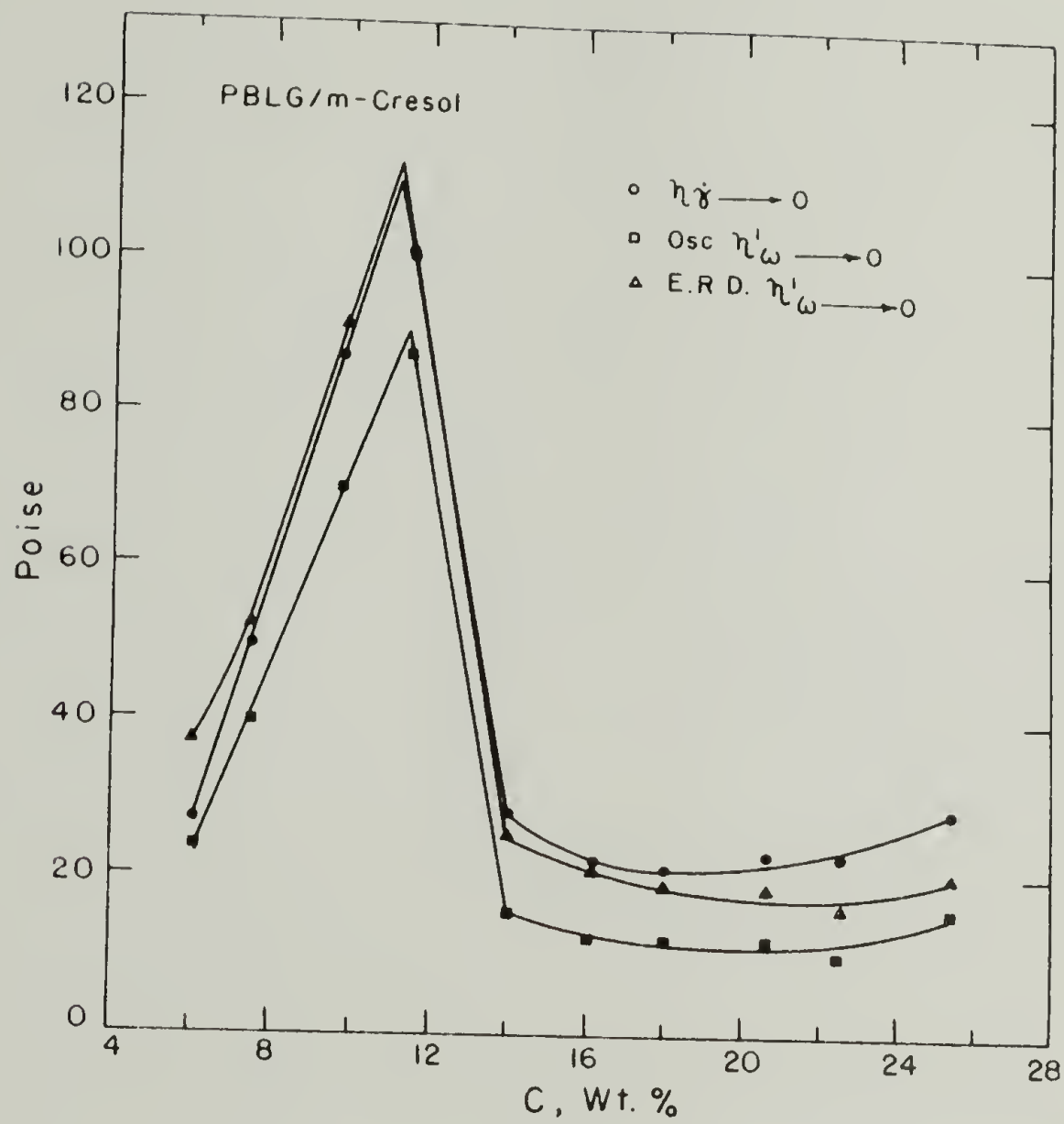


Figure 110. Limiting Viscosity Values vs. Concentration for 150,000 M.W. PBLG Solutions.

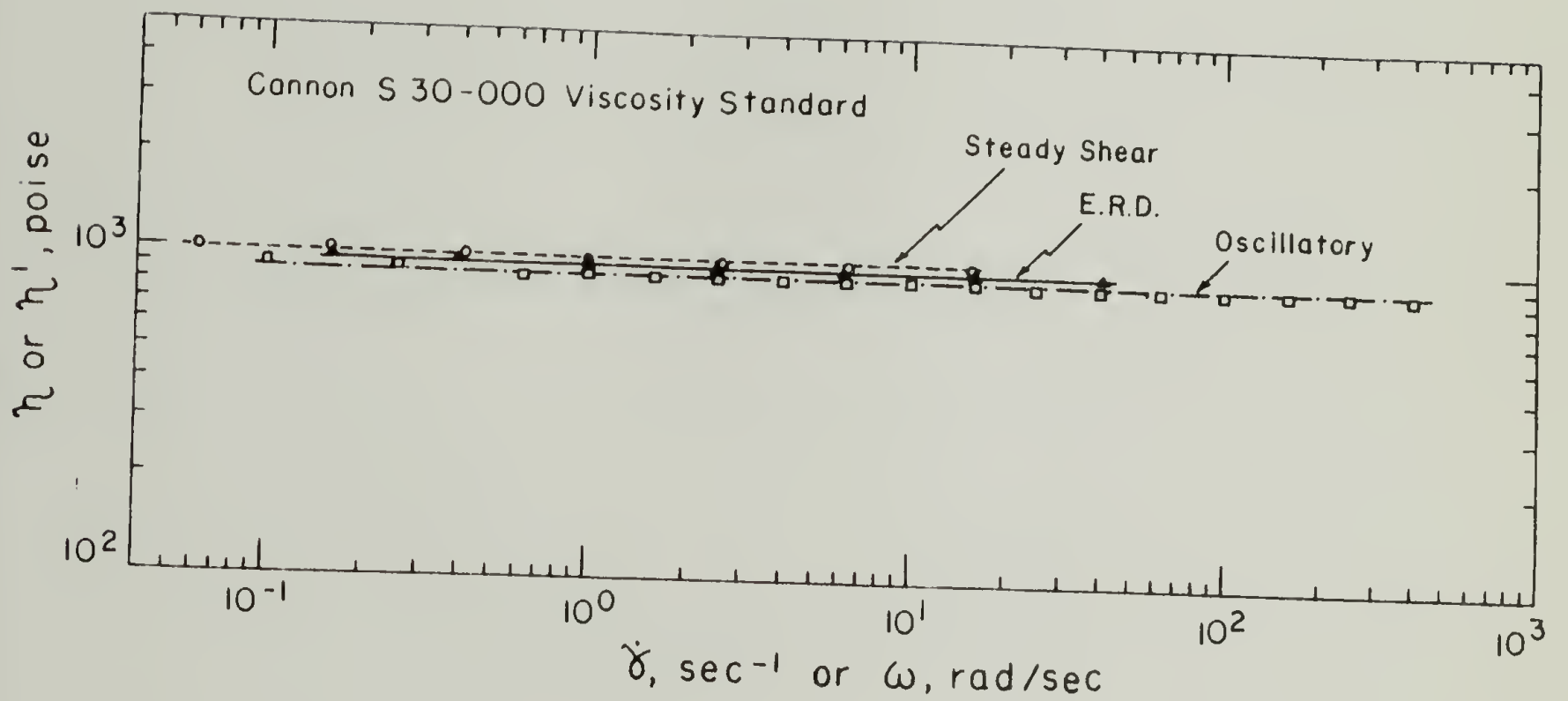


Figure 111. Steady Shear Viscosity vs. Shear Rate and Dynamic Viscosity vs. Frequency (Oscillatory Shear and Eccentric Rotating Disc) for Newtonian Viscosity Standard.

instrumentation. On the other hand, the trend in both figures is the same; steady shear giving the highest value, followed by E.R.D. and then oscillatory. This suggests that systematic errors in the instrumentation, which are no doubt present to some extent, since the accuracy of the data is less than the precision, may be more significant at the high sensitivities required to obtain low shear and low frequency limiting viscosity values for these low-viscosity fluids. We conclude that the disagreement in Figure 110 is not great enough to be certain that it is characteristic of the fluids.

More significant than the quantitative agreement, or lack of it, among  $\eta$ , E.R.D.  $\eta'$  and osc.  $\eta'$  at any particular concentration is the fact that all three give values of  $C_{\eta}^*$  which agree very closely (see Table 5).

The results of oscillatory measurements of  $\eta'$  for the PCBZL solutions is shown in Figures 112 and 113. The solutions of concentration below  $C_{\eta}^*$  are again well-behaved, with well-defined low-frequency Newtonian plateaus, followed by power-law behavior in the frequency-dependent region. Too few points are available in the power-law regions of the 13.9% and the 17.3% solutions to establish the variation of slope with concentration. However, extending the linear regions gives break points (not shown) at decreasing frequency as concentration is increased, as was found for the PBLG solutions: approx. 72 rad/sec for 13.9%, approx 46 rad/sec for 17.3%, 23 rad/sec for 20.6%, 13 rad/sec for 22.5%.

The first two solutions with concentration greater than  $C_{\eta}^*$  (which showed no negative normal stress behavior) do not exhibit power-

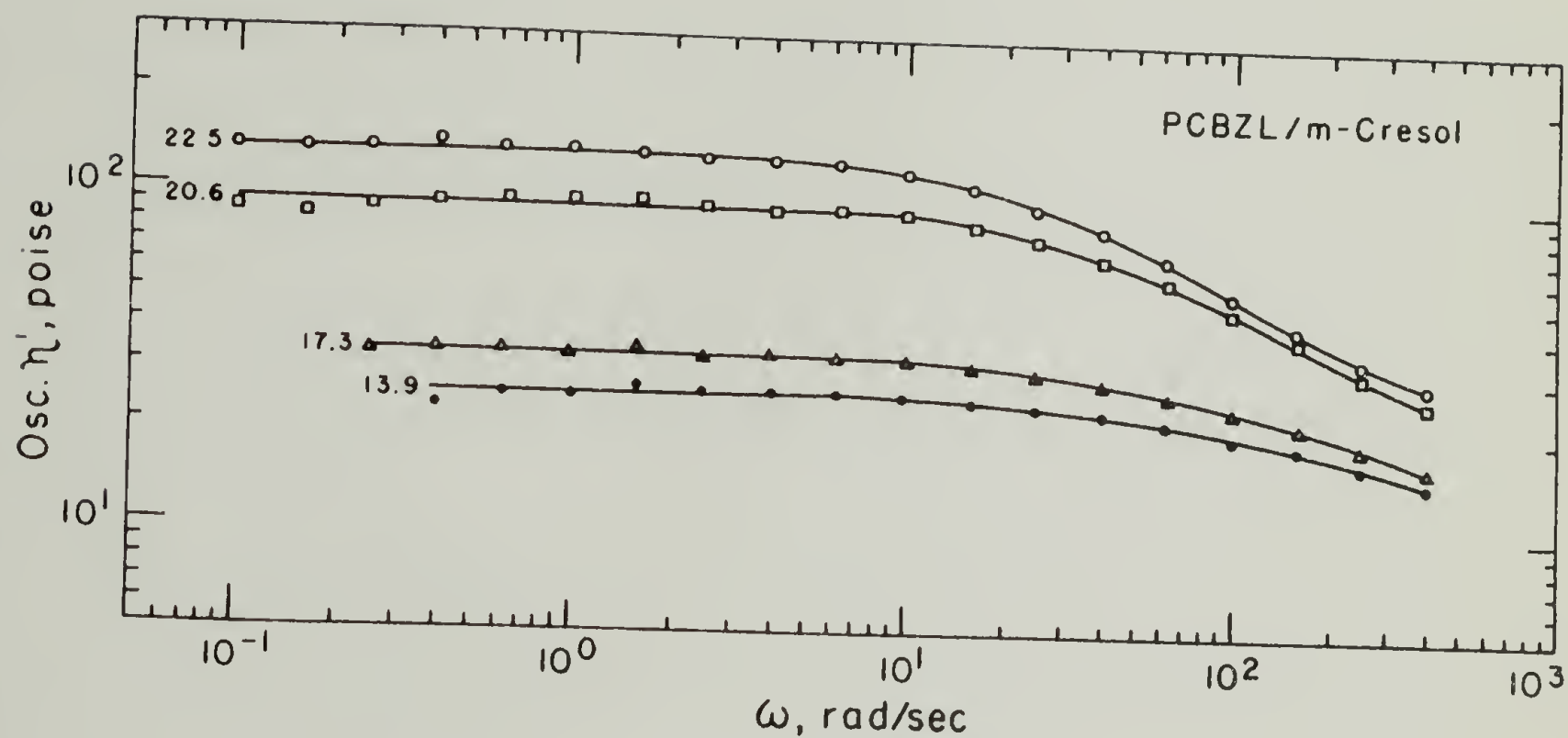


Figure 112. Dynamic Viscosity vs. Frequency (Oscillatory Shear) for 200,000 M.W. PCBZL Solutions.

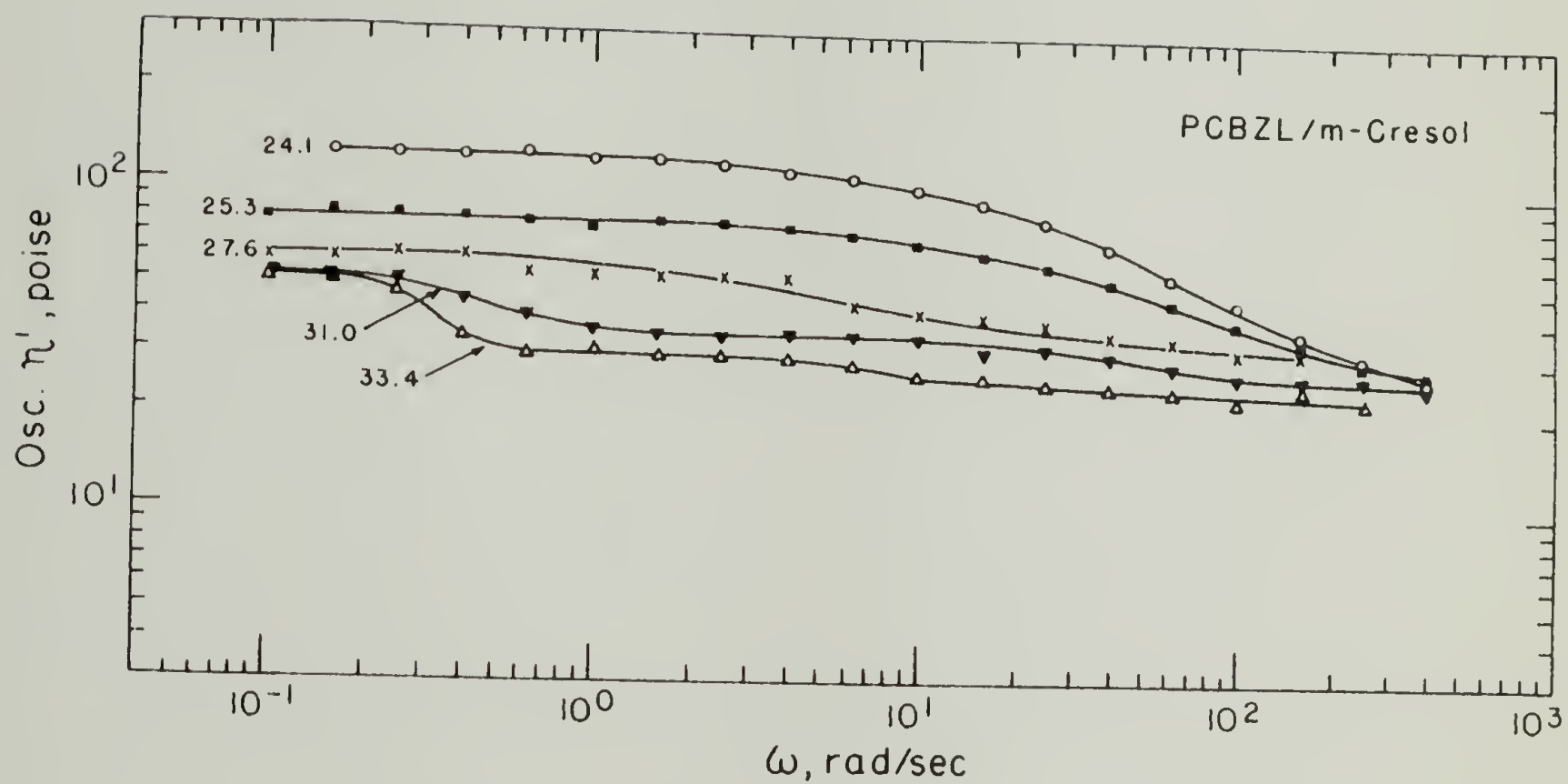


Figure 113. Dynamic Viscosity vs. Frequency (Oscillatory Shear) for 200,000 M.W. PCBZL Solutions.

low shear-thinning behavior, but appear to be curving toward high frequency plateaus. The 33.4% and 31.0% solutions have more complex behavior with two high-frequency plateaus. The difference in values of  $\eta'$  in the two high frequency plateaus is such that it is possible but not probable that the second plateau is an artifact of experimental scatter. There is indisputably at least one high frequency plateau for these two concentrations. Unfortunately, the crucial 27.6% solution (the lowest concentration of PCBZL which exhibited the negative normal stress effect) gave abnormally scattered data so one can draw a line with either one or two high-frequency plateaus through the data points with equal lack of justification.

It appears possible that the existence of three plateaus in  $\eta'$  vs.  $\omega$  (the low-frequency limit and the two high-frequency plateaus) corresponds to the three regimes of normal stress (positive-negative-positive) in liquid-crystalline PCBZL solutions. From the limited amount of information in hand, it appears that the difference in plateau levels and the sharpness of the change from one plateau value to another both decrease with concentration (i.e., the plateaus become less distinct with decreasing concentration). (Note in particular the sharp drop in  $\eta'$  at .4 rad/sec for the 33.4% solution which is similar to the steady shear behavior previously alluded to in Figure 86.) However, the frequencies at which the transitions occur seem to increase with decreasing concentration: approx .4 and 10 rad/sec for 33.4%, approx 1 and 60 rad/sec for 31.0%. This is in contrast with the observation that the shear rates at which the two changes in sign of  $N_1$  occur decrease with decreasing concentration.

The E.R.D. measurements of  $\eta'$  vs.  $\omega$  shown in Figure 114 does not clarify the situation greatly due to the limited frequency range accessible. Some similarities in shape with the osc.  $\eta'$  vs. curves can be seen. The four most concentrated solutions exhibit one high-frequency plateau. Again, the change from low-frequency limiting value to high-frequency plateau becomes less distinct as concentration decreases. Again, the frequencies at which this change occurs increases with decreasing concentration:  $\sim 0.6$  rad/sec for 33.4%,  $\sim 1.0$  rad/sec for 31.0%,  $\sim 1.5$  rad/sec for 27.6%, and  $\sim 2$  rad/sec for 25.3%. None of the E.R.D.  $\eta'$  curves exhibited two high-frequency plateaus. In sum, although there does seem to be some indication of differences in the dynamic viscosity behavior for PCBZL solutions which do or do not exhibit the negative normal stress effect, it is not as striking and clear-cut as for the PBLG solutions.

The values of osc.  $\eta'_{\omega \rightarrow 0}$  and E.R.D.  $\eta'_{\omega \rightarrow 0}$  are plotted versus concentration in Figure 115, as well as  $\eta_{\dot{\gamma} \rightarrow 0}$  for comparison. The differences among the values obtained by the three techniques seems to be too great to be attributable to experimental error, especially at the three highest concentrations. In fact, the shapes of the three curves are quite different in the concentration regime in which the negative normal stress effect was observed. As for PBLG, osc.  $\eta'_{\omega \rightarrow 0}$  gave the lowest values at all concentrations; however, for most concentrations the values of E.R.D.  $\eta'_{\omega \rightarrow 0}$  was higher than  $\eta_{\dot{\gamma} \rightarrow 0}$ . Significantly, the agreement among the three measurements is very good at the two lowest concentrations; since these two solutions had the lowest viscosities, it would be anticipated that they would have exhibited

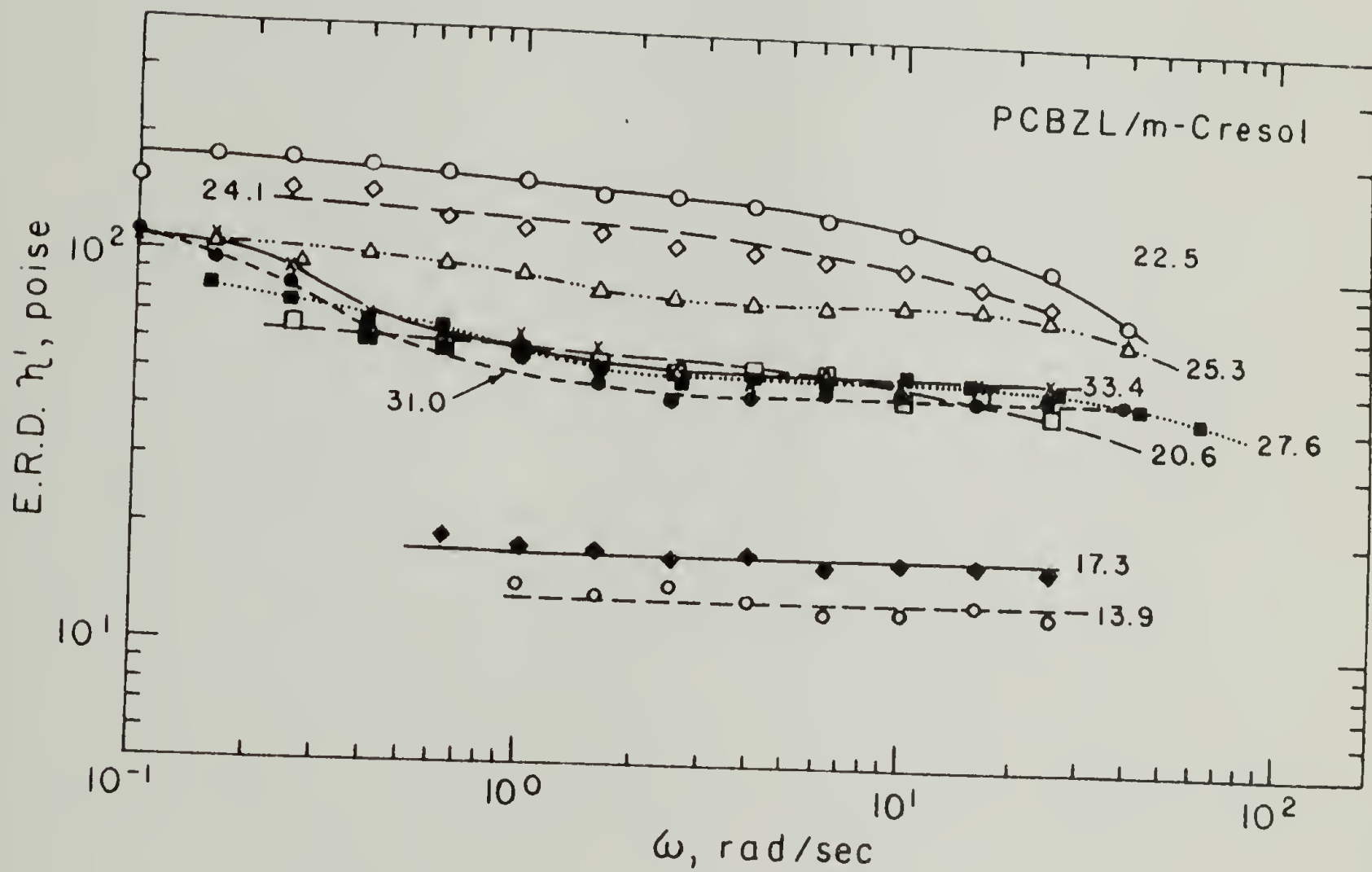


Figure 114. Dynamic Viscosity vs. Frequency (Eccentric Rotating Disc) for 200,000 M.W. PCBZL Solutions.



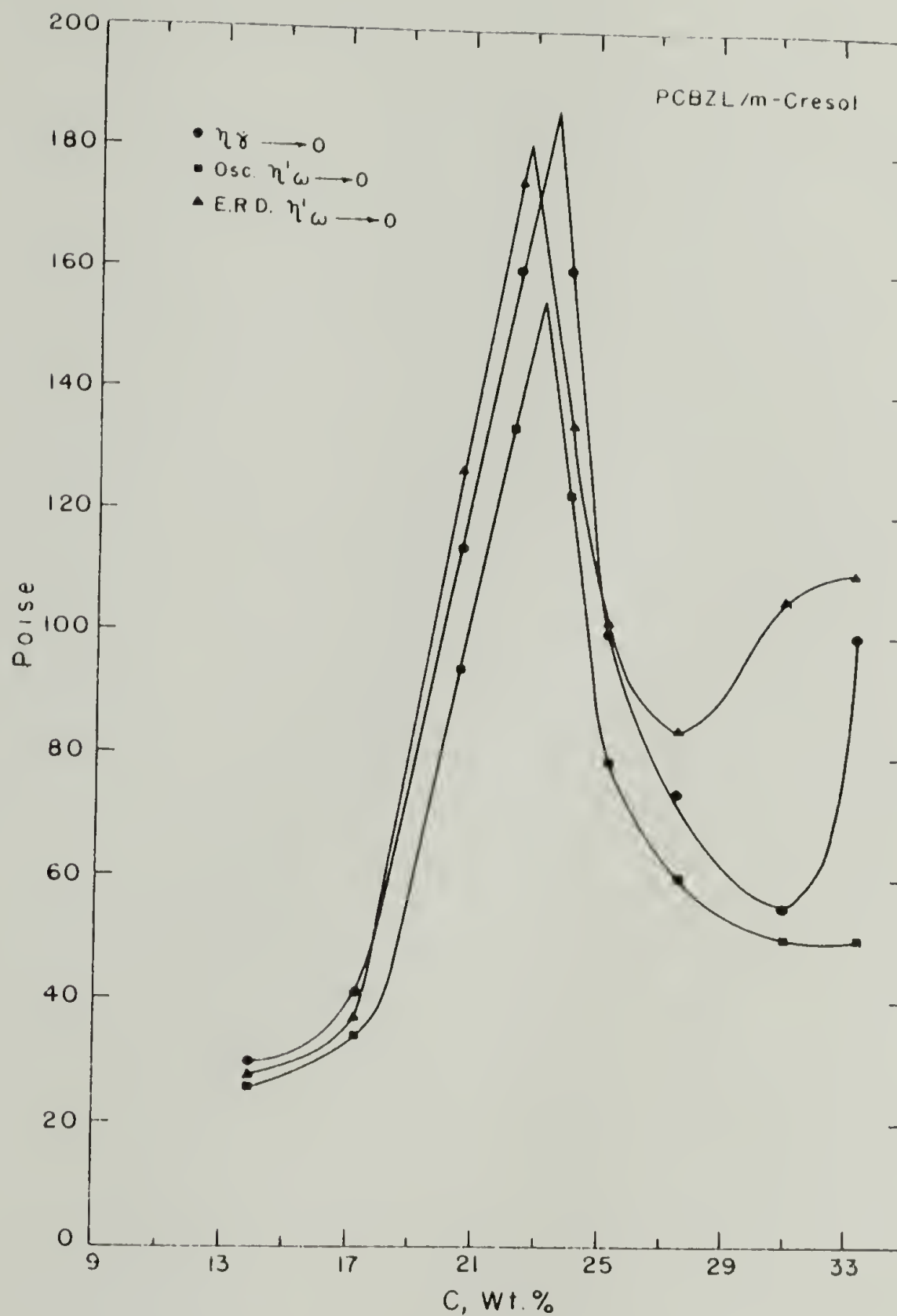


Figure 115. Limiting Viscosity Values vs. Concentration for 200,000 M.W. PCBZL Solutions.

the greatest discrepancy whether due to random errors or systematic errors. The agreement in values of  $C_{\eta}^*$  given by the three techniques is fair but not as good as in the case of the PBLG solutions. It is difficult to assess the error limits on values of  $C_{\eta}^*$  since it is a derived quantity; however, it appears that the differences are great enough to be significant.

In conclusion, it appears that a fairly strong case can be made for the assertion that the various limiting values, osc.  $\eta'_{\omega \rightarrow 0}$ , E.R.D.  $\eta'_{\omega \rightarrow 0}$ , and  $\eta_{\dot{\gamma} \rightarrow 0}$  are identical for the low-concentration isotropic solutions but diverge as  $C_{\eta}^*$  is approached and in the high-concentration liquid-crystalline solutions in the case of PCBZL, and possibly also in the case of PBLG.

Dynamic modulus. The results of measurements of dynamic modulus  $G'$  on PBLG solutions via oscillatory shear are shown in Figures 116 and 117. All solutions below 14.1% behave in a very similar manner;  $\log G'$  increasing linearly with  $\log \omega$  with a slope of 1.5-1.6, and curving below this line at high  $\omega$ . The departure from linearity occurs at decreasing values of  $G'$  and  $\omega$  as concentration is increased; 480 dyne/cm<sup>2</sup> at 65 rad/sec for 6.1%, 380 dyne/cm<sup>2</sup> at 33 rad/sec for 7.5%, 210 dyne/cm<sup>2</sup> at 14 rad/sec for 9.8%, 135 dyne/cm<sup>2</sup> at 8.0 rad/sec for 11.5%. The change in behavior between the 11.5% and 14.0% solutions is very striking (recall that 14.0% was the lowest concentration which exhibited the negative normal stress effect). Solutions of concentration 14.1% and greater were linear throughout the frequency range with slopes of 1.6 (with the exception of 20.6% at low frequencies). E.R.D.

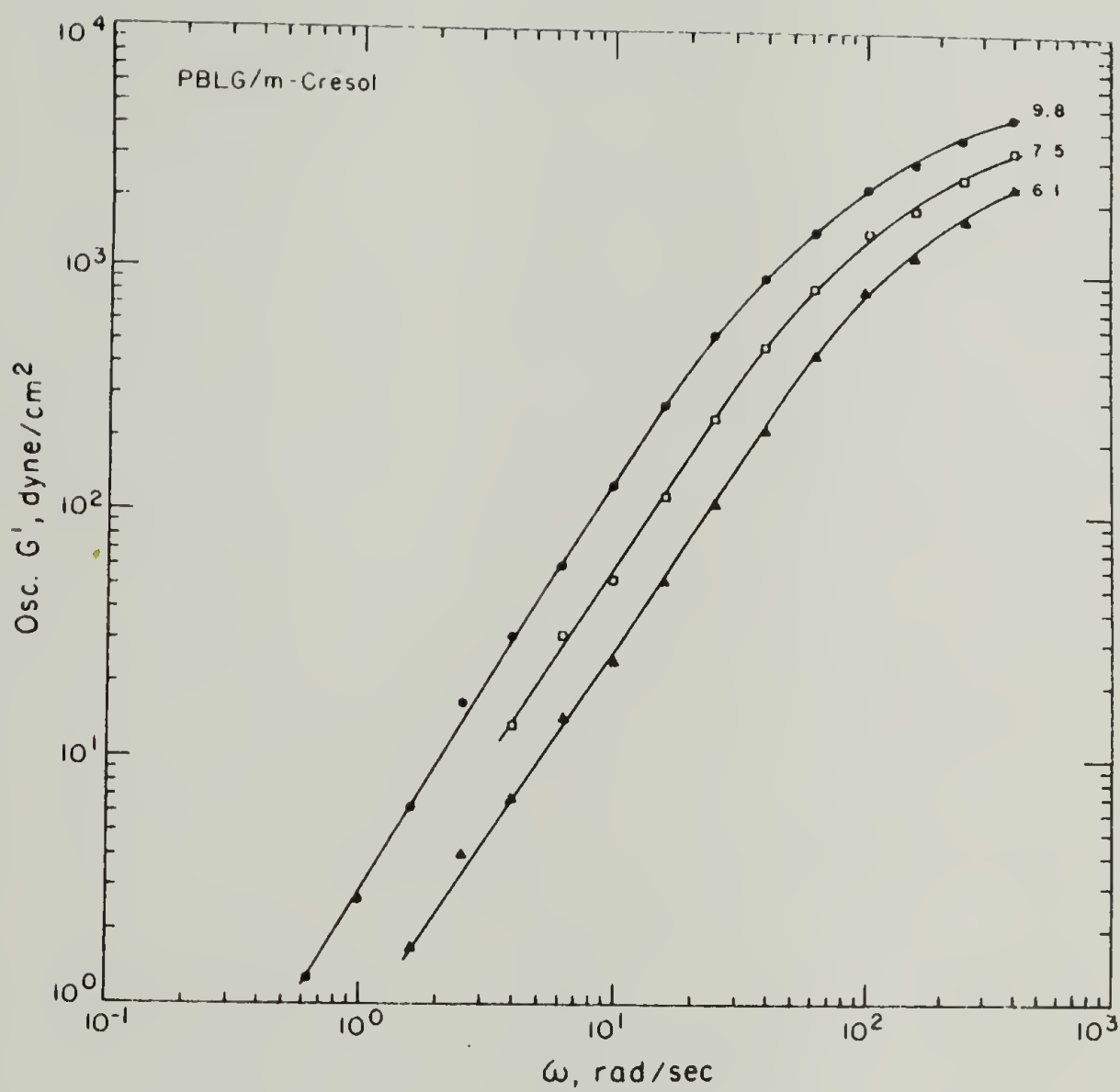


Figure 116. Dynamic Storage Modulus vs. Frequency (Oscillatory Shear) for 150,000 M.W. PBLG Solutions.

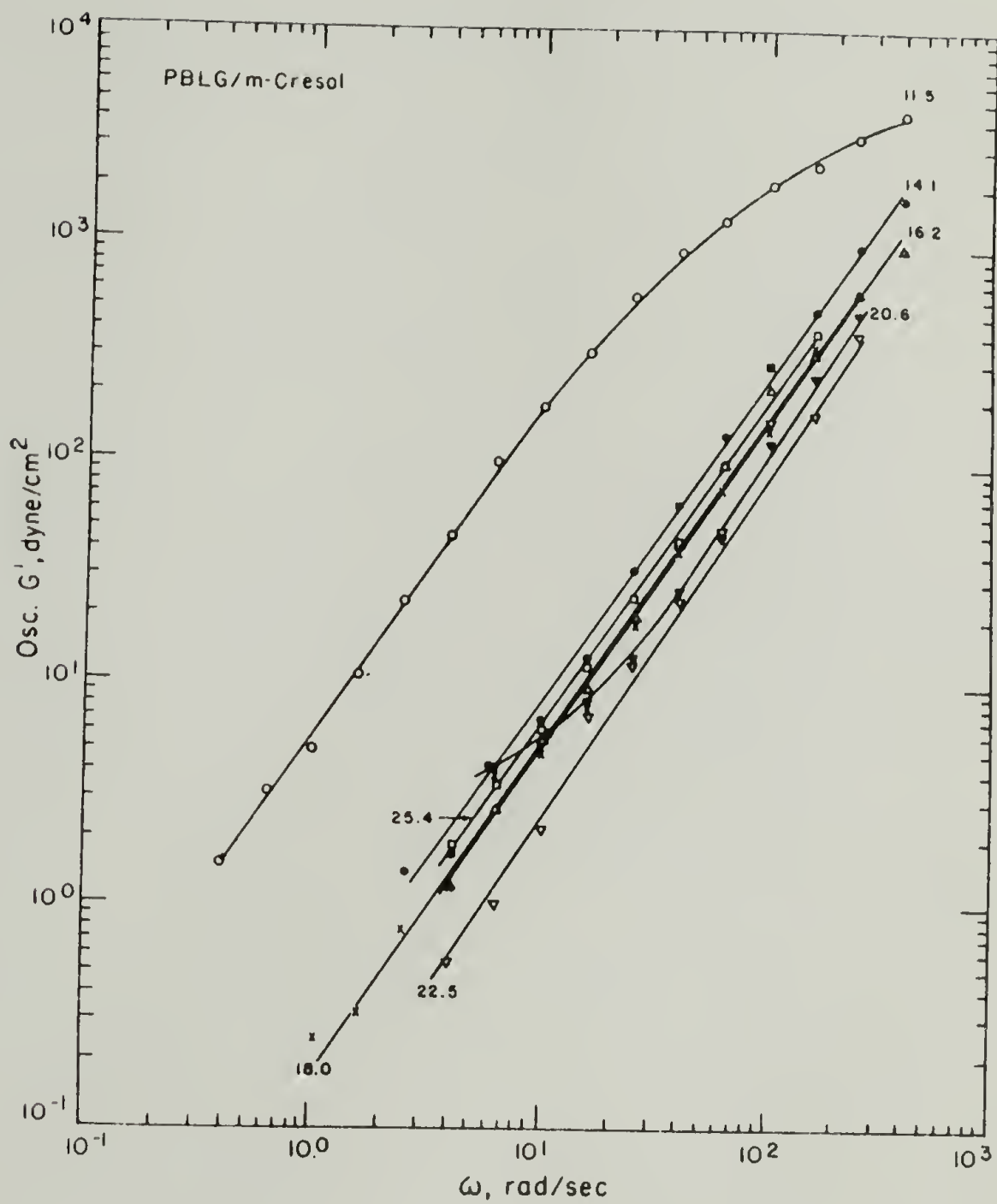


Figure 117. Dynamic Storage Modulus vs. Frequency (Oscillatory Shear) for 150,000 M.W. PBLG Solutions.

measurements of  $G'$  for these solutions are shown in Figure 118 for comparison. Due to the extremely limited frequency range accessible and the large uncertainty associated with the measurement of very low forces, we hesitate to draw any conclusions from these curves.

Values of  $G'$  at a frequency of 16 rad/sec (arbitrarily chosen in the accessible frequency range for most solutions) as measured by E.R.D. and oscillatory shear are plotted against concentration in Figure 119. Surprisingly, the agreement is quite good. The values of  $C_G^*$  are in close agreement and are also very close to values of  $C_\eta^*$  (see Table 5).

Results of oscillatory measurements of  $G'$  for PCBZL solutions are given in Figures 120 and 121. As with the lower concentration PBLG solutions, solutions below 24.1% exhibit linear  $\log G'$  vs.  $\log \omega$  with a slope of 1.5 and departure from linearity at high frequency. In this case, although the departure from linearity occurs at decreasing frequency as concentration increases, the values of  $G'$  are independent of concentration; 640 dyne/cm<sup>2</sup> at 100 rad/sec for 13.9%, 640 dyne/cm<sup>2</sup> at 75 rad/sec for 17.3%, 680 dyne/cm<sup>2</sup> at 24 rad/sec for 20.6%, 700 dyne/cm<sup>2</sup> at 17 rad/sec for 22.5%. The behavior of the solutions of concentration 24.1% and greater is more complex with several inflection points, perhaps corresponding to the plateaus in dynamic viscosity. As with the plateaus in osc.  $\eta'$  (see Figure 113), the inflection points become less distinct and occur at higher frequency in the 31.0% solution than the 33.4% solution. It is hard to perceive any trends in the behavior of the 27.6, 25.3 and 24.1% solutions.

E.R.D. measurements of  $G'$  for PCBZL solutions are shown in

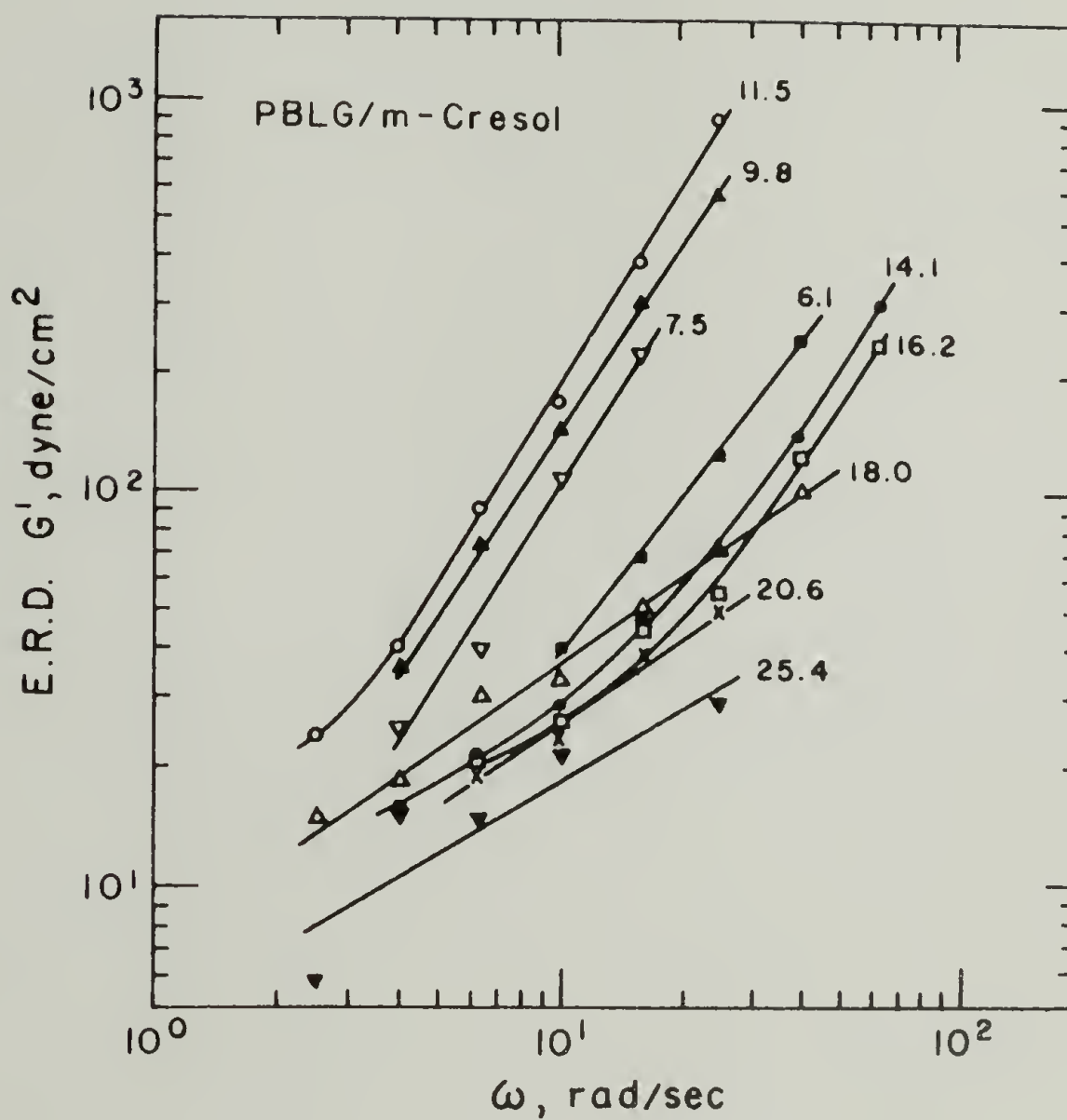


Figure 118. Dynamic Storage Modulus vs. Frequency (Eccentric Rotating Disc) for 150,000 M.W. PBLG Solutions.

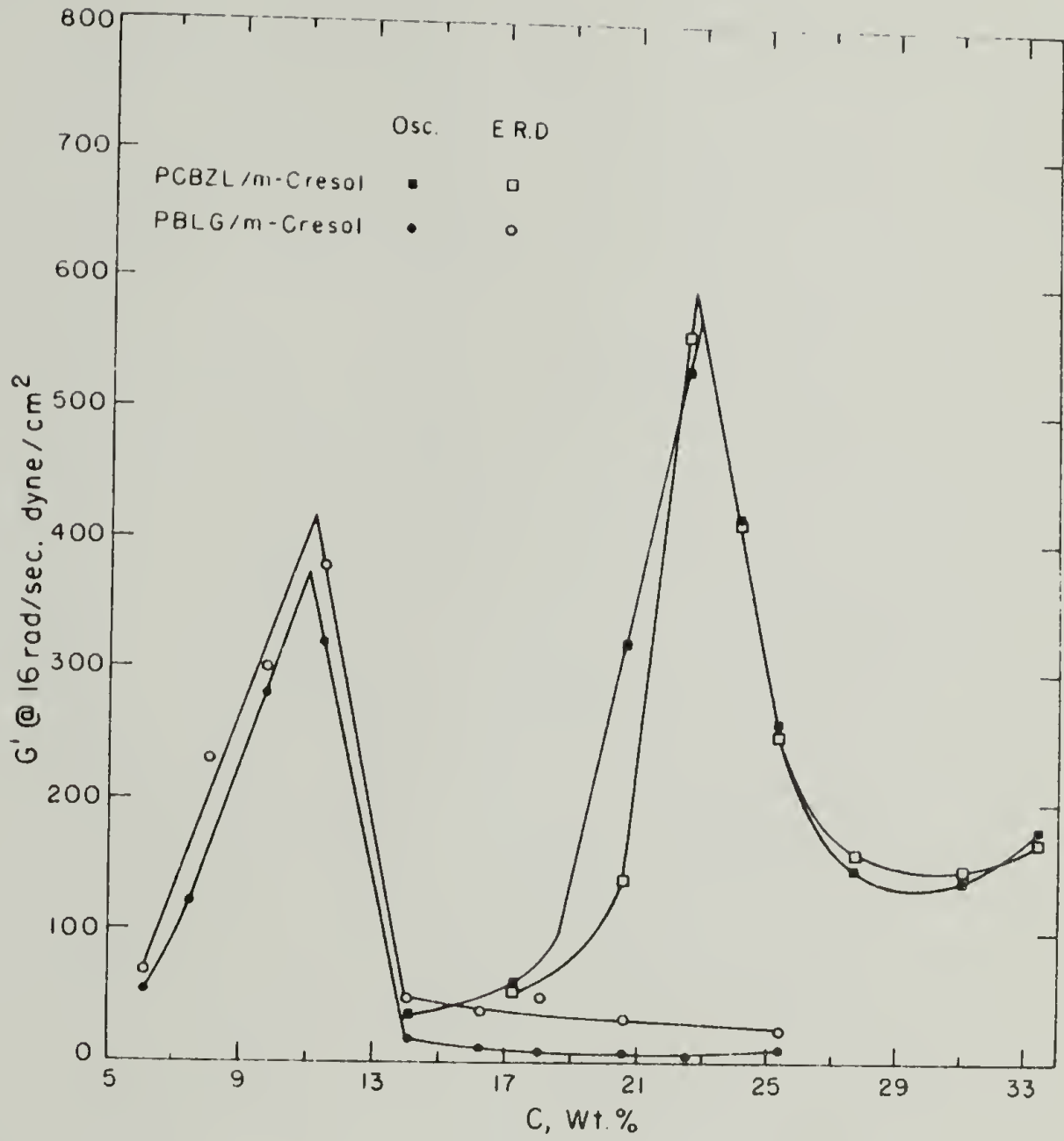


Figure 119. Dynamic Storage Modulus at 16 rad/sec vs. Concentration for 150,000 PBLG and 200,000 M.W. PCBZL Solutions.

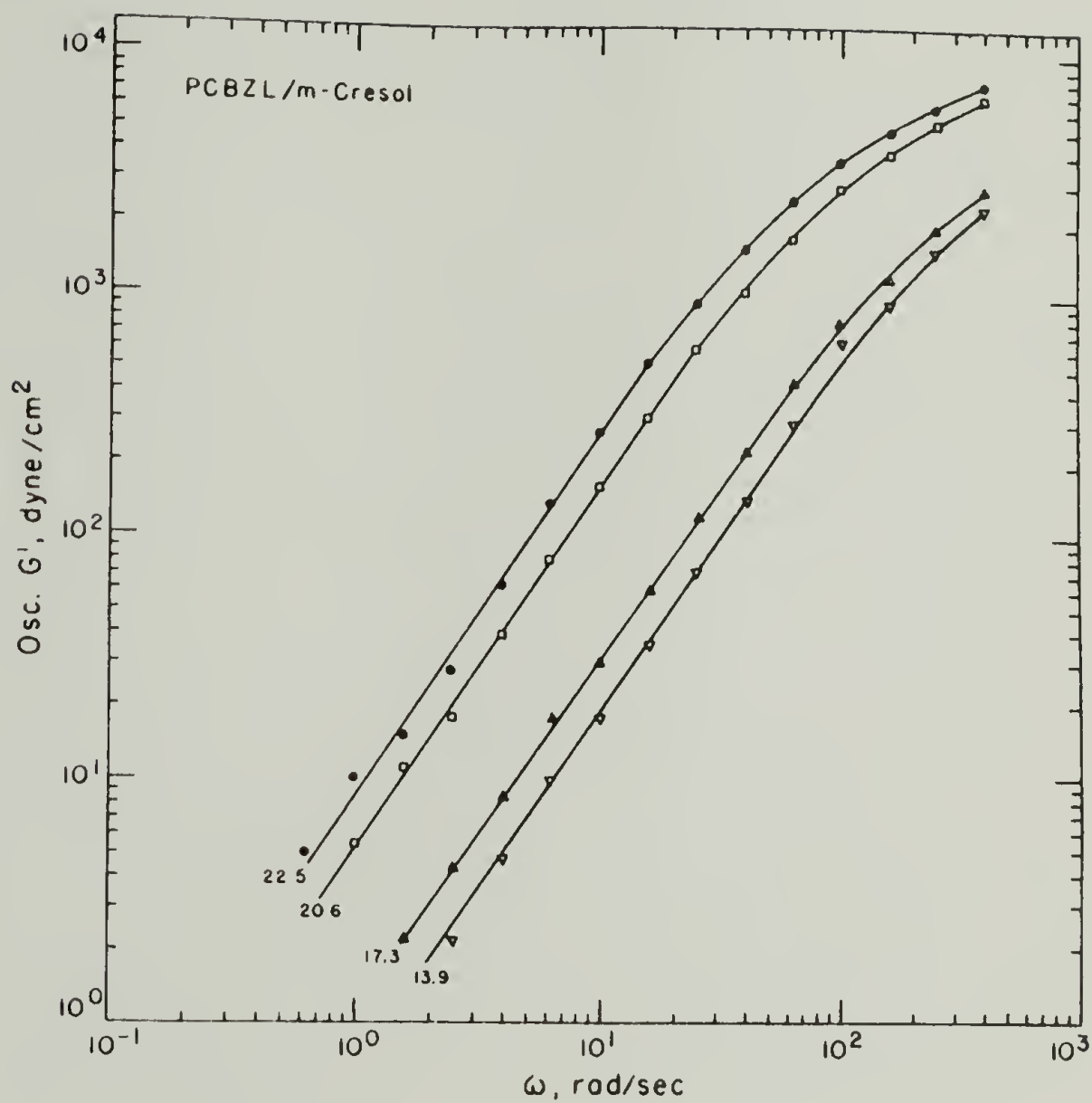


Figure 120. Dynamic Storage Modulus vs. Frequency (Oscillatory Shear) for 200,000 M.W. PCBZL Solutions.



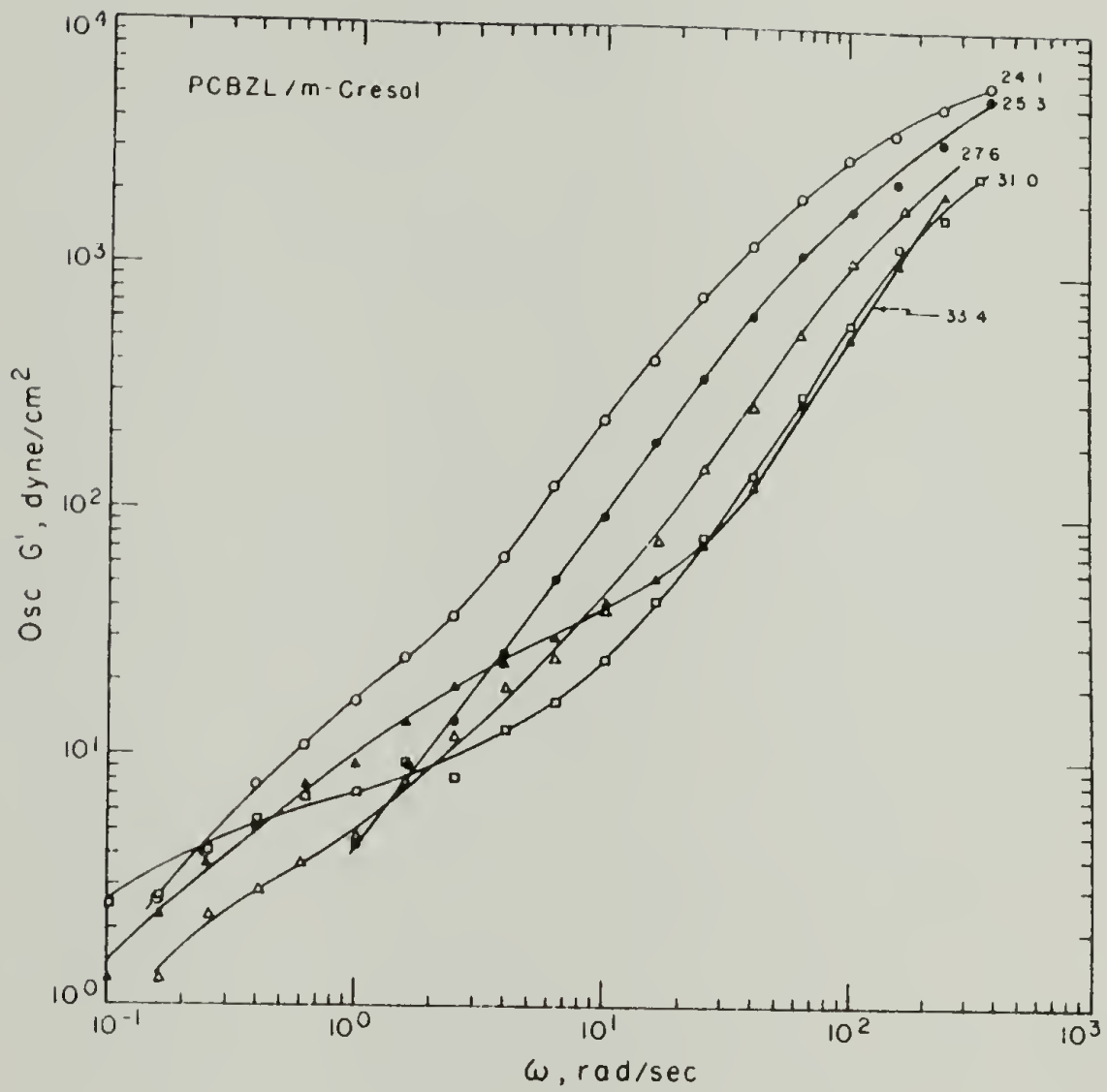


Figure 121. Dynamic Storage Modulus vs. Frequency (Oscillatory Shear) for 200,000 M.W. PCBZL Solutions.

Figure 122. Again, due to limited frequency range and large experimental error, no new information can be extracted from these curves. However, they do confirm the occurrence of inflection points in some of the higher concentration solutions.

Values of  $G'$  at the arbitrarily chosen frequency of 16 rad/sec are plotted against concentration in Figure 119. The quantitative agreement between osc.  $G'$  and E.R.D.  $G'$  is very good at most concentrations, better than the agreement between osc.  $\eta'_{\omega \rightarrow 0}$  and E.R.D.  $\eta'_{\omega \rightarrow 0}$ . Values of  $C_G^*$  also agree well with each other and with  $C_\eta^*$  as measured by E.R.D. (which is the lowest of the three  $C_\eta^*$  values for PCBZL).

### Discussion

Clearly, both PBLG and PCBZL form liquid-crystalline solutions when dissolved in *m*-cresol at sufficiently high concentration. Both polymers exhibited a bewildering variety of rheological phenomena, but showed similar behavior in two respects, one being a maximum in various rheological material functions at a critical concentration, and the other being the negative normal stress phenomenon in liquid crystalline solutions. Table 5 summarizes the various values of critical concentrations given by the different solution properties. It is apparent that the critical concentration for the formation of the anisotropic phase is much higher for the PCBZL, this despite the higher molecular weight and hence higher axial ratio for PCBZL than PBLG (axial ratios calculated on the basis of literature values for the diameter of the equivalent hydrodynamic cylinder in DMF of 15.0 Å<sup>o</sup>

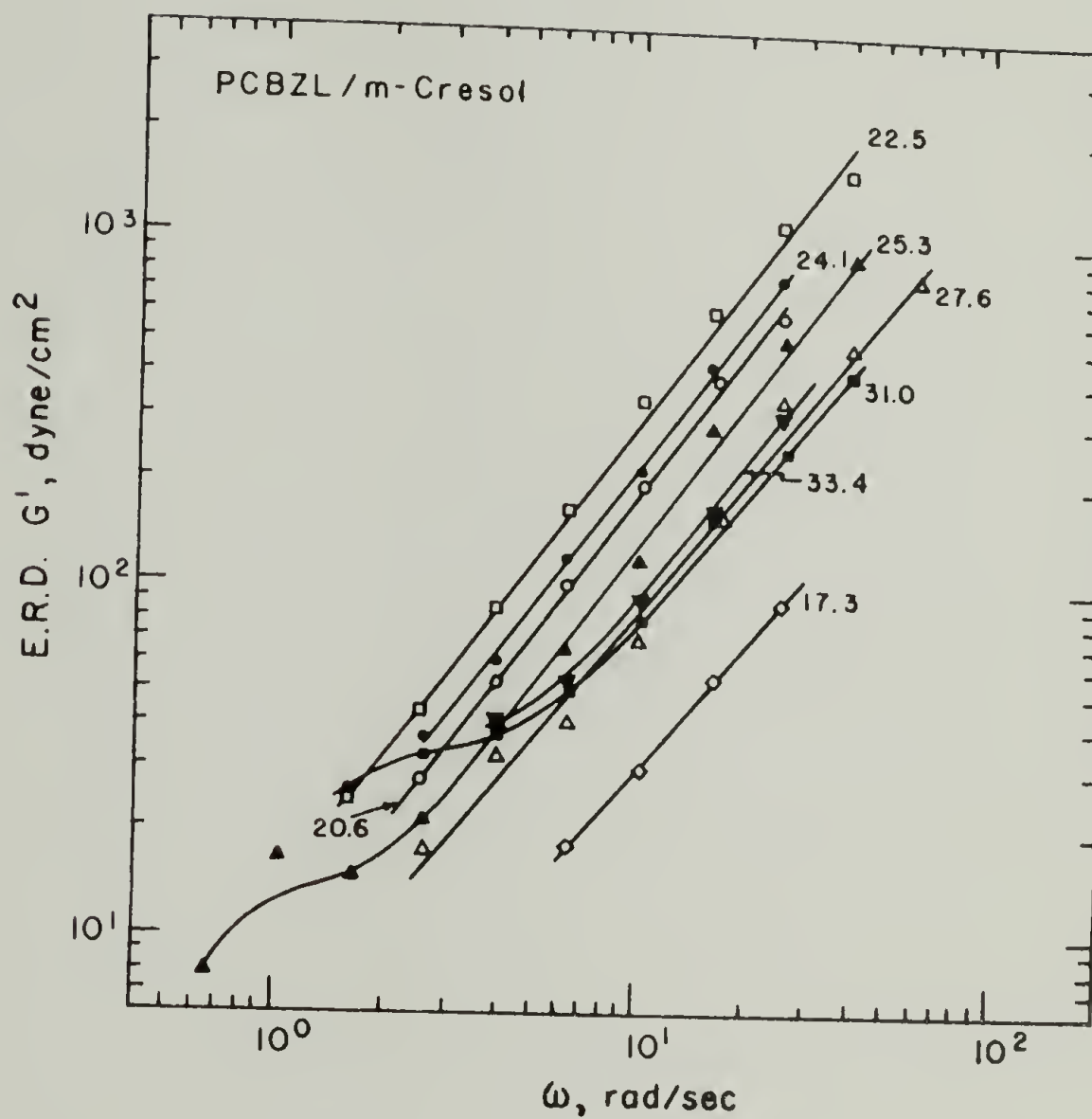


Figure 122. Dynamic Storage Modulus vs. Frequency (Eccentric Rotating Disc) for 200,000 M.W. PCBZL Solutions.

for PBLG (206) and  $17.2 \text{ \AA}$  for PCBZL (207) and length of  $1.5 \text{ \AA}$  per residue characteristic of the  $\alpha$ -helix (215) were 68.5 and 85, respectively).

This apparent paradox is resolved immediately upon consideration of the effect of helix flexibility, which would be to delay the liquid crystal transition to a higher concentration (208).

The postulate that PCBZL helices are less rigid than PBLG helices is amply supported. Using the composition of solvent ( $\text{CHCl}_3$ -dichloroacetic acid) at which the helix-coil transition occurred as a criterion of helix stability (and hence of helix flexibility (207, p. 189)), revealed that PBLG helices are more rigid than PCBZL helices (209). End-to-end distances of a variety of PCBZL samples as measured by light scattering and flow birefringence in DMF were consistent with a worm-like chain with a persistence length of  $262 \text{ \AA}$  (210). The Kuhn statistical segment length  $A$  (which is twice the persistence length (211)) for PCBZL in DMF ranged from  $146 \text{ \AA}$  at a molecular weight of 100,000 to  $438 \text{ \AA}$  at a molecular weight of 550,000 (207). This suggests that the fraction of helix imperfections decreases with molecular weight. However,  $A$  increases with molecular weight to a power less than unity, hence the number of statistical segments per molecule increases slowly with molecular weight, leading to an overall increase in flexibility. The length of the Kuhn statistical segment for PBLG over a range of molecular weight of 33,000 to 330,000 has been given as  $2400 \text{ \AA}$  (211). The molecular weight exponent in the Mark-Houwink equation is expected to approach 1.7 for rod-like solutes (212), and has been reported as 1.7 for PBLG in DMF and *m*-cresol (206)

or 1.54 in DMF (213). The value for PCBZL has been reported as 1.26 in DMF (207), 1.08 in m-cresol at 35°C and .74 in m-cresol at 15°C (214). As evidenced by the temperature dependence of the intrinsic viscosity behavior, the system PCBZL/m-cresol has the peculiarity of exhibiting an inverse coil-helix transition in the range of 22-30°C. Even at temperatures well past the coil-helix transition, the Moffitt parameter  $b_0$  is not as high as that obtained in other helix-forming solvents, indicating incomplete helix formation (214). At room temperatures the authors considered PCBZL to be completely in the random conformation. Bearing in mind that intrinsic viscosity and optical rotation measurements are performed on dilute solutions, the detection of the lyotropic liquid-crystal transition by rheological methods described herein represents crude empirical evidence that the coil-helix transition is shifted to lower temperatures at high concentrations of PCBZL in m-cresol.

In any case, it appears that not only is the PCBZL helix intrinsically less rigid than that of PBLG, but that in m-cresol at room temperature the helix is probably interrupted at intervals, leading to even higher flexibility. This is completely consistent with our observation that liquid crystalline behavior is achieved in PCBZL at a higher concentration than that expected on the basis of molecular weight.

By far the most unusual result of this investigation is the confirmation of the report in Chapter II of the observation of negative values of the first normal stress difference, under well-defined and reproducible circumstances. It has been observed to date in three

systems; two molecular weights of PBLG and one of PCBZL, all dissolved in m-cresol. Since all of the systems studied were helical polypeptides dissolved in m-cresol, it is impossible to assess the generality of this phenomenon. Nevertheless, within their narrow category, these two polymers represent extremes of flexibility. PBLG has the highest value of  $A$  known, exceeding those of poly(p-benzamide) and poly(p-phenylene terephthalamide) (211), whereas not only is the PCBZL helix intrinsically less rigid, but in m-cresol at room temperature the PCBZL helix is probably not even perfect. Hence, it would appear that if volume-filling considerations are the only relevant factors, the degree of rigidity required is not particularly stringent and the phenomenon should be quite general. On the other hand, if specific solute-solvent interactions or specific inter-molecular interactions are involved, there is as yet insufficient data for speculations concerning generality.

It would be difficult to be more skeptical of this strikingly anomalous phenomenon than we ourselves. In attempting to uncover experimental artifacts, we have considered four possible sources: inertial effects, secondary flow phenomena, surface tension effects, and the possibility of surface orientation or adsorption. The techniques we have employed have been: calculation of and numerical correction for inertia, experiments with a variety of edge conditions, and data collection utilizing five different cone-and-plate combinations. While there is undoubtedly some error accruing from these various sources, we believe that they are minor perturbations and far from sufficient to produce the phenomenon itself. If so, the question

arises, how has such a dramatic effect in a well-studied system escaped detection for so long? We believe the answer to rest with instrumentation. Accurate normal force measurements on solutions demands great stability and accuracy in the drive system, transducers, and electronics, as well as great precision in machining and alignment of cones and plates. The Rheometrics Mechanical Spectrometer has excelled in all respects. Perhaps the crucial item of instrumentation was a tunable active (zero-insertion loss) low pass filter (A.P. Circuit Corp., N.Y.) inserted between the signal-conditioning amplifiers and the chart recorder. This eliminated two problems which have doubtless frustrated previous investigators. The first is random high-frequency noise due to environmental vibrations which make it difficult to make normal force measurements at the high sensitivities required at low shear rates. The second is a periodic oscillation in normal force at a frequency equal to the rotation speed of the cone, due no doubt to minute errors in machining and alignment. This oscillation becomes quite large at the high rotation speeds necessary to achieve high shear rates and is further exacerbated when using very shallow cone angles to achieve extremely high shear rates. By tuning the cutoff frequency of the filter to achieve the proper balance between pen response and suppression of unwanted signals, we were able to extract the desired normal force measurement (essentially a D.C. voltage) over a wide range of shear rates. Purists will object to this extensive signal conditioning procedure, but the results speak for themselves.

The other extraordinary result of this investigation is the

difference in viscosity and normal stress behavior at high shear rates as concentration was varied. At shear rates on the order of  $10,000 \text{ sec}^{-1}$  the maximum in  $\eta$  vs.  $C$  is greatly or entirely suppressed (see Figures 87 and 88), whereas the maximum in  $N_1$  vs.  $C$  is still very much in evidence (see Figures 105 and 106). This result is completely independent of the negative normal stress effect and is not affected by whatever credibility, or lack of it, is accorded the latter phenomenon. The implications of both phenomena are the same; that normal stress effects in these solutions are profoundly influenced by the supra-molecular structure and that the effect of shear-induced orientation on the supermolecular structure is not equivalent to that of the organization resulting from the formation of liquid crystalline structure (which is the conclusion suggested by the viscosity measurements). An effort at modeling the structural changes giving rise to these phenomena will be presented in Chapter IV, which will also reveal the results of rheo-optical studies of these solutions.

A comparison of the results of dynamic measurements on the two systems reported herein shows less consistency of behavior than the steady shear measurements. In the case of PBLG/m-cresol, a dramatic difference in dynamic behavior was observed between solutions which exhibited the negative normal stress effect and those that did not (Newtonian  $\eta'$  against non-Newtonian  $\eta'$ , linear  $\log G'$  vs.  $\log \omega$  against departures from linearity in  $\log G'$  vs.  $\log \omega$ ). In the case of PCBZL/m-cresol a difference in dynamic behavior was not observed between solutions that did or did not give negative  $N_1$ , but rather in solutions above and below  $C^*$  (plateaus in  $\log \eta'$  vs.  $\log \omega$  against



simple power-law shear thinning behavior, inflection points in  $\log G'$  vs.  $\log \omega$  against simple linear dependence followed by departure from linearity at high  $\omega$ ). Thus not only was the point in the concentration sequence at which a recognizable change in dynamic behavior occurred different between the two systems, but the nature of the change also differed. This further increases the difficulty of creating a model of the structural changes occurring in these solutions which is capable of predicting the wide variety of observed phenomena.

This work represents a classic example of how our understanding of a relatively well-studied problem can be overturned by the application of new techniques made possible by improvements in instrumentation. The results presented here confirm our feeling that flow of lyotropic solutions of rod-like helical molecules is a process of astonishing complexity. We have raised many questions and attempt to answer a few of them in Chapter IV, but we recognize that we are very far from unravelling the puzzle.

TABLE 5

VALUES OF CRITICAL CONCENTRATION FOR LIQUID CRYSTAL FORMATION  
(wt%)

Polymer	$C_{\eta}^*$			$C_{N1}^*$	$C_{G1}^*$		Disappearance of $-N_1$		$C^*$ biref	Flory Theory	
	Steady Shear	osc. Dynamic	E.R.D. Dynamic		osc.	E.R.D.	From $\sigma_{12}$ vs. C see Fig. 22	From $N_1$ vs. C see Fig. 23		vol. %	wt. %
PBLG	11.2	11.4	11.2	11.6	11.1	11.2	11.2	12.6	10.5	11.3	14.7
PCBZL	23.6	23.2	22.8	24.0	22.8	22.6	27.6	25.2	25.3	9.2	11.9

C H A P T E R   I V  
RHEO-OPTICAL STUDIES OF CONCENTRATED SOLUTIONS OF  
HELICAL POLYPEPTIDES

Introduction

In Chapters II and III we have reported the observation of many unusual rheological phenomena in concentrated solutions of poly- $\gamma$ -benzyl-glutamate (single enantiomers as well as racemic mixtures, PBLG and PBDG), poly- $\epsilon$ -carbobenzoxy-L-lysine (PCBZL), and poly- $\beta$ -benzyl-L-aspartate (PBA) in the helicogenic solvent, *m*-cresol. We observed that the transition from isotropic to liquid-crystalline state at a critical concentration  $C^*$  of the rod-like helical polypeptide solute is manifested dramatically in all of the rheological properties which were examined.

The observations reported in this chapter will consist of photographs taken during shear, after the cessation of shear, and of dried films made from solutions of PBLG in a volatile helicogenic solvent, 1,4-dioxane. In order to avoid unnecessary redundancy, background material which is available in Chapters II and III has been kept to a minimum and interested readers are referred thereto.

Experimental

An exploded schematic diagram of the shearing stage apparatus utilized in this study is shown in Figure 123. The apparatus consists

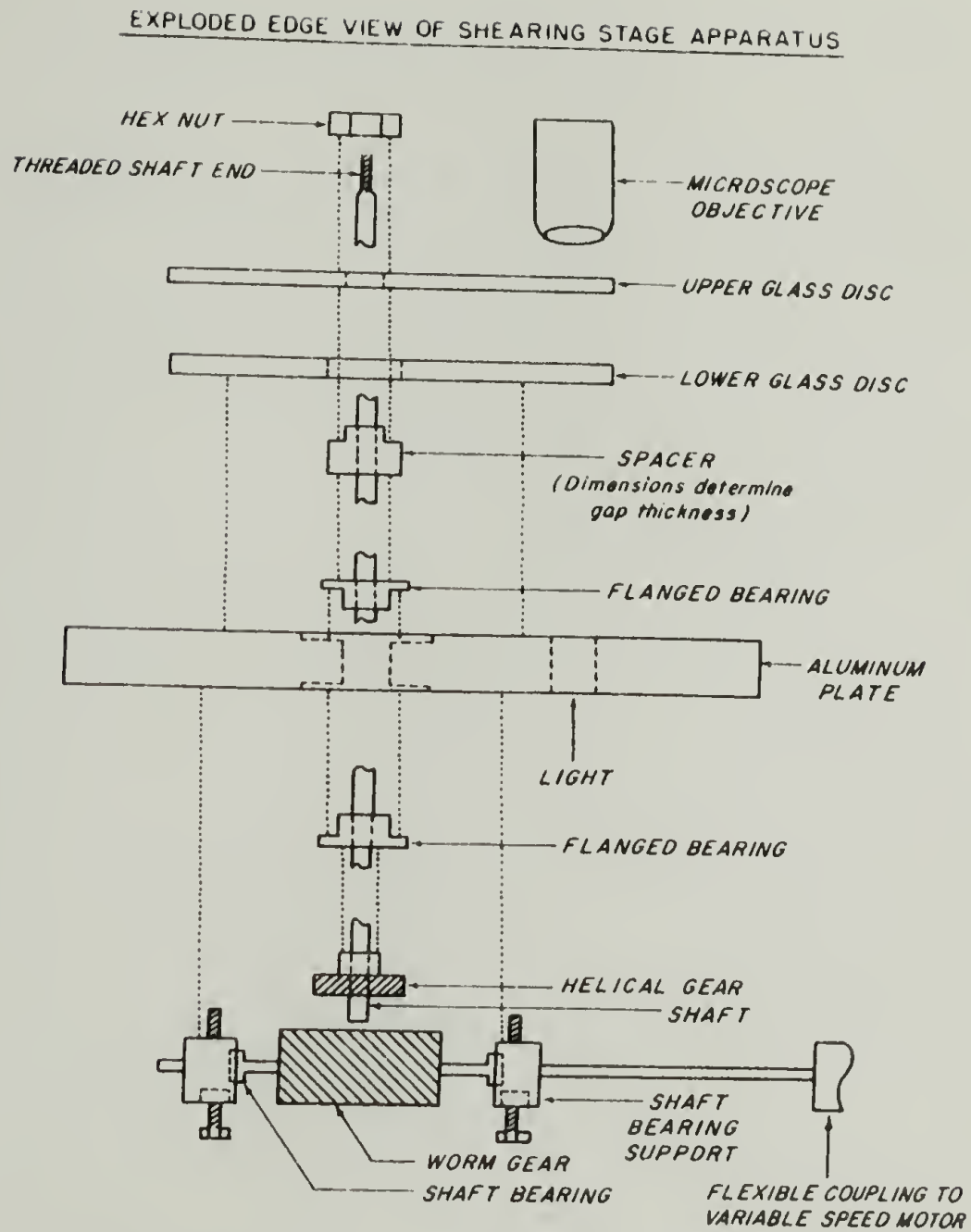


Figure 123. Exploded Schematic Diagram of Shearing Stage Apparatus.

simply of two glass discs, separated approx. .5 mm by a brass spacer, one fixed and one driven at any chosen speed, which can be inserted into a polarizing microscope. Since the field of view of the microscope objective is small compared to the distance from the observed spot to the axis of rotation, it can be assumed that the shear rate is constant throughout the field of view. The range of accessible shear rates is approximately  $.50\text{-}200 \text{ sec}^{-1}$ . It was found impossible to increase the shear rate further by reducing the spacing of the discs since lack of precision in machining caused slight non-parallelism of the discs which would have produced unacceptably large variations in shear rate in the course of each revolution. The accuracy of the shear rate values given in this chapter is approximately 30%.

Dried films were made from 1,4-dioxane solution by pressing a drop of solution between glass slides and pulling them apart lengthwise at various speeds for low and high shear. The films dried in approximately one minute.

The 350,000 M.W. PBLG used in this study was obtained from Biopolymer Corp. (Moreland Hills, Ohio) and the 150,000 M.W. PBLG was obtained from Sigma Chemical Co. (St. Louis, Mo.). Steady shear viscosity  $\eta$  and first normal stress difference  $N_1$  as a function of shear rate for a 17.0 wt% solution of the 350,000 M.W. PBLG in m-cresol are shown in Figure 124. Note in particular the occurrence of two sign changes in  $N_1$  at shear rates of 3.5 and  $80 \text{ sec}^{-1}$ ; this region of negative  $N_1$  is a feature which we have observed in other liquid crystalline polypeptide solutions but which has not appeared previously in the rheological literature.

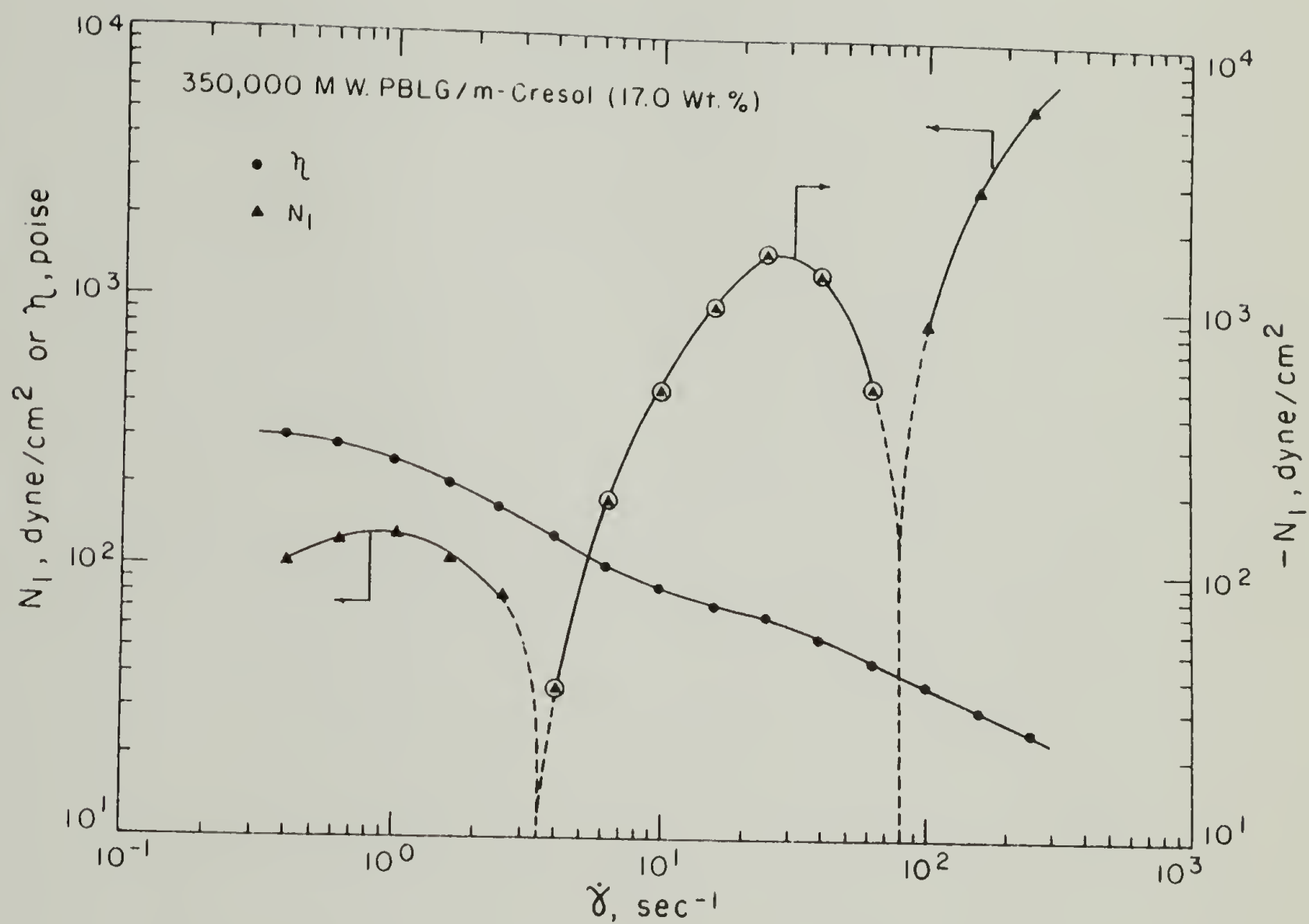
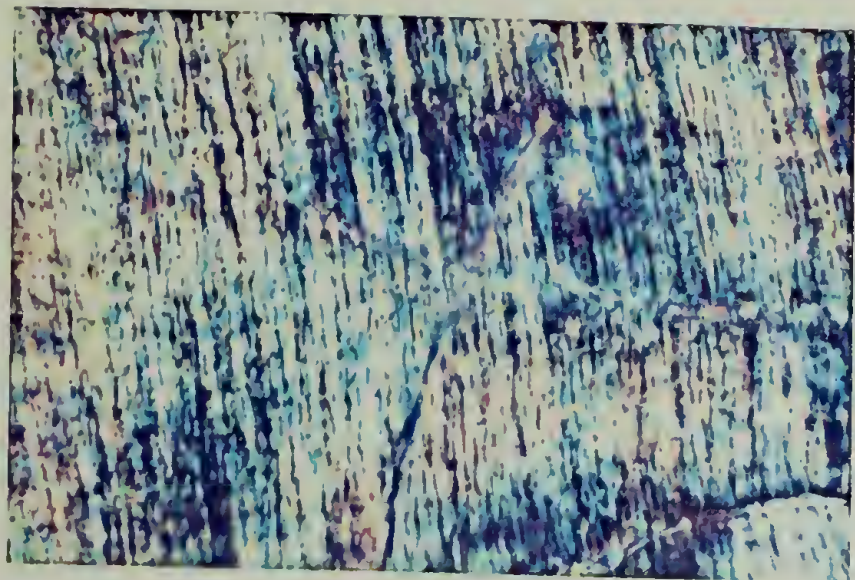


Figure 124. Steady Shear Viscosity and First Normal Stress Difference versus Shear Rate for 17.0% 350,000 PBLG.

## Results

During shear. Photomicrographs taken at a magnification of 170X between crossed polars with a flash lamp to freeze the structure at a variety of shear rates are shown in Figure 125. Some of the features which will be referred to in the description which follows may be obscure in black and white reproduction but were more clearly visible in the original Ektachrome slides due to the vivid birefringence colors. The direction of shearing is vertical in every case.

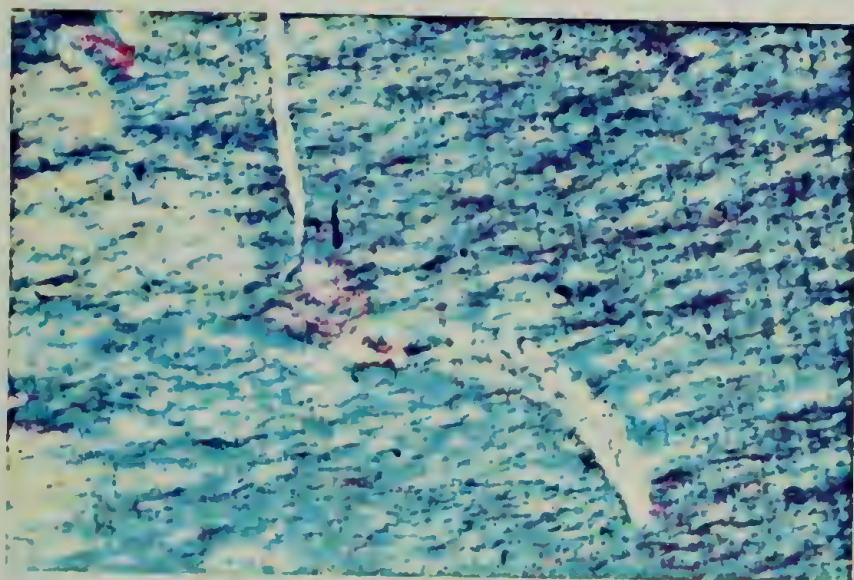
Figure 125a ( $1.1 \text{ s}^{-1}$ ) clearly shows streaks parallel to the shearing direction. In Figures 125b and 125c ( $3.3$  and  $5.5 \text{ s}^{-1}$ ) these streaks are disappearing and the beginnings of a structure exhibiting orientation perpendicular to the shearing direction is seen. In Figures 125d and 125e ( $16$  and  $19 \text{ s}^{-1}$ , resp.), the transverse striations are clearly visible and no streaks parallel to the shearing direction are in evidence. (We have nicknamed these transverse striations the "row-nucleated" texture, due to the similarity of appearance with structures formed during stress-induced crystallization of polyethylene (216, Figure 17). No assumptions about the origin of this texture are implied by this terminology.) In Figure 125f ( $25 \text{ s}^{-1}$ ), the row-nucleated texture is still clearly defined but in Figure 125g ( $40 \text{ s}^{-1}$ ) it is starting to fade. Note the air bubbles elongated in the direction of shear. In Figure 125h ( $70 \text{ s}^{-1}$ ) the transverse striations are just barely visible and finally in Figure 125i ( $100 \text{ s}^{-1}$ ) only a relatively featureless field remains, with what appears to be occasional disclinations scattered throughout. It is apparent that the correlation between the



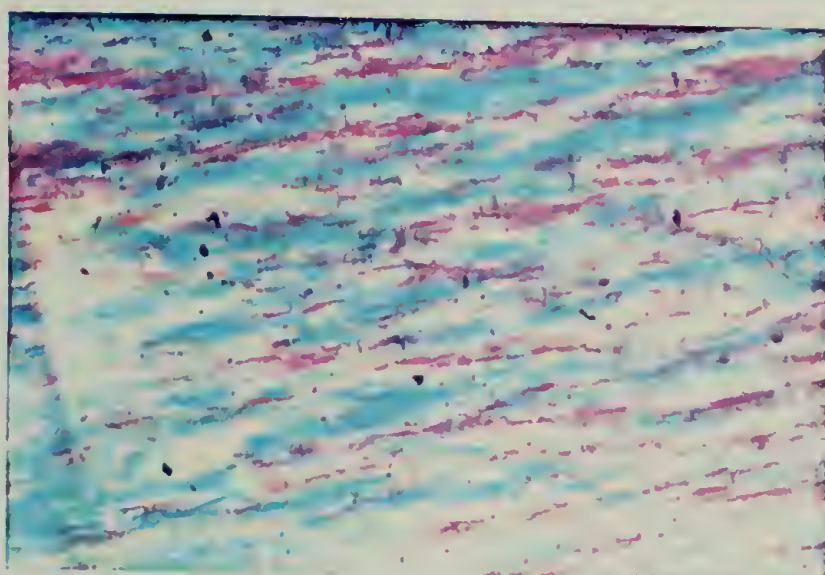
a



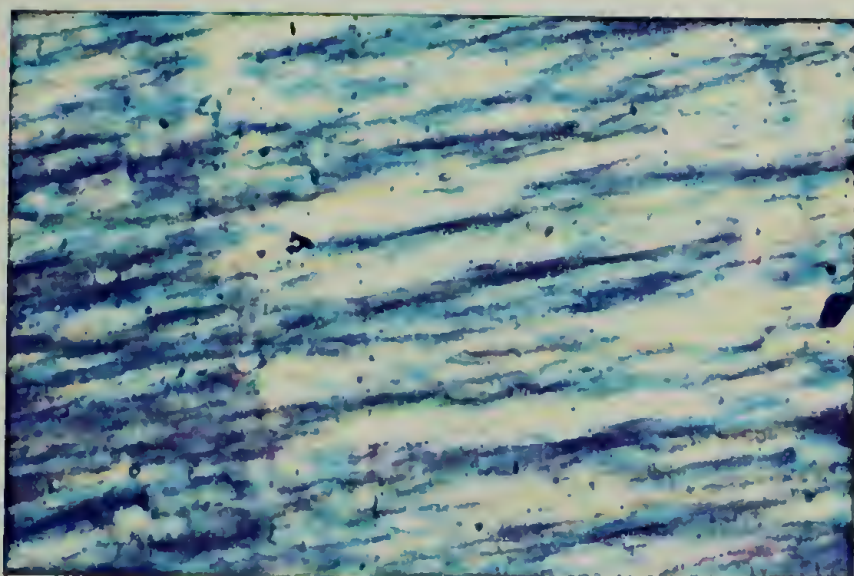
b



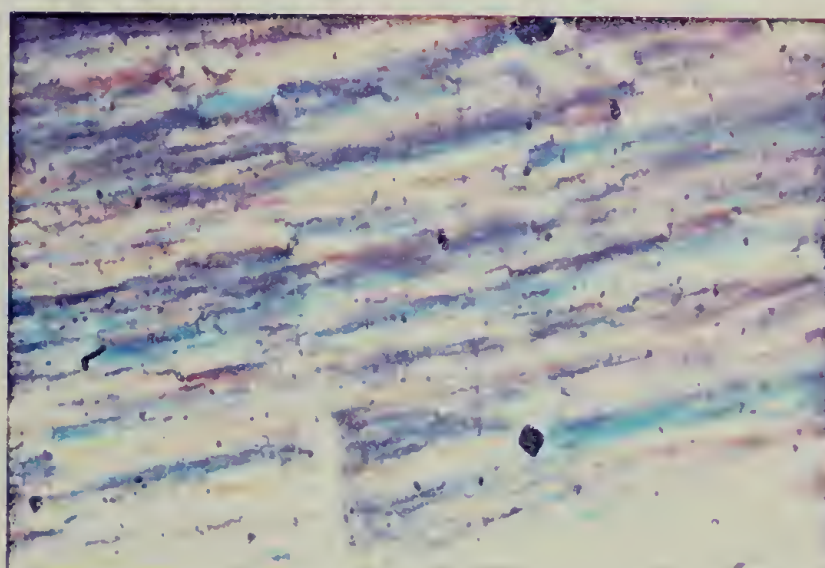
c



d



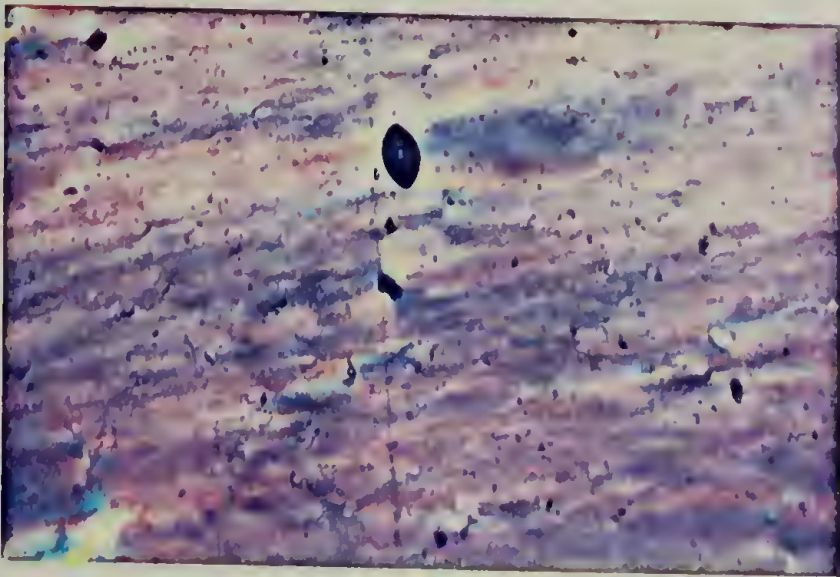
e



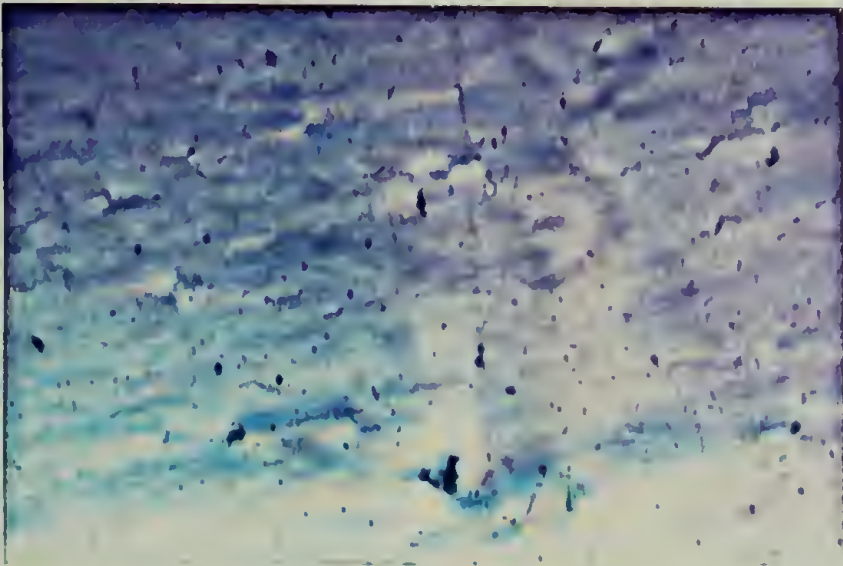
f

Figure 125. Polarized Light Micrographs of 17.0% 350,000 M.W. PBLG at Various Shear Rates 170X. (a)  $1.1 \text{ s}^{-1}$ . (b)  $3.3 \text{ s}^{-1}$ . (c)  $5.5 \text{ s}^{-1}$ . (d)  $16 \text{ s}^{-1}$ . (e)  $19 \text{ s}^{-1}$ . (f)  $25 \text{ s}^{-1}$ . (g)  $40 \text{ s}^{-1}$ . (h)  $70 \text{ s}^{-1}$ . (i)  $100 \text{ s}^{-1}$ .

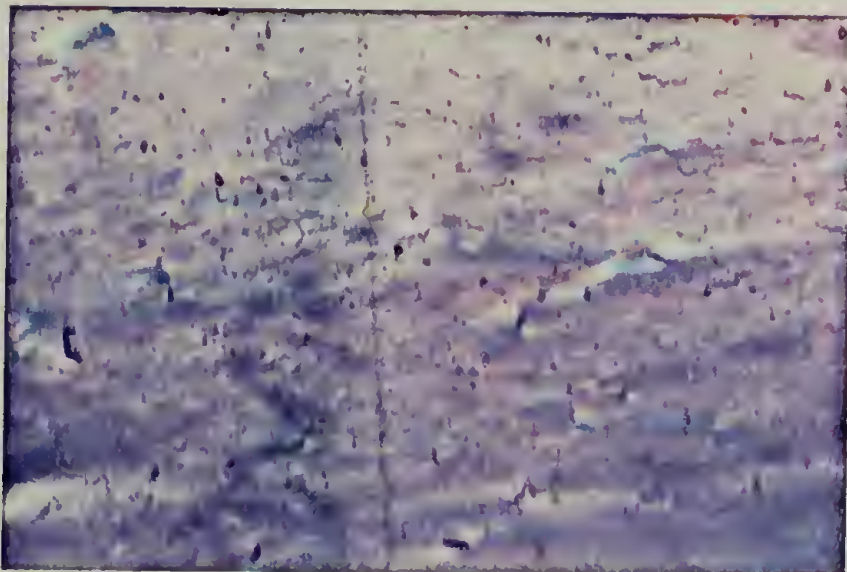




g



h



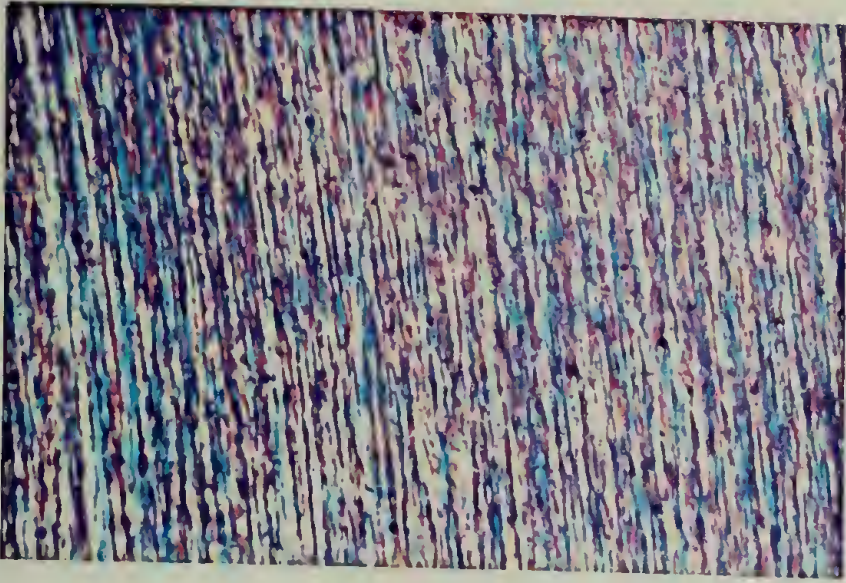
i

Figure 125. Continued.

appearance of the row-nucleated texture and a negative value of  $N_1$  is quite close.

After cessation of shear. Photographs taken after the cessation of shear for a 14.1 wt% solution of the 150,000 M.W. PBLG are shown in Figures 126-128. (This solution did not exhibit negative  $N_1$  at shear rates within the range of the shearing stage and the row-nucleated texture did not appear in photographs taken during shear.) In Figure 126a, taken immediately after the cessation of shear at  $3.3 \text{ s}^{-1}$ , long thin streaks, oriented parallel to shear and speckled in appearance, are visible. In Figures 126b and 126c (.3 min and 1 min after cessation) the appearance is only slightly changed with slight coarsening of the speckling and thickening of the streaks. In Figure 126d (2 min) the coarsening is more visible and the first hint of horizontal organization appears. Finally, in Figure 126e (5 min), the coarsening is very pronounced so that the streaks have become lines of ellipsoidal regions. Ellipsoidal regions of the same color have come roughly into horizontal register so that a coarse, irregular variation of the row-nucleated texture results.

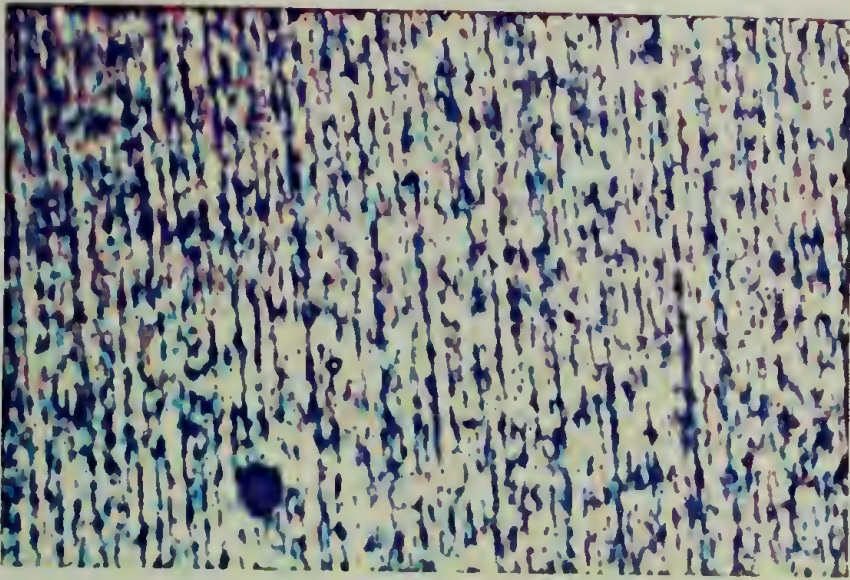
Photographs taken after cessation of shear of  $19 \text{ s}^{-1}$  are shown in Figure 127. Figure 127a (immediately after cessation) once again shows speckled streaks parallel to the shearing direction. Figure 127b (.1 min) still shows the parallel streaks but superimposed is the beginnings of transverse striations. In Figure 127c (.3 min) the row-nucleated texture superimposed on the streaks is well developed, with greater overall perfection and finer scale than the texture which



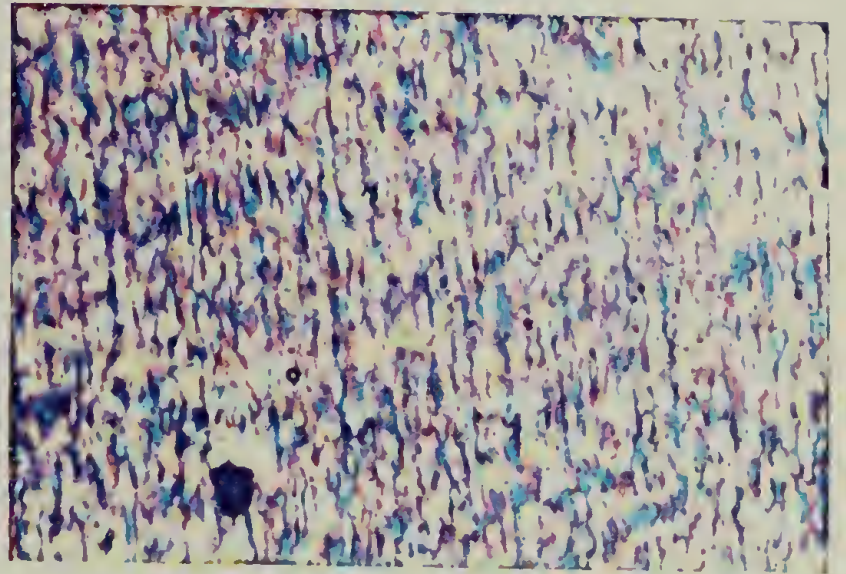
a



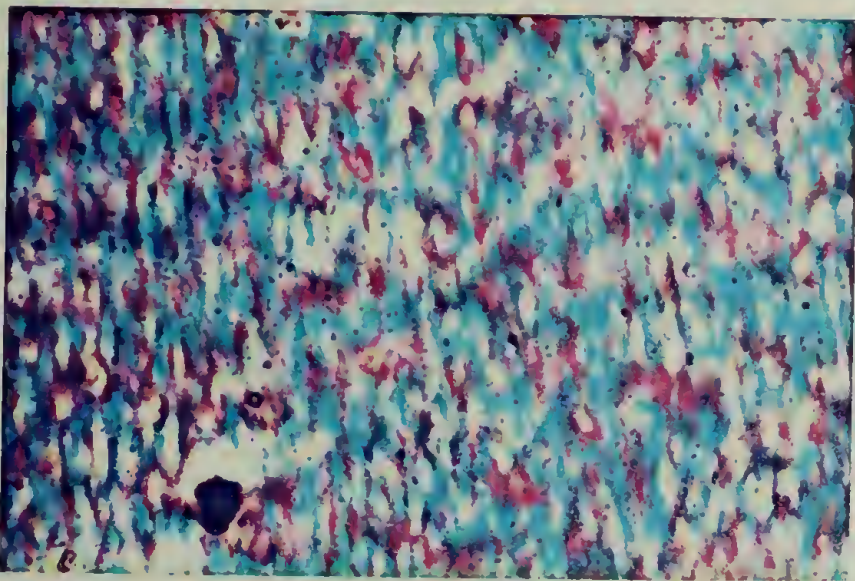
b



c

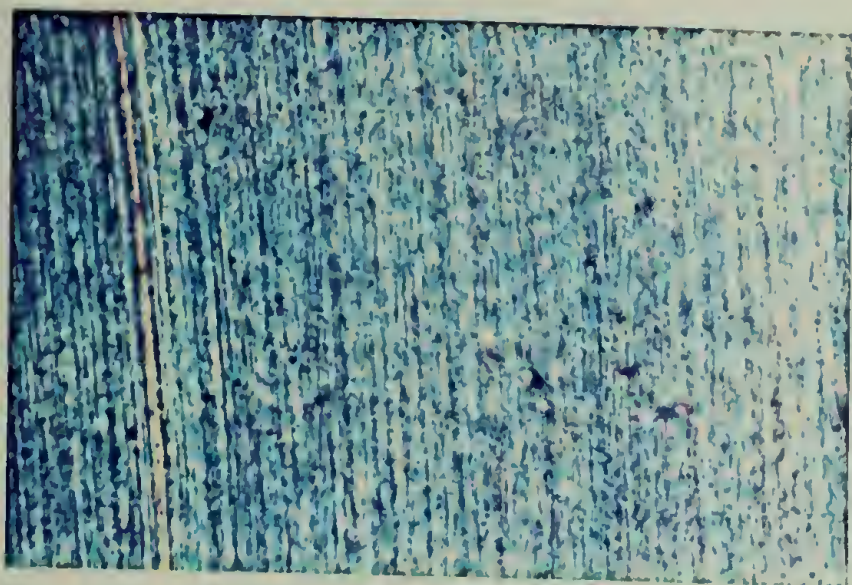


d

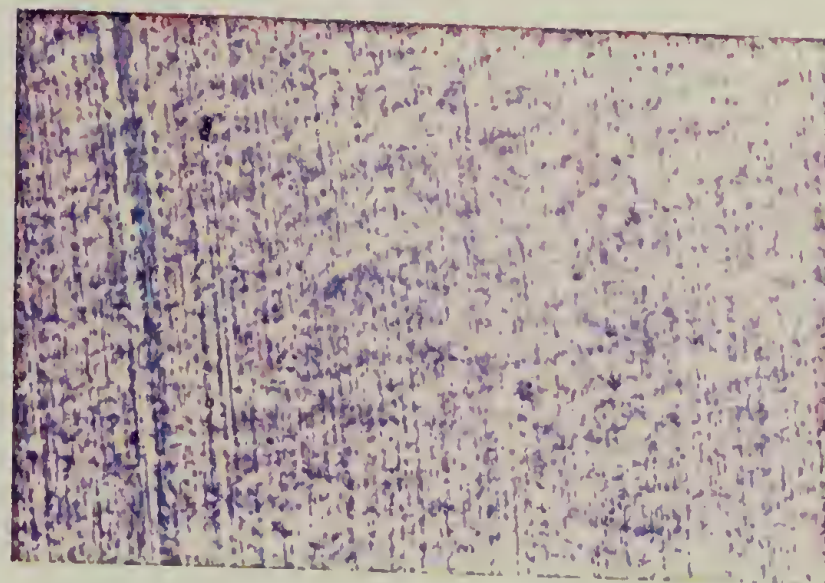


e

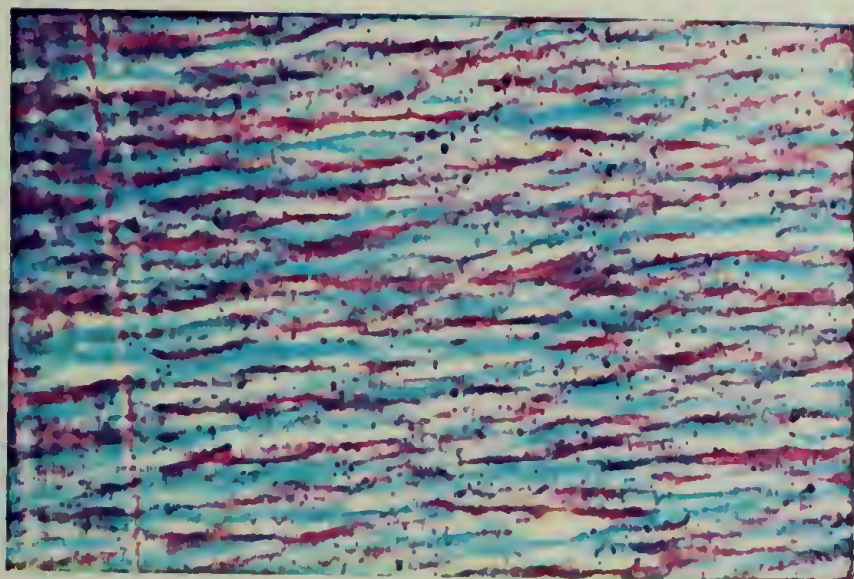
Figure 126. Polarized Light Micrographs of 14.1% 150,000 M.W. PBLG at Various Times after Shearing at  $3.3 \text{ s}^{-1}$  170X.  
(a) Immediately. (b) .1 min (c) .3 min (d) 1 min  
(e) 5 min



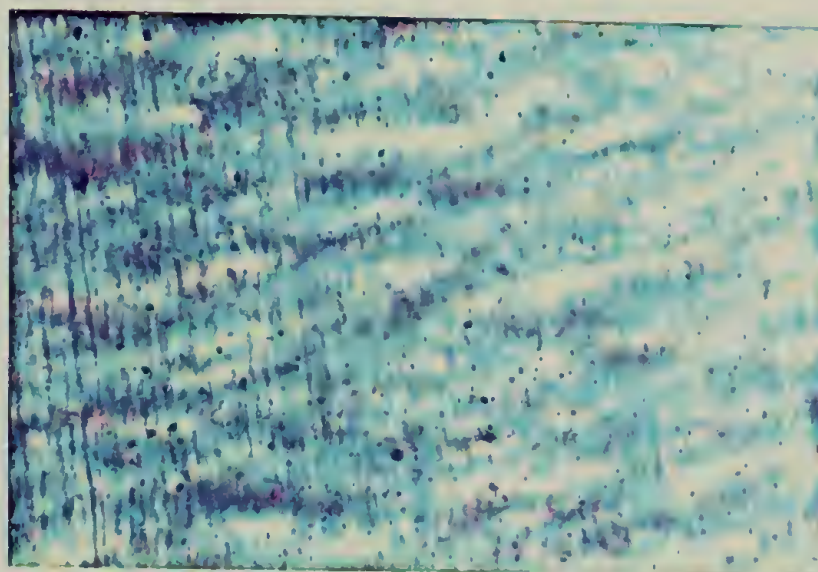
a



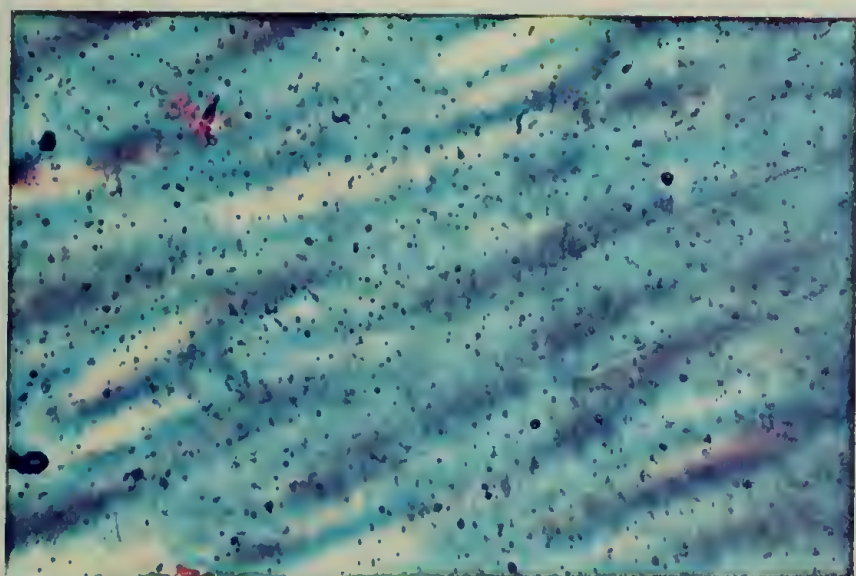
b



c



d



e

Figure 127. Polarized Light Micrographs of 14.1% 150,000 M.W. PBLG at Various Times after Shearing at  $19 \text{ s}^{-1}$  170X.  
(a) Immediately. (b) .1 min (c) .3 min (d) 1 min  
(e) 5 min

developed after 5 minutes after shear at  $3.3 \text{ s}^{-1}$  (Figure 126e). In Figure 127d (1 min) the row-nucleated texture is already beginning to fade, with coarsening and loss of definition. After 5 minutes (Figure 127e), the row-nucleated texture has almost completely disappeared.

Photographs taken after the cessation of shear of  $100 \text{ sec}^{-1}$  are shown in Figure 128. Figure 128a (immediately after cessation) reveals only a uniform speckled appearance. After only .05 min, very fine and well-defined transverse striations have already formed (Figure 128b). At .1 min (Figure 128c), the striations are slightly more perfect than in the previous photograph, and neighboring striations are much better differentiated on the basis of color. By .3 min (Figure 128d), the row-nucleated texture is already thickening and losing definition. This process continues and after 2 min the striations are quite thick, though reasonably well defined.

The behavior of this solution after the cessation of shear can be summarized as follows: with increasing rate of prior shear the row-nucleated texture forms more rapidly, with better definition and thinner striations, and also degenerates more quickly. It is significant that the solution shown in Figures 126-128 did not exhibit a negative value of  $N_1$  at the shear rates used, nor did they show the row-nucleated texture immediately upon cessation of shear. The horizontal striations were not present during shear, but formed after cessation. However, the propensity of the molecular organization to re-organize into the row-nucleated texture increased with shear rate, i.e., as the sign change in  $N_1$  was approached. One final observation linking the negative normal stress and the row-nucleated structure: in those solutions which



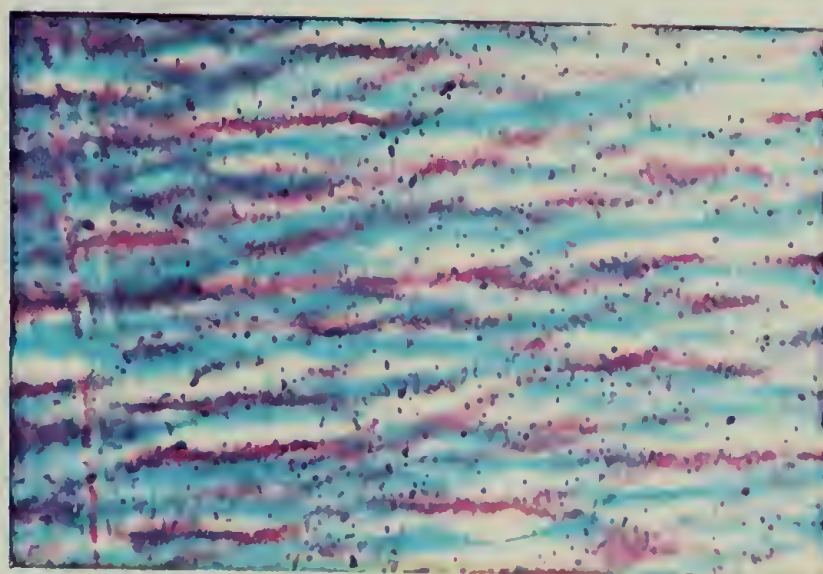
a



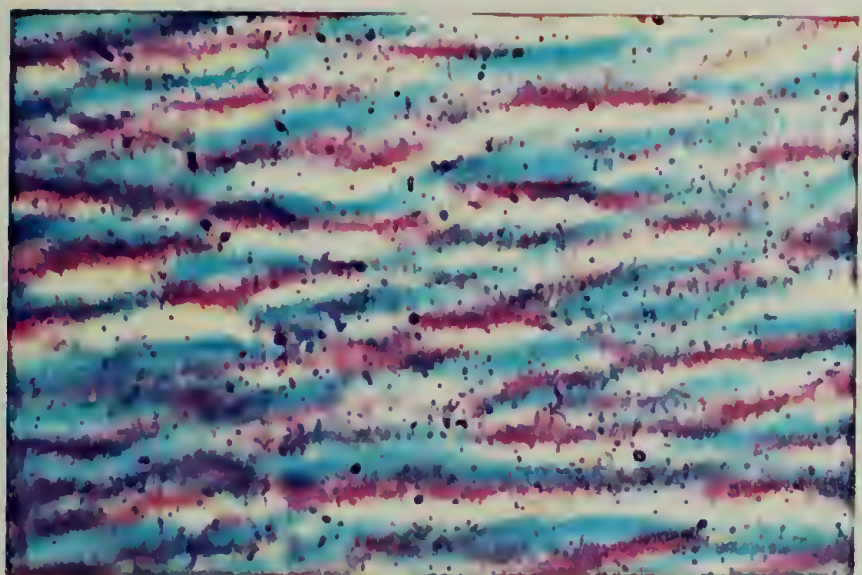
b



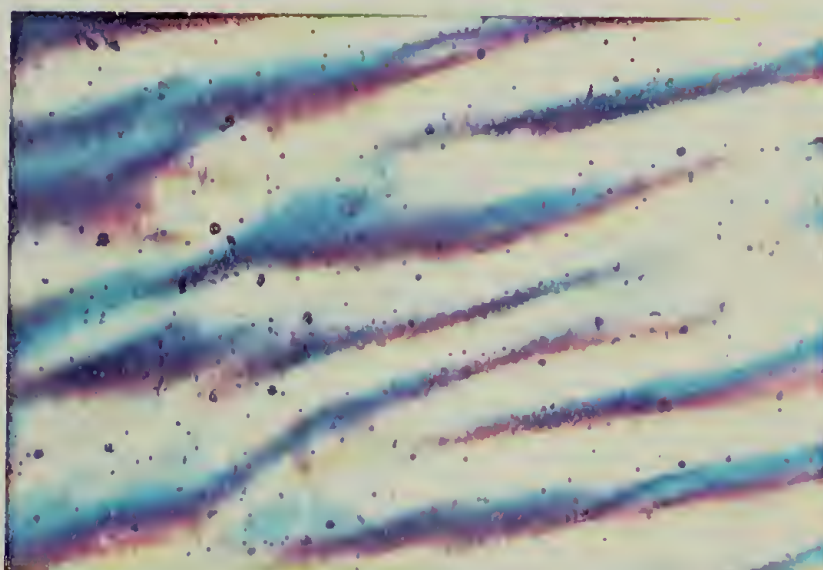
c



d



e



f

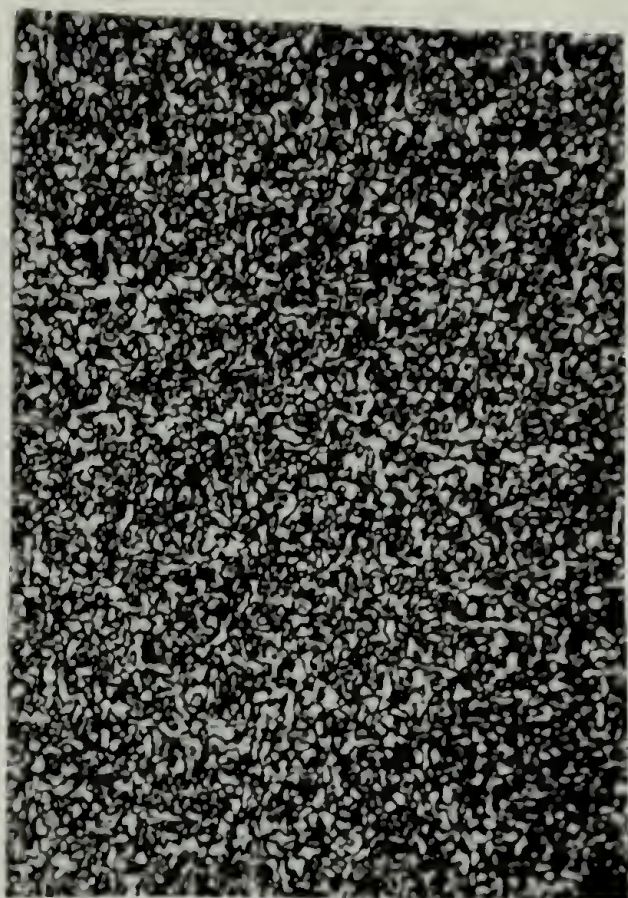
Figure 128. Polarized Light Micrographs of 14.1% 150,000 M.W. PBLG at Various Times after Shearing at  $100 \text{ s}^{-1}$  170X.  
(a) Immediately. (b) .05 min (c) .1 min (d) .3 min  
(e) 1 min (f) 2 min

were birefringent at rest (liquid crystalline) but did not exhibit negative  $N_1$  values the row-nucleated texture was not observed under any circumstances, either during or after cessation of shear.

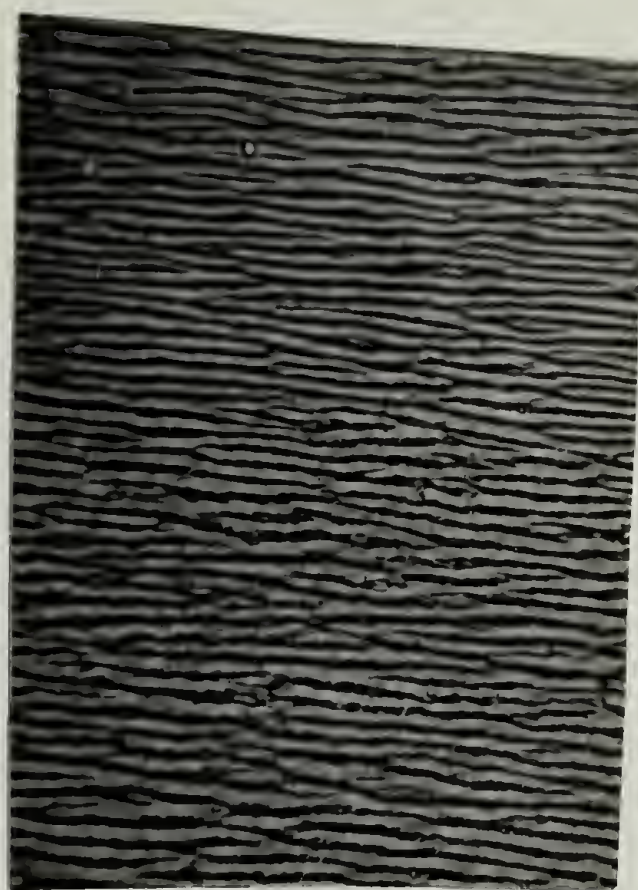
Dried films. Experiments were conducted with 15.0 and 6.8 wt% solutions of the 350,000 M.W. PBLG in 1,4-dioxane. This solvent was chosen since it is helicogenic and moderately volatile so that the structures formed after the cessation of shear (see Figures 126-128) would be made permanent by evaporation of solvent. An assumption inherent in this procedure is that the structures formed by shear are the same in m-cresol and dioxane solution, i.e., that they result from inter-molecular interactions (steric or electrostatic) and not from specific solute-solvent interactions. This assumption is supported by the similarity of behavior of the m-cresol solutions and the dried films.

Films made from the isotropic solution (6.8%) revealed a uniform spherulitic morphology, regardless of the rate of prior shear (Figure 129a). Recall that the "row-nucleated" texture was not observed in any circumstances for isotropic m-cresol solutions, nor for the anisotropic m-cresol solutions which did not exhibit the negative normal stress effect.

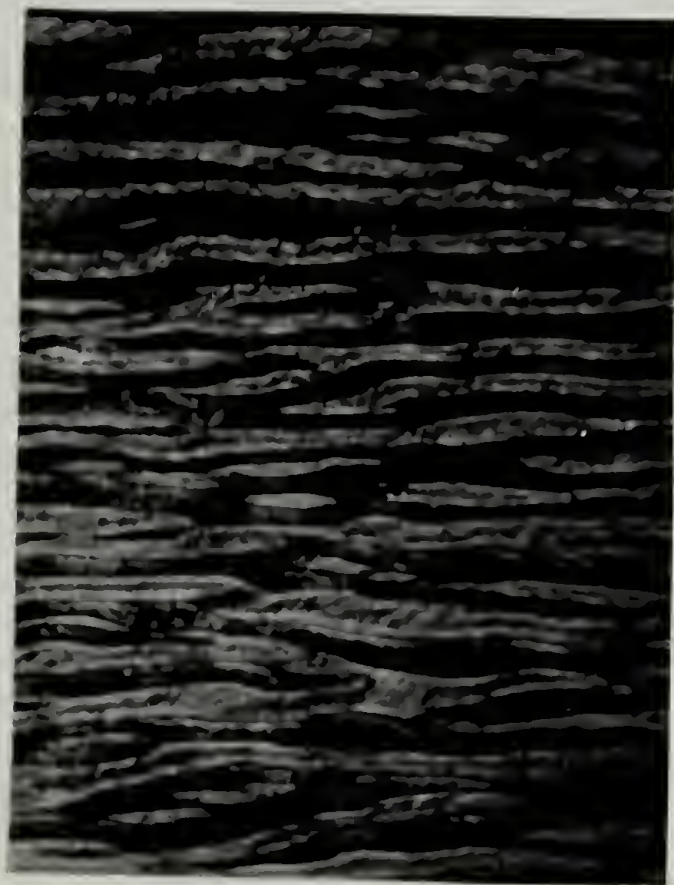
Films made from the anisotropic (15.0%) solution after shearing showed the transverse striations characteristic of the "row-nucleated" texture. As with the m-cresol solutions, films made at high shear exhibited fine striations (approx. 10  $\mu$  width) and those made at low shear exhibited wider striations (approx. 30  $\mu$  width) (see Figures 129b and c). The length of the striations was indeterminate, although



a



b



c

Figure 129. (a) Dried Film from 6.8% 350,000 M.W. PBLG in Dioxane 100X. (b) Dried Film from 15.0% 350,000 M.W. PBLG in Dioxane 100X--High Shear. (c) Dried Film from 15.0% 350,000 M.W. PBLG in Dioxane 100X--Low Shear.



occasional terminations were visible. Also, striations were occasionally seen to fork into two striations which then continued side-by-side.

In most cases the striations appeared smooth but on occasion consisted of long runs of a very pronounced helical structure, always of the same sense. In these regions the field of view had the appearance of a series of coarse ropes strung perpendicular to the direction of shearing (see Figure 130).

Insertion of a first order red plate at  $45^\circ$  to the crossed polaroids gave alternately blue and yellow colors to the striations, indicating that the molecules within the striations were alternately parallel and perpendicular to the red plate. The molecules were therefore oriented alternately  $\pm 45^\circ$  to the shearing direction. This was observed both for the smooth striations and the helical, ropy striations.

### Discussion

Previous reports of a feature similar to the row-nucleated texture described above, formed by various means, have appeared in the literature. Toth and Tobolsky (217) report that an electric field gradient perpendicular to a thin film of 15% PBLG in  $\text{CHCl}_3$  produces a dark field between crossed polars due to perpendicular orientation of the solute molecules, however, slight mechanical shearing instantaneously restored birefringence colors in the form of "parallel, multi-colored bands whose long direction is perpendicular to the direction of shear." 15% methylene dibromide solutions of PBLG allowed to stand for 20 hours in a magnetic field of 9600 Gauss formed a structure

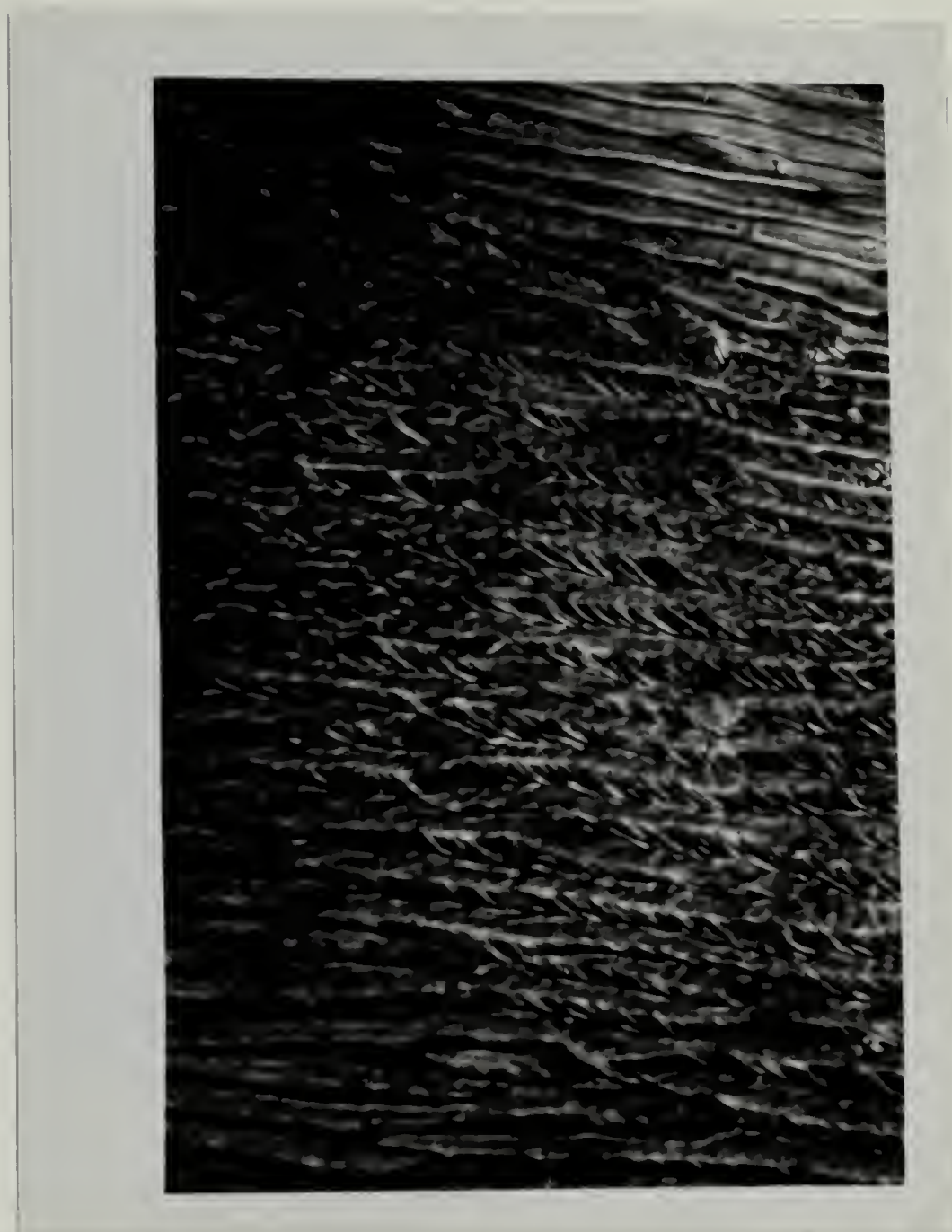


Figure 130. Helical Transverse Striations in Dried Film of 350,000 M.W. PBLG in Dioxane 100X.

consisting of lines perpendicular to the magnetic field (218). The same authors also state that "rubbing" the solution also yields lines perpendicular to the direction of rubbing. A similar effect is reported by Iizuka upon reversal of an electrostatic field in a 14.0% solution of PBLG in  $\text{CH}_2\text{Br}_2$  (219). A series of photographs taken during the process (ref. 219, Figure 6) is strikingly similar to Figure 128 of this work. Initially the structure was that of speckled streaks parallel to the electric field. Upon reversal of the field many equidistant lines perpendicular to the electric field were rapidly formed (less than 2 sec.). After 140 sec. the perpendicular pattern had visibly decayed.

None of these authors advanced speculations concerning the mechanism of formation of these structures. The model which we will propose presently for structural re-arrangement within liquid crystalline solutions under shear must be consistent with the important results of our rheological and rheo-optical investigations, viz. two changes in sign in  $N_1$  corresponding to two distinct changes in texture, with negative values of  $N_1$  correlating with the appearance of the transverse striations characteristic of the "row-nucleated" texture.

The results of the microscopic investigation of dried sheared films of anisotropic solution indicate that molecules within striations are oriented  $\pm 45^\circ$  to the direction of shear. We make the assumption that the transverse striations seen in m-cresol solution during shear (at rates such that the negative normal stress effect is observed) is the same structure. We propose that the transverse striations seen in thin films form planes on the order of 10-30  $\mu$  in width which traverse

the entire sample volume in the cone-and-plate rheometer, forming a physical link between the cone-and-plate (Figure 131a). We propose that the negative normal stress is the result of elasticity within these planes which are stretched as the cone rotates (see Figure 131b). We envision a dynamic steady state as these planes are continuously stretched, broken, and re-created in a constantly fluctuating orientation pattern. Adjacent striations do not coalesce since molecules within them are perpendicular to each other.

The sequence of events occurring as a liquid crystalline solution is sheared at ever increasing shear rates in a transparent cone-and-plate rheometer would be as follows:

Low shear - molecules orient parallel to shear direction.

Observe streaks parallel to shear and positive  $N_1$ .

Medium to high shear - molecules orient  $\pm 45^\circ$  to shear direction in wedge-shaped planes 10-30  $\mu$  wide.

Observe transverse striations from top view (planes seen edge on) and negative  $N_1$  (due to tension within planes).

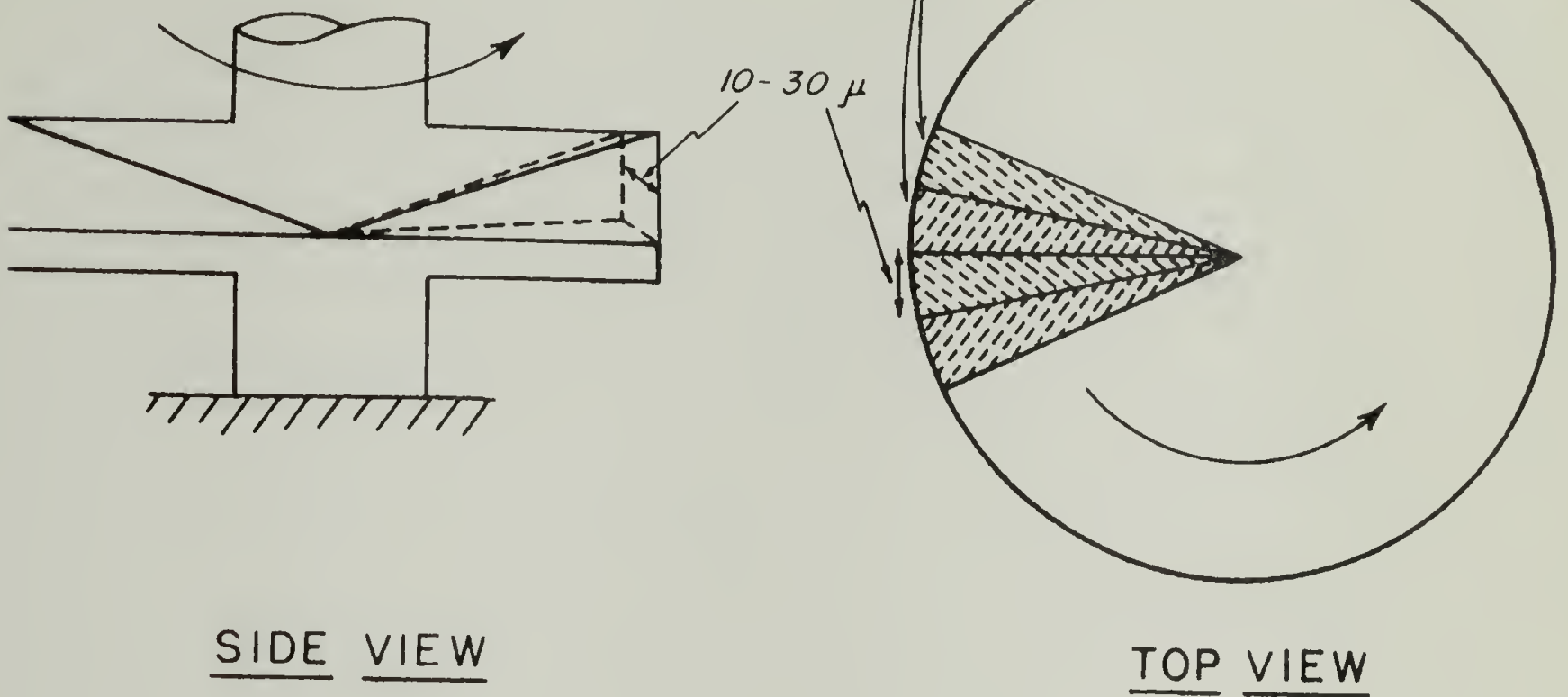
Very high shear - planes break up into rapidly tumbling molecular domains. Observe featureless field and positive  $N_1$ .

This speculative model accounts for the important observations of this work; three regimes of normal stress including one with negative values, and three different shear-induced textures including one characterized by striations perpendicular to the shear direction. It also accounts for the correlation between the "row-nucleated" texture and the negative

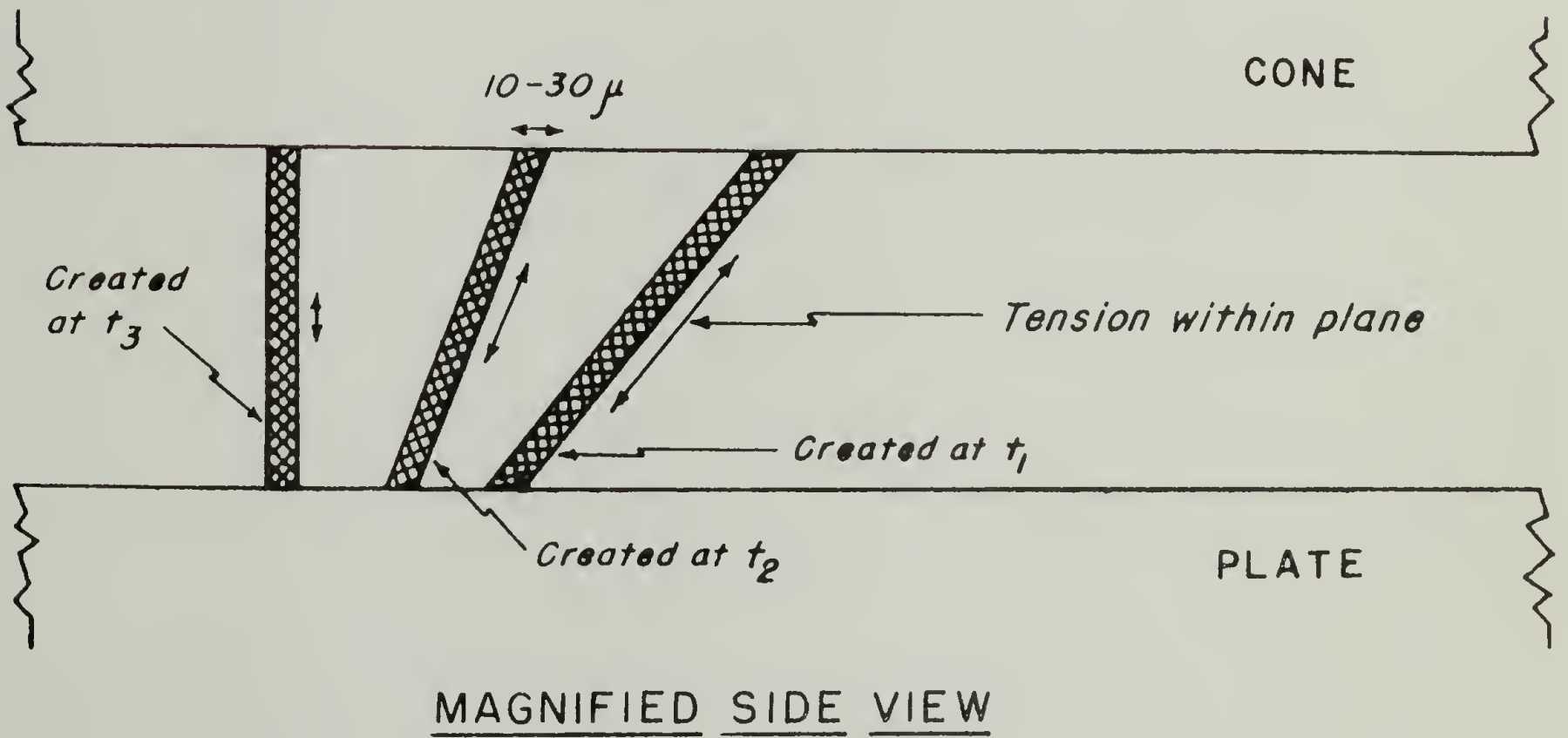
247

WEDGE - SHAPED PLANES OF FLUID GREATLY EXAGGERATED  
FOR CLARITY

Molecules Within Planes Oriented  $\pm 45^\circ$  To Shear Direction



(a)



(b)

Figure 131. Proposed Model Linking "Row-nucleated" Texture and Negative Normal Stress Effect in Cone-and-Plate Rheometer: (a) side view and top view; (b) magnified side view.

normal stress effect.

The crucial unanswered question is why the molecules assume the  $\pm 45^\circ$  orientation. Once they are thus oriented it is not surprising that they should come into register to form the transverse striations. Significantly, it appears that the  $\pm 45^\circ$  orientation possessed a degree of stability. Recall that liquid crystalline solutions sheared at rates within the first positive regime of  $N_1$  were oriented parallel to the shear direction immediately upon cessation, but evolved into the row-nucleated texture (cf. Figures 126-128) within seconds or minutes. Eventually, of course, Brownian motion destroyed these textures. It is also significant that the rate of prior shear in these cases influenced the rate of evolution into the row-nucleated texture, the degree of perfection of the texture, and the width of the striations. This was also noted for the liquid-crystalline dioxane solutions and evaporation of the solvent served to further enhance the perfection of the texture (cf. Figures 129b and c).

The  $90^\circ$  change in orientation of molecules within alternate planes makes this model similar to the phenomenon of "alignment-inversion walls" which has been observed in p-azoxyanisole (220) and treated theoretically (221). The creation of alignment inversion walls in closed shells was proposed as the mechanism leading to formation of tactoidal shell defects in PBLG/dichloromethane solutions under the influence of a magnetic field. Possibly shear fields as well as magnetic fields are capable of creating alignment-inversion walls in solutions of helical polypeptides.

This model is as yet highly speculative and could prove to be

entirely unrealistic, at which point we will painlessly abandon it.

It is, however, consistent with all rheological and rheo-optical observations we have made to date on PBG and PCBZL solutions.

C H A P T E R   V  
RHEOLOGY AND RHEO-OPTICS OF PBA GEL

The results of rheological characterization of a concentrated solution of poly- $\beta$ -benzyl-aspartate is being given separately, since the behavior is radically different from the PBLG and PCBZL solutions described previously. Only one solution was studied rather than the whole concentration series because a decision was made to concentrate our efforts on the relatively familiar though unusual phenomena observed in PBLG and PCBZL solutions.

The results of steady shear measurements ( $\eta$  vs.  $\dot{\gamma}$  and  $N_1$  vs.  $\dot{\gamma}$ ) on an optically anisotropic 33.2 wt% solution of 60,000 m.w. PBA are shown in Figures 132 and 133. The behavior of this solution is remarkably different from any seen previously in this work. Both  $\eta$  and  $N_1$  were critically dependent on shear history. An effort to elucidate this dependence involved the following shear sequence (the curves are numbered correspondingly):

- (1) Load sample, shear from  $.025$ - $625 \text{ sec}^{-1}$  increasing shear rate 5 steps per decade.
- (2) Continue making measurements at  $625 \text{ sec}^{-1}$  until the viscosity value becomes constant, then reduce shear rate back to  $.025 \text{ sec}^{-1}$  in 5 steps per decade.
- (3) Increase shear rate from  $.025$ - $625 \text{ sec}^{-1}$  in 5 steps per decade.



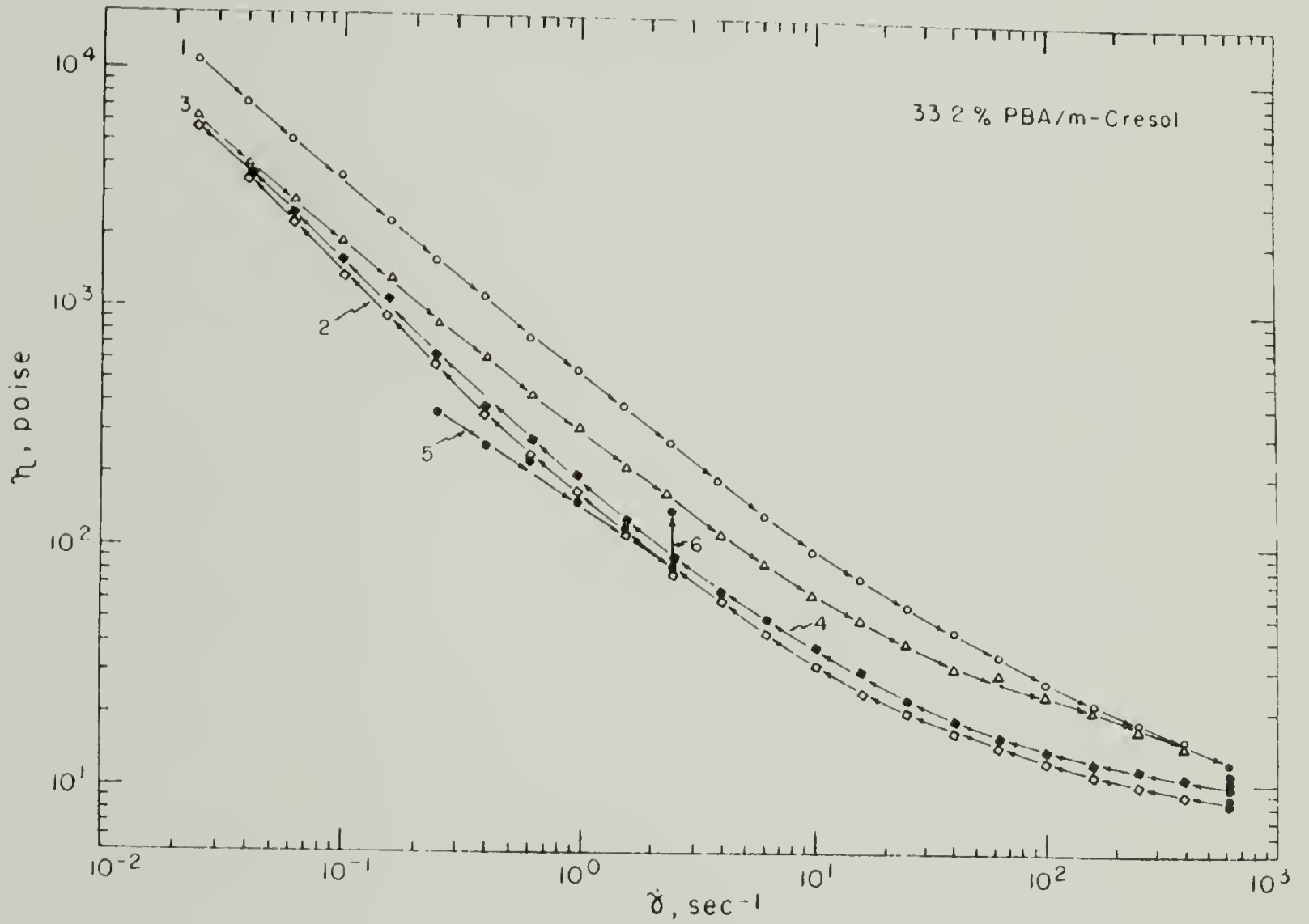


Figure 132. Steady Shear Viscosity versus Shear Rate for 33.2% 60,000 M.W. PBA.

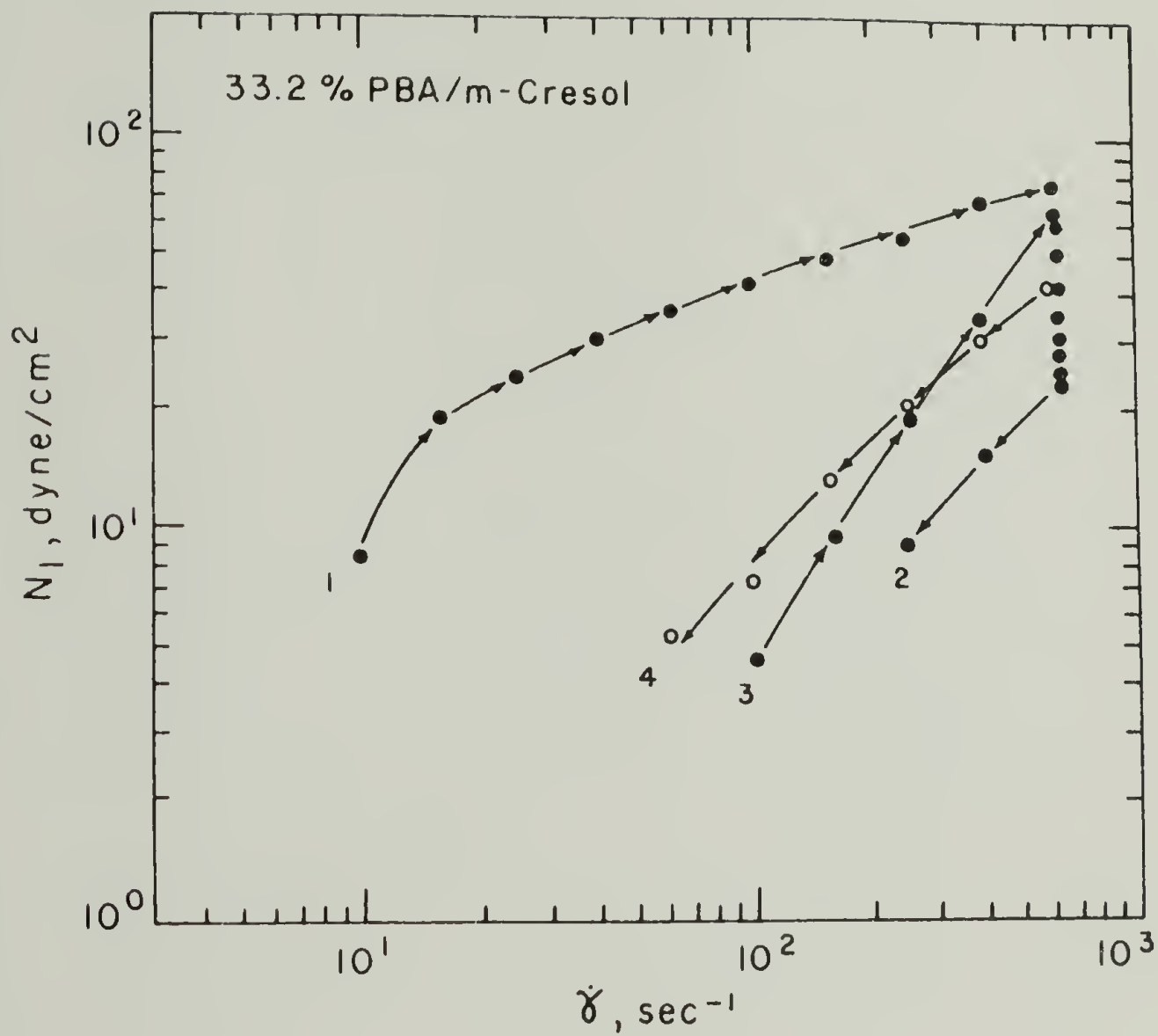


Figure 133. First Normal Stress Difference versus Shear Rate for 33.2% 60,000 M.W. PBA.

- (4) Repeat step 2.
- (5) Shear at  $625 \text{ sec}^{-1}$  for 10 minutes, then make measurements from  $.25$  to  $2.5 \text{ sec}^{-1}$ .
- (6) Shear at  $2.5 \text{ sec}^{-1}$  for 10 minutes, then make a measurement at  $2.5 \text{ sec}^{-1}$ .

The consequent curves of  $\log \eta$  vs.  $\log \dot{\gamma}$  have the appearance of a hysteresis loop, with viscosity measurements made at decreasing shear rate significantly higher than those made at increasing shear rate. The appearance suggests that a structure is present in the fluid which is broken down gradually by shear. It also appears that the structure can "heal" itself over a period of time when the rate of shearing is reduced (e.g., compare values of  $\eta$  at  $\dot{\gamma} = .25 \text{ sec}^{-1}$  for the second series of increasing shear rate, either series of decreasing shear rate, and after shearing for 10 minutes at  $625 \text{ sec}^{-1}$ ). The healing effect can be seen explicitly in step 6 of the shearing sequence in which measurements at  $2.5 \text{ sec}^{-1}$  are compared before and after a ten minute shearing period. The structure of the fluid is broken down gradually rather than instantly even at rather high shear rates, e.g., measurements were made continuously at  $625 \text{ sec}^{-1}$  (see Figure 132) for approximately ten minutes before reaching a stable value. At low shear rates  $\log \eta$  vs.  $\log \dot{\gamma}$  has a slope of approximately -1, indicating shear stress independent of shear rate. This behavior is characteristic of fluids which exhibit yield stress.

The first normal stress differences measured simultaneously with the viscosity measurements discussed above are presented in Figure 133 (data for  $N_1$  is not available for the entire shearing

sequence). The change in properties upon shearing is even more visible in  $N_1$  than in  $\eta$ . Note in particular curves 2 and 4, both made after shearing at  $625 \text{ sec}^{-1}$  until the viscosity had apparently stabilized. Evidently the period of shearing prior to embarking on the measurements for series 4 was insufficient, since viscosity values for series 4 (see Figure 132) were slightly higher than for series 2 throughout the entire shear rate range. The difference in  $N_1$  values between series 2 and series 4 is more dramatic. Note also that magnitudes of  $N_1$  are low, especially after prolonged shearing at  $625 \text{ sec}^{-1}$ ; on the order of 10-100  $\text{dyne/cm}^2$  at  $625 \text{ sec}^{-1}$ , rather than 1000-10,000  $\text{dyne/cm}^2$  typical for PBLG and PCBZL (see Figures 89 and 90). Finally, the negative normal stress effect was not observed on this PBA solution at any time.

The dynamic properties of the PBA solution are shown in Figures 134 and 135. The behavior of  $\log \eta'$  vs.  $\log \omega$  is similar to that of  $\log \eta$  vs.  $\log \dot{\gamma}$ , with a slope approaching -1 at low frequencies, indicating the existence of a yield stress. The behavior of  $G'$  is quite unusual by reason of the very shallow curve of  $\log G'$  vs.  $\log \omega$ . Both  $\eta'$  and  $G'$  were extremely sensitive to strain amplitude. This is consistent with the hypothesis of a structure which is broken down incrementally as shear rate is increased, since oscillatory shear performed over a larger distance (amplitude) in the same time (constant frequency) constitutes a higher shear rate. Healing of the fluid structure can be seen in a second test at low amplitude. As with  $N_1$  and  $\eta$ ,  $G'$  seems more sensitive to breakdown of the structure than  $\eta'$ , both in terms of decreased magnitude with increased amplitude and in terms of extent of healing after a short waiting period.

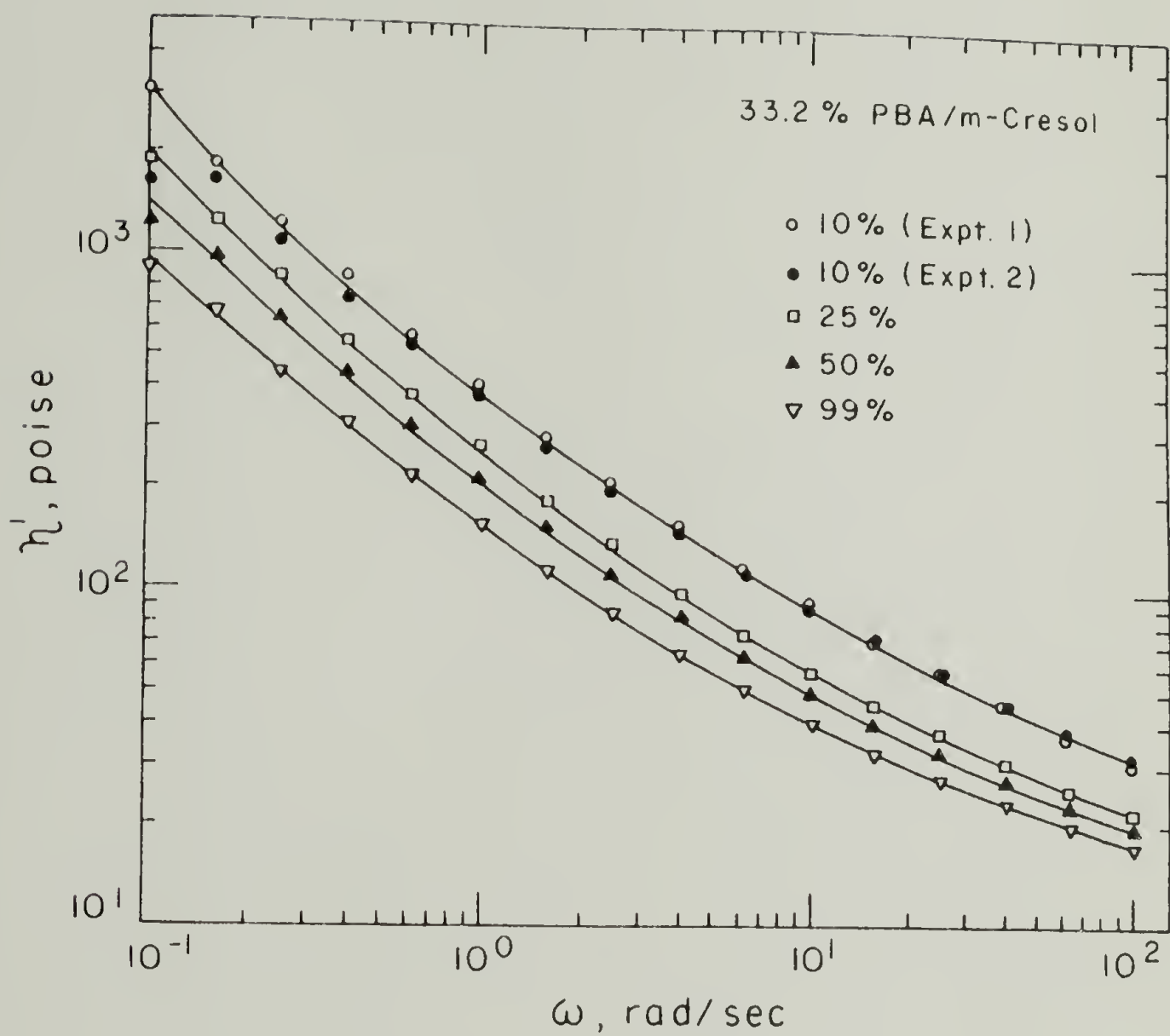


Figure 134. Dynamic Viscosity at Various Strain Amplitudes versus Frequency for 33.2% 60,000 M.W. PBA.

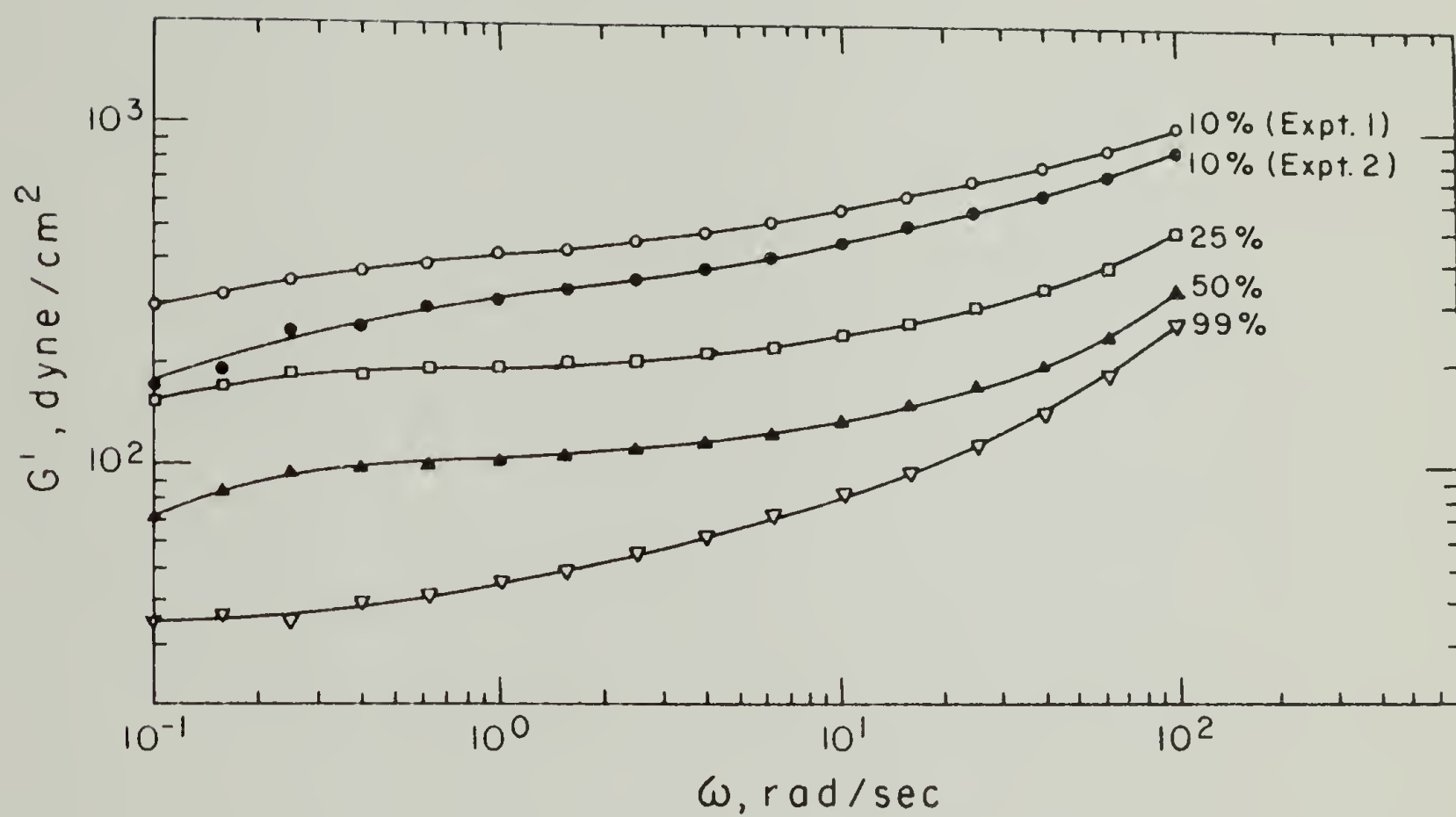


Figure 135. Dynamic Storage Modulus at Various Amplitudes versus Frequency for 33.2% 60,000 M.W. PBA.

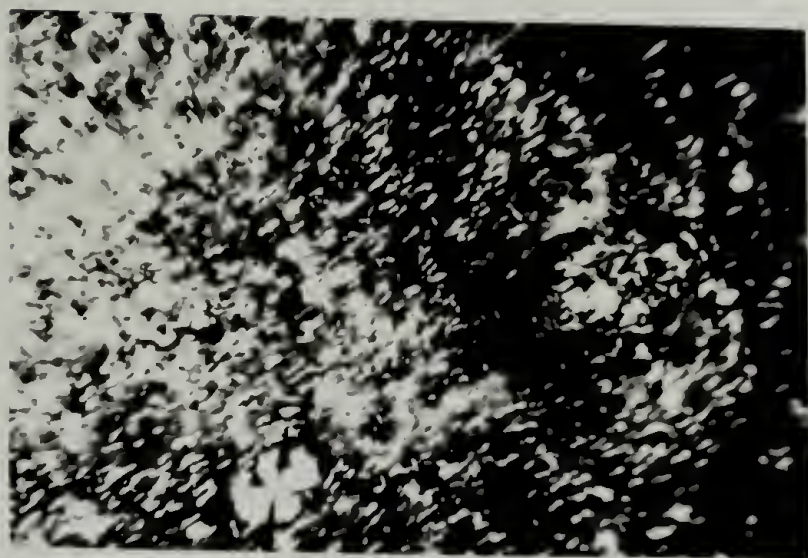
Polarized light micrographs of the solution at rest and during shear at  $6 \text{ sec}^{-1}$ , and  $200 \text{ sec}^{-1}$  are shown in Figure 136, a, b, and c respectively. Not visible in the black and white reproduction are the faint birefringence colors with a few widely scattered circular regions of vivid birefringence color. The uniform structure of the solution at rest is unremarkable. Surprisingly, even during shear, no preferred direction can be seen in the photographs (shearing direction is vertical). This is in marked contrast to the orientation phenomena observed in liquid crystalline PBLG and PCBZL solutions (3).

### Discussion

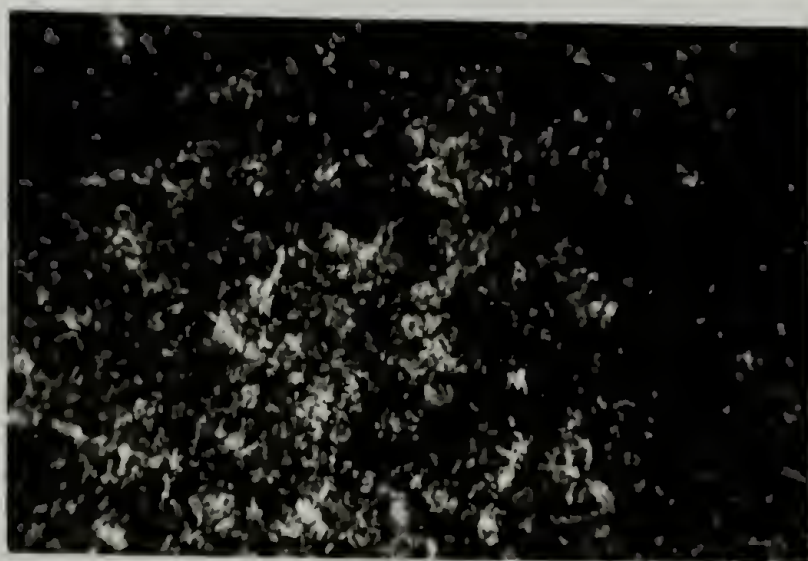
The results presented in this chapter are consistent with a network structure maintained through the action of temporary crosslinks. A crosslink density dependent on level of shear stress may arise in two ways. One is a situation in which the rate of formation and rate of destruction of temporary crosslinks are dependent both on crosslink density and shear stress, leading to a steady state value of crosslink density at any shear stress. The other is to postulate a distribution of crosslink strengths. In the latter case a specific fraction of crosslinks will be sufficiently strong to remain intact at any shear stress, again leading to any "equilibrium" crosslink population. The former case implies a dynamic equilibrium and the latter a static equilibrium.

Upon initiation of shear the crosslink density drops gradually from its rest value to the "equilibrium" value characteristic of the ultimate shear stress at the chosen shear rate. Upon subsequent

a



b



c



Figure 136. Polarized Light Micrographs of 33.2% 60,000 M.W. PBA 170X.  
(a) Rest (b)  $6 \text{ s}^{-1}$  (c)  $200 \text{ s}^{-1}$



reduction of shear rate the crosslink density increases gradually to the value characteristic of the ultimate shear stress at the lower shear rate. The time required to establish the equilibrium value of crosslink density probably decreases with shear rate and is at least 10 minutes even at  $625 \text{ sec}^{-1}$ .

The great difference in behavior between PBA/m-cresol solutions and PBLG/m-cresol solutions is even more unexpected since PBA and PBLG are quite similar chemically, differing only by the methyl group (see Figure 82). The difference between PBLG and PCBZL is much greater, yet the rheology of liquid crystalline solutions of these polymers is quite similar. The photographs taken during shear (see Figure 136) show that flow in the PBA/m-cresol gel occurs by translation of molecular clusters on the order of  $100 \mu$  in diameter. These clusters do not seem to be significantly elongated at shear stress of at least  $2000 \text{ dyne/cm}^2$ , hence the clusters are somewhat rigid. The specific interactions which lead to the observed behavior must occur between clusters. Physical entanglement is an unlikely mechanism for stiff helical molecules. Perhaps electrostatic interactions are involved; one can imagine "hairy" clusters with portions of molecules of various lengths protruding and overlapping laterally when two clusters encounter, leading to a distribution of crosslink strengths.

The reason for formation of such clusters for PBA but not for PBLG or PCBZL is unknown. Also an open question is the mechanism responsible for the normal force when the gel is sheared.

## C H A P T E R   V I

### FUTURE WORK

As in any research endeavor, new areas of inquiry opened up constantly which we were unable to pursue due to limited time and resources. In this section we will present the best ideas and propose future work which could profitably be undertaken, given sufficient resources.

The greatest weakness of the work described in this thesis was the necessity of re-using the same solutions after each measurement and of producing the concentration series by successive dilutions of one original highly concentrated solution. The most obvious consequence of this procedure was the accumulation of significant quantities of dust in the solutions, as can be seen quite clearly in some of the photographs. Although this did not seem to affect the rheological measurements greatly, it is nevertheless inelegant. More to the point, it made it impossible to perform light-scattering experiments. Therefore, if this work were to be continued, the first step would be to construct an apparatus for large scale synthesis of the polymers. Quantities on the order of several hundred grams would be ideal. Then one could make sufficient quantities of each concentration simultaneously in a dust-free environment and then, after measurement, return the sample to a waste container for later recovery. This procedure would increase the speed at which the work could proceed,

since a major bottleneck in this work was time spent waiting for solutions to equilibrate after dilution. Another consequence would be the opportunity to extend the work to more volatile solvents. This was impossible in the present case since evaporation of solvent during each measurement would have caused great uncertainty in the concentration upon returning the sample to the bottle.

The next suggestion would be to re-construct the shearing stage apparatus taking advantage of the services of a professional machinist so that the range of accessible shear rate could be increased by the use of thinner gaps (this would also allow study of surface orientation effects using very thin gaps), and so that the accuracy of the shear rate values would be improved. This reconstructed apparatus should be self-contained to the point that it could be detached from the microscope and inserted in the path of a laser beam for dynamic light-scattering experiments. This would be a very powerful tool to use in conjunction with several microscopy techniques (polarized light, phase, interference contrast) for elucidating details of molecular organization in the solutions under shear.

It was observed during experiments with the present shearing-stage apparatus that a very rapid sequence of color and possibly intensity changes immediately follows the cessation of shear. Undoubtedly a great deal of information could be extracted by measuring transmitted light intensity at a variety of wavelengths as a function of time and prior shear rate. This would also allow flow-birefringence measurements on the isotropic solutions as the critical concentration is approached from the dilute side.

The most dramatic and unanticipated result of this work has been the observation of the negative normal stress effect. On the basis of a thorough literature search and personal communications with many eminent rheologists, it appears that reproducible, steady-state, large magnitude negative normal force in steady shear has never before been reported. We have observed this effect on three distinct though fairly similar polymer/solvent systems but only in the cone-and-plate geometry (although a variety of cones and plates were employed). An essential extension of this work would be to look for this astonishing phenomenon in other geometries. Probably the concentric cylinder geometry would be the best choice. Again, the availability of large quantities of sample would be an asset.

Another approach to the more thorough exploration of the negative normal stress phenomenon would be to determine the radial dependence of normal stress in the cone-and-plate geometry, as opposed to the total normal thrust method used so far which in effect integrates normal stress over the entire sample area. This can be done conveniently in the mechanical spectrometer by installing a very small flush-mounted pressure transducer in a large bottom plate. By using an excess of sample under a smaller cone ("infinite sea") and scanning the sensitive spot of the large plate by means of the two-axis translational stage, one can develop the normal force profile at various radial positions under the cone. This information could be used in a variety of ways. First, one could simply integrate the area under the experimental normal stress profile to double-check the total normal thrust (which could be measured simultaneously). Also, if normal

stress turns out to be an exponential function of radius, the exponential constant is a measurement of the second normal stress difference, which to our knowledge has never been reported for any liquid crystalline system. Another possible use of such an apparatus would be to use a flat plate rather than a cone as the upper platen; then one could obtain normal stress as a function of shear rate immediately by scanning along a radius as another check of the total normal thrust results.

A "point-normal stress" transducer has been designed, but attempts at constructing the apparatus have so far met with little success. The chief problem is that in order to consider the measurement to be made at a point, the sensitive area of the transducer must be quite small. This, combined with relatively low values of the normal stress (from fractions of a P.S.I. to several P.S.I.) make the forces which must be measured very small. There is still much room for optimization, and we feel that moderate investment in time from a person with the necessary instrumentation skills would bear fruit.

Another rheological technique which could be applied thanks to the capabilities of the mechanical spectrometer is to measure total normal thrust during E.R.D. measurements. This would give another estimate of the second normal stress difference to compare with the result of radial variation of normal stress.

One of the interesting coincidences of this work is the fact that the system PCBZL/m-cresol undergoes an inverse coil-helix transition slightly above room temperature in dilute solutions. The effect

of helix imperfections were felt as flexibility in the molecules, which shifted the critical concentration for the formation of the liquid crystalline phase upward. It was also noted previously that the fact that liquid crystalline behavior was observed at all at room temperature constitutes evidence that the coil-helix transition is shifted to lower temperatures in concentrated solutions. This was completely fortuitous since both components of the system were chosen for other reasons: m-cresol since it is a helicogenic solvent of low vapor pressure, PCBZL since it is a helical polypeptide available in high molecular weights at reasonable prices. It would be quite elegant to combine some optical techniques to examine this coil-helix transition in concentrated solution (a subject which has received little attention) with the measurements of rheological properties at different temperatures. One can envision an interesting sequence of events. Consider a solution barely above the critical concentration but below the transition temperature, that is, the molecules are in the coil form, so that the solution is isotropic. As temperature is increased to the coil-helix transition, the molecules become rod-like helices so that the solution becomes liquid crystalline. As the temperature is increased further the liquid crystalline structure cannot be maintained in the face of the violent thermal motions, hence the order "melts" out to reform an isotropic solution. Thus one could anticipate a rather unique isotropic→anisotropic→isotropic mesomorphic transition as temperature is increased.

Another sequence of events can also be envisioned. Consider a solution well above the critical concentration and barely below the

coil-helix transition temperature. Upon shearing this solution a high viscosity will be observed. However, the viscosity of this solution would be lower were the molecules in helical form, since the solution would then be liquid crystalline, thus reducing the amount of energy dissipated in shearing. It is possible therefore that one might observe a shear-driven inverse coil-helix transition, as the system responds to the perturbation in such a way as to minimize the perturbation, in accordance with Le Châtelier's principle.

As this brief presentation makes clear, there are a number of interesting problems in rheology and physical chemistry which merely await investigation. It is ironic that so many exciting observations and possibilities for future work have arisen in this thesis, since one gets the impression from the literature that the rheology of liquid crystalline polypeptide solutions is rather old hat. The pioneering work was done almost twenty years ago and more recent efforts have been desultory. Certainly the instrumentation which made this work possible has been available for at least five years. It is our fervent hope that this subject receive the attention which it deserves, and in fact we hope that circumstances will allow us to continue the work ourselves one day.

## REFERENCES

1. C.F. Goodeve, Trans. Far. Soc., 35, 349 (1939).
2. G.B. Jeffrey, Proc. Roy. Soc., A, 102, 161 (1923).
3. A. Einstein, Ann Physik 19, 289 (1906); 34, 591 (1911).
4. R. Simha, J. Phys. Chem., 44, 25 (1940).
5. J.M. Burgers, "Second Report on Viscosity and Plasticity," Academy of Sciences at Amsterdam, Nordemann Inc., N.Y., 1938.
6. E. Guth, Kolloid Z., 74, 147 (1936).
7. B.H. Zimm and A.J. Haltner, Nature, 184, 265 (1959).
8. M.A. Nawab and S.G. Mason, J. Phys. Chem., 62, 1248 (1958).
9. L. Nicodemo and L. Nicolais, Chem. Eng. J., 8, 155 (1974).
10. J.G. Brodnyan, Trans. Soc. Rheo., 3, 61 (1959).
11. W.R. Blakeney, J. Colloid Sci., 22, 324 (1966).
12. O.L. Forgacs and S.G. Mason, J. Colloid Sci., 14, 473 (1959).
13. A. Peterlin, J. Physik, 111, 232 (1938).
14. R. Simha, J. Phys. Chem., 44, 25 (1940).
15. W. Kuhn and H. Kuhn, Helv. Chim. Acta., 28, 97 (1945).
16. J.G. Kirkwood, Rec. Trav. Chim., 68, 649 (1959).
17. N. Saito, J. Phys. Soc. Jap., 6, 297 (1951).
18. N. Saito, J. Phys. Soc. Jap., 6, 302 (1951).
19. H.A. Sheraga, J. Chem. Phys., 23, 1526 (1955).
20. R. Simha, J. Phys. Chem., 44, 25 (1940).
21. J.W. Mehl, J.L. Oncley, and R. Simha, Science, 92, 132 (1940).
22. J.T. Yang, J.A.C.S., 81, 3902 (1959).



23. J.T. Yang, Adv. Prot. Chem., 16, 323 (1961).
24. M.E. Reichmann, J. Phys. Chem., 63, 638 (1959).
25. E. Fukada and M. Date, Biorrheology, 1, 101 (1963).
26. F.E. Helders and J.D. Ferry, J. Phys. Chem., 60, 1536 (1956).
27. F. Bueche, J. Chem. Phys., 22, 1570 (1954).
28. A.B. Robins, Trans. Far. Soc., 60, 1344 (1964).
29. A.B. Robins, Biorrheology, 3, 153 (1966).
30. H. Eisenberg, J. Polym. Sci., 25, 257 (1957).
31. W. Kuhn and H. Kuhn, Helv. Chim. Acta., 28, 1533 (1945).
32. A. Wada, Biopolymers, 2, 361 (1964).
33. E. Wada, J. Polym. Sci., 14, 305 (1954).
34. J.T. Yang, J.A.C.S., 83, 1316 (1961).
35. F. Perrin, J. Phys. Radium, 5, 497 (1934).
36. R.C. Williams in T.M. Rivers and F.L. Horsfall (ed.), Viral and Rickettsial Infections of Man, 34d E.D., J.B. Lippincott Co., Philadelphia, 1959.
37. P. Doty, J.H. Bradbury, A.M. Holtzer, J.A.C.S., 78, 947 (1956).
38. H. Edelhoeh and R.E. Lippolot, Biochim. et. Biophys. Acta., 45, 205 (1960).
39. J.T. Yang, J.A.C.S., 80, 1783 (1958).
40. W.P. Gaskins and F.H. Philipoff, J. Phys. Chem., 63, 985 (1959).
41. Y.H. Pao, J. Appl. Phys., 28, 591 (1957).
42. J.T. Yang, J.A.C.S., 81, 3902 (1959).
43. H.A. Scheraga, J.T. Edsall, J.O. Gadd, J. Chem. Phys., 19, 1101 (1951).
44. A. Peterlin and H.A. Stuart, Z. Physik, 112, 129 (1939).
45. J.T. Yang, J. Am. Chem. Soc., 83, 1316 (1961).
46. J.T. Yang, J. Polym. Sci., 54, S14 (1961).

47. J.G. Kirkwood and P.L. Auer, J. Chem. Phys., 19, 281 (1951).
48. J.G. Kirkwood and R.J. Plock, J. Chem. Phys., 24, 665 (1956).
49. T. Kotaka, J. Chem. Phys., 30, 1566 (1959).
50. E. Fukada and M. Date, Biorrheology, 1, 101 (1963).
51. N. Hirai, Bull. Inst. Chem. Res. Kyoto Univ., 33, 21 (1955).
52. N.W. Tschoegl and J.D. Ferry, J. Am. Chem. Soc., 86, 1474 (1964).
53. B.H. Zimm, J. Chem. Phys., 24, 269 (1956).
54. H. Tanaka, A. Sakanishi, J. Furuichi, Reports on Progress in Polymer Physics in Japan, 8, 193 (1965).
55. H. Tanaka, A. Sakanishi, M. Kaneko, J. Furuichi, 14th Annual Symposium on Rheology, Paper #19, Sendai, Japan.
56. N.W. Tschoegl and J.D. Ferry, J. Am. Chem. Soc., 86, 1474 (1964).
57. L. Onsager, Ann. N.Y. Acad. Sci., 51, 627 (1949).
58. A. Isihara, J. Chem. Phys., 19, 1142 (1951).
59. P.J. Flory, Proc. Roy. Soc. London, A234, 60 (1956).
60. E.A. DiMarzio, J. Chem. Phys., 35, 658 (1961).
61. J.P. Staley, Mol. Cryst. Liq. Cryst., 22, 333 (1973).
62. S.Ya Frenkel, J. Polym. Sci., C44, 49 (1974).
63. A. Ciferri, Polym. Eng. Sci., 15, 191 (1975).
64. A. Ciferri and T.A. Orofino, J. Phys. Chem., 70, 3277 (1966).
65. S.Ya Frenkel, L.G. Shalytko, G.K. Elyashevich, J. Polym. Sci., C30, 47 (1970).
66. G. Oster, J. Gen. Physiology, 33, 445 (1950).
67. F.C. Bawden and N.W. Pirie, Proc. Roy. Soc., B123, 274 (1937).
68. J.D. Bernal and I. Frankuchen, J. Gen. Physiol., 25, 111 (1941).
69. S.Ya Frenkel, V.G. Baranov, T.I. Volkov, J. Polym. Sci., C16, 1655 (1967).

70. C. Robinson, J.C. Ward, R.B. Beevers, Disc. Faraday Soc., 25, 29 (1958).
71. C. Robinson, Trans. Faraday Soc., 52, 571 (1956).
72. H.L. DeVries, Acta. Cryst., 4, 219 (1951).
73. C. Robinson and J.C. Ward, Nature, 180, 1183 (1957).
74. R.D. Orwoll and R.L. Vold, J. Am. Chem. Soc., 93, 5335 (1971).
75. A. Nakajima, T. Hayashi, M. Ohmori, Biopolymers, 6, 973 (1968).
76. E.L. Wee and W.G. Miller, J. Phys. Chem., 75, 1446 (1971).
77. V.N. Tsvetkov et al., Eur. Polym. J., 9, 481 (1973).
78. A. Skoulios and G. Finaz, Journal De. Chemie Physique, 59, 473 (1962).
79. "Organized Polymers," Chemistry and Industry, 1231 (1962).
80. S. Hokikiri, K. Kodera, Polymer J., 4, 213 (1973).
81. S.Ya Frenkel and B.M. Ginsburg, J. Polym. Sci., C22, 813 (1968).
82. R.H. Marchessault, F.F. Morehead, M.J. Koch, J. Colloid Sci., 16, 327 (1961).
83. B. Ranby, Disc. Far. Soc., 11, 158 (1951).
84. J. Hermans, Liquid Crystals and Ordered Fluids, Porter and Johnson (ed.), A.C.S. Advances in Chemistry Series 63 (1967).
85. J. Hermans Jr., J. Polym. Sci., C2, 129 (1963).
86. M. Litt, J. Colloid Sci., 16, 297 (1961).
87. A.A. Kovinski, G.J. Kizior, S.G. Wax, A.I. Ch. E. J., 20, 1104 (1974).
88. J. Hermans Jr., J. Colloid Sci., 17, 638 (1962).
89. S. Peter and H. Peters, Z. Physik. Chem., 3, 103 (1955).
90. E. Iizuka, Mol. Cryst. Liq. Cryst., 25, 287 (1974).
91. E. Iizuka, J. Phys. Soc. Jap., 35, 1972 (1973).
92. S. Timoshenko, Theory of Elasticity, McGraw-Hill, N.Y., 1934, p. 15.

93. D. Balasubramanian and R. Shakh, Biopolymers, 12, 1639 (1973).
94. L.H. Gan, P. Blais, D.J. Carlsson, T. Suprunchuk, D.M. Wiles, J. Polym. Sci., 19, 69 (1975).
95. H. Blades, "Dry-Jet Wet Spinning Process," U.S. Patent #3,767,756.
96. M.G. Northolt, J.H. Van Arsten, J. Polym. Sci. Polym. Letters, 11, 333 (1973).
97. S.P. Papkov, M.M. Iovleva, L.P. Mil'Kova, A.V. Volokhina, V.D. Kalmykova, G.I. Kudryavstev, Vysokomol. Soedin., 15A (1973).
98. S. Kwolek, "Optically Anisotropic Aromatic Polyamide Dopes," U.S. Patent #3,671,542.
99. J.J. Burke, J. Macromolec. Sci. Chem., A7, 187 (1973).
100. S.P. Papkov et al., Khim. Volokna, 1, 26 (1974).
101. T.S. Sokolova, S.G. Efimova, A.V. Volokhina, G.I. Kudryavtsev, S.P. Papkov, Vysokomol. Soedin. Ser., A15, 2501 (1973).
102. S.P. Papkov, A.Ya Malkin, V.G. Kulichikhin, J. Polym. Sci. Polym. Phys., 12, 1753 (1974).
103. G.V. Vinogradov, N.A. Plate, A.Y. Malkin, V.P. Shivaev, T.H. Poolak, Vysokomol. Soedin., 16A, 437 (1974).
104. J. Preston and W.B. Black, High Modulus Wholly Aromatic Fibers, Fiber Science Series, Marcel Dekker, Inc., N.Y., 1973.
105. R.S. Porter, J.H. Southern, N. Weeks, Polym. Eng. Sci., 15, 213 (1975).
106. D.G. Ballard, J.D. Griffiths, J. Watson, "Wet Spinning of Birefringent Solutions of Optically Active Polypeptide," U.S. Patent #3,121,766.
107. J. Preston, Polym. Eng. Sci., 15, 199 (1975).
108. J. Preston, "High Strength/High Modulus Organic Fibers," Monsanto Co. Internal Report.
109. S.P. Papkov et al., Khim. Volokna, 3, 25 (1974).
110. L.S. Ornstein and W. Kast, Trans. Faraday Soc., 29, 931 (1933).
111. V.N. Tsvetkov and B.A. Marinin, Acta. Physiochemica U.R.S.S., 13, 219 (1940).

112. W. Helfrich, J. Chem. Phys., 50, 100 (1969).
113. C.W. Oseen, Trans. Faraday Soc., 29, 883 (1933).
114. F.C. Frank, Disc. Faraday Soc., 25, 19 (1958).
115. J.L. Ericksen, Appl. Mech. Rev., 20, 1029 (1967).
116. J.L. Ericksen, Arch. Rat. Mech. Anal., 4, 231 (1960).
117. F.M. Leslie, Quart. J. Mech. Appl. Math., 19, 357 (1966).
118. M.J. Stephen, Phys. Rev., A2, 1558 (1970).
119. D. Forster, T.C. Lubensky, P.C. Martin, J. Swift, P.S. Pershan, Phys. Rev. Lett., 26, 1016 (1971).
120. Juey-Wen Huang, Phys. Rev. Lett., 26, 1525 (1971).
121. Ch. Gahwiller, Mol. Cryst. Liq. Cryst., 20, 301 (1973).
122. P. Martinoty and S. Candau, Mol. Cryst. Liq. Cryst., 14, 243 (1971).
123. J. Wahl and F. Fischer, Mol. Cryst. Liq. Cryst., 22, 359 (1973).
124. J. Wahl and F. Fischer, Optics Comm., 5, 341 (1972).
125. H.C. Tseng, D.L. Silver, B.A. Finlayson, Physics of Fluids, 15, 1213 (1972).
126. J. Fishers and A.G. Frederickson, Mol. Cryst. Liq. Cryst., 8, 267 (1969).
127. G.W. Gray, Molecular Structure and the Properties of Liquid Crystals, Academic Press, N.Y., 1962, pp. 70-71.
128. R.J. Atkin, Arch. Rat. Mech. Anal., 38, 224 (1970).
129. R.S. Porter and J.F. Johnson, J. Phys. Chem., 66, 1826 (1962).
130. J.L. Ericksen, Soc. Rheo. Trans., 13, 9 (1969).
131. Ch. Gahwiller, Phys. Lett., 36A, 311 (1971).
132. W. Helfrich, J. Chem. Phys., 56, 3187 (1972).
133. R.S. Porter, E.M. Barrall, J.F. Johnson, J. Chem. Phys., 35, 1452 (1966).

134. R.S. Porter and J.F. Johnson, Rheology, Theory and Applications, F.R. Eirich (ed.), Vol. IV, Academic Press, N.Y., 1967, pp. 317-345.
135. J.M. Pochan, P.F. Erhardt, W.C. Richards, J. Chem. Phys., 57, 3596 (1972).
136. D. Marsh, J.M. Pochan, P.F. Erhardt, J. Chem. Phys., 58, 5795 (1973).
137. W.J. Jackson and H.F. Kuhfuss, "Process for Preparing a Final Copolyester by Reacting a Starting Polyester with an Acyloxy Aromatic Carboxylic Acid," U.S. Patent #3,778,410.
138. W.J. Jackson, Tennessee Eastman Co., Kingsport, Tenn., Personal Communication.
139. W.J. Jackson, H.F. Kuhfuss, T.F. Gray, 30th Annual Technical Conference, 1975, Reinforced Plastics/Composites Institute of the Society of the Plastics Industry, Inc.
140. C.L. Beatty, J.M. Pochan, M.F. Froux, D.O. Hinman, Macromolecules, 8, 547 (1975).
141. P.P.A. Smit, Kolloid Z.U.Z. Polymere, 250, 27 (1972).
142. D.L. Beck and A.A. Hiltz, S.P.E. Trans. Jan. 1965, 15 (1965).
143. J.R. Collier and L.M. Neal, Polym. Eng. Sci., 9, 182 (1969).
144. G.P. Adrianova, J. Polym. Sci., 13, 95 (1975).
145. W.G. Perkins, N.J. Capiati, R.S. Porter, Polym. Eng. Sci., 16, 200 (1976).
146. W.J. Jackson and H.F. Kuhfuss, J. Polym. Sci., Polym. Chem. Ed., 14, 2043 (1976).
147. Belgian Patents Nos. 828,935; 828,936.  
German Patents Nos. 2520-819; 2520-820.  
Netherlands Patent No. 7,505,551.  
U.S.A. Priorities Ser. Nos. 468,690; 468,695; 468,697.
148. I.I. Konstantinov, A.A. Baturin, V.S. Minaeva, Y.B. Amerik, B.A. Krentsel, Presented at the Sixth International Liquid Crystal Conference at Kent State University (1976).
149. C. Shih, J. Polym. Sci., Polym. Phys. Ed., 13, 95 (1975).
150. L. Onsager, Ann. N.Y. Acad. Sci., 51, 627 (1949).

151. A. Isihara, J. Chem. Phys., 19, 1142 (1951).
152. P.J. Flory, Proc. Roy. Soc. London, A234, 60 (1956).
153. E.A. DiMarzio, J. Chem. Phys., 35, 658 (1961).
154. J.P. Straley, Mol. Cryst. Liq. Cryst., 22, 333 (1973).
155. S.Ya Frenkel, J. Polym. Sci., C44, 49 (1974).
156. F.C. Bawden and N.W. Pirie, Proc. Roy. Soc. London, B123, 274 (1937).
157. J.D. Bernal and I. Frankuchen, J. Gen. Physiol., 25, 111 (1941).
158. S.Ya Frenkel, V.G. Baranov, and T.I. Volkov, J. Polym. Sci., C16, 1655 (1967).
159. C. Robinson, J.C. Ward, and R.B. Beevers, Disc. Faraday Soc., 25, 29 (1958).
160. P. Doty, J.H. Bradbury, and A.M. Holtzer, J.A.C.S., 78, 947 (1956).
161. C. Robinson and J.C. Ward, Nature, 180, 1183 (1957).
162. R.S. Porter and J.F. Johnson, Rheology, Theory and Applications, F.R. Eirich (ed.), Vol. IV, Academic Press, N.Y., pp. 317-345.
163. J. Hermans Jr., J. Colloid Sci., 17, 638 (1962).
164. E. Iizuka, Mol. Cryst. Liq. Cryst., 25, 287 (1974).
165. C.W. Macosko and W.M. Davis, Rheol. Acta, 13, 814 (1974).
166. J.T. Yang, J.A.C.A., 81, 3902 (1959).
167. Y. Layec and C. Wolff, Rheol. Acta, 13, 696 (1974).
168. J.G. Kirkwood and P.L. Auer, J. Chem. Phys., 19, 281 (1951).
169. K. Walters, Rheometry, Halsted Press, N.Y., 1975, p. 63.
170. E.T. Samulski and A.V. Tobolsky, Chap. 4.3 in Liquid Crystals and Plastic Crystals, Vol. 1, G.W. Gray and P.A. Winsor (ed.), Halsted Press, N.Y., 1974, pp. 175-199.
171. F.D. Saeva, Mol. Cryst. Liq. Cryst., 23, 171 (1973).
172. R.S. Porter, E.M. Barrall II, J.F. Johnson, J. Chem. Phys., 45, 1452 (1966).

173. J.M. Pochan and D.G. Marsh, J. Chem. Phys., 57, 1193 (1972).
174. S.P. Papkov et al., J. Polym. Sci., 12, 1753 (1974).
175. S. Kwolek, "Optically Anisotropic Aromatic Polyamide Dopes," U.S. Patent #3,671,542.
176. P.G. DeGennes, Solid State Commun., 6, 163 (1965).
177. P.F. Erhardt, J.M. Pochan, W.C. Richards, J. Chem. Phys., 57, 3596 (1972).
178. B.D. Coleman and H. Markovitz, J. Appl. Phys., 35, 1 (1964).
179. E. Iizuka, J. Phys. Soc. Jap., 35, 1792 (1973).
180. H.A. Scheraga, J.T. Edsall, J.D. Gadd, J. Chem. Phys., 19, 1101 (1951).
181. K. Walters, *ibid.*, p. 88.
182. N. Adams and A.S. Lodge, Phil. Trans. Roy. Soc., 256, 149 (1964).
183. R.W. Duke and L.L. Chapoy, Rheol. Acta, 15, 548 (1976).
184. T.A. Huang, Ph.D. Thesis, Univ. of Wisconsin, Dept. of Engineering Mechanics, 1976, p. 93.
185. E. Iizuka, Personal Communication, April, 1977.
186. F.M. Leslie, Arch. Rat. Mech. Anal., 28, 265 (1968).
187. M.C. Williams, A.I. Ch. E. J., 21, 1 (1975).
188. F.C. Bawden and N.W. Pirie, Proc. Roy. Soc. London, B123, 274 (1937).
189. J.D. Bernal and I. Frankuchen, J. Gen. Physiol., 25, 111 (1941).
190. S.Ya Frenkel, V.G. Baranov and T.I. Volkov, J. Polym. Sci., C16, 1965 (1967).
191. C. Robinson, J.C. Ward, R.B. Beevers, Disc. Faraday Soc., 25, 29 (1958).
192. J. Hermans Jr., J. Colloid Sci., 17, 638 (1962).
193. E. Iizuka, Mol. Crys. Liq. Crys., 25, 287 (1974).
194. E. Iizuka, J. Phys. Soc. Jap., 35, 1792 (1973).



195. G. Kiss and R.S. Porter, J. Polym. Sci. Polym. Symp., 65, (1978).
196. W.M. Kulicke, G. Kiss and R.S. Porter, Rheol. Acta, 16, 568 (1977).
197. C.W. Macosko and W.M. Davis, Rheol. Acta, 13, 814 (1974).
198. C. Onsager, Ann. N.Y. Acad. Sci., 51, 627 (1949).
199. P.J. Flory, Proc. Roy. Soc. London, A234, 73 (1956).
200. E.A. DiMarzio, J. Chem. Phys., 35, 658 (1961).
201. S.Ya Frenkel, J. Polym. Sci. Polym. Symp., 44, 49 (1974).
202. J.C. Slattery, J. Colloid Sci., 16, 431 (1961).
203. J.M. Pochan and D.G. Marsh, J. Chem. Phys., 57, 1193 (1972).
204. D.G. Marsh, J.M. Pochan, F.E. Erhardt, J. Chem. Phys., 58, 5795 (1973).
205. K. Walters, Rheometry, Halsted Press, N.H., 1975, p. 30.
206. P. Doty, J.H. Bradbury, A.M. Holzer, J.A.C.S., 78, 947 (1956).
207. E. Daniel and E. Katchalski, Polyamino Acids, Polypeptides, and Proteins, M.S. Stahmann (ed.), Univ. Wisconsin Press, Madison, 1962, p. 183.
208. P.J. Flory, Proc. Roy. Soc. London, A234, 60 (1956).
209. G.D. Fasman, M. Idelson and E.R. Blount, J.A.C.S., 83, 709 (1961).
210. J. Applequist and P. Doty, "Polyamino Acids," p. 161.
211. V.N. Tsvetkov, E.I. Rjuntsev, and I.N. Shtennikova, Liquid Crystalline Order in Polymer Molecules, A. Blumstein (ed.), Academic Press, N.Y., 1978, p. 58.
212. H. Bendit, L. Freund, and G. Spach, Poly- $\alpha$ -Amino Acids, G. Fasman (ed.), Marcel Dekker, Inc., N.Y., 1967, p. 105.
213. G. Spach, L. Freund, and H. Bendit, J. Mol. Biol., 7, 468 (1963).
214. M. Matsudka, T. Norisuye, A. Teramoto and H. Fujita, Biopolymers, 12, 1515 (1973).
215. L. Pauling, R.B. Corey and H.R. Branson, Proc. Nat. Acad. Sci., 37, 205 (1951).

216. A. Keller and M.J. Machin, J. Macromol. Sci. Phys., B1, 41 (1967).
217. W.J. Toth and A.V. Tobolsky, Polym. Lett., 8, 531 (1970).
218. Y. Go, S. Ejira, and E. Fukada, Biochim. et Biophys. Acta, 175  
454 (1969).
219. E. Iizuka, Advances in Polymer Sci., 20, 80 (1976).
220. R. Williams, J. Chem. Phys., 39, 384 (1963).
221. W. Helfrich, Phys. Rev. Lett., 21, 1518 (1968).
222. R.W. Filas, Ph.D. Dissertation, Princeton University, 1978.

APPENDIX I  
INERTIAL NORMAL-FORCE CORRECTIONS IN  
ROTATIONAL RHEOMETRY

1. Introduction

In order to completely characterize a fluid in simple, steady shear flow, three material functions must be known, viz., the steady viscosity  $\eta$ , the first normal-stress difference  $v_1 = p_{11} - p_{22}$  and the second normal-stress difference  $v_2 = p_{22} - p_{33}$ . In the special case of a Newtonian fluid, the viscosity is independent of shear rate and the normal-stress differences are zero.

Of these material functions,  $\eta$  and  $v_1$  are experimentally most easily accessible in a cone-and-plate viscometer by measurement of torque and total normal-force respectively. Several commercial instruments can provide these data. A rough estimate of  $v_2$  may be made by measuring total normal-force during an Eccentric Rotating Disc (E.R.D.) measurement, a test which is readily possible with a Rheometrics Mechanical Spectrometer, the instrument used herein. Thus, the measurement of normal-forces is commonplace in rotational rheometry. In order to make accurate measurements of total normal-force with such instruments, one must consider an inertial contribution which is neglected in the simple theory and which may be significant at high deformation rates or when large diameter measuring platens are used (1).

2. Theory

The simple theory (2) for flow between a rotating cone and a

stationary plate makes the following assumptions:

1. Inertial effects are negligible, i.e., the fluid density is zero.
2. The cone angle is very small so that  $\dot{\gamma} = \frac{\omega}{\theta_0}$  ( $\dot{\gamma}$  = shear rate,  $\omega$  = rotational velocity,  $\theta_0$  = cone angle).
3. The free surface of the liquid is part of a sphere of radius  $R$  ( $R$  = radius of the platens) and centered at the cone vertex.
4. Surface tension is negligible.

Solving for the stress distribution using the stress equations of motion in conjunction with these assumptions yields:

$$r \frac{d\bar{p}}{dr} = -(\nu_1 + 2\nu_2), \quad [1]$$

where  $\bar{p}$  is the pressure at a point in excess of atmospheric pressure.

Integrating this subject to the boundary condition  $\bar{p}(R) = p_0 - \nu_2$  yields:

$$\bar{p}(r) = (\nu_1 + 2\nu_2) \ln \frac{r}{R} - \nu_2, \quad (+ p_0 - \nu_2) \quad [2]$$

where  $p_0$  is atmospheric pressure.

The total normal-force on the plate is given by:

$$F_z = \int_0^R 2\pi r \bar{p}(r) dr. \quad [3]$$

Another integration gives:

$$F_z = \frac{\pi R^2}{2} \nu_1. \quad [4]$$

Hence by rearrangement the first normal-stress is given by:

$$v_1 = \frac{2F_z}{\pi R^2}, \quad [5]$$

which is the commonly used result.

In order to consider the effect of inertia, it is necessary to add a term to the pressure distribution equation. Adams and Lodge (3) adapted a result from Greensmith and Rivlin (4) to obtain this correction factor:

$$\left( r \frac{d\bar{p}}{dr} \right)_{\text{inertial}} = \frac{\rho \omega^2 r^2}{3}. \quad [6]$$

An alternate analysis by Walters yielded the same form with a slightly different constant:

$$\left( r \frac{d\bar{p}}{dr} \right)_{\text{inertial}} = \frac{3\rho \omega^2 r^2}{10}. \quad [7]$$

Using the latter, corrected pressure distribution is therefore:

$$r \frac{d\bar{p}}{dr} = -(v_1 + 2v_2) + \frac{3\rho \omega^2 r^2}{10} \quad [8]$$

Performing a double integration as before yields:

$$F_z = \frac{\pi R^2}{2} v_1 - \frac{3\rho \omega^2 R^4}{40} \quad [9]$$

For a Newtonian fluid  $v_1 = 0$  and the above equation becomes:

$$F_{z0} = - \frac{3\pi\rho\omega^2 R^4}{40} , \quad [10]$$

which is the contribution to the normal-force due solely to inertia: this will appear as an "apparent first normal-stress difference" for a Newtonian liquid (as per eq. [5]):

$$(v_1)_{\text{inertial}} = \frac{2F_{z0}}{\pi R^2}$$

or substituting eq. [10]:

$$(v_1)_{\text{inertial}} = - \frac{3\rho\omega^2 R^2}{20} . \quad [11]$$

Notice that this apparent first normal-stress difference is negative, hence a correction must be added to obtain the true value of  $v_1$  for a fluid exhibiting real normal-stress effects.

Greensmith and Rivlin in their original treatment were forced to make the assumption that the centrifugal force at any point within the fluid may be replaced by the value averaged over the gap between two parallel plates at the given value of  $r$ . Adams and Lodge reasoned that the value of centrifugal force at any point may be replaced by the value averaged over the cone angle at a given  $r$ . Hence the correction should be accurate to the same degree of approximation for both cone-and-plate and parallel plate systems. Furthermore, the inertial normal-force should be independent of cone angle, plate separation, and fluid viscosity; the only relevant quantities being fluid density, rotation speed and radius.

### 3. Experiments

In order to test the accuracy of the theoretically derived inertial normal force correction eq. [10], the total normal-force was measured in both cone-and-plate and parallel plate geometry for a variety of Newtonian fluids of widely varying viscosity and density. In the case of cone-and-plate geometry, both cone angle and platen radius were varied. In the case of parallel plate geometry both platen radius and separation were varied. The measured inertial normal-force values were normalized with respect to density and radius so that if data were in accord with theory, all data would fall on the same line:

$$\frac{F_{z0}}{\rho R^4} = \frac{\left( - \frac{3\pi\rho\omega^2 R^4}{40} \right)}{\rho R^4} = \frac{\omega^2}{4.244} \quad [12]$$

Figure 1 shows that all data indeed fell on the same line. In order to determine the dependence of  $F_{z0}$  on  $\omega$  the data were fit by a least square linear regression to the equation:

$$\log\left(-\frac{F_{z0}}{\rho R^4}\right) = m \log\omega + b, \quad [13]$$

a total of 56 data points were fit by a line with a slope of 1.986. The correlation coefficient was .99957. In order to determine if the constant in the denominator of eq. [12] is correct, an exact quadratic dependence on  $\omega$  was assumed and the data fit to the equation:

$$-\frac{F_{z0}}{\rho R^4} = \frac{1}{K} \omega^2 + b.$$

The same data points were fit by  $K = 4.135$  with a correlation coefficient of .99982. Thus the least squares analysis of a large body of data accumulated using many different fluids, platen radii, cone angles, and plate separations, resulted in values within 2.5% of those called for by theory for both the exponent of  $\omega$  and the constant in the denominator of eq. [12].

The treatment of inertial normal-force for Eccentric Rotating Disk (E.R.D.) systems is slightly different since the entire volume of fluid rotates at the same frequency (to a very good approximation) as opposed to the parallel plate and cone-and-plate systems in which a velocity gradient is set up.

By modelling the E.R.D. situation as a solid body rotation, Macosko and Davis (5) obtained for the contribution to the total normal-force due to inertia:

$$F_{z0} = - \frac{\pi p \omega^2 R^2}{4} \quad [14]$$

As before, this equation was normalized with respect to density and radius:

$$\frac{F_{z0}}{pR^4} = \frac{\left( -\frac{\pi p \omega^2 R^4}{4} \right)}{pR^4} = - \frac{\omega^2}{1.273} \quad [15]$$

The results are shown in curve A of Figure 1. As before, the dependence of  $F_{z0}$  on  $\omega$  was determined by a least squares fit to the equation:

$$\log \left( - \frac{F_{z0}}{pR^4} \right) = m \log \omega + b.$$



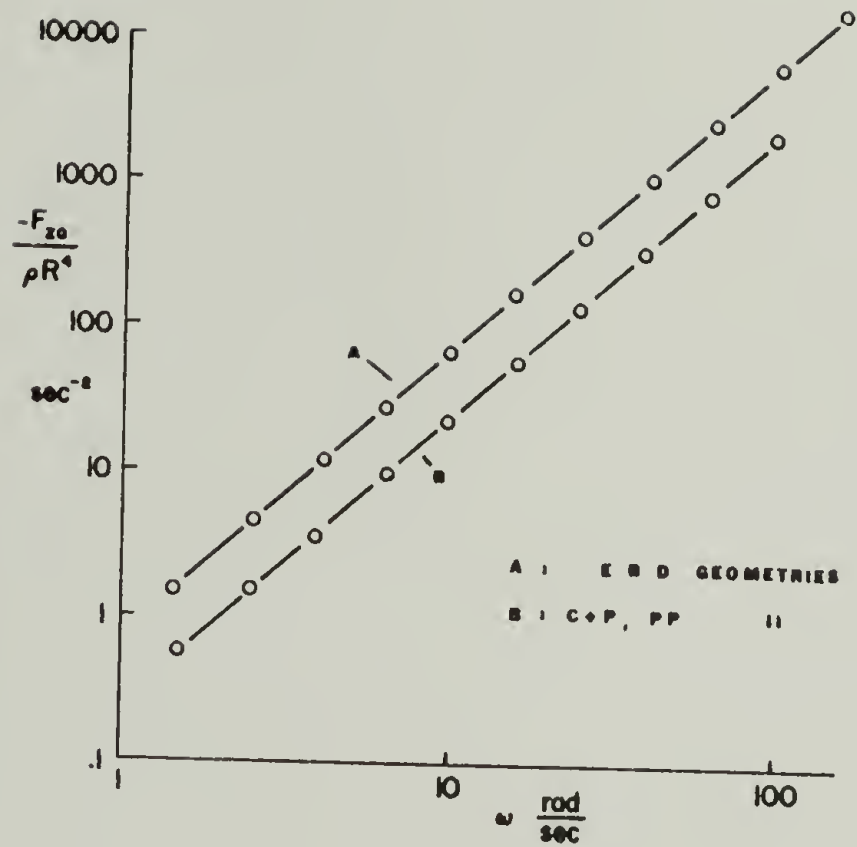


Fig. 1. Normalized inertial normal-force vs. angular velocity.

A - For eccentric rotating disc.

B - For cone-and-plate and parallel-plate geometries.

In the case of E.R.D., a total of 37 data points were fit by a line of slope 2.033. The correlation coefficient was .99884. In order to determine if the constant in the denominator of eq. [15] is correct, an exact quadratic dependence on  $\omega$  was assumed and the data fit to the equation:

$$-\frac{F_{z0}}{\rho R^4} = \frac{1}{K} \omega^2 + b.$$

The same E.R.D. data points were fit by  $K = 1.327$  with a correlation coefficient of .99989. Thus the least squares analysis of a large body of E.R.D. data resulted in values for the exponent of  $\omega$  and the constant in the denominator of eq. [15] within about 4% of those called for by theory. In view of the large oscillations which plagued normal force measurements in E.R.D. (mean values were used) this agreement was very satisfactory.

Thus it can be seen that when measuring first and second normal-stress differences via normal-force in parallel plate, cone-and-plate or Eccentric Rotating Disc geometries, one must be aware of the correction described herein. An example of the magnitude of the error which may otherwise be committed is shown in Figure 2 for typical viscoelastic polymer solutions (polyacrylamide in water). At high shear rates it is seen that the inertial effect can completely overwhelm the elastic response of the solution. An even more striking example of the effect of the inertial normal-force is provided by Figure 3. It is seen that the measured normal-force indicates an apparent first normal-stress difference which reaches a maximum with shear rate and

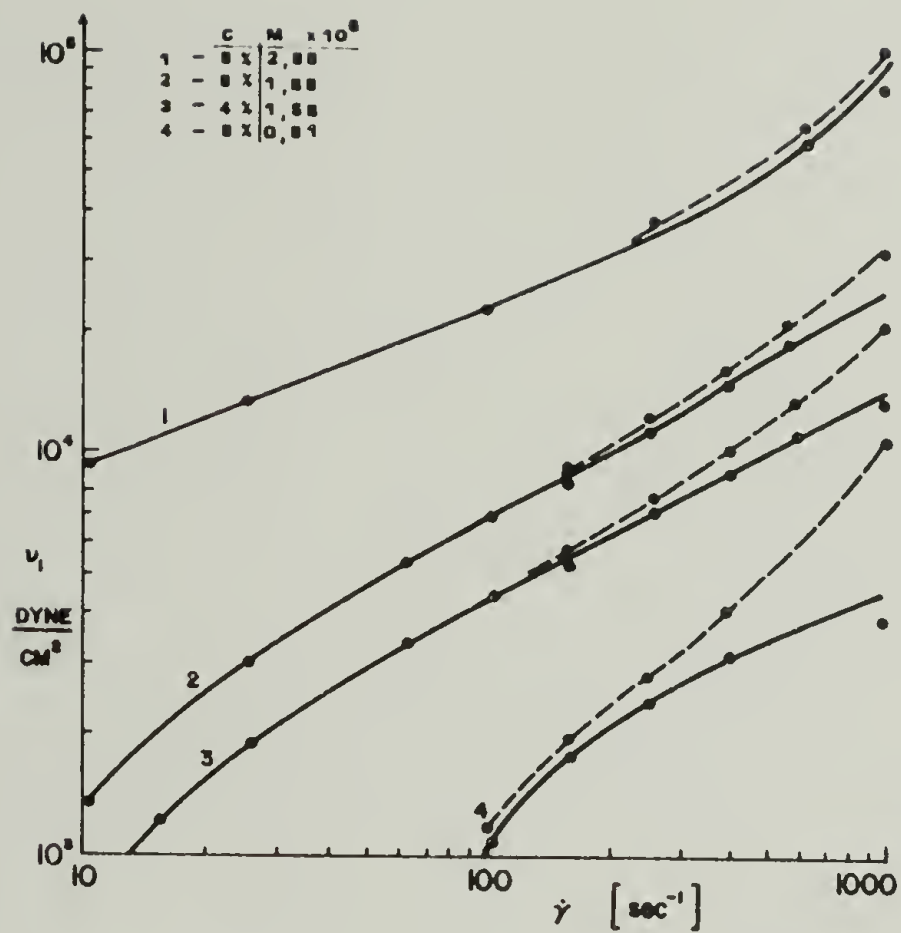


Fig. 2. Normal-force measurements of aqueous polyacrylamide solutions. Dotted lines are corrected for inertial normal force.  $T = 23^{\circ}\text{C}$ .

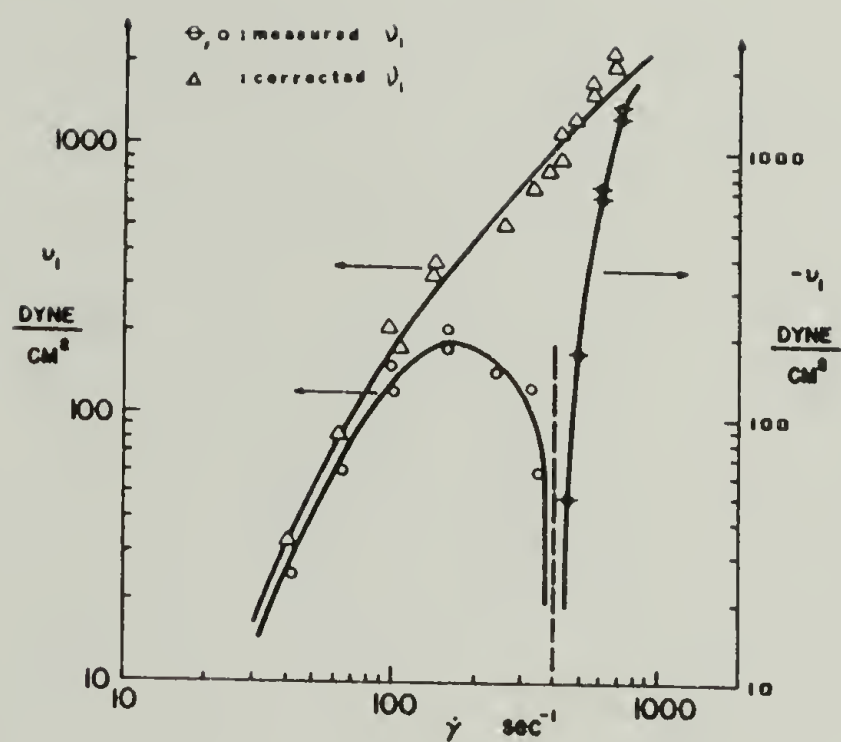


Fig. 3. Normal-force measurements for a 2% aqueous polyacrylamide solution.  $\bar{M}_\eta = 1.56$  mill

then decreases, become negative at  $\dot{\gamma} > 400 \text{ sec}^{-1}$ . That this observation is an artifact is emphasized by the fact that the flow curve (not shown) has no discontinuity at the "critical" shear rate of the "transition" from positive to negative  $v_1$ . The corrected data can be seen to indicate  $v_1$  increasing monotonically with shear rate.

#### 4. Conclusions

A number of measurements of spurious normal forces in Newtonian fluids in steady shear rotational flow indicated that inertial effects can be very significant. Secondary flow, edge and surface tension effects appeared to be negligible.

Corrections for the inertial normal-force found in the literature were accurate within experimental error. The magnitude of the inertial normal-force in cone-and-plate and parallel plate steady shear flow is given by:

$$F_{z0} = - \frac{3\pi\rho\omega^2 R^4}{40} .$$

The magnitude of the inertial normal-force in solid body rotation (Eccentric Rotating Disc flow) is given by:

$$F_{z0} = - \frac{\pi\rho\omega^2 R^4}{4} .$$

Examples of possible consequences of a failure to make the inertial normal-force correction were obtained for typical viscoelastic polymer solutions. In several cases, the error was confined to an

error in magnitude of the first normal-stress difference. However, in one instance an apparent reversal of sign in the first normal-stress difference was observed. This artifact was eliminated when the appropriate correction was applied. This example emphasized the extent to which inertial effects can dominate the behavior of polymer solutions in relatively ordinary circumstances in rotational rheology.

Table 1. Fluids, geometries and ranges (tested at T = 23°C).

Fluid	Approx. $\eta$ (CP)	$\rho$ (g/cc)	Shear mode	R (mm)	GAP (mm)	Cone angle(rad)	$\omega$ (rad/sec)
m-Cresol	15	1.03	C.+P.	50		.04	1.6-40
			C.+P.	25		.04	6.3-100
			C.+P.	25		.1	10-40
			C.+P.	12.5		.01	25-100
S-30,000-67-1b (Cannon Instrument Co. Viscosity Standard)	$3 \times 10^5$	.896	E.R.D.	25	1.5		10-157.5
			E.R.D.	25	1.0		10-157.5
S-600-65-2d (Cannon Instrument Co. Viscosity Standard)	600	.890	E.R.D.	25	1.0		10-63
			E.R.D.	25	.5		10-63
			P.P.	25	.5		10-100
			C.+P.	25		.04	10-100
Brookfield 500	500	.974	E.R.D.	50	1.5		1.6-25
			E.R.D.	50	1.0		2.5-25
			P.P.	50	1.0		4-40
			C.+P.	50		.04	1.6-40
CH <sub>2</sub> I <sub>2</sub>		3.32	P.P.	25	1.0		4-40
			C.+P.	25		.04	4-40
			E.R.D.	50	.3		2.5-25
Water, water + surfactant	1.0	.997	C.+P.	50		.04	16-40
Ethylene glycol	20	1.108	C.+P.	50		.04	4-40

## REFERENCES

- (1) Miller, M.J., E.B. Christiansen, Amer. Ind. Chem. Engg. J. 18, 600 (1972).
- (2) Walters, K., Rheometry (Halsted Press, New York, 1975).
- (3) Adams, N., A.S. Lodge, Phil. Trans. Roy. Soc. A256, 149 (1964).
- (4) Greensmith, H.W., R.S. Rivlin, Phil. Trans. Roy. Soc. A245, 399 (1953).
- (5) Macosko, C.W., W.M. Davis, Rheol. Acta 13, 818 (1974).



## APPENDIX II

### DOCUMENTATION OF COMPUTER PROGRAMS

In order to avoid duplication of effort by future users of the mechanical spectrometer, the computer programs developed during the course of this work will be described. These programs are written in APL and can be found in workspace GK1 of account number A78R000 as of December, 1979. This Appendix is divided into five parts: steady shear programs, oscillatory programs, Eccentric Rotating Disc programs, miscellaneous programs, and a description of the APL file system. The general strategy for each type of measurement is to break the process down into three programs; one to organize the data into a convenient form, one to make calculations, and one to calculate means and standard deviations. Listings of the programs appear in each section.

#### Steady Shear - "DATASORT"

Type "DATASORT." The computer will respond with "start-to stop type 123456789 - constants are sample I.D., Date, R, Beta, T-scale, Z-scale." (The quad symbol " $\square$ :" signifies that the computer is ready for input.) This means that the computer is asking for parameters which will stay the same for a number of data points. Note that R is radius in cm., and beta is cone angle in radians, and the sample I.D. must consist only of numbers. If you type "123456789" this will cause the program to terminate. After typing in the constants, press "Return." The computer will respond with "to change a constant type 987654321 and repeat whole line--data are omega, T, Z."

This means that if you wish to change one of the constants you should type "987654321" and press "return." Then the next line of input would be the entire set of six constants. If the constants are correct and you wish to start feeding in data, type in the values of rotation speed (in rad/sec) and torque and normal force in centimeters measured from the strip chart. Note that the program assumes that each measurement is made in both clockwise and counter-clockwise directions, thus the torque value is divided by two by the calculations program. If a measurement is made in one direction only, the torque value should be doubled before feeding in. (This does not apply to normal force.) Press "return" after typing in the data and continue the process of typing in the data three numbers at a time until you wish to change a constant (type "987654321" and press "return") or terminate the program (type "123456789" and press "return").

After terminating program "DATASORT," all of the data will be contained in an  $N \times 9$  array called "DATA" and also a  $9N$  vector called "DATASAVE." The dimensions of the data array may be found by typing " $\rho$  DATA." You should either use the data immediately or else save it in an APL file, since calling the program "DATASORT" again will cause the variable "data" to be written over, hence all the numbers stored therein will be lost. If the situation does arise that you call "DATASORT" again without properly preserving "DATA," you can attempt to input an array, e.g., " $(3\ 3)\rho 1$ ," which will give a rank error in step [12]. This will cause the program to exit before step [14], hence the previously inserted numbers will be retained in "DATASAVE" in vector form. However, it is better not to take a chance, since there is

nothing more annoying than losing an hour's work re-entering data lost because of carelessness.

On some occasions, especially when disc space becomes tight, the computer will go down abruptly and the contents of "DATA" will be lost. You may attempt a recovery procedure, but this is often unsuccessful. On such days it pays to exit from "DATASORT" frequently and save what you have so far. On the first occasion, after exiting from "DATASORT" type "TEMP+DATA," press "return," then type ")SAVE." On all subsequent occasions after exiting type "TEMP+TEMP,[1]DATA," press "return," then type ")SAVE." This will cause the additional rows of numbers to be tacked on below the previously saved numbers. Then when the data set has been exhausted you can save "TEMP" in the file system as described later.

If you have made a mistake in feeding in data and the number of numbers is not evenly divisible by 9, attempting to exit from "DATASORT" will produce an error in step [15]. The procedure for handling this situation is also described later.

#### "CONEPLATE"

The program "CONEPLATE" takes the  $N \times 9$  array as produced by "DATASORT" and calculates viscosity, first normal-stress difference, and shear rate. A correction for the negative inertial contribution to the normal stress difference (see Appendix One) is made automatically (values of this correction are contained in the variable "INCOR").

To use this program, type "CONEPLATE." When the computer responds with quad (" $\square$ :") type in the name of the data array (e.g.,

"DATA") or else read from a file (described later), and press "return." The computer will respond with "give sample I.D." Type in the identifying number of the sample for which you wish calculations made and press "return." This step is provided so that data on a number of samples can be contained in a single data array, yet results on individual samples can be called out separately. The computer will respond with "to write type 123456789." If you wish a printout of the results of the calculations, type "123456789" and press "return." If not, type any other number and the program will terminate. The results will be contained in the global variables "GAMMA," "ETA," and "NUONE," which will be used by the averaging program.

#### "GAMMASELECT"

This program takes the results from "CONEPLATE" and calculates mean and standard deviation of viscosity and normal force. Since this program requires input in the form of global variables created by "CONEPLATE," you must use "CONEPLATE" immediately prior to "GAMMASELECT" on the data of interest.

To use this program, type "GAMMASELECT." The computer will respond with "averages desired for which shear rate?" Type in the desired shear rate and press "return." The computer will select all viscosity and normal force numbers corresponding to shear rates within 5% of the selected value. This is done because the fixed rotational speeds combined with the available cone angles result in shear rates which are not precisely identical. Note that in many cases a torque measurement can often be made when a normal force measurement is not

possible and the reverse is also sometimes true. For this reason value of zero for either viscosity or first normal stress difference are not included in the averages. The computer will respond with the number of viscosity and normal force points, and the mean and standard deviation of each. Then type in the next desired shear rate and press "return." Continue in this manner until you are ready to exit, then type "123456789" and press "return."

### Oscillatory Shear - "OSCSORT"

The strategy of this program is similar to "DATASORT." There are five constants rather than six, since normal force is not measured. Note that the recommended procedure is to use a torque scale of 10,000  $g_f$ -cm. If the sample is not viscous enough to produce a visible response in the torque pen at this scale, results may be erratic and it is beneficial to use a more sensitive scale. Note that on the highest sensitivity settings (200, 500, 2000  $g_f$ -cm) the amplifiers may phase-shift the torque signal at higher frequencies (e.g.,  $4H_z$ - $63H_z$ ) which will be interpreted by the rheophaser as a material property. If in doubt, make measurements on several scales. Note also that the setting of the low-pass filter affects the pen response but not the input to the rheophaser.

As before, the signal to change a constant is "987654321" and to exit the program, "123456789." The data are frequency in Hertz, voltage (amplitude of oscillation), A, B. Ignore the negative signs in front of A and B on the rheophaser.

As with "DATASORT," the data is organized into a N x 9 array

(called "DATAOSC"). However, the backup location (again called "DATASAVE") is also an  $N \times 9$  array rather than a  $9N$  vector. The same precautions about saving data also apply here. If you make a mistake feeding data into "OSCSORT" an error message on step [9] will result immediately rather than when you attempt to exit.

#### "OSCCOMP"

This program makes calculations from the  $N \times 9$  data array produced by "OSCSORT." It is used exactly the same as "CONEPLATE." The results given are frequency (in rad/sec), strain amplitude, storage modulus, loss modulus, and dynamic viscosity. Note that the factor of 14.1 in step [3] converts displacement from volts to radians. This arises since the voltage values used by the rheophase are R.M.S. values. Thus a 1 v. amplitude on the rheophaser gives a sine wave with a baseline-to-peak value of 1.41 volts. The angular position control and drive system deflect the cone by .141 radian. Multiplying by 100 for % gives 14.1. The results produced by this program are deposited in global variables called "FREQ," "GSTO," and "ETAPRIME," for use by the averaging program.

#### "OSCSELECT"

This program takes results from "OSCCOMP" and calculates means and standard deviations of storage modulus and dynamic viscosity. This program is used in exactly the same way as "GAMMASELECT" and all comments pertaining thereto are also valid here.

Eccentric Rotating Disc - "ERDSORT"

The strategy for making E.R.D. measurements is usually to make several measurements at one frequency by changing the displacement. For this reason rotation speed is considered a constant. Other constants are sample I.D. (numbers only), date, radius (cm.), plate separation (cm.), rotational speed (rad/sec),  $X_0$  (mm),  $Y_0$  (mm), X-scale, Y-scale.  $X_0$  and  $Y_0$  are those values of X and Y which give no pen deflection upon reversal of the direction of rotation. These values will be close to 15,000 and 20,000 resp., but will depend on plate radius, gap, and to a lesser extent on rotation speed. Best accuracy can be achieved by determining  $X_0$  and  $Y_0$  anew for each rotational speed.

Data are X (mm), Y (mm),  $F_x$  (cm., measured on strip chart), and  $F_y$  (cm.). Since in general the displacement during an E.R.D. measurement is parallel to one or the other of the axes, either X or Y will be equal to the zero-displacement value. The "ERDCOMP" program automatically selects the appropriate forces to calculate storage and loss moduli, according to the direction of displacement. A problem arises if rotation in only one direction is used, since "ERDCOMP" assumes rotation in both directions and halves the appropriate force. In this case, for displacement along the X-axis, double  $F_y$ , for displacement along the Y-axis double  $F_x$ .

For "ERDSORT," as for "DATASORT," a mistake in feeding in data will not be discovered until attempting to exit the program, at which point step [16] will bomb out. Successfully exiting the program

leaves the data in an  $N \times 13$  array called "DATAERD" and in a  $13N$  vector called "DATASAVE."

#### "ERDCOMP"

This program makes calculations based on the  $N \times 13$  data array produced by "ERDSORT." It is used exactly the same as "CONEPLATE" and "OSCCOMP." Since this program was written to handle data generated by solutions, it was not felt necessary to compensate for instrument compliance. However, this may be a significant source of error for elastomers and polymer melts, especially at high frequencies. A FORTRAN program written by George Senich (also, unfortunately, called "ERDCOMP") exists in the library of account #A78R000 as of November, 1979. This program bears no relation to any of the other programs described in this Appendix.

#### "ERDSELECT"

This program is used exactly the same as "GAMMASELECT" and "OSCSELECT."

### The APL File System

This section describes some of the programs copied from the "FILESYS" workspace into workspace "GK1." APL files are indirect access files (unless specifically defined as a direct access file). This means that all manipulations are performed on a temporary copy of the file (generated by "tying" the file to an access number). The temporary copy becomes the permanent copy when the file is "untied."



This means that if the file is not untied before signing off the system, any new information is lost. On the other hand, if part of the information in a tied file is accidentally lost (e.g., by writing over the wrong location), one can simply sign off without untying, sign on again, and start with another copy of the permanent file.

To create a file, use the "FCREATE" function: type "'NAME' FCREATE n." "NAME" is in quotation marks and must be seven or less alphanumeric characters. "n" is an integer file-tie number. Note that files are tied upon creation, the permanent copy is produced upon untying. If you try to create a file using a name which is already being used for a file, you get an error. However, you can use the name of an existing variable for a file, thus a convenient, mnemonic procedure is to, e.g., define a file called "DATA," and write in the variable "DATA" produced by the program "DATASORT" every time you use it. To find out what files already exist in the account, use ")LIB."

To use an existing file, tie the file to a number: "'NAME' FTIE n." To find out what the status of a tied file is, type "PSTATUS." This gives the names of all tied files, the file-tie numbers, and the last filled location (the first location is #0), as well as some obscure information. To write into a file, type "VAR FWRITE (n m)," where "VAR" is the name of the variable (don't use quotation marks), "n" is the file-tie number, and "m" is the desired location (the location need not be empty). To read from a file type "FREAD(n m)." This expression can be used exactly like a variable, e.g., when inputting data into "OSCOMP," you can read directly from the file. You can only

"TOM" and ties it to number 9, therefore "TOM" must exist in the library (if not, create it) and no files should be tied to 9. This program repeatedly calls "OSCCOMP" and places the results in temporary storage. When you exit from "FINESSE" the results are placed into variables "FREQ," "GSTO," and "ETAPRIME," so that you may use OSC-SELECT immediately.

Correcting errors made while inputing data. Errors made while feeding data into "DATASORT" and "ERDSORT" will not be discovered until exiting from the program, at which point an error will be caused by the number of numbers not being evenly divisible by 9 or 13 respectively. Let's assume that you forgot to feed in a normal force value in measurement 10 out of 30. You typed in "123456789" and got an error message for DATASORT [15]. Type "p DATA" and the computer responds 269 (one short of 30 x 9). Type " $\square \leftarrow (30 \ 9)p(\text{DATA},0)$ ." This prints out a 30 x 9 array consisting of all the numbers in "DATA" with a zero tacked on the end. The location of the error will be obvious immediately since the last column will have normal force values for the first nine rows but a long sample I.D. number in row 10, column 9. This tells you that row 10 only has 8 entries rather than 9. You establish that the normal force value is missing by reference to the strip chart and that the correct value is 3.05. The missing number should be in position number 89, which means inserting the number between position 88 and position 89 of "DATA" as it stands. To do this use the following procedure:

```
TEMP←(88↑DATA), 3.05, (88↓DATA)
```

```
DATA←(30 9)ρ TEMP
```

The last step reshapes the corrected data vector into the desired N x 9 array.

```

VMM:MSUB: LUJ
DATA=0
START - TOSTOP TYPE 123456789 - CONSTANTS ARE SAMPLE I.D., DATE ,R(CM),BETA,T-SCALE,Z-SCALE
CONST=0
+(CONST=123456789)/BRANCH
TO CHANGE A CONSTANT TYPE 987654321 AND REPEAT WHOLE LINE
DATA ARE OMEGA,T(CM),Z(CM)
LOOP:DATA=0
+(DATA=123456789)/BRANCH
+(DATA=987654321)/CONSTCHANGE
CONST=0
+LOOP
CONSTCHANGE:DATA=DATA,CONST,DATA
+LOOP
BRANCH:DATA=DATA
DATA=((PDATA)+9),9)PDATA

```

```

OCONEPLATE [0]
OCONEPLATE
DATA=0
ETA=234.1299X(((DAC[8]+25)XDAC[5]XDAC[4])+(DAC[7]XDAC[3]*3))
NUMEAS+624.333X(((DAC[9]+25)XDAC[6])+(DAC[3]XDAC[3]))
INCOR+(0.15XDAC[3]XDAC[3]XDAC[7]XDAC[7])
NUONE+NUMEAS+INCOR
GIVE SAMPLE I.D.
SAMPLE=0
GAMMA+(DAC[7]+DAC[4])
SELECT+DAC[1]@SAMPLE
RESULT+(SELECT/(DAC[1])),(SELECT/GAMMA),(SELECT/ETA),(SELECT/NUONE)
TO WRITE TYPE 123456789
+(123456789=0)/WRITE
+END
WRITE:'SAMPLE',' SHEAR',' ETA ','NUONE '
Q(4,(+/SELECT))PRESULT
END

```

```

OGAMMASELECT [0]
OGAMMASELECT
' AVERAGES DESIRED FOR WHICH SHEAR RATE?'
GAMSELVAL=0
+(GAMSELVAL=123456789)/STOP
GAMSEL+(PSELECT)PGAMSELVAL
SELECT2+(((SELECT/GAMMA)-GAMSEL)X((SELECT/GAMMA)-GAMSEL))*0.5*((GAMSELVAL*0.05)
SELETA+((ETA#0)^(SELECT2))/(SELECT/ETA)
SELNU+((NUMEAS#0)^(SELECT2))/(SELECT/NUONE)
' VISCOSITY POINTS 'PSELETA;' NORMAL FORCE POINTS 'PSELNU
' AVE. ETA=';(+/SELETA)+PSELETA;' STANDARD DEVIATION IS';(((+/SELETA*2))+PSELETA)*2))X
0.5
[10] 'AVE. NUONE=';(+/SELNU)+PSELNU;' STANDARD DEVIATION IS';(((+/SELNU*2))+PSELNU)-(((+/SELNU)+PSELNU)*2))*0.5
[11] +2
[12] STOP

```

## SAMPLE CALCULATIONS USING STEADY SHEAR PROGRAMS

TEMP2

1122778	10278	5	0.04	200	20	0.1	13.9	1.18
1122778	10278	5	0.04	1000	20	0.16	4.27	2.53
1122778	10278	5	0.04	1000	20	0.25	6.08	5.76
1122778	10278	5	0.04	1000	20	0.4	10.13	12.25
1122778	10278	5	0.04	1000	20	0.25	6.6	5.8
1122778	10278	5	0.04	1000	20	0.16	4.28	2.5
1122778	10278	5	0.04	2000	100	0.4	5.02	2.58
1122778	10278	5	0.04	2000	100	0.63	7.44	5.24
1122778	10278	5	0.04	2000	100	1	10.47	10.52
1122778	10278	5	0.04	2000	100	1.6	13.62	19.77
1122778	10278	5	0.04	2000	100	0.63	7.42	5.19
1122778	10278	5	0.04	2000	100	0.4	5.07	2.49
1122778	10278	5	0.04	2000	500	1	10.42	2.39

## CONEPLATE

0:

TEMP2

GIVE SAMPLE I.D.

0:

1122778

TO WRITE TYPE 123456789

0:

123456789

SAMPLE	SHEAR	ETA	NUOME
1122778	2.5	83.31278	23.61231
1122778	4	79.97877	50.642
1122778	6.25	72.8837	115.3114
1122778	10	75.89555	245.3385
1122778	6.25	79.11718	116.1106
1122778	4	80.16608	50.04264
1122778	10	75.22125	258.3247
1122778	15.75	70.78304	524.9292
1122778	25	62.75431	1054.627
1122778	40	51.02159	1984.49
1122778	15.75	70.59277	519.9345
1122778	10	75.97047	249.3343
1122778	25	62.45462	1197.475

## GAMMASELECT

AVERAGES DESIRED FOR WHICH SHEAR RATE?

0:

2.5

VISCOSITY POINTS 1 NORMAL FORCE POINTS 1

AVE, ETA=83.31278 STANDARD DEVIATION IS 0

AVE, NUOME=23.61231 STANDARD DEVIATION IS 0

0:

4

VISCOSITY POINTS 2 NORMAL FORCE POINTS 2

AVE, ETA=80.07243 STANDARD DEVIATION IS 0.09365196

AVE, NUOME=50.34232 STANDARD DEVIATION IS 0.2996798

0:

6.3

VISCOSITY POINTS 2 NORMAL FORCE POINTS 2

AVE, ETA=76.00044 STANDARD DEVIATION IS 3.116737

AVE, NUOME=115.711 STANDARD DEVIATION IS 0.3995731

0:

10

VISCOSITY POINTS 3 NORMAL FORCE POINTS 3

AVE, ETA=75.69576 STANDARD DEVIATION IS 0.3369157

AVE, NUOME=250.9992 STANDARD DEVIATION IS 5.4307

0:

123456789

```

VARIABLES
[1] I+1
[2] DATAOSC+(0,9)P0
[3] TYPE IN SAMPLE, DATE, RADIUS (CM), BETA (RAD), T-SCALE (G/25CM),
[4] CONSTCHANGE:PARAM+D
[5] TYPE IN OMEGA (HZ), V, A,B - TO STOP TYPE 123456789 - TO CHANGE TYPE 987654321,
[6] LOOP:DATA+D
[7] +(DA=123456789)/STOP
[8] +(TA=987654321)/CONSTCHANGE
[9] DATAOSC+DATAOSC,[1](PARAM,DA)
[10] +LOOP
[11] STOP:DATA SAVE+DATAOSC
      0
POSSECOMP [0] 0
POSSECOMP
      'GIVE DATA'
DATA+D
CONST+( (3xDAC[4]x156.08xDAC[5])÷(DAC[3]*3) )
INT+(DAC[6]x6.283), (DAC[7]x10÷DAC[4]), (CONSTxDAC[8]), (CONSTxDAC[9])+(DAC[6]x6.283)
INT+B(5, ((PINT)+5))PINT
GSTOP+INT[3]
ETAPRIME+INT[5]
FREQ+INT[1]
      'TO WRITE TYPE 123456789'
+(D=123456789)/WRITE
+STOP
WRITE: 'SAMPLE ' ;DAC[1]; ' DATE ' ;DAC[1;2]
      ' W DISPL./o G-STORAGE G-LOSS ETAPRIME '
INT
STOP:
      0
POSSELECT [0] 0
POSSELECT
      'AVERAGES DESIRED FOR WHICH FREQUENCY? - TYPE 123456789 TO STOP'
FREQSELVAL+D
+(FREQSELVAL=123456789)/STOP
FREQSEL+(PGSTO)PFREQSELVAL
SELECT+( ( (FREQ-FREQSELVAL) )÷(FREQSELVALx0.1) )
SELSTA+( (ETAPRIME#D)^(SELECT) )/ETAPRIME
SELSTO+( (GSTO#D)^(SELECT) )/GSTO
      'NUMBER OF STORAGE POINTS ' ;PSELSTO; ' NUMBER OF LOSS POINTS ' ;PSELETA
      'AVE. ETAPRIME=' ;((+ /SELSTA)÷PSELSTA); ' STANDARD DEVIATION IS ' ;(((+ / (SELSTA*2))÷PSELSTA)-((+ /SELSTA)÷PSELSTA) )
      'AVE. G-STORAGE=' ;((+ /SELSTO)÷PSELSTO); ' STANDARD DEVIATION IS ' ;(((+ / (SELSTO*2))÷PSELSTO)-((+ /SELSTO)÷PSELSTO) )
[10]
[11] +2
[12] STOP:
      0

```

SAMPLE CALCULATIONS USING OSCILLATORY PROGRAMS

TEMP

1123776	92578	2.5	0.1	200	1	0.1	0.097	1.16
1123776	92578	2.5	0.1	200	1	0.1	0.179	1.123
1123776	92578	2.5	0.1	200	1	0.2	0.124	1.14
1123776	92578	2.5	0.1	200	1	0.2	0.194	1.184
1123776	92578	2.5	0.1	200	0.63	0.15	0	0.7612
1123776	92578	2.5	0.1	200	0.63	0.15	0.0878	0.8103
1123776	92578	2.5	0.1	200	0.63	0.3	0.0535	0.7643
1123776	92578	2.5	0.1	200	0.63	0.3	0.1108	0.7537
1123776	92578	2.5	0.1	200	0.4	0.15	0.0178	0.4944
1123776	92578	2.5	0.1	200	0.4	0.15	0.0271	0.4935

OSCCOMP

GIVE DATA

□:

TEMP

TO WRITE TYPE 123456789

□:

123456789

SAMPLE	1123776	DATE	92578				
ω	DISPL. %	G-STORAGE	G-LOSS	ETAPRIME			
6.283	10	58.13668	695.2428	110.6546			
6.283	10	107.2831	673.0669	107.1251			
6.283	20	74.31905	683.2558	108.7467			
6.283	20	116.2734	709.6271	112.944			
3.95829	15	0	456.2231	115.2576			
3.95829	15	52.62268	485.651	122.6921			
3.95829	30	32.06508	458.0811	115.727			
3.95829	30	66.40767	451.728	114.122			
2.5132	15	10.66838	296.3173	117.9044			
2.5132	15	16.24231	295.7778	117.6897			

OSCSELECT

AVERAGES DESIRED FOR WHICH FREQUENCY? - TYPE 123456789 TO STOP

□:

2.5

NUMBER OF STORAGE POINTS 2 NUMBER OF LOSS POINTS 2  
 AVE, ETAPRIME=117.7971 STANDARD DEVIATION IS 0.1073159  
 AVE, G-STORAGE=13.45534 STANDARD D2.786964

□:

4

NUMBER OF STORAGE POINTS 3 NUMBER OF LOSS POINTS 4  
 AVE, ETAPRIME=116.9497 STANDARD DEVIATION IS 3.366359  
 AVE, G-STORAGE=50.36514 STANDARD DEVIATION IS 14.11089

□:

6.3

NUMBER OF STORAGE POINTS 4 NUMBER OF LOSS POINTS 4  
 AVE, ETAPRIME=109.8676 STANDARD DEVIATION IS 2.171475  
 AVE, G-STORAGE=89.00306 STANDARD DEVIATION IS 23.69696

```

[1] PERISORT [0]
[2] DATAE+10
[3] *STAFF - TO STOP TYPE 123456789 - CONSTANTS ARE:
[4] *SAMPLE I.D., DATE, R(CM), GAP(CM), OMEGA, X0(MM), Y0(MM), X-SCALE, Y-SCALE.
[5] *CONST+0
[6] +(CONST=123456789)/BRANCH
[7] *TO CHANGE A CONSTANT TYPE 987654321 AND TYPE WHOLE LINE.
[8] *DATA ARE X(MM), Y(MM), FX (CM), FY (CM).
[9] LOOP:DATAE+0
[10] +(DATAE=123456789)/BRANCH
[11] +(DATAE#987654321)/CONSTCHANGE
[12] CONST+0
[13] *LOOP
[14] CONSTCHANGE:DATAE+DATAERD,CONST,DATAE
[15] *BRANCH:DATAE+DATAERD
[16] DATAERD+((PDATAERD)/13),13)PDATAERD

```

```

[1] PERDCOMP [0]
[2] PERICOMP
[3] I+1
[4] ZAPD
[5] GSTO+GLOSS+ETAPRIME+A+(PFA)[1]P0
[6] LOOP:+(FA[6]=FA[10])/YDISFL
[7] A[I]+((1(FA[6]-FA[10]))+(DA[4]))x0.1
[8] GSTO[I]+((DA[3]xDA[12])x(980.7+25))+(3.1416xFA[3]xDA[3]xA[I])
[9] GLOSS[I]+((DA[9]xFA[13])x(980.7+50))+(3.1416xDA[3]xDA[3]xA[I])
[10] ETAPRIME[I]+GLOSS[I]+DA[5]
[11] I+I+1
[12] *INDEX
[13] YDISFL:A[I]+((1(FA[7]-FA[11]))+(DA[4]))x10
[14] GSTO[I]+((FA[9]xFA[13])x(980.7+25))+(3.1416xDA[3]xDA[3]xA[I])
[15] GLOSS[I]+((DA[8]xFA[12])x(980.7+50))+(3.1416xDA[3]xDA[3]xA[I])
[16] ETAPRIME[I]+GLOSS[I]+DA[5]
[17] I+I+1
[18] *INDEX:+(I((PFA)[1])/LOOP
[19] INT+IA[5],(AX100),GSTO,GLOSS,ETAPRIME
[20] *TO WRITE TYPE 123456789.
[21] +(123456789#D)/WRITE
[22] *U DISPL./O
[23] G-STORAGE G-LOSS ETAPRIME.
[24] D+Q((PINT)/(PDA)[1]),((PDA)[1])PINT
[25] WRITE:

```

```

[1] PERDSELECT [0]
[2] PERDSELECT
[3] *AVERAGES DESIRED FOR WHICH FREQUENCY?-TYPE 123456789 TO STOP.
[4] FRESELVAL+0
[5] +(FRESELVAL=123456789)/STOP
[6] FRESEL+((PFA)[1])PFRESELVAL
[7] SELECT2+((FA[5]-FRESEL)x(DA[5]-FRESEL))x0.5((FRESELVALx0.05)
[8] SELLOSS+((ETAPRIME#0)(SELECT2))/ETAPRIME
[9] SELSTO+((GSTO#0)(SELECT2))/GSTO
[10] *NUMBER OF STORAGE POINTS 'JSELSTO: NUMBER OF LOSS POINTS 'JSELLOSS
[11] *AVE ETAPRIME '=';(+/SELLOSS)+JSELLOSS; PLUS/MINUS 'J((+/SELLOSS)-((+/SELSTO)+JSELLOSS)x2))x
[12] *AVE G-STORAGE '=';(+/SELSTO)+JSELSTO; PLUS/MINUS 'J((+/SELSTO)+JSELSTO)-((+/SELSTO)+JSELSTO)x2))x0.5
[13] *STOP:
[14] STOP:

```



TEMP1

1123775	91878	2.5	0.15	1	15.091	20.034	20	20	14.95	20.034	0	0.49
1123775	91878	2.5	0.15	1	15.091	20.034	20	20	14.8	20.034	0.19	1.2
1123775	91878	2.5	0.15	1	15.091	20.034	20	20	14.65	20.034	0.29	1.85
1123775	91878	2.5	0.15	1	15.091	20.034	20	20	14.4	20.034	0.32	2.95
1123775	91878	2.5	0.15	1	15.091	20.034	20	20	14.25	20.034	0.4	3.54
1123775	91878	2.5	0.15	0.63	15.091	20.034	20	20	14.95	20.034	0	0.41
1123775	91878	2.5	0.15	0.63	15.091	20.034	20	20	14.8	20.034	0	0.77
1123775	91878	2.5	0.15	0.63	15.091	0.034	20	20	14.65	20.034	0	1.16
1123775	91878	2.5	0.15	0.63	15.091	20.034	20	20	14.5	20.034	0.23	1.49
1123775	91878	2.5	0.15	0.63	15.091	20.034	20	20	14.35	20.034	0.3	1.89

ERRDCOMP

D:

TEMP1

TO WRITE TYPE 123456789

D:

123456789

W	DISFL./°	G-STORAGE	G-LOSS	ETAPRIME
1	9.4	0	104.1438	104.1438
1	19.4	39.13336	123.579	123.579
1	29.4	39.41358	126.3953	126.3953
1	46.06667	27.7561	127.9383	127.9383
1	56.06667	28.50693	126.1432	126.1432
0.63	9.4	0	87.14074	138.3186
0.63	19.4	0	79.29654	125.8675
0.63	29.4	0	78.82717	125.1225
0.63	39.4	23.32528	75.55363	119.9264
0.63	49.4	24.26552	76.43638	121.3276

ERRDSELECT

AVERAGES DESIRED FOR WHICH FREQUENCY?-TYPE 123456789 TO STOP

D:

1

NUMBER OF STORAGE POINTS 4 NUMBER OF LOSS POINTS 5

AVE ETAPRIME =121.6399 PLUS/MINUS 8.8593

AVE G-STORAGE =33.70249 PLUS/MINUS5.578178

D:

.63

NUMBER OF STORAGE POINTS 2 NUMBER OF LOSS POINTS 5

AVE ETAPRIME =126.1125 PLUS/MINUS 6.499129

AVE G-STORAGE =23.7954 PLUS/MINUS0.4701187

D:

123456789



